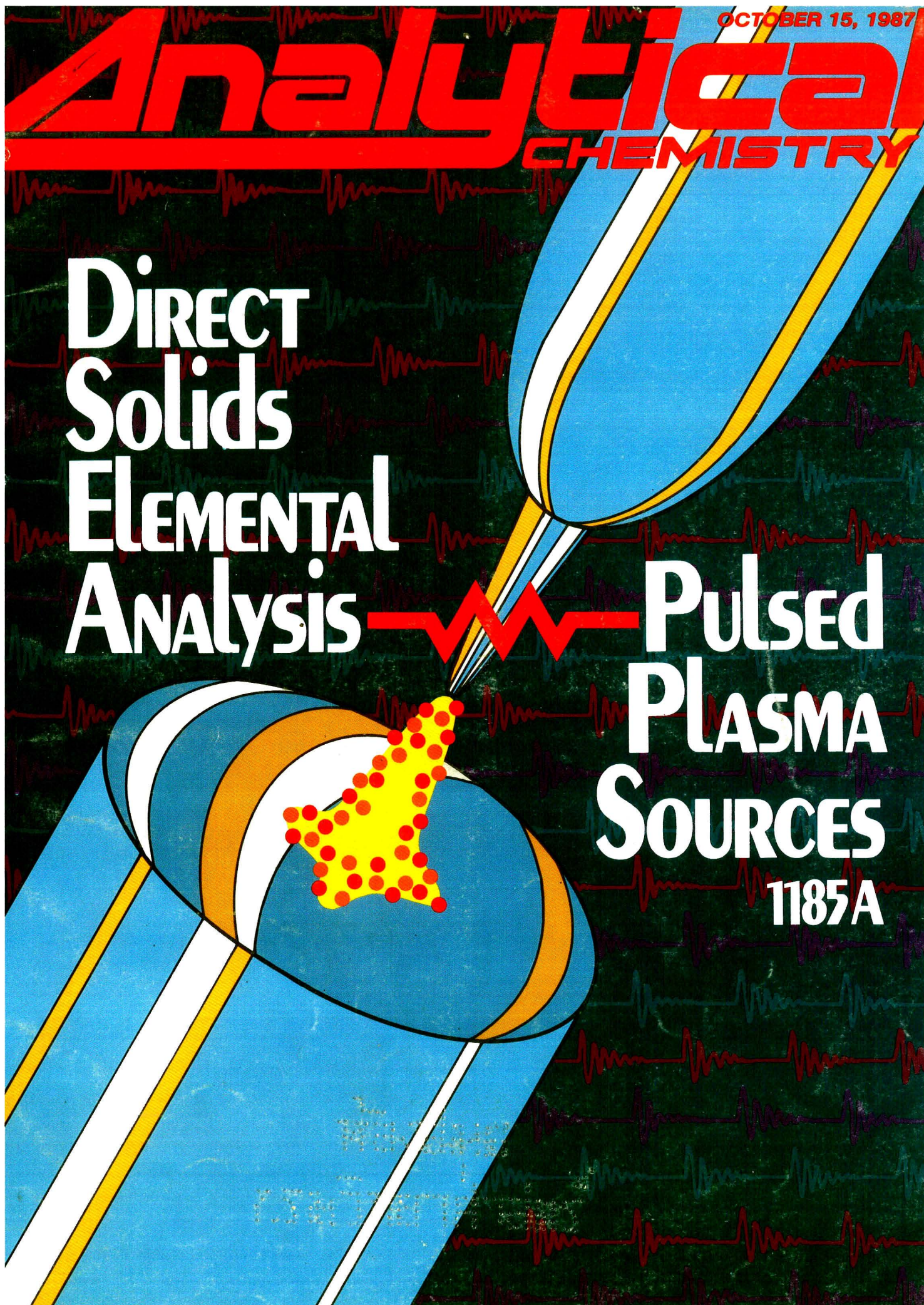


OCTOBER 15, 1987

Analytical CHEMISTRY

**DIRECT
Solids
ELEMENTAL
Analysis**

**Pulsed
PLASMA
SOURCES**
1185A





**The ability to store, recall and
evaluate the results makes differential
weighing more efficient.
Now you can do it more easily with
a METTLER DeltaTrac balance.**

Ask for more information and a free copy
of the new METTLER DeltaTrac applications guide.

CIRCLE 104 ON READER SERVICE CARD

We understand.
Precisely.

METTLER



**Staying ahead at the leading edge in performance
and versatility, at yesteryears' lower prices...**

Introducing the new DL25 and DL21 Titrators

- designed to meet your specific needs
- extensive automation possibilities
- available with new PC software
- exclusive two-year METTLER Service Plus® Protection:
on-site repair or a loaner unit guaranteed within 48 hours

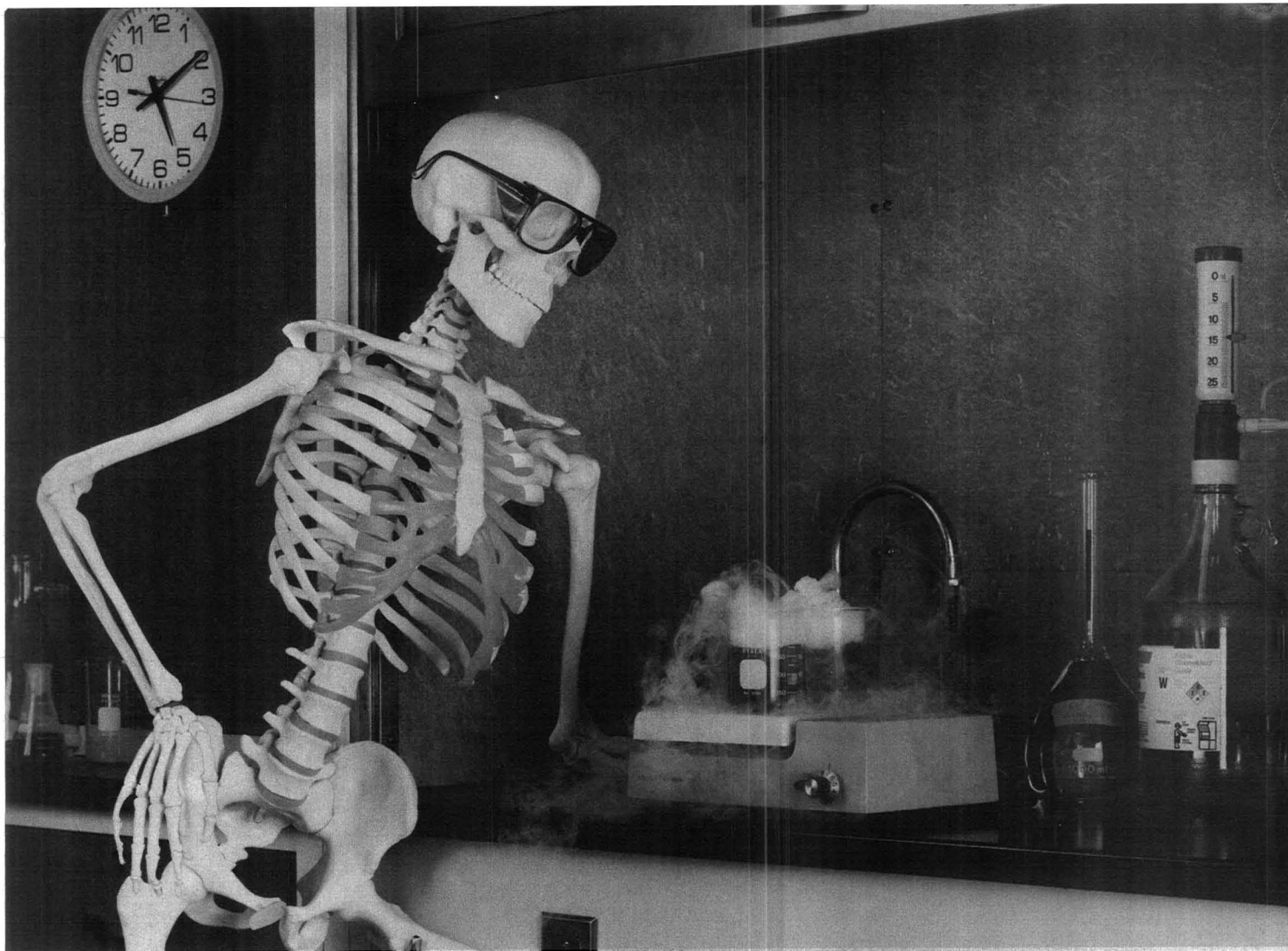
METTLER, whenever titration is your concern.

Mettler Instrument Corporation, Box 71, Hightstown, N.J. 08520
Phone 1-800-METTLER, in New Jersey 609-448-3000

METTLER

CIRCLE 105 ON READER SERVICE CARD

6713.73



Been waiting long for your samples to dissolve?

Your brand new AA sits idle while you dissolve samples by techniques that haven't changed in a century. Doing acid digestions over a hot plate is tedious, hazardous, time consuming . . . and totally unnecessary!

The CEM Microwave Digestion System reduces AA/ICP sample preparation time from hours to just minutes without generating clouds of acid fumes. The system uses closed vessels of PFA Teflon® which are specially designed for safety at high pressure. The CEM Microwave Digestion System holds a carousel of 12 such vessels. Each vessel has a control valve which opens if excess pressure builds up. These closed vessels allow the acids used for sample digestion to reach temperatures well above their normal boiling point.

Dramatic reductions in sample preparation time are achieved by a combination of rapid microwave heating and elevated digestion temperature. The Microwave Digestion System can be programmed to automatically carry out a digestion in various stages. This frees the operator to attend to other duties while the digestion is taking place.

The CEM system is ideal for sample digestions in nitric, hydrochloric and hydrofluoric acids. It puts you on the cutting edge of laboratory technology with maximum safety, ease of use, lower blanks and reduced acid usage.

And it's a system that drastically cuts the time you spend waiting for dissolutions.

If you'd like more information, or if you want to talk to us about your application, call us now at 800/334-6317. (In NC, call 704/821-7015.)

CEM

P. O. Box 200
Matthews, NC 28106





ANCHAM
59(20) 1173A-1216A/2449-2544 (1987)
ISSN 0003 2700

Registered in U.S. Patent and Trademark Office;
Copyright 1987 by the American Chemical Society

ANALYTICAL CHEMISTRY (ISSN 0003-2700) is published semimonthly by the American Chemical Society at 1155 16th St., N.W., Washington, D.C. 20036. Editorial offices are located at the same ACS address (202-872-4600; TDD 202-872-8733). Second-class postage paid at Washington, D.C., and additional mailing offices. Postmaster: Send address changes to ANALYTICAL CHEMISTRY Membership & Subscription Services, P.O. Box 3337, Columbus, Ohio 43210.

Claims for missing numbers will not be allowed if loss was due to failure of notice of change of address to be received in the time specified; if claim is dated (a) North America: more than 90 days beyond issue date, (b) all other foreign: more than one year beyond issue date, or if the reason given is "missing from files."

Copyright Permission: An individual may make a single reprographic copy of an article in this publication for personal use. Reprographic copying beyond that permitted by Section 107 or 108 of the U.S. Copyright Law is allowed, provided that the appropriate per-copy fee is paid through the Copyright Clearance Center, Inc., 27 Congress St., Salem, Mass. 01970. For reprint permission, write Copyright Administrator, B&J Division, ACS, 1155 16th St., N.W., Washington, D.C. 20036.

Registered names and trademarks, etc., used in this publication, even without specific indication thereof, are not to be considered unprotected by law.

Advertising Management: Centcom, Ltd., 500 Post Rd. East, Westport, Conn. 06880 (203-226-7131)

1987 subscription rates include air delivery outside the U.S., Canada, and Mexico

	1 yr	2 yr
Members		
Domestic	\$ 25	\$ 42
Canada and Mexico	50	92
Europe	77	146
All Other Countries	104	200
Nonmembers		
Domestic	37	62
Canada and Mexico	62	112
Europe	127	231
All Other Countries	154	285

Three-year and other rates contact: Membership & Subscription Services, ACS, P.O. Box 3337, Columbus, Ohio 43210 (614-421-3776).

Subscription orders by phone may be charged to Visa, MasterCard, Barclay card, Access, or American Express. Call toll free at (800) ACS-5558 from anywhere in the continental United States; from Washington, D.C., call 872-8065. Mail orders for new and renewal subscriptions should be sent with payment to the Business Management Division, ACS, P.O. Box 57136, West End Station, Washington, D.C. 20037.

Subscription service inquiries and changes of address (Include both old and new addresses with ZIP code and *recent mailing label*) should be directed to the ACS Columbus address noted above. Please allow six weeks for change of address to become effective.

ACS membership information: Bebe Olsen, Washington address.

Single issues, current year, \$5.00 except review issue and LabGuide, \$10.00; **back issues and volumes and microform editions** available by single volume or back issue collection. For information or to order, call (800) ACS-5558 or write the Sales Department at the Washington address.

Nonmembers rates in Japan: Rates above do not apply to nonmember subscribers in Japan, who must enter subscription orders with Maruzen Company Ltd., 3-10 Nihonbashi 2-chome, Chuo-ku, Tokyo, 103, Japan. Tel: (03) 272-7211.

Analytical[®] CHEMISTRY



INSTRUMENTATION

1185 A

On the cover. Direct Solids Elemental Analysis: Pulsed Plasma Sources. Alexander Scheeline of the University of Illinois and David M. Coleman of Wayne State University discuss electrical plasma sources that can directly vaporize solids for elemental analysis

BRIEFS

1176 A

NEWS

1183 A

►Division of Analytical Chemistry summer internship program. ►Division announces undergraduate awards. ►SACP sponsors the Instrumental Analysis Enhancement Program

MEETINGS

1201 A

FOCUS

1203 A

Alzheimer's disease. Genetic testing, imaging techniques, and immunoassay methods show promise for biochemical diagnosis of Alzheimer's disease

NEW PRODUCTS & MANUFACTURERS' LITERATURE

1206 A

AUTHOR INDEX

2449

Performance of Flowing and Quiescent Free-Diffusion Junctions in Potentiometric Measurements at Low Ionic Strengths 2450

A stable, well-defined solution boundary, rather than cylindrical symmetry, is the major requirement for stable, free-diffusion junctions that can be used to precisely (± 0.001 pH) measure the pH of 10^{-4} M solutions.

Terence R. Harbinson and William Davison*, The Freshwater Biological Association, The Ferry House, Ambleside, Cumbria LA22 0LP, United Kingdom *Anal. Chem.*, 59 (1987)

Investigation of pH-Dependent Complex Equilibria at Low Ligand to Metal Ratio by Nonlinear Least-Squares Fit to Linear-Sweep or Cyclic Voltammetric Data 2456

The voltammetric determination of stability constants in the case of stepwise formation of stable complexes is illustrated for the copper(II)-oxalate system.

Harald Gampp, Institut de Chimie, Université de Neuchâtel, CH-2000 Neuchâtel, Switzerland *Anal. Chem.*, 59 (1987)

Infrared Studies of the Liquid Crystal *N*-(*p*-Cyanobenzylidene)-*p*-octyloxyaniline Coated on Underivatized and Trimethylsilane-Derivatized Silica 2460

Variations in the IR band shape from the nitrile stretch region for varying amounts of CBOA coated on underivatized and trimethylsilane-derivatized silica are postulated to arise from differences in relative populations of hydrogen-bonded and nonhydrogen-bonded cyano groups.

C. J. Hann and R. K. Gilpin*, Department of Chemistry, Kent State University, Kent, Ohio 44242 *Anal. Chem.*, 59 (1987)

Direct Correlation of Ion and Electron Microscopic Images by Digital Image Superpositioning 2463

Correlation of ion and electron micrographs is successfully achieved using a computer algorithm that digitally superimposes the images upon one another. The method allows for the verification and correction of artifacts that can degrade ion image quality.

Lisa K. Turner, Yong-Chien Ling, Mark T. Bernius, and George H. Morrison*, Baker Laboratory of Chemistry, Cornell University, Ithaca, N.Y. 14853-1301 *Anal. Chem.*, 59 (1987)

Determination of Arsenic, Selenium, and Antimony Using Metastable Transfer Emission Spectrometry 2468

Analytes are directly determined from aqueous solution, unlike most other atomic spectrometric techniques that require a separation-preconcentration procedure to achieve good sensitivity. Detection limits for As, Se, and Sb are 22, 16, and 65 pg, respectively.

William H. Hood and Thomas M. Niemczyk*, Department of Chemistry, The University of New Mexico, Albuquerque, N.M. 87131 *Anal. Chem.*, 59 (1987)

Resonance Ionization Spectrometric Determination of Gallium Using an Electrothermal Graphite Atomizer 2472

Ga is determined at concentrations below the $\mu\text{g/g}$ level in water solutions and in solid germanium. Reproducibility is better than 15% when 50 pg of Ga is determined. Detection limits of 5×10^7 atoms for pure Ga samples and 3×10^{10} atoms/cm³ in germanium samples are obtained.

George Bekov and Vladimir Radaev, Institute of Spectroscopy, USSR Academy of Sciences, SU-142092 Troitsk, Moscow Region, USSR, and **Jari Likonen, Riitta Zilliacus, Iiro Auterinen, and Eeva-Liisa Lakomaa***, Technical Research Centre of Finland, Reactor Laboratory, Otakaari 3 A, SF-02150 Espoo, Finland *Anal. Chem.*, 59 (1987)

Radiotracer Investigation of the Interference of Hydrofluoric Acid in the Determination of Arsenic and Antimony by Hydride Generation Atomic Absorption Spectrometry 2476

Improved procedures are proposed to eliminate the interference of hydrofluoric acid in the hydrogenation and absorption measurement stages and also in the reduction of Sb(V) to Sb(III).

Kilian Petrick and Viliam Krivan*, Sektion Analytik und Höchstreinigung, Universität Ulm, Oberer Eselsberg, D-7900 Ulm/Donau, FRG *Anal. Chem.*, 59 (1987)

Determination of Boron Isotope Ratios in Geological Materials by Inductively Coupled Plasma Mass Spectrometry 2479

Boron isotope ratios can be determined with a precision of 0.7% in materials containing as little as 0.5 ppm B.


D. Conrad Gregoire, Geological Survey of Canada, Ottawa, Ontario, Canada K1A 0E8 *Anal. Chem.*, 59 (1987)

Characterization of Radiation-Induced Damage to Polyadenylic Acid Using High-Performance Liquid Chromatography/Tandem Mass Spectrometry 2484

Polyadenylic acid is irradiated to 1000 Gy in N₂O-saturated aqueous solution at neutral pH and then enzymatically hydrolyzed to the mononucleoside level. HPLC/MS-MS is used to characterize a number of molecular products that result from the radiation-induced modifications to the model nucleic acid.

Anthony J. Alexander and Paul Kebarle, Department of Chemistry, University of Alberta, Edmonton, Alberta, Canada T6G 2E3, and **Alfred F. Fuciarelli and James A. Raleigh***, Department of Radiobiology, Cross Cancer Institute, Edmonton, Alberta, Canada T6G 1Z2 *Anal. Chem.*, 59 (1987)

*Corresponding author



Mighty LIMS from ORACLE[®] kernels grow.

Put down roots for laboratory information management today, knowing you're backed by the strongest combination of mainstream computer technology as your lab grows tomorrow. Choose ACCESS*LIMS, a laboratory information management system which integrates the latest technology for information management into the analytical laboratory.

We began with Oracle Corporation's proven relational data base management system as the kernel for ACCESS*LIMS. Then we added the

most modern computer technology available — the DEC VAX[™] series, VMS[™] operating systems and Ethernet[™] communications. These elements have been expertly crafted by our team of programmers — who are also chemists — to produce a LIMS that delivers information meaningful to the analytical laboratory.

If you're interested in a LIMS with roots to grow on, write or give us a call. Nelson Analytical, Inc.
10040 Bubb Road, Cupertino, CA 95014
408/725-1107.

nelson ANALYTICAL

We're Always Thinking Ahead.

ORACLE is a trademark of Oracle Corporation. Ethernet is a trademark of Xerox. DEC, VAX and VMS are trademarks of Digital Equipment Corp.

CIRCLE 110 ON READER SERVICE CARD

Preconcentration of Trace Metals from Seawater with 7-Dodeceny-8-quinolinol Impregnated Macroporous Resin 2491

The extraction behavior of the DDQ resin for 12 metals is studied, and column extraction with the resin is successfully applied to the preconcentration of metals at nanogram-per-liter levels.

Kenji Isshiki, Fumito Tsuji, and Tooru Kuwamoto, Department of Chemistry, Faculty of Science, Kyoto University, Kyoto 606, Japan, and **Eiichiro Nakayama***, Instrumental Analytical Research Center, Faculty of Science, Kyoto University, Kyoto 606, Japan
Anal. Chem., 59 (1987)

Reversed-Phase High-Performance Liquid Chromatography of Substituted Anilines Utilizing Molecular-Recognizing Ability of Crown Ether: Comparison with Ion-Pair Chromatography 2496

The addition of 18-crown-6 to the mobile phase enhances retention of substituted anilines. The degree of enhancement reflects number, position, and functionality of substituent groups, which enables specific separation of positional isomers.

Akimasa Shibukawa, Terumichi Nakagawa*, Atsunori Kaihara, Kumiko Yagi, and Hisashi Tanaka, Faculty of Pharmaceutical Sciences, Kyoto University, Sakyo-ku, Kyoto-shi 606, Japan
Anal. Chem., 59 (1987)

Synthesis and Characterization of 2- μ m Wide-Pore Silica Microspheres as Column Packings for the Reversed-Phase Liquid Chromatography of Peptides and Proteins 2501

Separation of ribonuclease, insulin, lysozyme, myoglobin, and ovalbumin is accomplished in 50 s using 2- μ m C_4 -modified silica packed in a 3.3 \times 0.62 cm column.

Neil D. Danielson* and J. J. Kirkland, E. I. du Pont de Nemours and Company, Central Research and Development Department, Experimental Station, Wilmington, Del. 19898
Anal. Chem., 59 (1987)

Detection Limits with Specified Assurance Probabilities 2506

A detection limit-estimation methodology that protects against both false positives and false negatives is described. The method is demonstrated with an experiment involving extractable analytes.

C. Andrew Clayton*, John W. Hines, and Phyllis D. Elkins, Research Triangle Institute, Research Triangle Park, N.C. 27709
Anal. Chem., 59 (1987)

Three-Component Self-Modeling Technique Applied to Luminescence Spectra 2515

Selection of pure component spectra coefficients is improved when additional applicable constraints are imposed. The method is applied to resolve experimental spectra composed of the fluorescence of two conformers of *trans*-1,2-di(2-naphthyl)ethene and a background spectrum dominated by Raman emission in the excitation wavelength region.

Ya-Ping Sun, Donald F. Sears, Jr., and Jack Saltiel*, Department of Chemistry, Florida State University, Tallahassee, Fla. 32306-3006
Anal. Chem., 59 (1987)

Photoacoustic Immunoassay Using Sensitivity Size Dependency for Determination of Turbid Solutions 2519

The rheumatoid factor is determined with a latex agglutination method and photoacoustic spectroscopy. The detection limit of this method is three orders of magnitude lower than conventional immunoassay using turbidimetry.

Takehiko Kitamori* and Kazumichi Suzuki, Energy Research Laboratory, Hitachi, Ltd., Hitachi, Ibaraki 316, Japan, and **Tsuguo Sawada and Yohichi Gohshi**, Department of Industrial Chemistry, Faculty of Engineering, University of Tokyo, Bunkyo-ku, Tokyo 113, Japan
Anal. Chem., 59 (1987)

Improvement in the Definitions of Sensitivity and Selectivity 2522

New definitions of selectivity and sensitivity allow the prediction of analytical error for multicomponent analysis. The estimated error is always the lower limit of the experimentally verified analytical error.

Gerhard Bergmann, Birgit von Oepen, and Peter Zinn*, Lehrstuhl fuer Analytische Chemie, Ruhr-Universitaet Bochum, 4630 Bochum 1, West Germany
Anal. Chem., 59 (1987)

Parametric Mode Operation of a Hyperbolic Penning Trap for Fourier Transform Mass Spectrometry 2527

Symmetries of the hyperbolic Penning trap are reviewed en route to development of a mass calibration law, which is tested at a magnetic field of 1.2T using 1,1,1,2-tetrachloroethane major fragment ions and a new pulse excitation method.

D. L. Rempel, E. B. Ledford, Jr., S. K. Huang, and M. L. Gross*, Department of Chemistry, University of Nebraska, Lincoln, Neb. 68588
Anal. Chem., 59 (1987)

Correspondence

Mixed-Mode Column Thermospray Liquid Chromatography/Mass Spectrometry 2533

John R. Lloyd, Mary Lou Cotter, David Otori, and Alan R. Oyler*, Research Laboratories, Ortho Pharmaceutical Corporation, Raritan, N.J. 08869-0602
Anal. Chem., 59 (1987)

Aids for Analytical Chemists

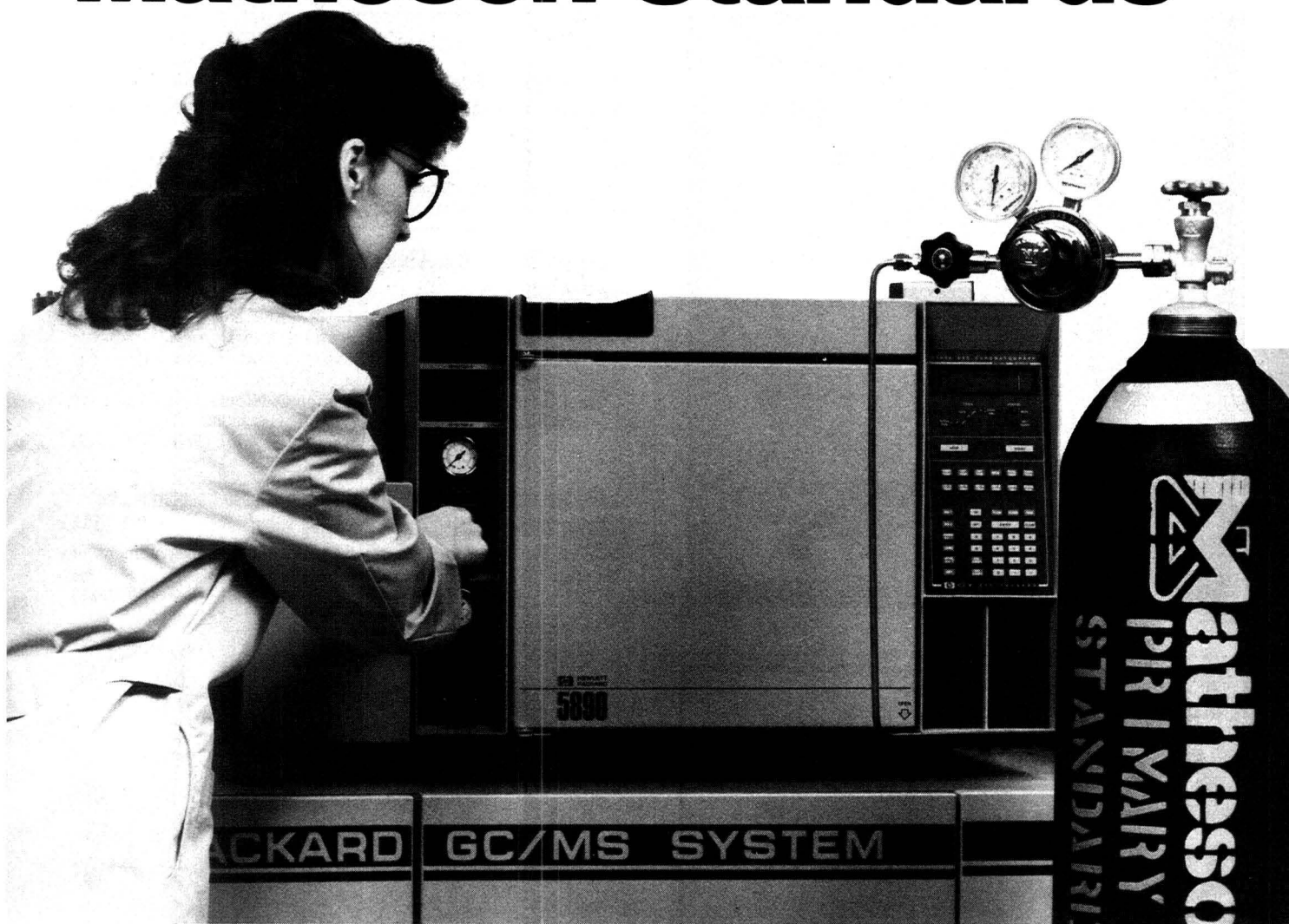
Automated Sample Cell Cleaner 2534

D. E. Bautz and J. D. Ingle, Jr.*, Department of Chemistry, Oregon State University, Corvallis, Ore. 97331
Anal. Chem., 59 (1987)

Selective Separation of 2,3,7,8-Tetrachlorodibenzofuran by High-Resolution Gas Chromatography and by Alumina Column Liquid Chromatography 2536

Maximilian Swerev and Karlheinz Ballschmiter*, Analytische Chemie, Universität Ulm, Oberer Eselsberg, D-7900 Ulm, Federal Republic of Germany
Anal. Chem., 59 (1987)

Move Up to Matheson Standards



Accurate gas chromatography is dependent upon your technique, your equipment, and your gases. A skilled gas chromatographer can enhance the accuracy of his results by using Matheson products exclusively. Three special products are of utmost importance.

Primary Standard Calibration Mixtures

The heart of your work centers around your calibration standards. Consider Matheson's Primary Standards to improve your results. The accuracy of these mixtures usually exceeds that of most analytical instruments. Matheson Primary Standards are prepared on high load, high sensitivity analytical balances. Each gas component is carefully quality controlled before being weighed into the

cylinder. Only weights traceable to the National Bureau of Standards are used. These mixtures give the highest degree of accuracy, precision and confidence. Move up today! Insist on Matheson Primary Standards.

Carrier Gases

The same exacting quality you get in Matheson Primary Standard Calibration Mixtures is also available in Matheson's carrier gases. No slipping in quality control here. Each Matheson UHP, Zero Gas, Ultra Zero Gas, and, of course, Matheson Purity Gas is guaranteed to be exactly what the label says. Nothing more, nothing less. Improve your GC operation today with the right carrier gas from Matheson.

Gas Handling Systems

Don't jeopardize the integrity of your gases with gas handling equipment of inferior quality. Matheson has

the right piece of equipment for every job. From regulators that don't outgas impurities, to filters for protecting delicate valves, to flowmeters that measure precisely, Matheson equipment is **the standard**.

When your work requires the best, don't settle for less than Matheson Standards.

From pharmaceuticals to petroleum, from laser technology to aerospace, when only the best will do, do what so many experienced scientists do, move up to Matheson Standards.

For more information, contact Matheson, at (201) 867-4100, or circle the Reader Service Number below.

Matheson®
Gas Products
World Leader in Specialty Gases & Equipment
30 Seaview Drive, Secaucus, NJ 07094

CIRCLE 102 ON READER SERVICE CARD

Chem Service

Reference & Analytical Standards

Over 13,000 high-purity, pre-analyzed lab chemicals. Available in gram- size quantities. Individually or in kit format.

Chem Service, Inc.
P.O. Box 3108
West Chester, PA 19381
215/692-3026

CIRCLE 28 ON READER SERVICE CARD

BRIEFS

Ultraviolet-Visible Absorption Spectra of Biological Molecules in the Gas Phase Using Pulsed Laser-Induced Volatilization Enhancement in a Diode Array Spectrophotometer 2538

Liang Li and David M. Lubman*, Department of Chemistry, The University of Michigan, Ann Arbor, Mich. 48109

Anal. Chem., 59 (1987)

Measurement of Vapor Deposition and Extraction Recovery of Polycyclic Aromatic Hydrocarbons Adsorbed on Particulate Solids 2541

Robert J. Engelbach, Arlene A. Garrison, E. L. Wehry*, and Gleb Mamantov*, Department of Chemistry, University of Tennessee, Knoxville, Tenn. 37996

Anal. Chem., 59 (1987)

Vibrating Tumblers as Cleaning Devices for Mass Spectrometer Ion Source Parts 2543

Louis R. Alexander*, Vince L. Maggio, Vaughn E. Green, James B. Gill, Elizabeth R. Barnhart, and Donald G. Patterson, Jr., Toxicology Branch, Environmental Health Laboratory Services, Center for Environmental Health, Centers for Disease Control, Atlanta, Ga. 30333, and Lance C. Nicolaysen, Chemistry Department, Emory University, Atlanta, Ga. 30322

Anal. Chem., 59 (1987)

Correction. Comparison of Inorganic Mobile Phase Counterions for Cationic Indirect Photometric Chromatography 2544

Jeffrey H. Sherman and Neil D. Danielson*, Department of Chemistry, Miami University, Oxford, Ohio 45056

Anal. Chem., 59 (1987)

Depend on **DRIERITE**.....
the desiccant for your laboratory drying needs



- * **DRIERITE**
- * **Indicating DRIERITE**
- * **Laboratory Gas Drying Unit**
- * **Drying Tubes**
- * **Technical Advice**

Write or call for free catalog

W. A. Hammond DRIERITE Co.
P. O. Box 460
Xenia, Ohio 45385
513-376-2927

See our catalog in
THOMCAT

CIRCLE 71 ON READER SERVICE CARD

Gain the Full FT-IR Advantage...

The performance of any FT-IR spectroscopy system relies on the interrelationship of optical quality, advanced electronics, data processing capability, and a systems approach that increases its versatility as your needs grow. *That's the Nicolet Advantage.* The highly acclaimed 700 Series expresses that advantage to its fullest.

New System 730 Benchtop Spectroscopy™: A research-quality system that delivers exceptional performance and value. The new System 730 provides the same superb stability, sensitivity, and spectral processing capabilities as the highly successful System 740 in a compact, economical benchtop form.

The Nicolet 700 Series incorporates the latest innovations to provide exceptional sensitivity and stability. System 730's quiet signal processing electronics and high dynamic range achieve excellent signal-to-noise performance for all of your applications.

Specify your spectral range. You can choose from a comprehensive selection of beamsplitters and detectors ranging from 15,250 to 50 cm^{-1} and optimize your System 730 to cover near-IR, mid-IR, or far-IR. Interchangeable modules allow you to quickly and conveniently change detectors for different experimental requirements.

Mainframe computer speed and versatility from a compact benchtop data system. Nicolet's dual-bus architecture gives you uncompromising real-time data acquisition and processing performance, as well as industry-standard interfacing to the latest data system peripherals including the new high-performance DMA SCSI storage devices.

The most comprehensive, field-proven software in the industry gives you full access to the complete problem-solving power of FT-IR, whether you are a novice user or an experienced spectroscopist. You also have full access to Nicolet's extensive on-line spectral search libraries, industry-standard communication and networking capabilities, and advanced PLS multicomponent quantitative software.

System 730 gives you the versatility to handle a wide range of applications, including rapid-scan kinetics studies, real-time GC-IR separation and identification, TGA-IR for materials characterization, SFC-IR, and microspectroscopy.

The Nicolet 700 Series enables you to fully achieve the problem-solving power of FT-IR. Contact us for the full story.

Nicolet International Offices

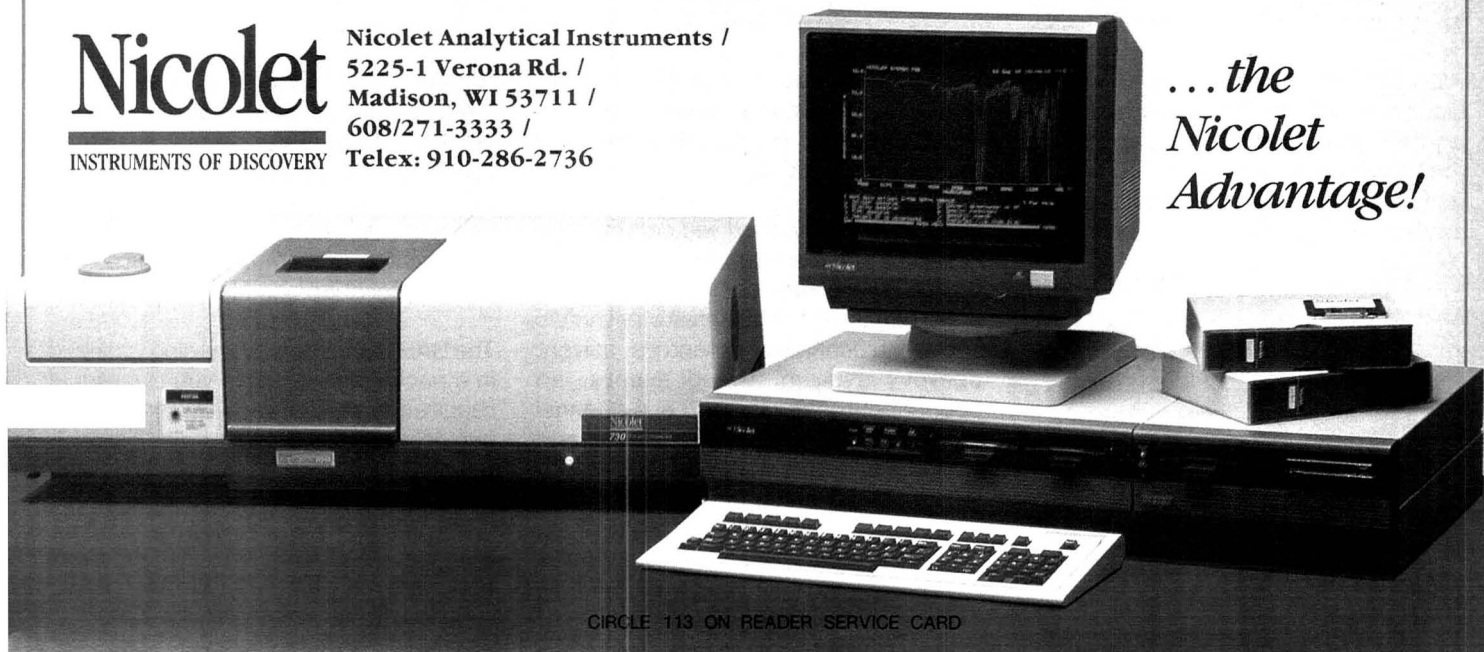
Belgium	02-762-2511	France	13-055-8300	Japan	06-863-1550	Switzerland	01-251-6133
Canada	416-625-8302	Germany	069-837001	Netherlands	03403-74754	United Kingdom	0926-494111

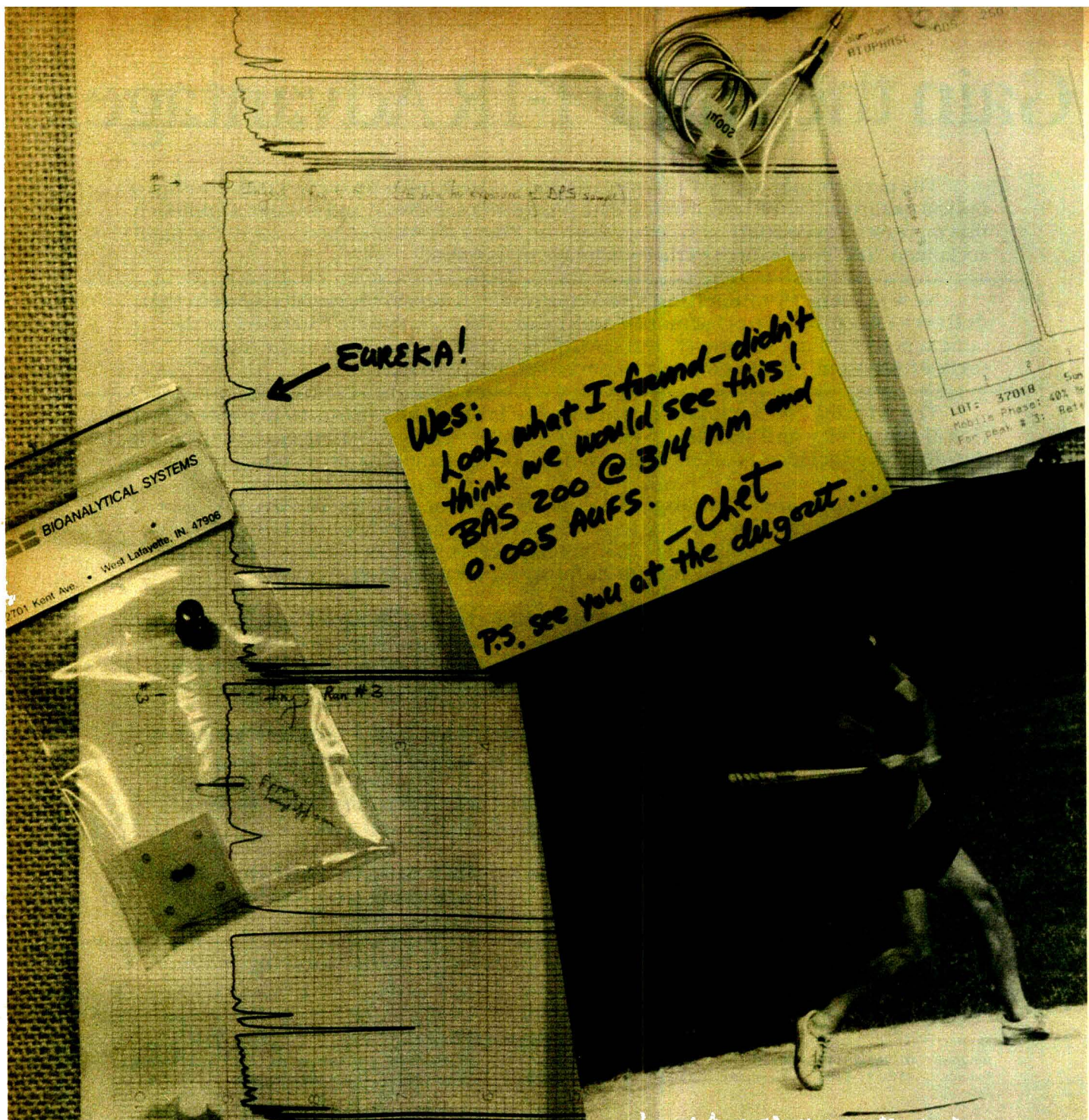
Nicolet

INSTRUMENTS OF DISCOVERY

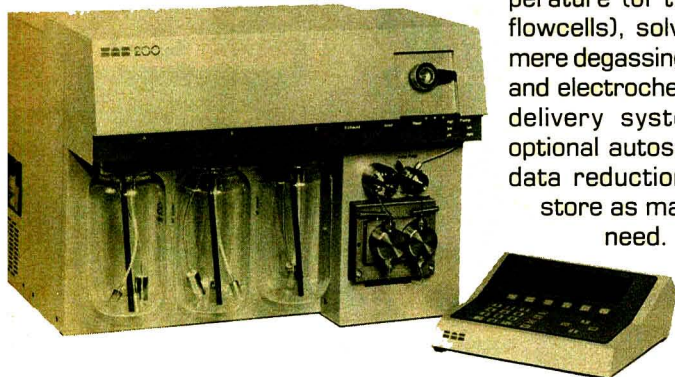
Nicolet Analytical Instruments /
5225-1 Verona Rd. /
Madison, WI 53711 /
608/271-3333 /
Telex: 910-286-2736

...the
*Nicolet
Advantage!*





We can't promise that the BAS 200 Liquid Chromatograph will make you a legend in your own time. We can promise that it will be a big hit in a busy laboratory. It's the tidiest set of answers available for trace analysis problems.



Convenience, automation, and extra performance features relieve the drudgery and let you concentrate on more important activities.

With a single keyboard you control temperature (of the injector, column and flowcells), solvent deoxygenation (not mere degassing), high sensitivity UV/Vis and electrochemical detectors, solvent delivery system, timed events, an optional autosampler and a 4-channel data reduction package. Create and store as many methods files as you need. Each one can control a gradient profile of up to 9 segments, as well as

temperature and 8 changes in electrode potential, electrode gain, wavelength and AUFS during any analytical run. Route the output from other detectors directly into the BAS 200 data reduction system and print out chromatograms or complete reports with peak integration and identification.

The BAS 200 offers everything you need in a package tailored to your individual requirements. Call for a demonstration (we promise to give you the soft pitch).



2701 Kent Ave
West Lafayette
Indiana 47906

Bioanalytical Systems, Inc. Telex: 276141
(317) 463-4527

CIRCLE 17 ON READER SERVICE CARD

Division of Analytical Chemistry Summer Internship Program

The Division of Analytical Chemistry of the American Chemical Society is seeking applicants for the 1988 summer internship program. The program is aimed at introducing talented undergraduates to modern analytical chemistry. Students chosen to participate will be employed by industrial, government, or academic analytical laboratories, where they will carry out various phases of fundamental or applied research.

Participating laboratories agree to hire one or more students during the summer. Applicants are screened and evaluated by the division's Professional Status Committee. Applications and reference letters of the most qualified students are sent to several participating laboratories. These organizations then select the individuals most suited to their needs. The Professional Status Committee acts as a broker, soliciting applications from both students and organizations. Salary and details of employment are negotiated by the organization and the undergraduate student.

To qualify for the program, students must have completed two years of college, preferably including an instrumental analysis course or its equivalent, and have an interest in analytical chemistry. Ideally, students should be attending a four-year college and be between their junior and senior years at the start of summer 1988. The Analytical Division will also accept applications from current graduate students in analytical chemistry and from college seniors graduating in 1988 who have applied to graduate school with the intention of majoring in analytical chemistry.

The deadline for receipt of student applications is Feb. 15, 1988. Additional information and application forms can be obtained from R. A. Osteryoung, Chairman, Professional Status Committee, ACS Division of Analytical Chemistry, c/o Department of Chemistry, State University of New York at Buffalo, Buffalo, N.Y. 14214.

For the 1987 program, 42 student applications were received. Some were rejected on the basis of a low grade-point average, insufficient background in analytical chemistry, or restrictive geographic requirements. Eventually, nine students were placed with eight organizations.

A list of organizations employing students, students' names, and their undergraduate institutions follows.

- Ames Laboratory**, Iowa State University, Ames, Iowa
Linda Dreifke, University of Wisconsin, Madison, Wis.
- E.I. du Pont de Nemours & Company**, Wilmington, Del.
Laural Boone, Barnard College, New York, N.Y.
- Hoechst-Roussel Pharmaceuticals**, Somerville, N.J.
Brenda Schwartz, Mary Washington College, Fredericksburg, Va.
- Inhalation Toxicology Research Institute**, Albuquerque, N.M.
Robert Averkamp, University of Wisconsin, Madison, Wis.
Kheng Lim, Coe College, Cedar Rapids, Iowa

- Phillips Petroleum**, Bartlesville, Okla.
Juliette Lantz, Loyola University, Chicago, Ill.
- U.S. Borax Research**, Anaheim, Calif.
Steven Simon, Stanford University, Stanford, Calif.
- University of Denver**, Denver, Colo.
Scott Brenkecke, Northern Arizona University, Flagstaff, Ariz.
- University of Tennessee**, Knoxville, Tenn.
Jennifer Thomas, Ohio Northern University, Ada, Ohio.

Undergraduate Awardees to Receive ANALYTICAL CHEMISTRY

The ACS Division of Analytical Chemistry has announced that 386 students have been chosen as winners of the 1987-88 undergraduate awards in analytical chemistry.

The awards are given annually to chemistry students at U.S. colleges and universities to recognize outstanding scholastic achievement and to stimulate interest in the field of analytical chemistry. Awardees will receive 16 issues of ANALYTICAL CHEMISTRY (October 1987 to May 1988) and the Division of Analytical Chemistry newsletter. The winners were selected by the chemistry departments of their respective institutions.

Instrumental Analysis Enhancement Program Funded for 1987-88

The 1987-88 academic year is the fifth year that the Society for Analytical Chemists of Pittsburgh (SACP) is sponsoring a program to provide copies of ANALYTICAL CHEMISTRY to undergraduate students enrolled in instrumental analysis courses in U.S. colleges and universities. This year, 943 subscriptions will go to 355 academic institutions participating in the program, referred to as the Enhancement Program for Students in Instrumental Analysis Courses.

The program supplies copies of ANALYTICAL CHEMISTRY for student use in undergraduate instrumentation courses. The subscriptions are intended to enrich course content and to encourage more students to continue the study of analytical chemistry at the graduate level. Professors participating in the program ensure that the issues are available to students in the laboratory. In addition, some of them assign student projects based on material in the JOURNAL.

The program begins each September and continues through February. In addition to copies of ANALYTICAL CHEMISTRY, a guide is provided that contains suggestions for the JOURNAL'S use as a supplemental teaching tool.

The program originated at the Allerton Conference in 1981 and in its first year (1982) was funded by the ACS Corporation Associates. SACP, one of the sponsors of the Pittsburgh Conference, has funded the program since 1983.

You can't replace microcoulometry. But you can make it better.



For trace sulfur and trace chlorine analyses, no other methodology offers you the sensitivity, selectivity, dynamic range and speed. And it is a standard method worldwide.

But even a proven methodology can benefit from cost and labor saving improvements. Even an established procedure can be made more reliable.

Introducing the Dohrmann MCTS-130 system for sulfur analysis and the MCTS-120 system for chlorine analysis. The fully automated microcoulometric analyzers with complete sample introduction, analysis and results reporting capabilities.

The MCTS systems can handle any sample: gas, liquid, tar-like material, solids. Choose from a variety of manual or automatic sample inlets. Want to switch between S and Cl analysis modes? It takes only minutes.

Just program the MCTS-130/120 systems for the

analysis procedure required. The MCTS will take care of the rest. You can even set your system up for unattended operation. Analysis time is less than 5 minutes per sample.

Report your results with confidence. Microprocessor control replaces manual adjustments. Automated data analysis eliminates errors in computation and results reporting.

Depend on Dohrmann.

Best of all, the MCTS-130/120 systems come with Dohrmann's worldwide sales and service network — backed by over 25 years of experience in microcoulometry and an extensive applications laboratory at our California headquarters.

Now's the time to replace your sulfur or chlorine analyzer. Contact Dohrmann today and see how much better microcoulometry can be.

Rosemount Analytical Division

DOHRMANN®

3240 Scott Boulevard
Santa Clara, CA 95054, U.S.A.
Telephone (800) 538-7708
(408) 727-6000
Telefax (408) 727-1601
Telex 346395

CIRCLE 35 ON READER SERVICE CARD

Direct Solids Elemental Analysis: Pulsed Plasma Sources

Alexander Scheeline
School of Chemical Sciences
University of Illinois
1209 W. California Ave.
Urbana, Ill. 61801

David M. Coleman
Department of Chemistry
Wayne State University
Detroit, Mich. 48202

INSTRUMENTATION

If one wishes to determine the elemental composition of a solid sample, a measurement can be made in situ or the solid can be converted to a more convenient form in which its composition can be revealed. X-ray fluorescence is the most common of the in situ methods. Because this method suffers from poor detection limits for low-atomic-number elements and usually requires samples to be extensively prepared so that effects attributable to

crystal structure are reproducible, it will not be considered further here.

An alternative approach to determining the elemental makeup of the solid sample is to dissolve the sample and then aspirate the resulting solution into an appropriate source for atomic spectroscopy. This approach suffers from such problems as contamination from solvents, conflicting requirements for dissolution of various elements, and substantial time requirements for sample preparation.

In contrast, a variety of systems can be used to directly sample solid materials. This article discusses electrical plasma sources that are capable of di-

rectly vaporizing solids for elemental analysis. Although spontaneous light emission is typically the detection method used, mass spectrometry (MS) also can be used with each of these sampling devices. Our opinion is that sampling is the crucial issue to consider. This is not to say that excitation or ionization are unimportant, but rather that representative and effective sampling of solids is less well understood and more difficult to achieve than is reproducible excitation. Two challenging steps remain: generating the ion, or its parent free atom, from the vaporized material and providing a functional relationship between the concentra-

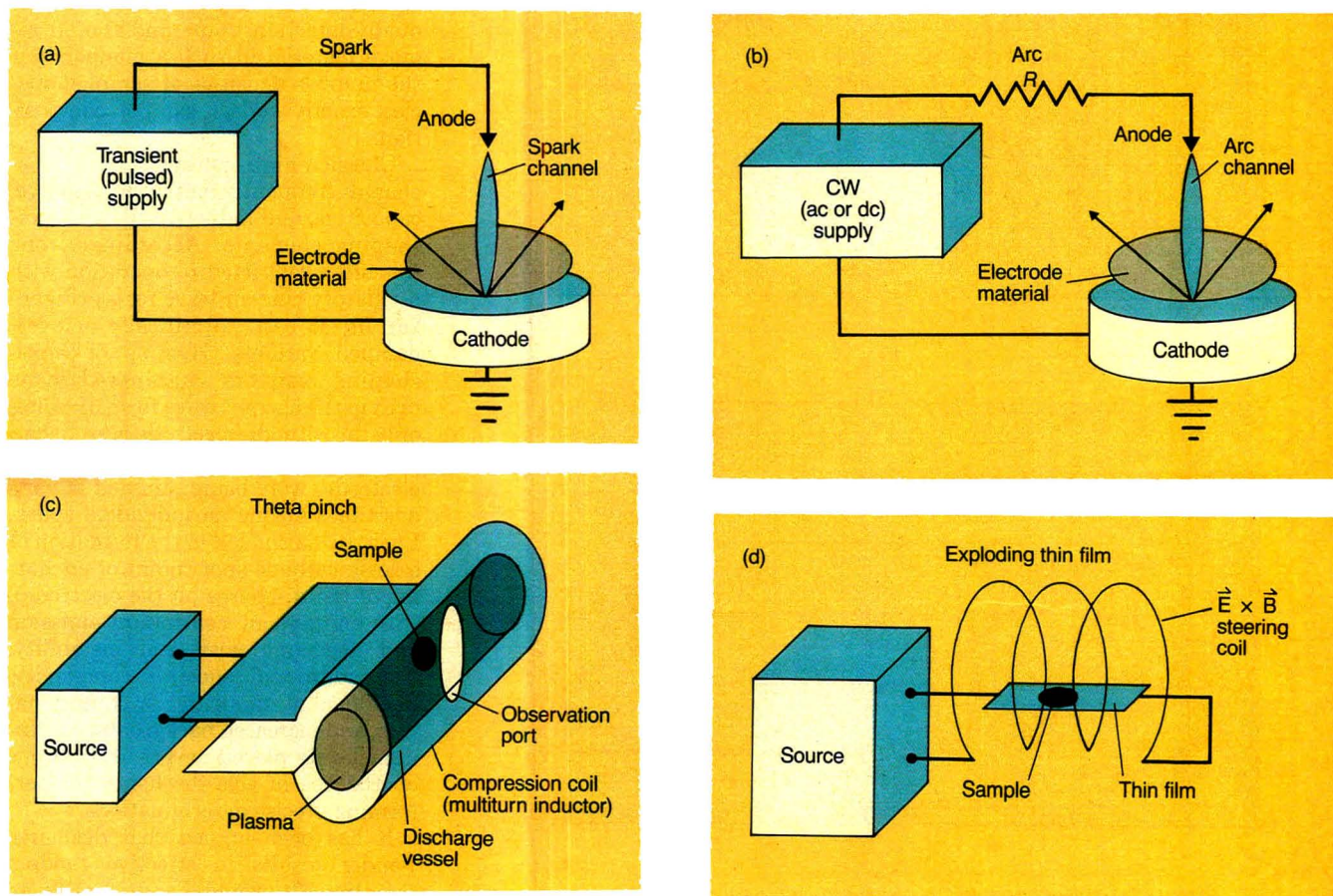


Figure 1. Stylistic representation of (a) spark, (b) ac or dc arc, (c) theta-pinch, and (d) exploding thin-film discharge systems. CW = continuous wave power supply. Arrows in (a) and (b) represent propagation of sampled material. In (d), \vec{E} = electric field, \vec{B} = magnetic field.

tion of sensed species in the sampled vapor cloud and the original solid sample.

When choosing an approach for solids analysis, one must consider dc low-power discharges as well as the transient discharge approaches that we emphasize here. Discussions of glow discharge and hollow cathode sources, observed both with emission and mass spectrometry, have recently appeared in *ANALYTICAL CHEMISTRY* (1). An interesting combination of comparatively high-pressure sampling and low-pressure emission (or absorption) has also appeared recently (2). In this system a gas jet impinges on the sample surface in a hollow cathode configuration. Laser microprobe sampling will not be discussed. In general, such sampling can be considered a subset of the separated sampling and excitation techniques to which we refer. A discussion that highlights some of the paral-

els between spark matrix effects and laser microprobe matrix effects can be found (3), and a discussion of sampling mechanisms also can be found (4). We emphasize transient discharges because of their known utility, complicated spectrophysics, and a scientifically established potential for improved performance. Technical limitations to the commercial realization of such performance continue to challenge researchers in this field of study.

Spark discharges

The transient spark (5, 6) remains an excellent tool for the ablation of material from conductive solids. Many diverse forms of this discharge are used, including low-voltage resistor-capacitor (RC) circuits with auxiliary ignited breakdown, high-voltage discharges, and less routine sources such as the high-frequency quarter-wave spark source (7).

A majority of industrially applied spark discharges are of the high-voltage type. A stylistic representation of the source is shown in Figure 1a. Even here great diversity is common; variations in current wave form and in the switch element are used to initiate the discharge. The current wave form may range from fully unidirectional to fully oscillatory. Peak currents from a few amperes to more than 1000 are not uncommon. The duration of an individual spark may range from less than one microsecond to several hundred microseconds. Repetition rates range from a few Hz to approximately 2.5 kHz. The application of a discharge with particular characteristics has tended to be based on "what worked before" rather than on any detailed understanding of discharge physics. A systematic explanation of many phenomena related to wave forms was published some 15 years ago (8).

The common denominator for various forms of the spark discharge is that a significant amount of electrical energy is imparted to the surface of interest in a short period of time and in a physically restricted area. The resultant processes (see below) are efficient in removing quantities of material from most electrode surfaces and converting that material into an appropriate "atom reservoir." Ideally, the spark should remove a sufficient amount of the electrode surface to achieve adequate detection limits and should remove material in such a manner that the number densities of sampled species exactly reflect sample composition.

Classic high-voltage spark discharges frequently employed resistive, capacitive, and inductive (RLC) wave-shaping elements. Accordingly, one was often restricted to operation with oscillatory current wave forms (Figure 2a), or, at best, to critically or overdamped variants. Heating of wave-shaping resistors guaranteed some drift in the current wave form. Because only the cathodic electrode is eroded to a significant degree, it is clear that *both* electrodes were being sampled at various times during an individual spark. Each oscillation led to the formation of a fresh cathode spot (point of anchoring of the discharge on the electrode), with consequent continuum emission and discharge positional instability. The additional spectral complexity, likelihood of impurities or contamination, and increased background continuum levels placed severe restrictions on the use of this discharge for performing precise determinations.

It has been argued that discharge wander results in effective random sampling. It would be preferable to achieve random sampling using a positionally stable discharge and moving

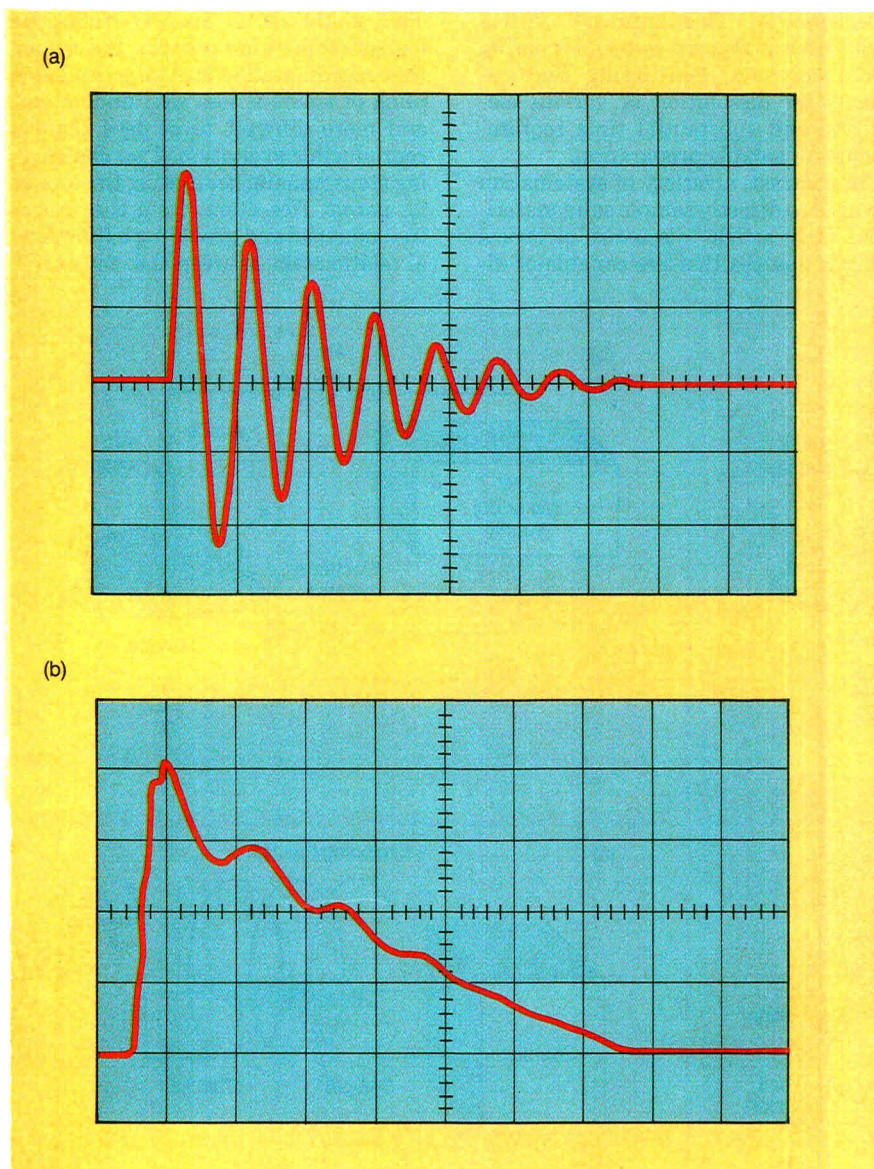
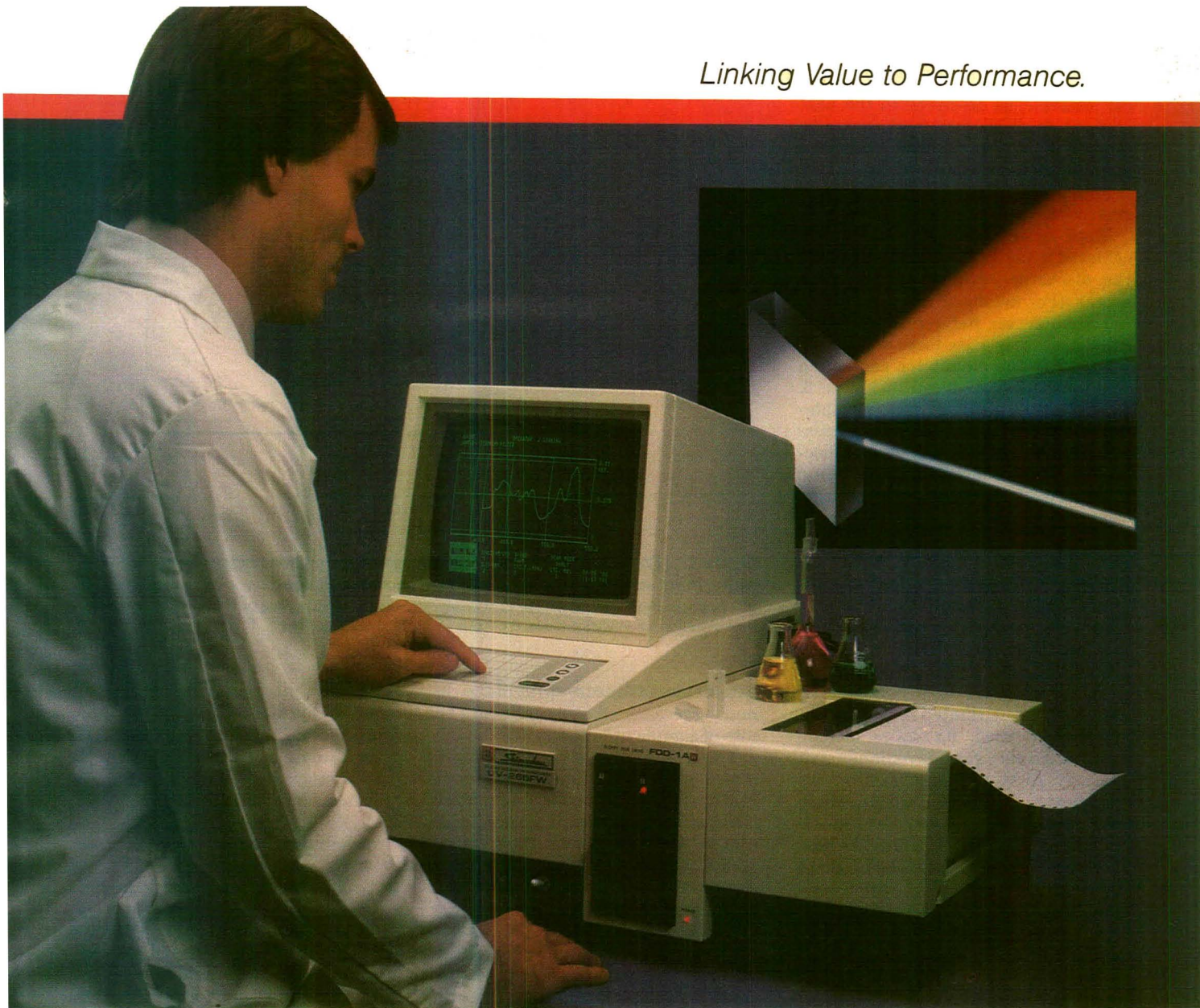


Figure 2. Typical high-voltage spark current wave forms.

(a) Fully oscillatory wave form (damped RLC oscillator). (b) Unidirectional wave form (diode-inductor-rectified).

Linking Value to Performance.



The new UV-265: a UV-VIS with a fundamental difference.

Good, basic optics. Since good spectroscopy has to start with good optics, we've put our best "back-to-basics" thinking into our advanced UV-VIS model UV-265. Fully-sealed optics and completely separate lamphouse without a mirror for *long term integrity of results*; proven symmetrical, double beam design for a flat baseline—every time; a blazed, holographic grating for increased energy throughput; and adjustable slits ensure high spectral resolution (better than 0.1nm)



Advanced software power. To fully utilize the information obtained from the UV-265 high-resolution optics and integrated recording system, we've added complete microprocessor control, comprehensive applications software, a full line of accessories and

the largest memory yet. A full 2.4 Mbyte memory lets you store and retrieve up to 75 spectra or over 200 parameters and calibration sets per disk. And, of course, it comes with IBM PC/Apple II interface.

So, compare the fundamental differences in UV-VIS instrumentation, write or call for our "Back-to-basics in UV-VIS" booklet and details on the new UV-265.

Shimadzu Scientific Instruments, Inc.
7102 Riverwood Drive, Columbia, MD 21046
(301) 381-1227



SHIMADZU

Shimadzu Corporation International Marketing Div.: Shinjuku-Mitsui Building, 1-1, Nishishinjuku 2-chome, Shinjuku-ku, Tokyo 160, Japan. Tel: Tokyo 03-346-5641 Telex: 0232-3291 SHMDT J.
Shimadzu (Europe) GmbH: Acker Strasse 111, 4000 Düsseldorf, F.R. Germany. Tel: (0211) 666371 Telex: 08586839

Circle 151 for literature. Circle 152 for a call from our representative.

the electrode rather than the spark (with consequent improvement in optical behavior, as described in the next section). An oscillatory spark cannot be used to obtain the required positional stability. Microspark discharges have been reported that permit profiling of surfaces with 5- μm spatial resolution.

More versatile wave shaping can be achieved using inductors and diodes in the discharge network of the spark source. (For details of this wave-shaping circuitry, see Reference 9). A typically achievable wave form is shown in Figure 2b. The circuit for generating this wave form is shown in Figure 3. Through the use of high-melting materials (e.g., thoriated tungsten), no emission is observed from the counter electrode. An individual unidirectional spark remains anchored at the position where the initial space charge is formed on the electrode surface. As a result, spark positional stability is greatly enhanced. Photographs of unstable oscillatory sparks and positionally stable unidirectional sparks are shown in Figures 4a and 4b, respectively.

Many of the problems associated with the classical high-voltage discharge can be attributed to the switching element used. Examples include motorized rotary gaps, UV-illuminated auxiliary gaps, and an effective but complicated switch of Bardocz, which used a mercury vapor switch tube and multiple auxiliary gaps. Under the best of operating conditions the latter could be triggered accurately at low repetition rates, but it was accompanied by high levels of radiofrequency interference (RFI). Under the worst of conditions the earlier switches could be dangerous and unpredictable. The use of hydrogen thyratrons (e.g., Reference 9) and silicon-controlled rectifiers as switching elements in recent years has resulted in sources that can be triggered with low ignition jitter (a few nanoseconds), low levels of RFI, and high repetition rates. The use of fiberoptic components for switching and data collection purposes has greatly simplified the solution of problems resulting from RFI.

Sampling efficiency (mass of sample eroded per unit energy dissipated by the spark) is very much matrix- and support gas-dependent. For example, using identical discharge conditions, sampling from an aluminum cathode is far more effective than sampling from a copper cathode. Erosion resulting from spark sampling of a pure graphite pellet is much less than erosion from the same pellet containing 20% of a high sodium coal ash. It has long been believed that, for a given matrix, sample uptake is proportional to the "coulombic integral," $\int i dt$, of the spark current wave form. Recent results contradict this theory (10). It is clear that other

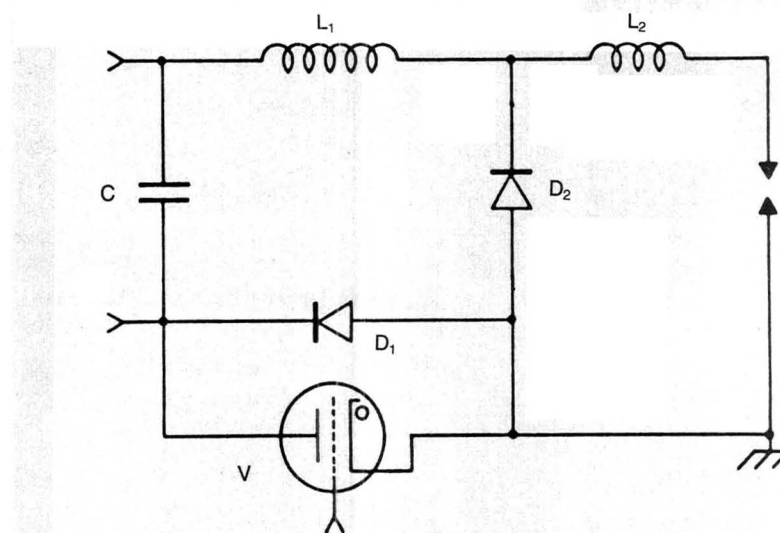


Figure 3. Spark source circuitry used to generate pulsed unidirectional discharges with current wave forms similar to those shown in Figure 2b.

V = hydrogen thyatron switch tube, C = energy storage capacitor, L₁ and L₂ = wave-shaping inductors, D₁ = thyatron commutation diode, D₂ = gap-shunt wave-shaping diode.

parameters such as the di/dt of the current wave form strongly influence the rate of sample uptake.

The case for representative sampling is also unclear. Watters and DeVoe recently attempted to collect all particulate matter generated by spark sampling of an electrode (11). This material subsequently was dissolved and analyzed by solution inductively coupled plasma (ICP) spectrometry. Based on their results, representative sampling was not substantiated. Earlier, it was demonstrated that an electrode's surface composition also differed from that of the bulk, unsparked material (12). In spite of a genuine need to unravel the above problems, accurate atomic and ionic number densities have never been measured for species sampled in a spark discharge, nor is a quantitative theory describing electrode erosion available.

When viewed in a more-or-less conventional manner (e.g., temporally and spatially integrated), even using unidirectional spark discharges, spark emission is characterized as complex, broadened, and self-absorbed and as having high background levels. The analytical consequences have tended to include poor detection limits, unusually short dynamic ranges, excessive spectral interferences, and the use of heuristic algorithms for quantitation. We mention these results not to imply that useful information is not routinely extracted, but rather to point out that the true utility of this discharge is not often fully exploited.

Raw working curves obtained from spark emission systems have a variety of shapes. Because sample uptake var-

ies with alloy composition, working curves represent a convolution of many processes. In Figure 5 a hypothetical set of alloys containing elements A and B is assayed for the concentration of element B. The relative amount of material sampled, m_s , is given by the following equation:

$$m_s = 1 - 0.9 \exp(-f_A)$$

where f_A is the mole fraction of element A. That is, A is easier to sample than B. In Figure 5a, the emission signal from B is plotted as a function of its mole fraction in the sample. One might naively suspect self-reversal of the emission line of B from such a curve, although proof of such behavior would require the use of a high-dispersion spectrometer. In fact, intensity in this inset is exactly proportional to the number of atoms of B that were vaporized from the sample. If emission from a line emitted by A were used as an internal standard, the curve shown in Figure 5b results. It has long been recognized that an internal standard, if used as in Figure 5b, must be at a constant concentration. In Figure 5b, the internal standard in fact varies in concentration.

If intensity ratio is plotted as a function of concentration ratio, the graph in Figure 5c results. The oft-sought linear working curve results, but it is unrealistic. Spark emission is subject to self-absorption and self-reversal. If the dependence of reversal on analyte concentration is the same for species A and B, and if self-absorption is neglected, a working curve of intensity ratio as a function of concentration ratio results,

...necessity for the successful chemist. To meet this need, BBN Software Products Corporation presents ChemText, the chemical document processor for the IBM personal computer. The excerpts and demonstrate some of the capabilities of ChemText.

The Ester Enolate Claisen Rearrangement of α -Amino Acid Derivatives: Approaches to Borreline

Borreline

standard procedure for the Ireland-Claisen rearrangement, using the two allylic esters of N-acyl α -amino acids are converted to the rearranged γ,δ -unsaturated esters in moderate to good yield and diastereoselectivity. Moderate variation of stereochemistry is seen using different solvents or conditions. The also applied successfully to the synthesis of highly hindered amino acids and substituted analogs.

Molecules, reactions, forms and equations are produced in ChemText's powerful drawing editors, and included in documents. The extensive set of science and mathematics symbols enable you to rapidly build complex multi-level equations in ChemText documents.

CHEMTEXT.TM CHEMISTRY NEVER LOOKED THIS GREAT.

Every chemical structure looks just right. Mathematical formulas are proportioned the way they should be. Your European colleagues' names are spelled properly, with their native alphabets. You've created the perfect document with ChemText—the first integrated image and text processor designed specifically for chemistry.

Who would have guessed this professional-looking document is so easy to produce? With ChemText, you draw the molecules, free-form, with a mouse. Click. ChemText "cleans up" the structures, normalizing bond lengths and angles. Click again. And

the images are sized to your liking, ready to be integrated with the text. You can store them for future use, too—even transfer the structures to and from other computer programs. No more plastic templates. No more cutting and pasting.

Pull-down menus guide you through ChemText's powerful capabilities, from text editing to drawing structures to file management. ChemText will even import other graphic images and integrate them into your document: Hewlett-Packard graphics, HPGLTM, RS/1[®] graphics, chromatograms, spectra... and,

of course, ChemBase[™], REACCS, MACCS-II and CHEMLAB-II images.

Now every document from your lab can reflect your great chemistry. All it takes is ChemText and your IBM[®] Personal Computer. Call Molecular Design Limited at (800) MDL-0064. In California call (415) 895-1313. Or write us at 2132 Farallon Drive, San Leandro, CA 94577.

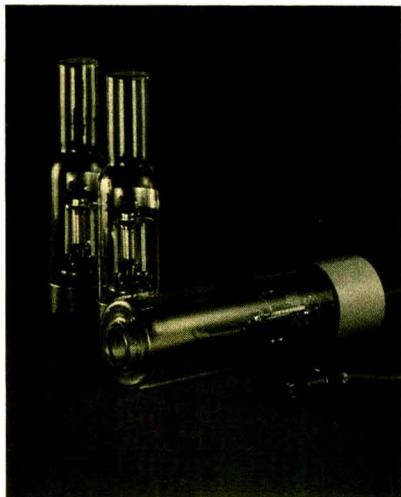


Helping You Communicate Good Chemistry.

ChemText and ChemBase are trademarks of Molecular Design Limited. IBM is a registered trademark of International Business Machines Corporation. RS/1 is a registered trademark of BBN Software Products Corporation. CHEMLAB-II is the product of Chemlab Incorporated and licensed to Molecular Design Limited for exclusive worldwide distribution. HPGL is a trademark of Hewlett-Packard Company.

CIRCLE 98 ON READER SERVICE CARD

GOOD NEWS FOR ATOMIC ABSORPTION SPECTROSCOPY



Hamamatsu Hollow Cathode Lamps are now available from major lab suppliers.

Hamamatsu single and multi-element Hollow Cathode Lamps offer superior stability, spectral purity and output intensity, even for such elements as arsenic and selenium. They are compatible with most commercial spectrophotometers, including Beckman, Zeiss and Perkin-Elmer. And best of all, they're available from your local lab supplier.

For Application Information, Call
1-800-524-0504
1-201-231-0960 in New Jersey

HAMAMATSU

HAMAMATSU CORPORATION
360 FOOTHILL ROAD
P. O. BOX 6910
BRIDGEWATER, NJ 08807
PHONE: 201/231-0960
International Offices in
Major Countries of
Europe and Asia.

© Hamamatsu Photonics, 1986

CIRCLE 67 ON READER SERVICE CARD

as shown in Figure 5d. We have seen working curves shaped as in each of the four parts of Figure 5. All have been fitted heuristically. In fact, the sets of absorption and sampling parameters that would be needed to establish working curves from first principles have never been measured. The heterogeneity of the discharge in space and time complicates derivation of such parameters.

Importance of temporal and spatial resolution

It has been known since at least 1909 (see Reference 13, which cites a reference from 1862!) that spark discharges display spatial and temporal heterogeneity. When the discharge channel anchors to the cathodic electrode, sample vaporization and emission from analyte ions commence. The plume of vapor travels across the spark gap at a velocity related to the boiling point of the material; the velocity is about $1 \text{ mm}/\mu\text{s}$. The plume also expands radially; neutral atom emission comes from spatial regions outside the current-conducting channel. Not only does the channel excite emission mainly from ionic species, but the arrival of the excitation front from the cathode is necessary before substantial support gas ionic line emission commences.

The brightest region of continuum emission is adjacent to the cathode in the space charge that develops above the electrode surface. In this extremely complex system, the following general-

izations appear to hold: Spectral complexity is highest near the discharge axis early in time, continuum appears adjacent to the electrode surface only during times when the electrode is becoming more cathodic (i.e., current is increasing in magnitude), and optimal signal-to-background ratios can be obtained by observing emission away from the discharge axis during times when current is decreasing or has ceased. Neutral atom emission continues for a significant period after current has died away completely.

To permit spatial filtering for removal of continuum radiation, the spark must be positionally stable. Stability is most readily accomplished when there is a well-defined boundary between an argon support gas channel and a surrounding atmosphere containing nitrogen (air works well). Unfortunately, diatomic molecular oxide bands appear when oxygen is present to a significant extent, so that most commercial instruments generate sparks in pure argon atmospheres. The degraded positional stability that results, in conjunction with a tradition of using highly unstable discharges to produce "good random sampling," has prevented the use of spatial resolution in commercial instruments to improve signal-to-background ratios.

Not only is emission a complex function of time and space during a single spark, but patterns of emission evolve during a train of sparks (14). If any analyte emission line is chosen for ob-

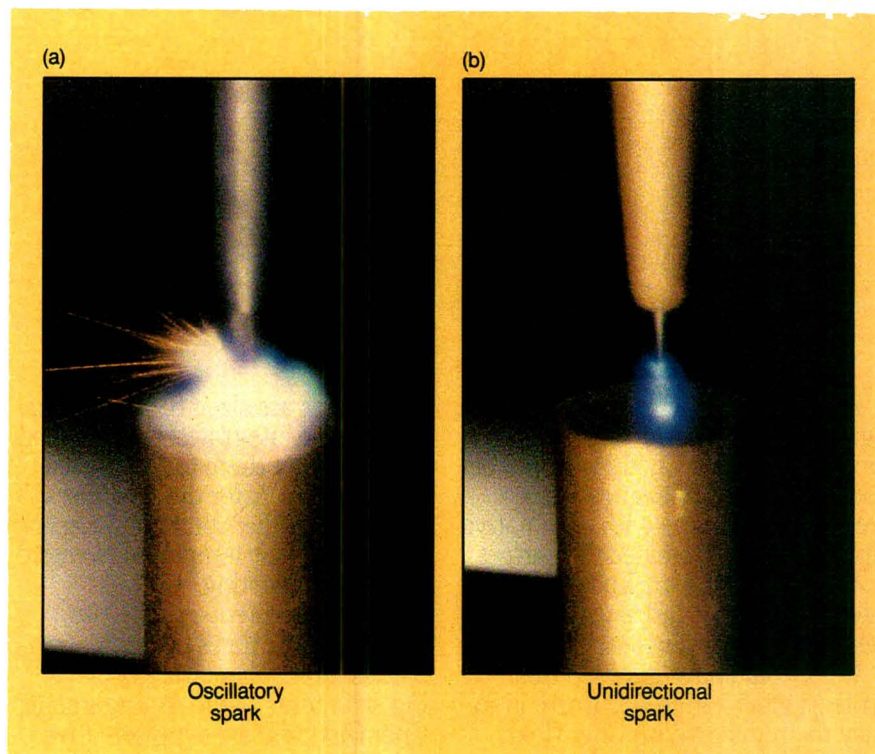


Figure 4. Time-integrated photographs of stable and unstable spark discharges.

(a) A low repetition rate, oscillatory wave form spark is ignited between an aluminum sample and a carbon counter electrode in air. (b) A high repetition rate, low-current, unidirectional spark is ignited. An argon flow jet and thoriated tungsten anode help assure positional stability.



Finnigan MAT TSQ[®] 70 Quadrupole MS/MS: A Generation Ahead

Ahead in high mass performance by a quadrupole MS/MS. FAB ionization with the TSQ 70 yields unsurpassed resolution of the molecular ion cluster from biomolecules like bovine glucagon (MW 3480). Get the facts in Technical Report #601: "High Mass Analysis Using FAB Ionization with the TSQ 70".

Ahead in combining the specificity of MS/MS with the sensitivity to measure dioxins at low picogram levels in complex matrices (Technical Report #602: "MS/MS Analysis of Dioxins").

Ahead in Instrument Control Language (ICL)* so advanced, it makes real-time data-dependent decisions that provide maximum information from a minimum of sample (Technical Report #603: "Data-Dependent Instrument Control on the Finnigan MAT TSQ 70").

Others *tell* you they have a new generation of MS/MS performance. We welcome the chance to *prove* what the TSQ 70 can do for you. Look at the data in these technical reports, and ask for a demonstration. See for yourself why the TSQ 70 is a generation ahead, again.

Mass spectrometry:
We make the difference.

Circle 50 for Literature.

Circle 51 for a Representative to call.



U.S.A., 355 River Oaks Parkway, San Jose, CA 95134. (408) 433-4800
Benelux, Landjuweel 7, 3905 PE Veenendaal. 08385 27266
France, 69, rue de Paris, F-91400 Orsay. (1) 69 28 52 53
Italy, Via Valadier, 37B, 00193 Rome. (06) 316000
Japan, Shijozaki Bldg. 27-1 Hirakawa-cho, Chiyoda-ku, Tokyo 102. (03) 221-100
Sweden, Årstadsvägen 1C, 117 43 Stockholm. (08) 190480
U.K., Paradise, Hemel Hempstead, Herts HP2 4TG. (0442) 233555
W. Germany, Postfach 14 40 62, D-2800 Bremen 14. (0421) 54 93-0

*patent applied for

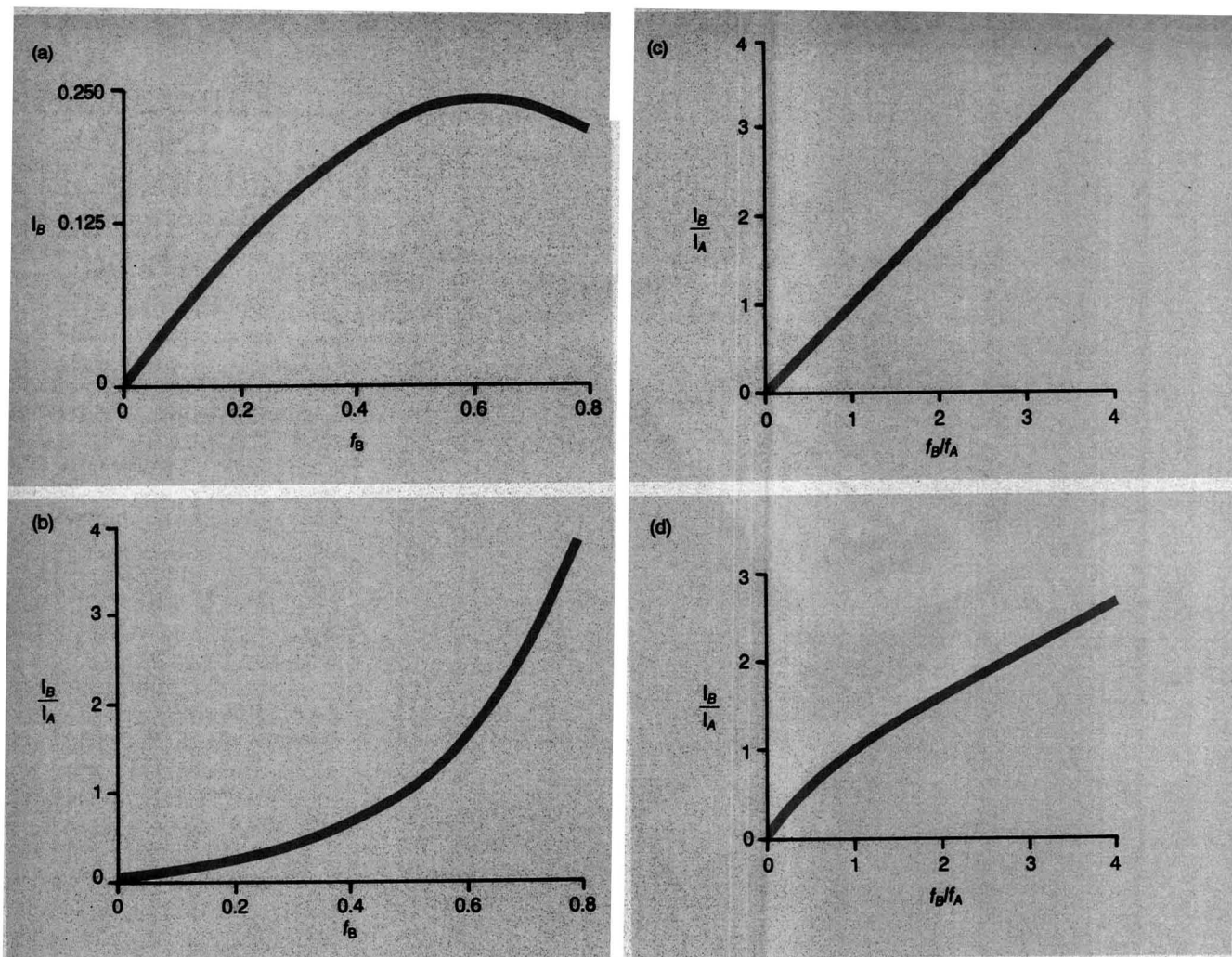


Figure 5. Typical spark working curves.

(a) Raw emission as a function of concentration. (b) Intensity ratio as a function of concentration. (c) Intensity ratio as a function of concentration ratio. (d) Same as (c), but including effects of self-reversal. (Reproduced with permission from Reference 6.)

servation, its intensity evolution from spark to spark will be a function of whether the electrode is stationary or rotating, whether the line is from an ionic or neutral species, and the bulk composition of the electrode. A unifying concept is that the spark samples both by sputtering and by bulk heating. Once electrode material melts, various elements can be differentially dissolved at the liquid-solid interface and thus preferentially sampled. The molten material resolidifies between discharges so that there is an aging effect when sparking continuously to a single point on the electrode surface. In addition, microheterogeneity in the electrode can be reflected in fluctuations from spark to spark in the elemental composition of sampled material (15).

Self-reversal can be seen for some resonance lines in the spark (magnesium ion is subject to particularly spectacular reversal). The absorbing cloud of material, which is thermally shaped and magnetically modified by interaction of the trajectories of ions with the field produced by the spark's discharge current, has toroidal geometry and

lasts for approximately 1 ms after discharge triggering. In many ways it is the intimacy of integrating the sampling and the excitation processes in a spark discharge that contributes to a lack of understanding of fundamental mechanisms and analytical complications.

Several researchers have concluded that, by segregating these steps using sequential samplers and excitors, each process may be independently understood and optimized. A brief review of these approaches is given in Reference 16. In this work a spark was used as a sampling device, and the resultant postdischarge torus was re-excited with a burst of radiofrequency energy (2.0 kW at 200 MHz). When compared with direct spark emission, spectral features resulting from this re-excitation process were simplified, possessed narrow line widths, were free from observable background continuum, and showed no evidence of self-reversal or self-absorption. Photographic detection limits approaching 10 ppb were reported for some elements. Working curves showing as many as four dec-

ades of linearity also were observed. Several workers have used a high-voltage spark to sample an electrode before transporting the effluent to a conventional ICP discharge (e.g., Reference 17). Again, significant improvements in detection limits and working curve linearity were evident. Commercial instruments based on the latter idea are now available.

Effect of sample matrix

Matrix effects are perceived differences between the signal obtained from a specific concentration of an analyte element and that expected, based on the behavior of some innocuous reference material. There is a substantial lore stating that sparks and arcs are subject to complex matrix effects. It is uncommon for matrix effects to be used for analytical benefit, despite the fact that there must be an algorithmic dependence of analytical signal on sample composition.

Some effects are well characterized. For example, it is known that Mn distills from steel furnace melts, so that the ratio of concentration of Mn in an



Demand high sensitivity at high mass. Demand the MAT 90.

When you need dynamic analysis of biomolecules. When you want to quantitate trace dioxin in complex matrices. When your analytical problem demands new capabilities in magnetic-sector mass spectrometry...

Only Finnigan MAT delivers. The MAT 90's novel ion optics and Instrument Control Language (ICL™) combine mass spectrometer performance with real-time, data-dependent optimization. The result: more useful information with less sample and less effort.

For example, the MAT 90 provides the necessary resolution and sensitivity with FAB to measure the molecular ion region of eglin-C, a 70-amino acid recombinant peptide (MW 8128). Automated peptide digest monitoring is now possible, with the continuous flow FAB probe (BioProbe™).

Demand a lower detection level than commercially available with any other mass spectrometer. Even at a resolution of 10,000, the MAT 90 can measure as little as 30 fg of 1,2,3,4-TCDD with a signal-to-noise ratio of better than 10 to 1.

Get the facts in Finnigan MAT application reports. And imagine what the MAT 90 can do in your laboratory. After all, shouldn't your next mass spectrometer meet your new analytical demands?

Mass spectrometry:
We make the difference.

Circle 52 for Literature.
Circle 53 for a Representative to call.



U.S.A., 355 River Oaks Parkway, San Jose, CA 95134, (408) 433-4800
Benelux, Landjuweel 7, 3905 PE Veenendaal, 08385 27266
France, 69, rue de Paris, F-91400 Orsay, (1) 69 28 52 53
Italy, Via Valadier, 37B, 00193 Rome, (06) 6878057
Japan, Shijozaki Bldg, 2-7-1 Hirakawa-cho, Chiyoda-ku, Tokyo 102, (03) 221 1001
Sweden, Årstadängsvägen 1C, 1117 43 Stockholm, (08) 190480
U.K., Paradise, Hemel Hempstead, Herts HP2 4TG, (0442) 233555
W. Germany, Postfach 14 40 62, D-2800 Bremen 14, (0421) 54 93-0

ICL and BioProbe are trademarks of Finnigan MAT.

aliquot to the concentration in the melt is time-dependent. This effect was recently rediscovered by a group investigating the use of a laser microprobe for *in situ* analysis! Resulturized steels have high sulfur concentrations only near the surface, so that slugs of such steels are highly heterogeneous. That a spark reports substantial fluctuations in sulfur signals is a function of the sample, not the analysis method.

Matrix variations that are a function of discharge behavior include self-reversal of major constituent emission lines and background shifts as major constituents change. These variations can be overcome largely by using data reduction algorithms that recognize the presence of the effects. As noted previously, spark working curves are generally nonlinear. This is not because of any mystical property of sparks. A spark exciting a solution sprayed into the spark produces emission intensity that is proportional to solute concentration. Spark-eroded analyte transported to an ICP results in emission that is proportional to analyte concentration in the virgin bulk sample. Only when both sampling and emission are observed simultaneously from the same spark is nonlinearity pronounced.

AC and DC arcs

Although not strictly a pulsed discharge, an arc (Figure 1b) may be regarded as a discharge system with a duty cycle approaching 100%. In many ways the behavior and chemistry of "arc-like" and "spark-like" discharges have sufficient common features to merit brief inclusion here. Although there has been some interest in microarc sampling of solution residues and the generation of radiofrequency arcs to directly aspirate solids into the ICP, there is little research activity on arc discharges going on in North America. Substantial research is being done in the rest of the world, however.

Two characteristics of arcs complicate their use: discharge wander and fractional distillation. Wander of the arc anode spot over the sample results in flicker noise in the analyte signal. Such noise must be integrated (most commonly with a photographic emulsion, although electronic approaches are feasible). Various combinations of magnetic fields and gas flow have somewhat successfully tamed this problem. Because bulk heating is the main means of sample volatilization in the arc, distillation of components rather than uniform sampling of the analyte material results. This result can be helpful for performing qualitative analysis, but it presents problems when performing quantitative analysis.

The time-temperature profile of the arc spot is dependent on the composi-

tion of the anode. Although one can compensate for this by recording spectra throughout the "burn" (period of sample excitation) and controlling the evolution through use of "spectroscopic buffers" (diluent to stabilize temperature at the buffer's boiling point), precision is limited. A concerted effort to record the time evolution of emission electronically and then to interpret the spectra based on the electrode temperature evolution as measured for a particular sample might well produce more precise results than those commonly obtained. Numerous papers have presented equations explaining the evolution of spectra and mass transport of analyte through the arc gap; these techniques have not yet been used on line.

Exploding conductors

R. D. Sacks and co-workers have developed methods for performing elemental analysis on powder samples for many years (18). Currently the most effective means for exciting refractory solids appears to be the use of an exploding thin film in a crossed magnetic field (Figure 1c). The powder is deposited on a film of gold, silver, or aluminum that is a few micrometers thick. Several kiloamperes are passed through the film, which is vaporized.

By appropriate use of magnetic fields, the thin-film plasma is constrained to be close to the plane of its origin, and particulates that initially were on the film are vaporized. Time resolution results in reproducible signals that are independent of particle size if the particulates are less than 30 μm in diameter. The shape of the current wave form can be optimized using passive components to separate the times of continuum emission from line emission. Reasonably concentrated solutions also can be analyzed by depositing a few microliters of solution on the thin film, then drying prior to detonation. In our opinion, the use of exploding conductors for elemental analysis is one of two as yet unexploited spectrochemical techniques most deserving of commercialization. (The other technique is the use of microwave discharges for gas and liquid elemental analysis.)

Imploding plasmas

The success of exploding conductors as atom reservoirs inspired two new approaches to the analysis of nonconducting and high-boiling solids. In both cases, the central idea is that an adiabatically compressed plasma is heated, so that high-boiling samples should be vaporized if a sufficiently compressed plasma interacts with the sample of interest.

In one case, a diffuse glow discharge is compressed with a pulsed magnetic

field in a solenoidal or theta-pinch configuration (Figure 1d) (19). Erosion of several micrograms per discharge of a variety of materials including aluminum oxide, boron nitride, and stainless steel has been demonstrated. The usual time resolution techniques are needed for freedom from continuum and line-broadening problems. In the other case, a thin film is imploded rather than exploded. A powder sample is distributed on the inside of a cylindrical thin film, and a coaxial discharge or Z-pinch plasma is initiated through the thin film (20). Early data indicate that such discharges are magnificent atomizers, but the intense continuum and line reversal produced have hampered design of convenient analytical methods. Although both theta- and Z-pinch plasmas show promise as solids samplers, they are not yet sufficiently developed for routine application.

Detection issues

A majority of commercial instruments are of the "direct reader" type (polychromator with photoelectric detection). These may be either simultaneous or sequential in nature. A variety of optical configurations, including the Czerny-Turner, Eagle, and Paschen-Runge, have been used. A majority of contemporary instruments are based on the Paschen mount and are built in massive (but stable) vacuum chambers.

In a simultaneous instrument, a fixed stationary entrance slit is used. A large number of exit slits and photomultiplier tube assemblies are precisely located at appropriate wavelength positions on the focal plane. Various approaches are used to individually "tweak" each spectral line into optimum alignment, including rotation of a quartz refractor plate in front of each exit slit. Instruments with 50–60 detection channels have been manufactured. Unfortunately, because spectral lines must be chosen in advance of instrument manufacture, and because crowded mechanical "realities" along the focal plane may restrict line choice, many compromises go into instrument design. Alignment of these instruments is a tedious art; realignment in the field by most operators is not possible.

Many manufacturers attempt to increase the flexibility of their instruments by attaching a small, stand-alone scanning monochromator to simultaneously observe the discharge. In practice, these are low-resolution air path appendages that rarely deliver detection limits or analytical performance approaching that of the polychromator. These instruments are expensive, but they remain the industrial workhorses in situations requiring repetitive analysis of similar samples.

Given the well-documented charac-

UNLOCK YOUR OPTIONS

WITH THE HAMAMATSU
PHOTONIC MULTICHANNEL
ANALYZER SYSTEM.



There's no longer any reason to lock yourself in with a dedicated photodiode array system. Because now there's a flexible tool that keeps pace with the latest technologies and delivers so much more.

The Hamamatsu PMA System consists of a Controller/Readout Console, an optional Ultrafast Gate, one of several interchangeable detector heads and an optional, modular image intensifier.

The Basic PMA permits multichannel (512 or 1024) spectral measurements of continuous phenomena. You can add our modular Image

Intensifier when your signal level gets too low. The Ultrafast PMA lets you capture transient spectra with an incredible 80 picosecond gate time, or analyze kinetic events with 10 picosecond resolution. The

Photon-Counting PMA is sensitive enough to detect a single photoelectron.

You can acquire the whole PMA System now. Or add components as your research needs change, and as we continue to advance detector technology. Best of all, you're buying Hamamatsu — a name that means the ultimate in quality, technology and service. For all the key facts, contact Hamamatsu Photonic Systems.



 **BREAKING OPTICAL
MEASUREMENT BARRIERS.**
HAMAMATSU
PHOTONIC SYSTEMS

360 Foothill Road, P.O. Box 6910, Bridgewater, NJ 08807, Phone: (201) 231-1116

teristics of photomultiplier tubes (especially dark current, dynamic range, and sensitivity) and the observed intensities of spectral lines, as many as three channels can be required for observance of a single element in different matrix-concentration situations. This requirement adds to the cost of the instrument and to operational complexity.

Recently much emphasis has been placed on so-called sequential instruments. Generally one optical element (the grating, a mirror, or a refractor plate) is caused to rotate such that spectral lines of interest are rapidly scanned across a single exit slit and detector. Appropriate means (optical encoding or laser diffraction) are used to ensure accurate wavelength positioning of each element of interest. Such instruments are far less expensive than their polychromator counterparts and can provide increased flexibility for analysis of nonroutine samples. Many of the advantages of rapid simultaneous determination are sacrificed using this approach. Ultimate performance remains an oft-debated issue. The patterned and random time evolution of emission characteristics from spark to spark suggest that simultaneous detection is preferable from a fundamental standpoint. Certainly for single-shot devices such as the various pinch discharges, simultaneous detection is essential.

A most auspicious development is the availability of two-dimensional electronic array detectors such as charge-coupled device arrays (CCDs) and charge injection device arrays (CIDs). These array detectors promise to provide linear dynamic range for any particular line of at least 3 orders of magnitude, low background, line selection after data collection, and cross-checking for line overlaps on every sample after data collection. With the addition of time gating, these devices appear to be nearly ideal spectrometric detectors (21). They overcome the nonlinearity, poor dynamic range, and slow readout of photographic emulsions while preserving the full spectral coverage that has remained the province of emulsions and scanning spectrometers. Capital costs are within an order of magnitude of those of a conventional direct reader. We anticipate that the availability of less expensive and more refined array detectors in commercial instruments will sound the death knell of the multiphotomultiplier direct reader.

We suspect that photographic photometry will survive, however, because the typical emulsion still has a spatial bandwidth that is orders of magnitude higher than that of any existing CCD. For utterly unknown matrices, the photographic emulsion provides a sig-

nificant window for the trained spectroscopist's eye. The CCD has sufficient resolution in conjunction with appropriate computing hardware to provide multielement determinations on reasonably complex materials. Only when backgrounds are clean and predictable and interferences are readily anticipated does the common direct reader serve adequately for analysis.

MS has been used for many decades to detect atoms sampled from solids. Spark source MS is a semiclassical method for determining elemental and isotopic composition of solids. Most such instruments work with the sample in vacuum. There have been a number of recent publications in this area by M. Bursey and colleagues. Atmospheric pressure sampling and excitation is uncommon. Spark sampling followed by ICP excitation and mass spectral detection would be workable with current commercial apparatus, although no reports have yet appeared in the literature. Harrison's work with glow discharges has already been cited. In short, there is little reason to doubt the efficacy of using MS for elemental analysis of solids. The lack of common use may say more about the sociological roots of atomic spectroscopists and the cost of vacuum equipment than it does about analytical utility.

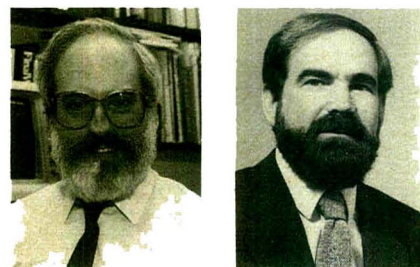
In conclusion, many exciting innovations, both instrumental and conceptual, in connection with pulsed plasma discharges have occurred in numerous research laboratories in recent years. Several of these have clear practical analytical ramifications. It is sad that spectrochemical instrument manufacturers have so steadfastly avoided capitalizing on this research. The solution to many classical discharge problems is within reach. The potential for useful, new, and innovative commercial analytical instrumentation is indeed high.

References

- (1) Harrison, W. W.; Hess, K. R.; Marcus, R. K.; King, F. L. *Anal. Chem.* **1986**, *58*(2), 341 A-356 A.
- (2) Bernhard, A. E.; Piepmeier, E. H.; Kim, H. J. Papers 130 and 415. Presented at FACSS 13th Annual Meeting, St. Louis, Mo., October 1986.
- (3) Carr, J. W.; Horlick, G. *Spectrochim. Acta, Part B* **1982**, *37*, 1.
- (4) Beenen, G. J.; Piepmeier, E. H. *Appl. Spectrosc.* **1984**, *38*, 851.
- (5) Walters, J. P. *Science* **1977**, *198*, 78.
- (6) Scheeline, A. *Prog. Anal. At. Spectrosc.* **1984**, *7*, 21.
- (7) Rentner, J. R.; Uchida, T.; Walters, J. P. *Spectrochim. Acta, Part B* **1977**, *32*, 125.
- (8) Walters, J. P. *Appl. Spectrosc.* **1977**, *26*, 17.
- (9) Coleman, D. M.; Walters, J. P. *Spectrochim. Acta, Part B* **1976**, *31*, 547.
- (10) Coleman, D. M.; Sainz, M. A. Wayne State University, unpublished results.
- (11) Watters, R. L., Jr.; DeVoe, J. R., National Bureau of Standards, personal communication.

- (12) Brewer, S. W.; Walters, J. P. *Anal. Chem.* **1969**, *41*, 1980.
- (13) Milner, S. R. *Philos. Trans. R. Soc. London Ser. A* **1909**, *209*, 71.
- (14) Ekimoff, D.; Walters, J. P. *Anal. Chem.* **1981**, *52*, 1644.
- (15) Olesik, J. W.; Walters, J. P. *Appl. Spectrosc.* **1983**, *37*, 105.
- (16) Coleman, D. M.; Sainz, M. A.; Butler, H. T. *Anal. Chem.* **1980**, *52*, 746.
- (17) Beaty, J. S.; Belmore, R. J. *J. Test. Eval.* **1984**, *12*, 212.
- (18) Sacks, R. D.; Goldberg, J. M.; Collins, R. J.; Suh, S. Y. *Prog. Anal. At. Spectrosc.* **1982**, *5*, 111.
- (19) White, J. S.; Scheeline, A. *Anal. Chem.* **1987**, *59*, 305.
- (20) Carney, K. M.; Goldberg, J. M. *Anal. Chem.* **1986**, *58*, 3108.
- (21) Sims, G. R.; Denton, M. B. In *Multi-channel Image Detectors*; Talmi, Y., Ed.; ACS Symposium Series 236; American Chemical Society: Washington, D.C., **1983**; Vol. 2, p. 117.

Much of the work summarized here was originally supported by the National Science Foundation and the Office of Basic Energy Sciences, U.S. Department of Energy.



Alexander Scheeline (l.) is an associate professor of chemistry at the School of Chemical Sciences, University of Illinois at Urbana-Champaign. He received his B.S. in chemistry at Michigan State University in 1974 and his Ph.D. in chemistry at the University of Wisconsin-Madison in 1978. He was a postdoctoral fellow at the National Bureau of Standards and an assistant professor at the University of Iowa prior to accepting his current position. His research interests are in atomic and plasma spectroscopy and in nonlinear dynamics.

David M. Coleman is an associate professor of chemistry at Wayne State University, Detroit, Mich. He received his B.S. in chemistry at Southern Illinois University in 1970 and his Ph.D. in chemistry at the University of Wisconsin-Madison in 1976. He was a postdoctoral fellow at Wisconsin prior to assuming his current position. His research interests are in atomic spectroscopy, specifically in the phenomenological separation of sampling and excitation, and occasionally in the application of spectroscopy to the arts.

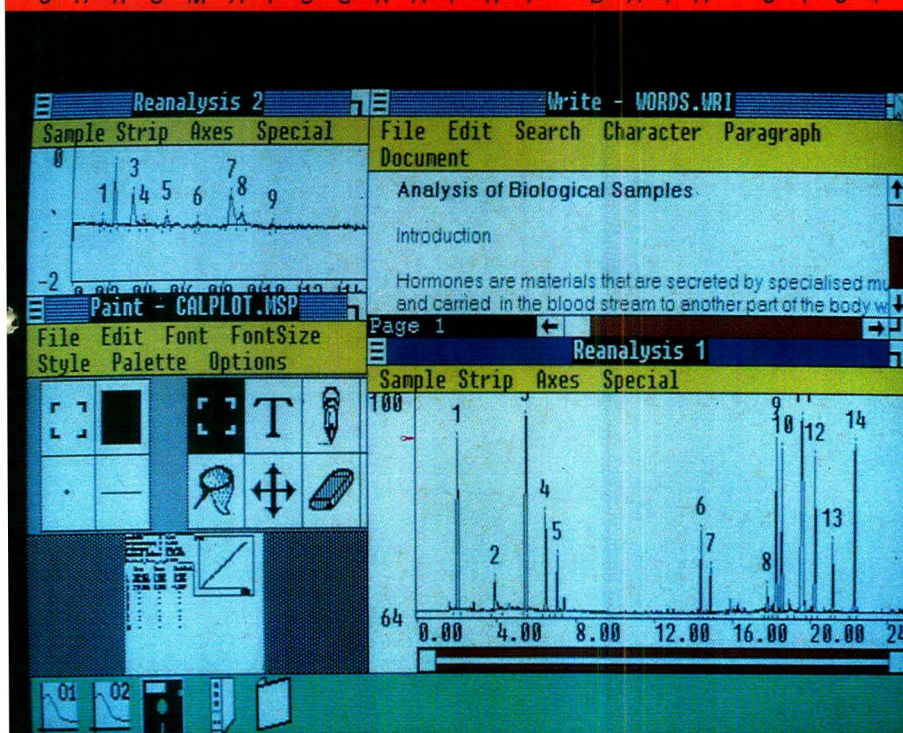
Both authors share a (not so) common mentor (John Walters), a passion for computer communication, an interest in music of other eras, and a predilection to invest inordinate amounts of time in organizing the annual FACSS meeting.



PHILIPS

PC, LC, GC integrated!

CHROMATOGRAPHY DATA SYSTEM



Simplified

set-up using mouse and windows. Operation couldn't be easier.

Logical

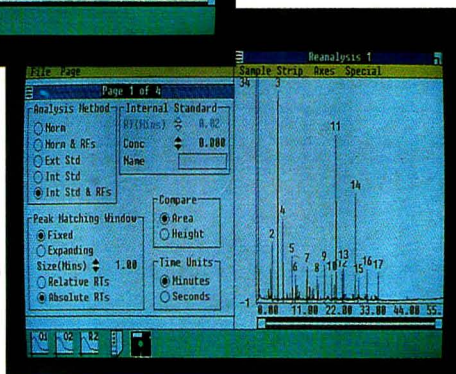
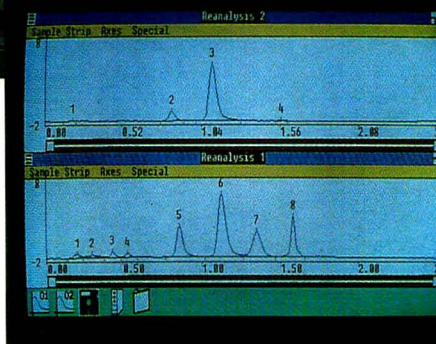
response to parameter changes inspires confidence. Gives the best in integration.

Interactive

software gives extra power to the analyst. Injects new professionalism with word processing, spreadsheets and custom reporting.

Chromatography

comes first! Unrivalled high resolution data collection from up to 6 on-line channels.



The new PU6000 Chromatography Data System.

More than just another data station running on a PC.
It's dedicated to get the results you need... FAST!

Write or 'phone now for details: Philips Analytical,
Pye Unicam Ltd, York Street, Cambridge, Great Britain CB1 2PX. Tel: (0223) 358866.

Bigger ideas for better analysis.

YOUR PROBLEM	THE AMICON SOLUTION		COMBINED RESULTS	AMICON MATREX PRICE 60Å MATERIAL (GERMAN MARKS) (1987 ave. European prices. Discounts available for bulk quantities)	
				DM/kg (100 kg order)	DM/kg (> 1 ton order)
Resolution \propto	Matrex Silica μm	Amicon N-Pack Column mm	Efficiency Obtained N (TP/m)		
1.05	15	50 x 500 300 x 500	27700 25800	950	850
1.10	20	50 x 500 300 x 500	19000 18000	200	180
1.15	35-70	50 x 500 300 x 500	10500 10000	29	24
1.20	70-200	50 x 500 300 x 500	5000 4800	21	15

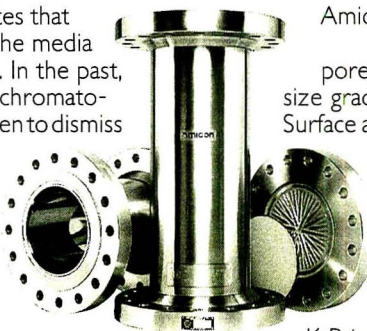
WHEN YOU START WITH AMICON CHROMATOGRAPHY TECHNOLOGY YOU STOP RELATING EFFICIENCY TO PARTICLE SIZE AND START SAVING MONEY.

In liquid chromatography, the equation states that the greater the efficiency required, the smaller the media particle size and, therefore, the greater the cost. In the past, this has led many people to consider preparative chromatography as an expensive separation technique or even to dismiss it completely.

New AMICON* technology is changing all that, by allowing a larger particle size to be used to achieve the required efficiency. This not only opens up a new era in efficiency vs. economy, but also makes the purity, speed and performance of chromatography a viable alternative for numerous new applications.

It starts with the new Amicon N-Pack packing/unpacking system. Used in conjunction with Amicon stainless steel chromatography columns, it eliminates the problem of uneven column packing which dictates the need to use small particle sizes to achieve high efficiency. The N-Pack's packing speed creates a high velocity in the exiting solvent stream, improving the packing density of particles at the bottom of the bed and ensuring uniform and homogenous packing throughout the column. Immediately, larger particle sizes can be used and costs reduced.

However, Amicon chromatography efficiency with economy is not just the sum of one new technology. It also covers the quality and cost of



Amicon MATREX™ silica packings themselves.

Firstly, rigid control of chemical purity, surface area, pore volume, pore size distribution and selective particle size grading ensures consistently reproducible characteristics. Surface area and pore volume are controlled to within $\pm 2\%$ within lots and batch-to-batch reproducibility is maintained to within $\pm 5\%$.

Secondly, as a member of the W. R. Grace & Co. group of companies, Amicon is the world's largest single source of silica media. As well as the ability to supply a comprehensive range, that means obvious economies, especially for bulk buyers. Add to that the K-Prime chromatograph, and you can even enjoy all those Amicon advantages in a single automated package.

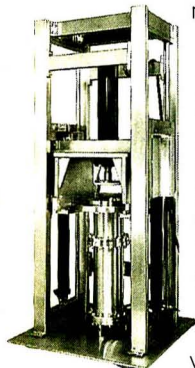
But if you're already using chromatography, don't take our word for it. Check the efficiency vs. cost figures above against your own. Alternatively, if you're in pharmaceuticals, biotechnology or fine chemicals recovery and have been hesitant about the economic viability of chromatography in the past, have a word with our international applications team by ringing one of the offices below.

We only do it if we do it better.

amicon®

Division of W. R. Grace & Co.

AMICON® and MATREX™ are registered trademarks of W. R. Grace & Co.



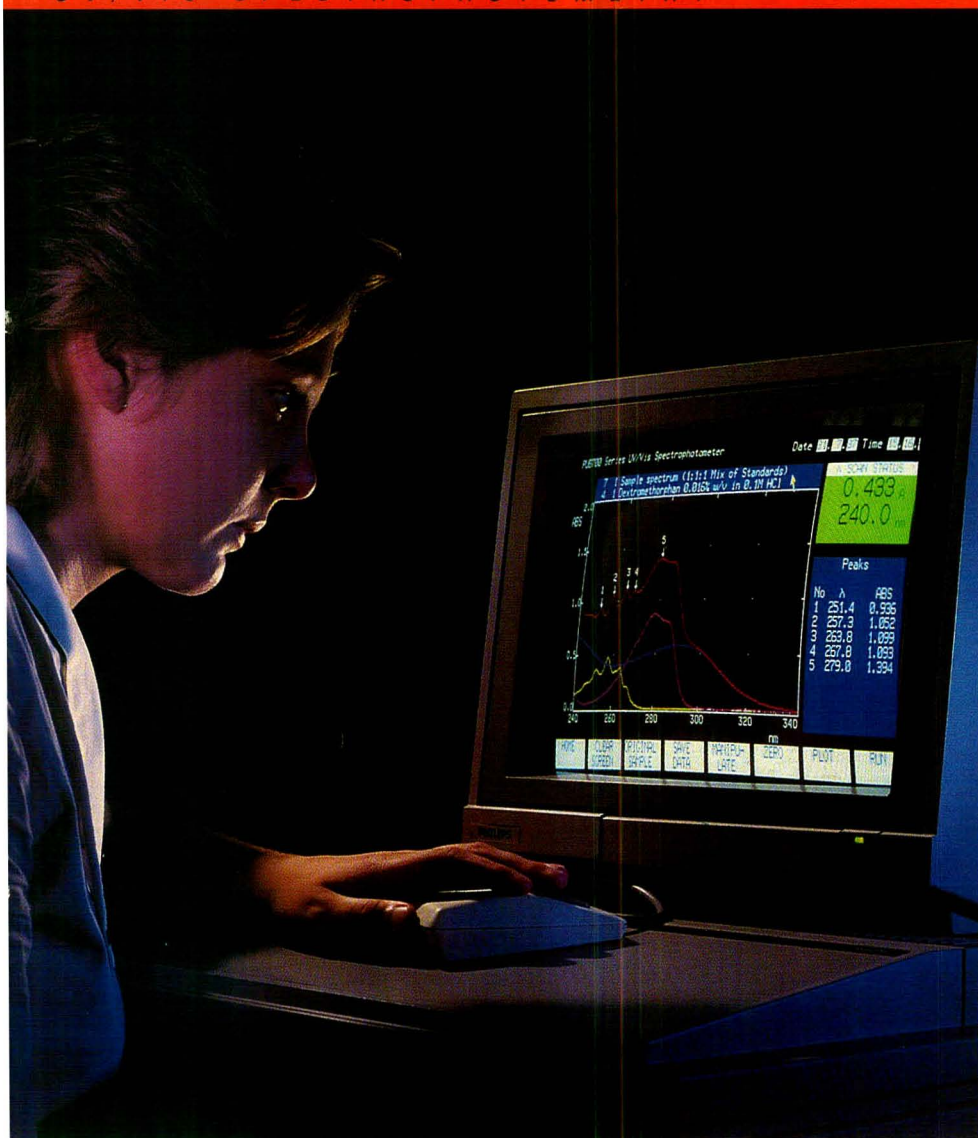
N-Pack 300AL



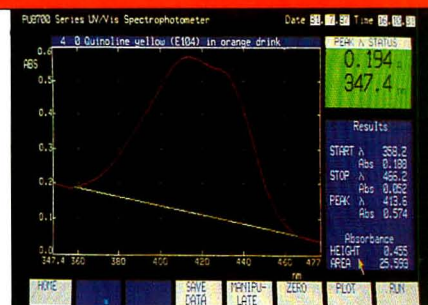
PHILIPS

UV: Visibly exciting!

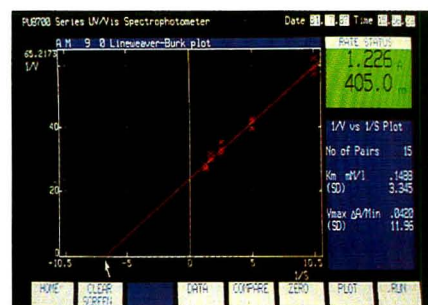
UV/VIS SPECTROPHOTOMETRY



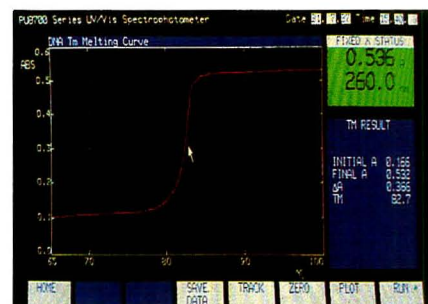
Multicomponent analysis. All the data points in each component's spectrum for high sensitivity quantification.



Many multi-wavelength methods of correcting for variable backgrounds and ratioing peaks.



Choice of automatic calculation of Michaelis-Menten parameters for enzyme characterisation.



Peltier temperature programming with full display of absorbance versus temperature.

Philips Analytical's popular PU 8700 series now offers the widest choice of easy-to-use software and sample handling options.

These are merely a selection from the exciting range. You need to know about the rest. Write or 'phone now. Philips Analytical, Pye Unicam Ltd, York Street, Cambridge, Great Britain CB1 2PX. Tel: (0223) 358866.

Bigger ideas for better analysis.

Here's a small sampling of what Europe's number one filtration expert can do for you

Sartorius. It pays to know us.

Discover the incredibly wide variety of our line of filterware and equipment for the fields of process chemistry and biochemistry. You'll find everything you need to make your work easier, more efficient and profitable: from the common disposable filter holder to the sophisticated, unique filtration system based on crossflow. All from the pioneer of innovative membrane filtration technology and a leading high-tech manufacturer of precision scales and balances worldwide:

Sartorius. With our unequalled expertise and results-oriented, dependable service, it pays to talk to us...

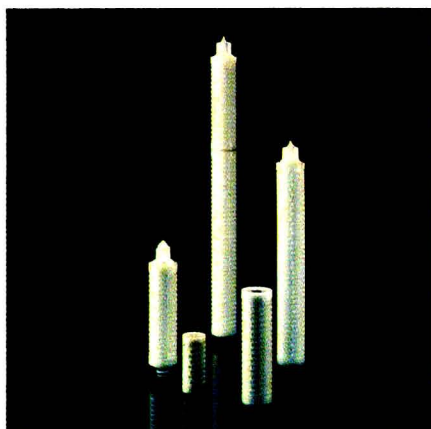
Sample # 1: Sartorius Sartocon II

Lets you scale up your profitability for biochemical separations.

Sartocon II is actually two crossflow filtration systems in one: you can readily convert it into an ultrafiltration or a microfiltration system just by exchanging the type of modules. Plus you can custom scale it to the performance you need.

- + High-grade stainless steel device holds 1 to 7 long-life modules
- + No more stacking; each module is a complete unit
- + Delivers high permeate flow rates at low operating pressures and recirculating rates
- + Highly versatile for clarification; separation of colloids; fractionation; and oil separations.
- + Also sized as a pilot system: Sartocon-Mini has a filter area of 0.1—0.5 m²

CIRCLE 153 ON READER SERVICE CARD



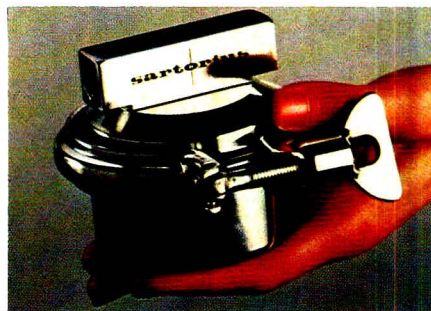
Sample # 2: Sartorius Cartridges

Give you unmatched filtration power.

Sartorius Filter Cartridges, top-quality pleated membrane & depth filters, have just what it takes to satisfy your special filtration needs for liquids and gases.

- + Wide array of designs, pore sizes, heights & housings
- + Superior & reliable retention efficiency
- + Broad chemical compatibility
- + Fast & low-cost clarification and removal of particulates/microbes

CIRCLE 154 ON READER SERVICE CARD



Sample # 3: Sartorius Maxisart-EL

Saves you time and trouble and helps maximize your productivity.

Maxisart-EL, the first completely heat-sealed inert gas filter, gives you maximum reliability for critical point-of-use applications.

- + Leak proof adaption system
- + Individually factory-tested for membrane integrity
- + Highly pressure-resistant pleated filter element
- + Factory purged & ready-to-use

CIRCLE 155 ON READER SERVICE CARD

Sample # 4: Sartorius Capsule

Simplifies your filtration work in the chemical industry.

This pleated filter cartridge sealed in a seamless polypropylene housing features just the kind of total convenience you need:

- + Preassembled & factory-tested
- + Wide choice of integrated connectors for the perfect custom fit
- + For sanitization, clarification and particulate removal of/from small volumes of liquids and gases

CIRCLE 156 ON READER SERVICE CARD



Sample # 5: Sartorius Sartocheck II

Programs reliability into your production run.

Sartocheck II is an easy-to-operate, programmable and automatic filter integrity tester that performs three integrity tests in one test run.



- + Determines the pressure drop, diffusion rate + bubble point
- + Tests both hydrophobic and hydrophilic filter materials in small-volume disc filtration systems or large-volume multiple element cartridge systems

CIRCLE 157 ON READER SERVICE CARD

Talk to the experts:

Sartorius GmbH

P.O. Box 3243
3400 Goettingen, W. Germany
Phone (51) 308-1, Telex 96723
Telefax 308289

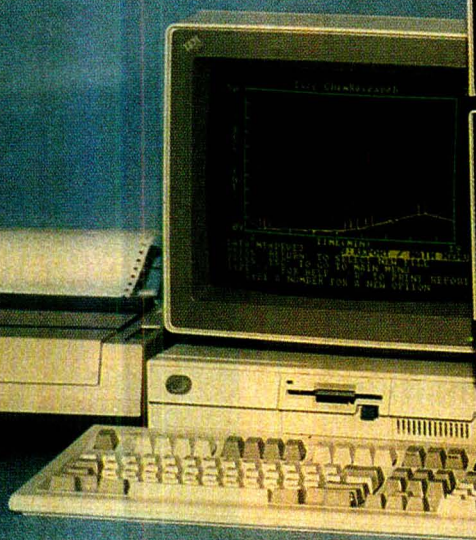
sartorius

The right chromatograph is going to cost you less



\$10,965

Binary/ternary gradient programmer, programmable pump, variable detector, recorder, valve, column.



\$16,640

Dual programmable pumps, variable detector, valve and column. Includes ChemResearch™ data management/gradient software and color monitor option. Now with IBM System 2/Model 30 and printer.

Isco chromatographs offer top value.

An Isco single-pump ternary or dual-pump binary gradient system complete with IBM computer can give you greater performance and capability than the two top-selling systems that cost much more. You'll get great value with any Isco HPLC system: analytical, microbore, or prep; stainless or inert.

With top performance. An Isco system gives you a precision pump that can be programmed to change flow rate based on either time or volume delivered. A

sensitive, stable 190-to-750 nm detector with flow cells down to 0.12 μ l. And a complete, powerful data management system that is actually easier to use than many simple integrators found in other chromatographs.

And top reliability. We've made over 50,000 detectors, pumps, and related instruments to earn our reputation for dependability. We back it up with the best system warranty offered anywhere—three years parts and labor.

Find out how much value Isco gives you by sending for a comparison of the leading HPLC systems. We'll also include our



80-page general catalog and 48-page HPLC catalog. Call toll free (800) 228-4250 (except NE, AK) or write: Isco, Inc., P.O. Box 5347, Lincoln, NE 68505.

**When testing
Optical Purity
leave nothing to chance**



**Check your products with
CHIRALPLATE**
simple · rapid · highly sensitive

Method: Thin layer chromatography
Principle: Ligand exchange
Application: Separation of enantiomers
and diastereomers

Without sample derivatization applicable for:

- amino acids • halogenated amino acids
- N-formylated and N-methylated amino acids
- lactones • dipeptides • thiazolidine derivatives

CHIRALPLATE unsurpassed for control of optical purity for pharmacologically important substances.

Request your free copy of our brochure
CHIRALPLATE today

MACHEREY-NAGEL



Macherey-Nagel GmbH & Co. KG
P. O. Box 307 · D-5160 Düren · West Germany
Tel. 0 24 21 / 6 10 71 · Telex 8 33 893 mana d

ENVIRONMENTAL SCIENCE & TECHNOLOGY

ES&T



**The premiere
research
publication in the
environmental
field.**

Environmental science continues to be one of the fastest growing fields. And ES&T has grown right along with it!

ES&T continues to give you the practical, hard facts you need on this science . . . covering research, techniques, feasibility, products and services.

Essential reading for environmental scientists both in the business and academic world . . . ES&T has increased its emphasis on peer-reviewed research dealing with water, air, and waste chemistry in addition to adding critical reviews of important environmental science issues—all relevant to understanding the management of our natural environment.

Also included are discussions on environmental analyses, governmental regulations, current environmental lab activities, and much more!

For rate information, and to subscribe, call toll free:

(800) 424-6747

CIRCLE 94 ON READER SERVICE CARD

Meetings

The following 1988 meetings are newly listed in ANALYTICAL CHEMISTRY. All 1987 meetings are listed in the January 15, March 15, April 15, May 15, July 15, and September 1 issues.

■ **Winter Conference on Plasma Spectrochemistry.** Jan. 3-9. San Diego, Calif. Contact: Ramon Barnes, Dept. of Chemistry, GRC Towers, University of Massachusetts, Amherst, Mass. 01003-0035 (413-545-0035)

■ **35th Annual Conference of the Western Spectroscopy Association.** Jan. 20-22. Pacific Grove, Calif. Contact: Heather Lafferty, WSA Conference Secretary, P.O. Box 10460, Eugene, Ore. 97440 (503-343-1200)

■ **2nd International Symposium on Preparative and Up-Scale Liquid Chromatography.** Feb. 1-3. Baden-Baden, F.R.G. Contact: Gesellschaft Deutscher Chemiker, Abt. Tagungen, Postfach 90 04 40, D-6000 Frankfurt/Main 90, F.R.G.

■ **OPTICS/ECOOSA '88.** March 22-25. Birmingham, U.K. Contact: Meetings Officer, The Institute of Physics, 47 Belgrave Square, London SW1X 8QX, U.K.

■ **2nd International Symposium on Analytical Methods and Problems in Biotechnology.** March 29-31. Noordwijkerhout, The Netherlands. Contact: Symposium Secretariat, ANABIOTEC '88, c/o QLT Convention Services, Keizersgracht 792, 1017 EC Amsterdam, The Netherlands

■ **CANBIOCHEM '88.** April 12-14. Montreal, Canada. Contact: John Luong, National Research Council, Biotechnology Research Institute, 6100 Royalmount Ave., Montreal, Que. H4R 2H2, Canada (514-496-6175)

■ **Flow Analysis IV.** April 17-20. Las Vegas, Nev. Contact: G. E. Pacey, Department of Chemistry, Miami University, Oxford, Ohio 45056

■ **4th International Symposium on Resonance Ionization Spectroscopy and Its Applications (RIS-88).** April 18-22. Gaithersburg, Md. Contact: Kathy Stang, National Bureau of Standards, Room A345, Physics Bldg., Gaithersburg, Md. 20899

■ **Handling of Environmental and Biological Samples in Chromatography.** April 27-29. Basel, Switzerland. Contact: R. Frei, Department of Analytical Chemistry, De Boelelaan

1083, Vrije Universiteit, 1081 HV Amsterdam, The Netherlands

■ **First International Symposium on Separation of Chiral Molecules.** May 31-June 2. Paris, France. Contact: Société Française de Chimie, 250 Rue Saint-Jacques, 75005 Paris, France

■ **36th ASMS Conference on Mass Spectrometry and Allied Topics.** June 5-10. San Francisco, Calif. Contact: Judith Watson, ASMS, P.O. Box 1508, East Lansing, Mich. 48823 (517-337-2548)

■ **195th ACS National Meeting and 3rd Chemical Congress of North America.** June 5-10. Toronto, Canada. Contact: B. Hodsdon, 1155 16th St., N.W., Washington, D.C. 20036

■ **ElectroFinnAnalysis.** June 6-9. Turku (Åbo), Finland. Contact: Ari Ivaska, Laboratory of Analytical Chemistry, Åbo Akademi, SF-20500 Turku (Åbo), Finland

■ **12th International Symposium on Column Liquid Chromatography.** June 19-24. Washington, D.C. Con-

tact: Symposium Manager, Barr Enterprises, P.O. Box 279, Walkersville, Md. 21793 (301-898-3772)

■ **9th International Congress on Thermal Analysis.** Aug. 21-26. Jerusalem, Israel. Contact: S. Shoval, Everyman's University, P.O. Box 39328, Tel-Aviv 61392, Israel

■ **102nd Annual AOAC International Meeting and Exhibition.** Aug. 29-Sept. 1. Palm Beach, Fla. Contact: Margaret Ridgell, AOAC, 1111 North 19th St., Suite 210, Arlington, Va. 22209 (703-522-3032)

■ **9th European Congress on Electron Microscopy (EUREM 88).** Sept. 4-9. York, U.K. Contact: Congress Secretariat, The Royal Microscopical Society, 37/38 St. Clements, Oxford, OX4 1AJ, U.K.

■ **Computer Applications in Analytical Chemistry—COMPANA '88.** Sept. 5-8. Jena, G.D.R. Contact: K. Danzer, c/o Friedrich Schiller University Jena, Department of Chemistry, Steiger 3, Jena, DDR-6900, G.D.R.

The Malvern MasterSizer does a fraction of what other particle sizers do.



Yes, it's true. The Malvern **MasterSizer** actually measures particles only a tenth of a micron in diameter. And it uses only two ranges to cover its entire size capability.

Admittedly, that capability extends to 600 microns and the two ranges, 0.1 to 80 μm and 1.2 to 600 μm , are each split into 64 size classes - that's rather more resolution than some other systems offer. And there is a third

range - 0.5-170 μm - should you require it.

But with **MasterSizer**, you'll find yourself doing less too. We have made alignment and sample handling, including flushing, completely automatic. And **MasterSizer** is so easy to use that it won't take you long to become completely familiar with it.

To learn more about doing less, contact Malvern, now.

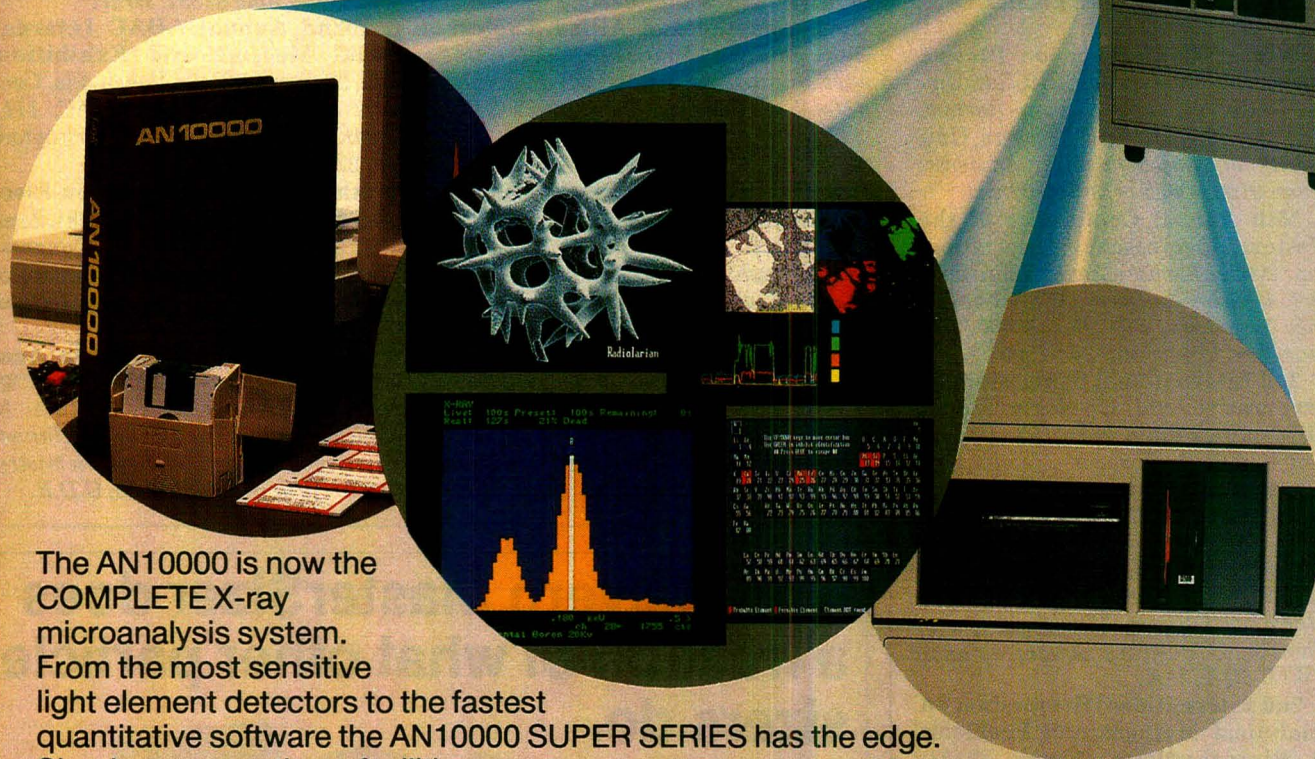
MALVERN

Malvern Instruments Inc
200 Turnpike Road, Southborough, MA 01772, USA
Telephone: (617) 480 0200 Telex: 311397

CIRCLE 96 ON READER SERVICE CARD

AN10000

So what's made
the AN10000 *Super*



The AN10000 is now the COMPLETE X-ray microanalysis system. From the most sensitive light element detectors to the fastest quantitative software the AN10000 SUPER SERIES has the edge. Simply compare these facilities.

- A totally upgradeable range of instruments to fit today's budget! but with tomorrow's requirements firmly in mind.
- LZ5 Light element detectors with guaranteed boron detection performance and a no compromise choice of totally windowless or UTW operation.
- "Time Variant Filter Pulse Processor" standard even on the base level system.
- Quantitative analysis! Using our exclusive "ON-LINE" quantitation routine the result is yours within seconds.
- "Position Beam" mode uniquely combines high resolution imaging with X-ray microanalysis.
- Graphics hardware for full 512×512 pixel images standard on all models.
- Extended graphics offers 256 discrete grey levels or 256 colours from a palette of 16 million.
- Extensive library of image processing and image analysis software.
- Exclusive MULTIPROGRAM operation provides maximum instrument time availability by implementing foreground/background operation.
- Latest data archiving peripherals offer low cost storage capacity.
- Complete range of microscope automation systems for stage, WDS and EELS control. There is even a system for the AUGER spectroscopist.

Why not call us today for further information about this fine range of instruments.

CIRCLE 90 ON READER SERVICE CARD

AN10000 *Super Series*



Link
ANALYTICAL

Link Analytical Inc,
240 Twin Dolphin Drive,
Suite D,
Redwood City,
California 94065 USA
Tel: (415) 595-LINK
Fax: (415) 595 5589

Link Analytical Limited,
Halifax Road, High Wycombe
Bucks HP12 3SE,
England
Tel: 0494 442255
Telex: 837542 LINK HWG
Fax: 0494 24129

Link Analytical (France) S.A.R.L.
9 Rue Fernand Leger,
Centre Val Courcelle,
91190 Gif Sur Yvette,
France
Tel: (1) 6907 7802
Telex: 603849S-LINK
Fax: (1) 6907 4469

Link Nordiska AB
Box 153,
181 22 Lindogoe,
Sweden.
Tel: 08-767 9170
Telex: 12645 SPECTAB

Link Analytical, (Aus) Pty. Ltd.
P.O. Box 7,
Pennant Hills,
N.S.W. 2120,
Sydney, Australia.
Tel: 2-8753130
Fax: 02-4841667

Diagnosis of Alzheimer's Disease

Genetic testing, imaging techniques, and immunoassay methods show promise for the biochemical diagnosis of Alzheimer's disease

It is estimated that two-and-a-half to three million Americans are afflicted with Alzheimer's disease, a degenerative brain disease that causes progressive loss of memory, language, and reasoning. There is no cure for Alzheimer's disease, although a new experimental drug, tetrahydroaminocrydine, does show promise for reducing memory loss in Alzheimer's victims. As many as 150,000 people are killed by Alzheimer's each year, and the annual cost of caring for these patients has been estimated at more than \$12 billion.

One of the most troubling aspects of Alzheimer's disease is the fact that it is extremely difficult to diagnose. Physicians must rely on physical examinations and psychological testing to diagnose the disease, and from 20 to 50% of all people who are told they have Alzheimer's actually have some other disease.

Absolute confirmation of the diagnosis can only be obtained by microscopic examination of brain tissue for signs of neuronal damage, either through a dangerous brain biopsy or during an autopsy. But research into both the cause and the means of distinguishing Alzheimer's disease from other brain disorders has intensified in the last few years. Research is proceeding in several different directions and includes efforts to identify products of the degenerative process, to detect neurochemical markers such as a decrease in various neurotransmitter levels, and to confirm a possible genetic defect on chromosome 21 that may be implicated in the development of Alzheimer's disease. These research efforts have led to the development of several promising methods for diagnosing Alzheimer's disease, including genetic testing, imaging techniques, and immunoassay methods.

One of the key findings in recent research on Alzheimer's is that the brain tissue of Alzheimer's patients contains distinctive protein tangles that do not appear to exist in normal brain tissue. An international team of neurologists, headed by Ron Polinsky at the National Institute of Neurological and Communicative Disorders and Stroke (Bethesda, Md.), in collaboration with a group of molecular biologists headed by James Gusella at Massachusetts General Hospital, have identified a region of chromosome 21 that appears to be linked with the disease in four fam-

FOCUS

ilies that have had Alzheimer's through several generations. A gene responsible for the production of one of the protein tangles also has been located on chromosome 21, leading to the postulation that the cause of Alzheimer's could be at least partially genetic. If further research confirms this genetic link, genetic testing could be used to determine whether a patient showing symptoms of Alzheimer's actually has the disease or has another neurological disorder.

Sophisticated imaging techniques that produce pictures of the brain, such as computer axial tomography (CAT scans), positron emission tomography (PET scans), and single-photon emission computed tomography (SPECT), have also been useful in distinguishing Alzheimer's disease from other brain disorders by noninvasively looking for the signs of neuronal damage that are found in postmortem examinations of brain tissue from Alzheimer's patients.

For example, a team from Harvard

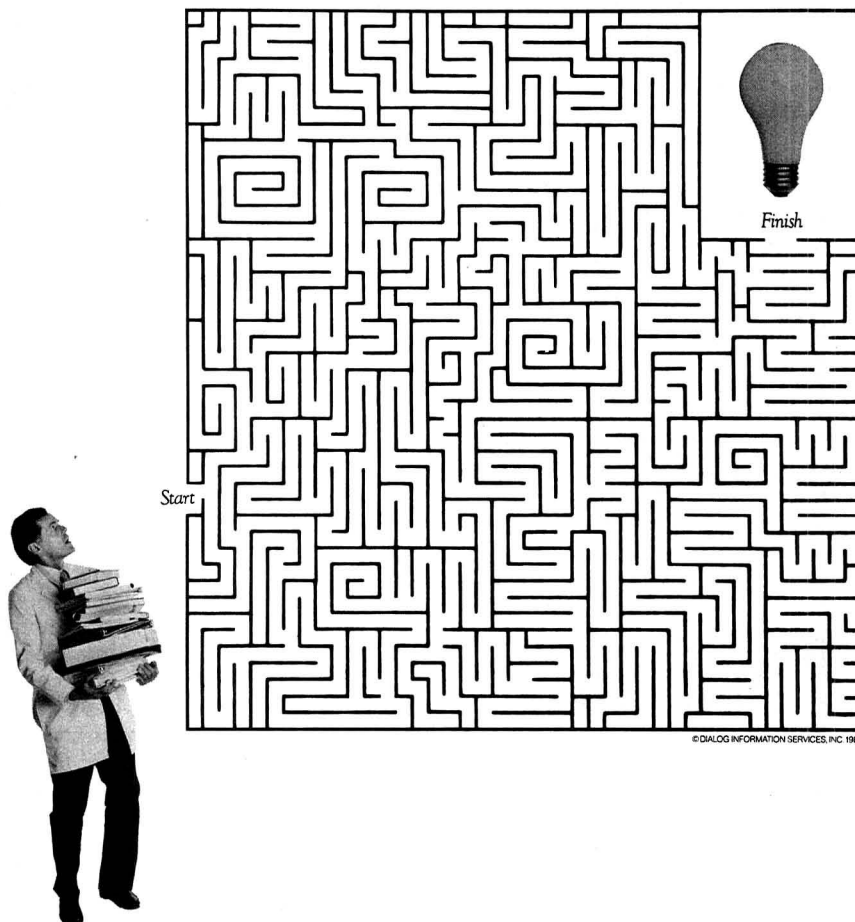
Medical School, Massachusetts General Hospital, and George Washington University Medical Center has used SPECT to study the muscarinic acetylcholine receptor binding function in an Alzheimer's patient. Iodine-123 labeled 3-quinuclidinyl-4-iodobenzilate was injected intravenously, and a high-resolution, high-sensitivity SPECT instrument was used to produce three-dimensional images of the brain.

These imaging techniques have the potential of providing a tool for early diagnosis of Alzheimer's cases. But because they are not widely available and are extremely expensive (a complete workup costs approximately \$1500), these techniques are not likely to become routine diagnostic tools soon.

Immunoassay techniques have been used both to determine levels of neurochemical markers in Alzheimer's patients and to detect an Alzheimer's-related protein in cerebral spinal fluid. Researchers at Duke University Medical Center (Durham, N.C.) recently measured the postmortem concentration of the neuropeptide neurotransmitter corticotropin-releasing factor (CRF) by radioimmunoassay in nine brain regions of both control patients and those with histologically confirmed Alzheimer's disease. Compared with tissue from control patients, the Alzheimer's tissue in the latter group shows a marked reduction of CRF concentration in three brain regions, indicating that CRF-containing neurons degenerate in Alzheimer's disease. Previous research has shown that levels of two other neurotransmitters, acetylcholine and somatostatin, are also depressed in Alzheimer's patients. Although all of this work has been done on brain tissue samples, methods that measure CRF, acetylcholine, or somatostatin levels in cerebrospinal fluid could possibly be used as diagnostic tools in the future.

Finally, a collaborative effort between researchers at the Institute for Basic Research in Developmental Disabilities (Staten Island, N.Y.), Immuno-Products Industries (Middlesex,

When it comes to research don't fight your way through the information maze.



If finding the right information on the latest patents, products and markets in biotechnology seems confusing, or if it takes too much valuable time, then you should know about DIALOG®.

Now you can quickly find the right information in databases such as CA SEARCH, with instant access to millions of articles indexed by Chemical Abstracts Service.

Or in SCISEARCH, offering a multidisciplinary index to the literature of science and technology. Or in BIOSIS PREVIEWS, providing worldwide coverage of research in life sciences.

And in EXCERPTA MEDICA, a leading resource for biomedical research.

In fact, DIALOG saves valuable

research time by giving you instant access to over 275 databases with information on literally millions of products and much more. So you'll spend less time in the library and more time doing what you do best.

Your company may already be using DIALOG. Check to see. To get acquainted, DIALOG offers \$100 worth of free time to first time users. Just call 800-3-DIALOG. Or write DIALOG, 3460 Hillview Avenue, Palo Alto, CA 94304.

DIALOG®

A SUBSIDIARY OF LOCKHEED CORP.

The world's largest online knowledgebank.

800-3-DIALOG

CIRCLE 33 ON READER SERVICE CARD

FOCUS

N.J.), and Senetek PLC (Mountain View, Calif.) has produced an immunoassay for the diagnosis of Alzheimer's disease. The method detects a cross-reacting antigen to a monoclonal antibody that was developed from protein tangles extracted from the brain tissue of confirmed Alzheimer's patients. According to John Bennett, president of Senetek, and Howard Rubinstein, president of Immuno-Products, two enzyme-linked immunosorbent assay (ELISA) methods have been developed: a competitive assay and a sandwich assay. Preliminary results indicate that the tests can distinguish Alzheimer's disease from other neurological disorders with about 75% accuracy, which is comparable to the best diagnostic studies using strict clinical and neuropsychological criteria. If these immunoassays can detect Alzheimer's disease earlier than can clinical methods, physicians can then start appropriate treatment for Alzheimer's disease sooner.

No cross-reactivity to drugs has been discovered thus far, and the immunoassay method can detect 1-3 ng/mL of the protein antigen in standards derived from the analysis of brain tissue of confirmed Alzheimer's patients. Clinical trials are now underway, and Senetek hopes to start marketing the test in Europe later this year. Plans are also underway to introduce the test in the United States after FDA regulatory requirements have been met.

Although Alzheimer's disease was first described by German neurologist Alois Alzheimer in 1907, it has received significant research interest only in the last 20 years or so. In the last 10 years, research on Alzheimer's has increased dramatically with the discovery of biological markers, proteins specific to Alzheimer's disease-afflicted brain tissue, and a possible genetic link. Because most victims of Alzheimer's are elderly (although it has been known to strike in middle age), the number of victims is sure to increase as the elderly population increases. Researchers expect that at least one of the promising lines of recent work on Alzheimer's disease will produce both a reliable diagnostic test and a means of treating the disease.

Mary Warner

Suggested reading

Wurtman, R. J. *Sci. Am.* January 1985, 62-74.

Ferry, G. *New Scientist*, Aug. 22, 1986, 33-5.
Edwards, D. D. *Science News*, Dec. 14, 1985, 374-75.

Holman, B. L.; Gibson, R. E.; Hill, T. C.; Eckelman, W. C.; Albert, M.; Reba, R. C. *J. Am. Med. Assoc.* 1985, 254, 3063-66.

Bissette, G.; Reynold, G. P.; Kilts, C. D.; Widerlov, E.; Nemeroff, C. B. *J. Am. Med. Assoc.* 1985, 254, 3067-69.

It Takes only \$4500 to Own the WINner.™



When it comes to chromatography workstations, you don't always get what you pay for. Unless you pick the WINner.

The WINner is a new and complete Workstation/INtegrator for chromatographers who want a complete solution at a completely affordable price.

With the WINner, you get an IBM-compatible Epson Equity computer, a 20-Mbyte hard disk, and Spectra-Physics' industry-standard integrator, the SP4290.

You also get a full complement of laboratory-proven Spectra-Physics chromatography applications software, high-resolution graphics, and direct data transfer to Lotus and other general purpose programs.

But what really puts the WINner out in front of its competition is the way it works. The WINner gives you true multi-tasking with continuous real-time plots and reports, from one or two data channels, right at your chromatographs. At the same time, the computer is always available for other tasks. And you never miss a run or lose data.

Best of all, you get it all—for \$4,500*.

So if you're looking for a chromatography workstation to put your money on, go with the WINner. It's a sure thing.

In the U.S., call toll free 800-424-7666. Spectra-Physics Autolab Division, 3333 North First Street, San Jose, CA 95134. In Europe, contact Spectra-Physics, GmbH, Siemensstrasse 20, D-6100, Darmstadt-Kranichstein, Fed. Rep. Germany.

*Price for U.S. only. For prices outside the U.S.A., contact your Spectra-Physics representative.

Spectra-Physics

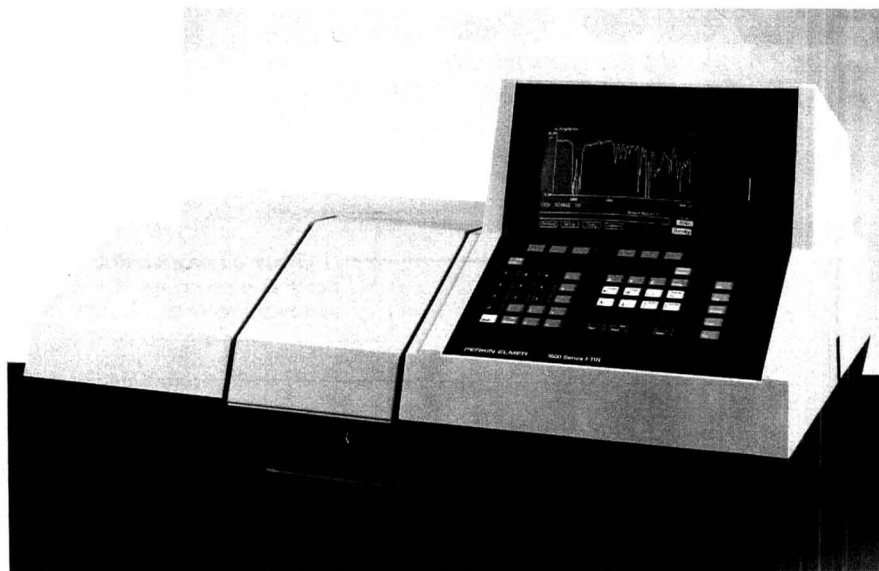
Discover the Quality

Epson is a registered trademark of Epson Corporation. Equity is a trademark of Epson America, Inc. IBM is a registered trademark of International Business Machines Corporation. Lotus and 1-2-3 are registered trademarks of Lotus Development Corporation.

CIRCLE 149 ON READER SERVICE CARD

ANALYTICAL CHEMISTRY, VOL. 59, NO. 20, OCTOBER 15, 1987 • 1205 A

NEW PRODUCTS



The 1600 series FT-IR is a stand-alone, benchtop instrument that features a sealed and desiccated optical system, advanced electronics, and software with interactive graphics and multitasking capabilities. Perkin-Elmer **401**

Data acquisition. SDA2000, designed for use with an IBM PC, PC-XT, PC-AT, or compatible computer, is a multichannel, high-speed data acquisition system that features a 2-megasample RAM and sampling rates up to 10 MHz (100 ns) with 12-bit resolution. Soltec **403**

Gas standards. Series 200 computerized generator produces precision gas standards for single- or multipoint calibration of gas chromatographs, mass spectrometers, in-plant monitors, and other gas analytical devices. A microcomputer with 32-bit computation precision accurately programs the mass flow controllers. Environics **404**

UV-vis. Model 1740 fixed-wavelength UV-vis monitor for LC incorporates 4 different lamps and 10 different filters to allow wavelength settings from 214 to 800 nm. Features include biocompatibility and cold room capability. Bio-Rad **405**

Flowmeter. EZ Cal I digital flowmeter provides primary airflow calibrations with instant digital readout and NBS traceability. A flow rate range of 5 mL/min to 4 L/min covers most personal monitoring applications. Sensidyne **406**

SEM. Stereoscan 240 offers 35-Å resolving power, accelerating voltages

ranging from 0.3 to 30 kV (in 100-V steps), and facilities for handling specimens up to 2 kg in weight and 150 mm in diameter. Additional features include 35° take-off angles and a 300-mm viewing screen. Cambridge Instruments **407**

Colorimeter. μ -Colorimeter allows sample absorbance or concentration to be read directly from microcuvette strips. Up to 12 wells can be measured, and results can be downloaded to a personal computer or printer using an RS-232 interface. Whatman **408**

LC detector. RI-4 refractive index detector, designed for the determination of nonabsorbing or weakly UV-absorbing compounds such as polymers, hydrocarbons, carbohydrates, alcohols, and fatty acids, is a deflection type of detector that covers the full 1.00 to 1.75 RI range. Varian **409**

pH and ion concentration. PHI 12 pH/ISE meter features direct readout of pH or most ion activity. The portable meter automatically recognizes five standard buffers—1.68, 4, 7, 10, and 12.45—and enters temperature-corrected values for standardization or calibration. Beckman **410**

LC/MS. The 700 series LC/MS interface, which is compatible with commercial mass spectrometers suitable for

chemical ionization, provides modular electronics, additional zones for temperature control and monitoring, a plug-in thermospray ion source assembly, and independent heater controls for the vaporizer tip and source block. Vestec **411**

Density/specific gravity. Model DA-210 meter is a microprocessor-based system that measures density and specific gravity of liquids and gases, plus the direct concentration of liquids, in 1–2 min with an accuracy of $\pm 1 \times 10^{-5}$ g/cm³. Seamark **412**

Software

Substructure searching. Tree, a program for retrieval of chemical structures and substructures from large databases, can search a database of 15,000 structures in ~20 s. The program can be used on the IBM PC, PC-XT, PC-AT, and compatible computers and can be linked to standard database packages and word-processing software. Technical Database Services **415**

Pascal library. The Pascal subprogram library is available for the Apple Macintosh; the Hewlett-Packard 200, 300, and 500 series; and the DEC VAX series. The library covers essential algorithms in mathematics, statistics, graphics, spectrometry, chromatography, thermodynamics, and kinetics. Scientific Logics **416**

Manufacturers' Literature

Chromatography data processor. Product literature describes the C-R5A chromatography data processor, which features 170Kbyte memory and an 8Kbyte insertable IC card for storing and automatically setting up programs, peak processing parameters, and user-defined applications packages. 13 pp. Shimadzu **427**

For more information on listed items, circle the appropriate numbers on one of our Readers' Service Cards



We can help take the headaches out of your projects and production. Profitably.

You face the same dilemma every day. Keeping productivity high. But also meeting strict regulatory and FDA compliance standards every step of the way — tedious and time consuming testing and documenting, over and over, again and again.

And the entire operation must run at a profit. Or it's not going to run at all.

It's enough to give you a headache. But you don't need an aspirin. You need Beckman.

We integrate robotics, instrumentation, computers and support into systems that provide *profitable* solutions to your productivity/compliance problems.

Our systems keep you up and running productively. At the same time they accurately verify, document and archive each step of your process.

That's why you'll find our integrated systems already working for over 30 pharmaceutical companies at 60 locations worldwide.

To get rid of *your* headaches, contact your local Beckman representative. Or write Beckman Instruments, Inc., 2500 Harbor Blvd., Fullerton, CA 92634-3100, U.S.A.

Discover all the benefits of our promise to you: Making science good businessSM.

BECKMAN

A SMITHKLINE BECKMAN COMPANY

CIRCLE 19 ON READER SERVICE CARD

U.S.A. (800) 742-2345. **Australia**, Gladesville (02) 816 52 88. **Austria**, Vienna (0222) 32 25 57. **Canada**, Mississauga, Ontario (416) 673 9844. **Denmark**, Birkerød (02) 81 92 11. **France**, Gagny (014) 381 93 00. **Germany**, Munich (089) 38 871. **Hong Kong** (05) 53 92 36. **Italy**, Milan (02) 69 911. **Japan**, Tokyo (03) 221 58 31. **Mexico**, Mexico City (5) 564 81 35. **Netherlands**, Mijdrecht (02979) 8 56 51. **Norway**, Oslo (02) 64 80 40. **Puerto Rico**, Carolina (809) 762 30 30. **Singapore** (065) 534 25 08. **South Africa**, Johannesburg (11) 805 2014. **Spain**, Madrid (01) 729 16 66. **Sweden**, Bromma (08) 98 53 20. **Switzerland**, Geneva (022) 35 64 80. **Taiwan**, Taipei (02) 700 22 33. **UK**, High Wycombe (0494) 411 81. © 1987, Beckman Instruments, Inc.

NEW FROM PLENUM

NONDESTRUCTIVE CHARACTERIZATION OF MATERIALS II

edited by **Jean F. Bussière, Jean-Pierre Monchalán, Clayton O. Ruud, and Robert E. Green, Jr.**

The multidisciplinary nature of characterizing materials nondestructively is reflected in this new review covering polymers and composites, ceramics and powder metallurgy, metals, layered structures/adhesive bonds/welding, degradation/aging, texture/anisotropy, stress, and new techniques.

0-306-42610-2/proceedings/788 pp. + index ill./1987/\$115.00

VIBRATIONAL SPECTROSCOPY OF MOLECULES ON SURFACES

edited by **John T. Yates, Jr. and Theodore E. Madey**

The contributors to this volume discuss the major methods used to measure vibrational spectra of surface species. Volume 1 in the series *Methods of Surface Characterization*.

0-306-42505-X/484 pp./ill./1987/\$75.00

COMPUTER-ENHANCED ANALYTICAL SPECTROSCOPY

edited by **Henk L. C. Meuzelaar and Thomas L. Isenhour**

An overview of advances in computerized optimization, data exploration, and spectral interpretation methods in mass spectrometry, infrared spectroscopy, and nuclear magnetic resonance spectroscopy. A volume in the series *Modern Analytical Chemistry*.

0-306-42644-7/267 pp. + index/ill. 1987/\$52.50

Modern Inorganic Chemistry

MÖSSBAUER SPECTROSCOPY APPLIED TO INORGANIC CHEMISTRY

edited by **Gary J. Long**

Volume 1

"... as a careful treatment of a number of fundamental theoretical aspects of Mössbauer-effect spectroscopy, this book is a must..."

—*Applied Spectroscopy*

0-306-41647-6/686 pp./ill./1984/\$92.50

Volume 2

Presents applications of Mössbauer spectroscopy in solving problems faced by the inorganic chemist.

0-306-42507-6/642 pp./ill./1987/\$92.50

PLENUM PUBLISHING CORPORATION
233 Spring Street
New York, NY 10013-1578

NEW PRODUCTS

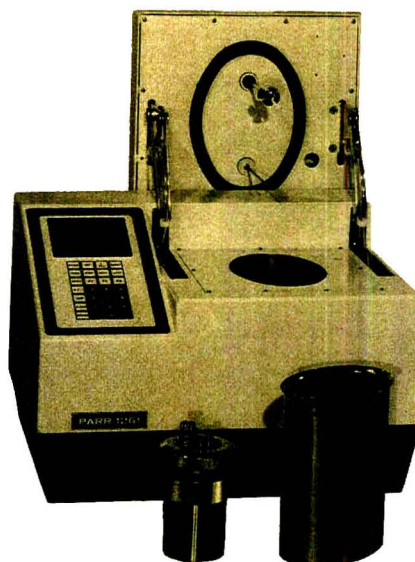
TLC. Brochure describing the Diamond series TLC plates, which feature extra-hard, high-reflectance surfaces, opens into a wall poster. A cross-reference guide helps the user to identify and order aluminum, plastic, and traditional glass-backed plates. Whatman 420

Chromatography newsletter. Vol. I, No. 3 of *The Separation Times* features articles on sulfur gas analysis, troubleshooting, column-coating efficiency, and analysis of fatty acid samples. J & W Scientific 421

Newsletter. Vol. VI, No. 4 of the *Supelco Reporter* includes articles on the contamination of GC carrier gases by gas-purifying devices and analyses of multiple industrial solvents using a single wide-bore capillary column. 12 pp. Supelco 418

Autosampler vials. Brochure features autosampler vials and related accessories for GC and LC. Products described include vials for microsampling, headspace vials, and materials for vial sealing. 16 pp. Chemical Research Supplies 419

Water analysis. Vol. 10, No. 1 of *In Focus* provides information on products for automated water analysis. FIA, ion chromatography, Kjeldahl analysis, and systems for the determination of chemical oxygen demand are described. 19 pp. Tecator 422



Model 1261 automatic isoperibol bomb calorimeter consists of a self-contained operating unit with fully integrated microprocessor control and built-in microcomputer and features electronic thermometry and a built-in bomb filling system. Parr 402

Semiconductor testing. Brochure describes the use of specialized instruments for semiconductor measurements. Low-level measurements, capacitance-voltage tests, and resistance and electromigration studies are discussed. 12 pp. Keithley 423

Balances. Brochure describes the GT series of electronic top-loading balances, which feature an electronic filling aid, a built-in bidirectional RS-232 interface, and the ability to weigh in both metric and nonmetric units. 6 pp. Ohaus 424

Catalogs

Biotechnology. Catalog features a selection of DNA transilluminators, DNA photodocumentation systems, DNA analysis systems, and scientific photodocumentation systems. Information on running and documenting DNA agarose gels is also included. 80 pp. Fotodyne 425

Labware. Catalog features Pyrex labware, including beakers; cylinders; boiling, distilling, volumetric, and Erlenmeyer flasks; funnels; separatory funnels; pipets; and centrifuge tubes. 16 pp. Corning 426

LC. Catalog features 1–20-mm ID columns for standard HPLC, fast LC, and microbore, small-bore, supercritical fluid, and preparative LC. Also listed are fittings, tubing, valves, and connectors. 16 pp. Keystone Scientific 428

Liquid measurement. Catalog includes information on adjustable, single-volume, and disposable pipets; pipet controllers and accessories; disposable tips; and dispensers. Rainin 430

Reagents and laboratory products. Catalog 870C features reagents, chemicals, and products for chromatography, sample preparation, and biochromatography. Information on spill control and safety products also is included. 282 pp. J.T. Baker 429

Laboratory equipment. Catalog contains scientific and process equipment, including purge and trap instrumentation, homogenizers, laboratory reactors, microcentrifuges, and electronic balances. 48 pp. Tekmar 431

Correction from August 1 issue

The company name for the wall chart of radionuclides listed under Manufacturers' Literature (p. 976 A) was published incorrectly. The correct company name is Packard Instrument.

CIRCLE 128 ON READER SERVICE CARD

Way out in front: 670 Titroprocessor



The 670 Titroprocessor typifies our latest generation of titrators: It is distinguished by a performance which reflects our many years of experience in titrating. Where until now could you determine the procedure of your methods with all auxiliary functions yourself?

- Do you require, for example
- Intelligible dialog with the instrument via a typewriter keyboard?
 - Complete problem solutions which you can easily adapt

to your needs, also for automatic titrations?

- Result outputs with designations and comments you can formulate yourself?
- Live information on the screen regarding the sequence of events during the titration?
- Printouts in A4 format on a built-in thermal printer/plotter?

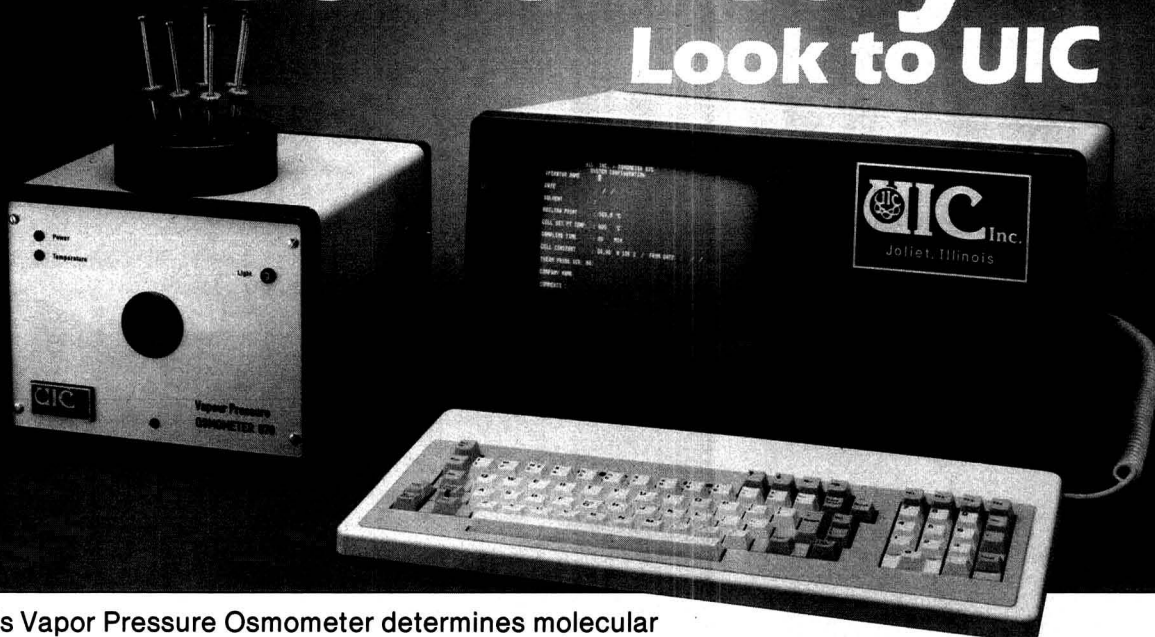
All this and much more is possible with the 670 Titroprocessor.

 **Metrohm**
Measurement in Chemistry
Worldwide with Metrohm

METROHM Ltd.
CH-9100 HERISAU Switzerland
Phone 071 / 53 11 33
Telefax 071 / 52 11 14
Telex 77267 metro ch

Brinkmann
INSTRUMENTS CO.
Cantiague Road, Westbury, New York 11590
Phone: (516) 334-7500, TWX: 510 222 8524

For Osmometry Look to UIC



UIC's Vapor Pressure Osmometer determines molecular weight from 40-35,000 g/mol. (standard and semi-automatic models are available)

The UIC Family of Osmometers also include:

Membrane
Cryoscopic
Colloidal

Call 800 DIAL UIC
800 FIND UIC in Canada
815 727-5431 in Illinois

UIC Inc.
Joliet, Illinois

P.O. BOX 863 JOLIET, ILLINOIS 60434
TELEX 723421 UAR JOL FAX 815-744-1561

CIRCLE 165 ON READER SERVICE CARD

LABORATORY SERVICE CENTER

Acetylthiourea • Aluminon • Aniline Sulfate • 4-Benzyl Pyridine
1-Bromonaphthalene • Bromosulphophthalein • 2,3-Butylene Glycol
Cesium Chloride • 1,2-Cycloheptanedione • Dithizone • Dulcitol
Ethyl Glycolate • 4-Hydroxybenzophenone • Hydroxylamine HCl & Sulfate
Iodobenzene • Isovaleraldehyde • α -Ketoglutaric Acid • Lacmoid
Luminol • Malonic Acid • 2-Mercaptobenzimidazole • Mucic Acid
4-Nitrophenylphosphate, DiNa & Ditriz Salts • Phenylthiourea
Toluene-3,4-dithiol • Triphenylphosphine • Vanillic Acid • Xylitol

Write for our Products List of over 3,000 chemicals

Tel: 516-273-0900 • TOLL FREE: 800-645-5566 • Telefax: 516-273-0858 • Telex: 497-4275

EASTERN CHEMICAL
A Division of UNITED-GUARDIAN, INC.

P. O. Box 2500
DEPT. AC
SMITHTOWN, N. Y. 11787

Laboratory Service Center (Equipment, Materials, Services, Instruments for Leasing), Maximum space — 4 inches per advertisement. Column width, 2-3/16"; two column width, 4-9/16". Artwork accepted. No combination of directory rates with ROP advertising. Rates based on number of inches used within 12 months from first date of first insertion. Per inch: 1" — \$141; 12" — \$139; 24" — \$136; 36" — \$131; 48" — \$128.

CALL OR WRITE JANE GATENBY

ANALYTICAL CHEMISTRY
500 Post Road East
P.O. Box 231
Westport, CT 06880
203-226-7131



Electron Transfer Technologies

PCSTAT—turn your IBM-PC/AT or compatible into a sophisticated potentiostat. The PCSTAT is a potentiostat on an expansion card that occupies one slot in the computer. Menu driven software includes built-in signal generator for potential sweeps (cyclic voltammograms) and potential steps. Text screen displays instrument set-up, selected and measured potentials, current, coulombs, and elapsed time when coulometer activated. Graphic screen displays I vs. E' plots. Data collected written to disk in ASCII format. A/D, D/A converters are 12 bit, maximum current 100mA. PCSTAT complete system (hardware and software) \$3250. High current version (1 A) \$4025. Electron Transfer Technologies, Inc., (609) 921-0070, P.O. Box 160, Princeton, NJ 08542.

FREE DATA, FAST

To quickly amass data on all of the products you need, consult the Lab Data Service section on our *Analytical Chemistry* reader reply card insert.

Laboratory Chemical Clean-Up, Packaging & Disposal



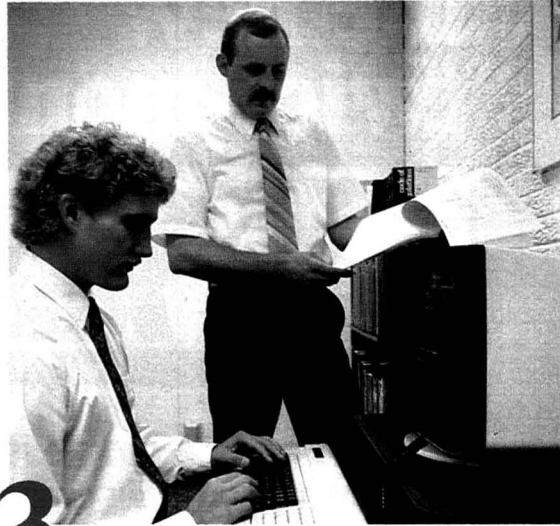
1

Inventory and screening



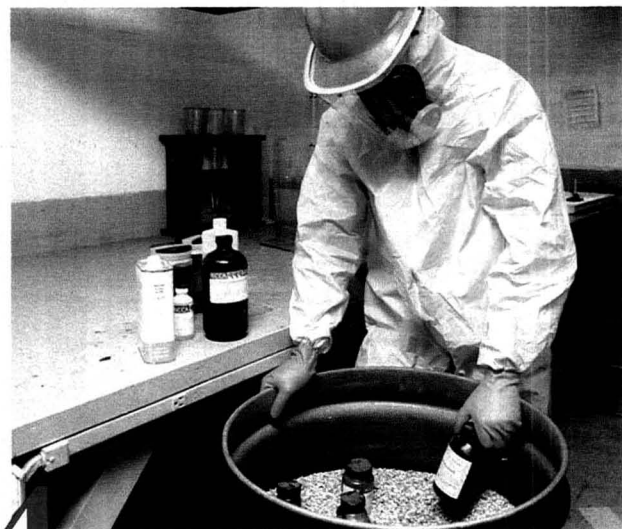
2

On-site testing and fingerprinting



3

Computerized identification - classification



4

D.O.T "Lab-Pack" packaging of compatible materials



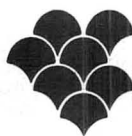
5

Environmentally secure packaging and transportation

This exclusive system is a self-designed and constantly updated computerized turnkey program. Experienced environmental chemists are fully equipped for on-site chemical inventory, fingerprinting and classification. Packaging and transport of chemicals to disposal facilities are in

compliance with all EPA and DOT regulations.

A wide assortment of laboratory and small quantity chemicals are efficiently identified, packaged and disposed of within one safe full service program.



**great lakes
environmental
services, inc.**

a subsidiary of environmental systems company

22077 Mound Rd., P.O. Box 1208, Warren, Michigan 48091 • (313) 758-0400 • MI 1-800-482-4484 • US 1-800-482-4482
Chicago Sales Office: 15 Spinning Wheel Rd., Suite 327, Hinsdale, Illinois 60521 • (312) 323-0410

CIRCLE 60 ON READER SERVICE CARD

ANALYTICAL CHEMISTRY, VOL. 59, NO. 20, OCTOBER 15, 1987 • 1211A

Introducing the new twice-monthly

**Quality
Research and
News In Your
Hands Twice
as Fast**

Analytical CHEMISTRY

Don't miss a single issue! The new, more timely ANALYTICAL CHEMISTRY, contains the same vital information in the field of measurement science. Twenty-four issues a year put the best in ANALYTICAL CHEMISTRY in your hands more often. You'll continue to find the same fine research articles, reports, special departments like Focus and A/C Interface, and the Annual Reviews and LabGuide issues.

There's never been a better time to subscribe

Call now and you can get your own subscription to the new twice monthly ANALYTICAL CHEMISTRY—including its sought-after annual "Application Reviews" and "LabGuide" issues.

SPECIAL RATES

Member*	1 Year	2 Years Save 15%	Nonmember	1 Year	2 Years Save 15%
U.S.	\$ 25	\$ 42	U.S.	\$ 37	\$ 62
Canada & Mexico	\$ 50	\$ 92	Canada & Mexico	\$ 62	\$112
Europe**	\$ 77	\$146	Europe**	\$127	\$231
All Other Countries**	\$104	\$200	All Other Countries**	\$154	\$285

*Member rates are for personal use only.

**Air service delivery included.

Call toll free: 800-424-6747

**Or write: American Chemical Society, Marketing Communications Department,
1155 Sixteenth Street NW, Washington, D.C. 20036**

This publication is available on microfilm, microfiche, and electronically through
Chemical Journals Online on STN International.

INDEX TO ADVERTISERS IN THIS ISSUE

CIRCLE INQUIRY NO.	ADVERTISERS	PAGE NO.	CIRCLE INQUIRY NO.	ADVERTISERS	PAGE NO.
1	**Amicon Hedges & Hughes Limited	1198C	149	Spectra-Physics Robert E. LaPointe & Company	1205A
19	Beckman Instruments BSG Cochrane, Chase, Livingston & Company	1207A	165	*UIC, Inc.	1210A
17	Bioanalytical Systems Kissinger Advertising Associates	1182A	<i>Directory section, see page 1210A.</i> <i>* See ad in ACS Laboratory Guide.</i> <i>** Company so marked has advertisement in Foreign Regional edition only.</i> <i>Advertising Management for the American Chemical Society Publications</i>		
30	CEM Corporation Union Agency	1174A	CENTCOM, LTD <i>President</i> Thomas N. J. Koerwer <i>Executive Vice President</i> <i>Senior Vice President</i> James A. Byrne Benjamin W. Jones Alfred L. Gregory, Vice President Clay S. Holden, Vice President Robert L. Voepel, Vice President Joseph P. Stenza, Production Director 500 Post Road East P.O. Box 231 Westport, Connecticut 06880 (Area Code 203) 226-7131 Telex No. 643310		
28	Chem Service, Inc. Bremble & Sewforth	1180A	ADVERTISING SALES MANAGER James A. Byrne, VP ASSISTANT ADVERTISING SALES MANAGER Bruce E. Poorman ADVERTISING PRODUCTION MANAGER Jane F. Gatenby SALES REPRESENTATIVES Philadelphia, PA . . . Patricia O'Donnell, CENTCOM, LTD., GSB Building, Suite 725, 1 Belmont Avenue, Bala Cynwyd, Pa. 19004. Telephone: 215-667-9666 New York, NY . . . Dean A. Baldwin, CENTCOM, LTD., 60 East 42nd St., New York, N.Y. 10165. Telephone: 212-972-9660 Westport, CT . . . Edward M. Black, CENTCOM, LTD., 500 Post Road East, P.O. Box 231, Westport, Ct. 06880. Telephone: 203-226-7131, Telex 643310 Cleveland, OH . . . Bruce E. Poorman, John C. Guyot, CENTCOM, LTD., 325 Front St., Suite 2, Berea, Ohio 44017. Telephone: 216-234-1333 Chicago, IL . . . Michael J. Pak, CENTCOM, LTD., 540 Frontage Rd., Northfield, Ill. 60093. Telephone: 312-441-6383 Houston, TX . . . Michael J. Pak, CENTCOM, LTD., Telephone: 312-441-6383 San Francisco, CA . . . Paul M. Butts, CENTCOM, LTD., Suite 1070, 2672 Bayshore Frontage Road, Mountain View, CA 94043. Telephone: 415-969-4604 Los Angeles, CA . . . Clay S. Holden, CENTCOM, LTD., Newton Pacific Center, 3142 Pacific Coast Highway, Suite 200, Torrance, CA 90505. Telephone: 213-325-1903 Boston, MA . . . Edward M. Black, CENTCOM, LTD., Telephone: 203-226-7131 Atlanta, GA . . . Edward M. Black, CENTCOM, LTD., Telephone: 203-226-7131 Denver, CO . . . Paul M. Butts, CENTCOM, LTD., Telephone: 415-969-4604 United Kingdom Reading, England . . . Malcolm Thiele, Technomedia Ltd., Wood Cottage, Shurlock Row, Reading RG10 0QE, Berkshire, England. Telephone: 073-434-3302, Telex #848800 Lancashire, England . . . Technomedia Ltd., c/o Meconomics Ltd., Meconomics House, 31 Old Street, Ashton Under Lyne, Lancashire, England. Telephone: 061-308-3025 Continental Europe . . . Andre Jamar, International Communications, Inc., Rue Mallar 1, 4800 Verviers, Belgium. Telephone: (087) 22-53-85, Telex #49263 Tokyo, Japan . . . Shuji Tanaka, International Media Representatives Ltd., 2-29 Toranomom, 1-Chome Minato-ku Tokyo 105 Japan. Telephone: 502-0656, Telex #22633		
33	*Dialog Information Services Humpal, Leftwich & Sinn, Inc.	1204A			
35	Dohrmann Lena Chow, Inc.	1184A			
50-53	Finnigan MAT Corporation Lena Chow, Inc.	1191A, 1193A			
60	Great Lakes Environmental Services Alden Design Associates	1211A			
67	*Hamamatsu Corporation Ketchum/Mandabach & Simms	1190A			
69	*Hamamatsu Photonic Systems Ketchum/Mandabach & Simms	1195A			
71	*W.A. Hammond DRIERITE Company J.P. Advertising Agency	1180A			
64	*Hewlett-Packard Company Pinné, Garvin, Herbers & Hock, Inc.	OBC			
75	*Isco, Inc. Farneaux Associates	1199A			
90	*Link Analytical	1202A			
94	Macherey-Nagel GmbH & Co. KG MP Design Werbeagentur	1200A			
96	Malvern Instruments, Inc.	1201A			
102	*Matheson Gas Products Kenyon Hoag Associates	1179A			
100	Metrohm AG Ecknauer & Schoch Werbeagentur	1209A			
104-105	*Mettler Instrument Corporation McKinney, Inc.	IFC, 1173A			
98	*Molecular Design Ltd. Lena Chow, Inc.	1189A			
110	Nelson Analytical Hayes/Rothwell	1177A			
113	*Nicolet Analytical Instruments Nicolet Advertising	1181A			
128	Plenum Publishing Corporation Plenum/Da Capo Advertising	1208A			
125-126	**Pye Unicam Ltd. Spectrum/SSC&B: Lintas Worldwide	1198B, 1198D			
153-157	**Sartorius GmbH Agentur Volker Baars	1198E			
151-152	*Shimadzu Scientific Instruments, Inc. Techmarketing, Inc.	1187A			

JOURNAL OF CHEMICAL AND ENGINEERING DATA

***The Only Publication Of Its Kind In The World
Featuring Contributions From Around The World!***

Editor:

Bruno J. Zwolinski
Texas A&M University

Associate Editor:

Randolph C. Wilhoit
Texas A&M University

Section Editor:

Joseph A. Dixon
The Pennsylvania State University

Multidisciplinary in nature and international in scope, JCED features contributions by distinguished physicists, chemists, chemical engineers, mechanical engineers, biological scientists, and applied mathematicians from many different countries. Their expert reports represent numerical data bases for private technical information systems, particularly in industry, that will broaden your scientific horizons and improve the quality of your work.

This unique journal offers you precise, accurate data on physical, thermodynamic and transport properties of well-defined materials. It also keeps you informed about the latest international standards on symbols, terminology and units of measurement for reporting data properly.

You'll find numerical property data measurements on:

- pure substances of defined purity
- well-defined gaseous, liquid and solid mixtures
- semi-empirical and theoretical correlations useful in interpolating, extrapolating and predicting properties of scientific and technological importance
- new substances—the physical and spectral properties of inorganic, organic, biochemical substances and other complex substances prepared by established synthetic procedures that may have major scientific and technological applications.

1987 Editorial Board

J.L. Margrave
Rice Univ.

B.D. Smith
Washington Univ.

R.H. Wood
Univ. of Delaware

J.M. Prausnitz
Univ. of California

H.J. White, Jr.
Nat'l Bureau of Standards

1987 SUBSCRIPTION INFORMATION

1987 Volume 32 4 Issues Per Year	U.S.	Canada and Mexico	Europe Air Service Included	All Other Countries Air Service Included
ACS Members	\$ 29	\$ 33	\$ 38	\$ 39
Nonmembers	\$160	\$164	\$169	\$170

Subscriptions at ACS member rates are for personal use only. Foreign payment must be made in U.S. currency by international money order, UNESCO coupons, U.S. bank draft, or use your subscription agent. Above rates do not apply in Japan. Contact Maruzen Co., Ltd. Journal subscriptions start January 1987.

Call toll-free (800) 424-6747 or write:

American Chemical Society, 1155 Sixteenth St., NW,
Washington, DC 20036

**Get A World Of Precise, Accurate Data.
Subscribe To JCED Today!**

This publication is available on microfilm, microfiche, and electronically through Chemical Journals Online on STN International.

EDITOR: **GEORGE H. MORRISON**

ASSOCIATE EDITORS: **Klaus Biemann,**
Georges Gulochon, Fred E. Lytle,
Robert A. Osteryoung, John A. Smith

Editorial Headquarters

1155 Sixteenth St., N.W.
Washington, D.C. 20036
Phone: 202-872-4570
Teletype: 710-8220 151

Managing Editor: Sharon G. Boots

Associate Editors: Stuart A. Borman,
Rani A. George, Louise Voress

Assistant Editors: Mary D. Warner,
Grace K. Lee

Production Manager: Leroy L. Corcoran

Art Director: Alan Kahan

Staff Artist: Amy A. Meyer

Production Editor: Elizabeth E. Wood

Circulation: Cynthia G. Smith

Editorial Assistant, LabGuide: Joanne Mullican

Journals Dept., Columbus, Ohio

Associate Head: Marianne Brogan

Associate Editor: Rodney L. Temos

Advisory Board: Shier S. Berman, Brian S. Bidlingmeyer, Henry N. Blount, Gary D. Christian, Harry V. Drushel, Larry R. Faulkner, Peter R. Griffiths, Gary M. Hieftje, Nobuhiko Ishibashi, Mary A. Kaiser, David L. Nelson, Erno Pungor, Dennis Schuetzle, Nicholas Winograd, Edward S. Yeung, Andrew T. Zander

Instrumentation Advisory Panel: Howard G. Barth, Richard F. Browner, James B. Callis, Richard S. Danchik, Thomas C. Farrar, Joel M. Harris, John F. Holland, Ronald E. Majors, Linda B. McGown

The Analytical Approach Advisory Panel: Edward C. Dunlop, Robert A. Hofstadter, Wilbur D. Shults

Published by the
AMERICAN CHEMICAL SOCIETY
1155 16th Street, N.W.
Washington, D.C. 20036

Books and Journals Division

Director: D. H. Michael Bowen

Journals: Charles R. Bertsch

Production: C. Michael Phillippe

Research and Development: Lorrin R. Garson

Manuscript requirements are published in the January 1, 1987 issue, page 219. Manuscripts for publication (4 copies) should be submitted to ANALYTICAL CHEMISTRY at the ACS Washington address.

The American Chemical Society and its editors assume no responsibility for the statements and opinions advanced by contributors. Views expressed in the editorials are those of the editors and do not necessarily represent the official position of the American Chemical Society.

Alexander, A. J., 2484
Alexander, L. R., 2543
Auterinen, I., 2472

Ballschmiter, K., 2536
Barnhart, E. R., 2543
Bautz, D. E., 2534
Bekov, G., 2472
Bergmann, G., 2522
Bernius, M. T., 2463

Clayton, C. A., 2506
Cotter, M. L., 2533

Danielson, N. D., 2501, 2544
Davison, W., 2450

Elkins, P. D., 2506
Engelbach, R. J., 2541

Fuciarelli, A. F., 2484

Gampp, H., 2456
Garrison, A. A., 2541
Gill, J. B., 2543
Gilpin, R. K., 2460
Gohshi, Y., 2519
Green, V. E., 2543
Gregoire, D. C., 2479
Gross, M. L., 2527

Hann, C. J., 2460
Harbinson, T. R., 2450
Hines, J. W., 2506
Hood, W. H., 2468
Huang, S. K., 2527

Ingle, J. D., Jr., 2534
Issiki, K., 2491

Kaihara, A., 2496
Kearle, P., 2484
Kirkland, J. J., 2501
Kitamori, T., 2519
Krivan, V., 2476
Kuamoto, T., 2491

Lakomaa, E.-L., 2472

Ledford, E. B., Jr., 2527
Li, L., 2538
Likonen, J., 2472
Ling, Y.-C., 2463
Lloyd, J. R., 2533
Lubman, D. M., 2538

Maggio, V. L., 2543
Mamantov, G., 2541
Morrison, G. H., 2463

Nakagawa, T., 2496
Nakayama, E., 2491
Nicolaysen, L. C., 2543
Niemczyk, T. M., 2468

Othori, D., 2533
Oyler, A. R., 2533

Patterson, D. G., Jr., 2543
Petrick, K., 2476

Radaev, V., 2472
Raleigh, J. A., 2484
Rempel, D. L., 2527

Saltiel, J., 2515
Sawada, T., 2519
Sears, D. F., Jr., 2515
Sherman, J. H., 2544
Shibukawa, A., 2496
Sun, Y.-P., 2515
Suzuki, K., 2519
Swerev, M., 2536

Tanaka, H., 2496
Tsuji, F., 2491
Turner, L. K., 2463

von Oepen, B., 2522

Wehry, E. L., 2541

Yagi, K., 2496

Zilliacus, R., 2472
Zinn, P., 2522

Performance of Flowing and Quiescent Free-Diffusion Junctions in Potentiometric Measurements at Low Ionic Strengths

Terence R. Harbinson and William Davison*

The Freshwater Biological Association, The Ferry House, Ambleside, Cumbria LA22 0LP, United Kingdom

Reference electrodes having free-diffusion liquid junctions (FDJs) created in quiescent and flowing solutions of 10^{-4} mol kg^{-1} HCl were tested against a previously evaluated "reference" FDJ. Junctions formed in 0.5 and 1 mm bore Perspex T pieces performed as well as those formed in cylinders (within 0.1 mV, 0.002 pH) and were independent of solution dynamics and configurational variations. Rather than cylindrical symmetry, the primary prerequisite for an accurate stable liquid junction was that the two solutions should meet at a sharply defined stable boundary which is not subjected to irregular convective influences. Junction material, bore size, and the ionic strength of simple electrolytes had little effect on junction performance. Although alternative designs of reference electrodes with renewable FDJs performed less well, they were precise to 0.01 pH. It is suggested that the operational definition of pH should be modified to state explicitly that measurements made with FDJs conforming to some simple design criteria will provide a good estimate of pH.

Potentiometric measurements with ion-selective electrodes require the use of a reference electrode to provide a constant reference potential. The most commonly used reference electrode elements, based on silver-silver chloride (Ag/AgCl) and calomel ($\text{Hg}/\text{Hg}_2\text{Cl}_2$), give rise to few problems. Use of a bridge electrolyte between the reference element and the sample solution ensures a constant potential at the solid interface but introduces other uncertainties associated with the liquid junction formed between the bridge electrolyte and the sample solution. If the liquid junction potentials are the same in calibration and test solutions, they cancel one another; but if there is a difference in the two potentials, known as the residual liquid junction potential, an error is introduced into the potentiometric determination. When the pH of dilute solutions are measured (<0.1 mol kg^{-1}), the residual liquid junction potential is assumed to be zero (1). In practice, however, the liquid junction potential depends on how the junction is formed, whether flowing or static, constrained or open (2). Unpredictable potentials may develop if a liquid junction is formed in an ill-defined constraining element, such as the commonly used ceramic frit, especially if the test solution has a low ionic strength (<1 mmol kg^{-1}). Free-diffusion liquid junctions formed in a cylinder as a sharp boundary between bridge electrolyte and sample have been found to perform well (3). In this case if convection cannot occur, concentration gradients are confined to a single plane. When the British Standards and NBS pH scales have been compared, using a junction formed at a sharp boundary in a cylinder so that the solutions can freely diffuse into one another, they have been in good agreement (4).

The determination of pH is the most commonly used potentiometric measurement. In some circumstances, such as geochemical investigations (5) of low ionic strength waters, the measured pH is interpreted in terms of hydrogen ion

activity or concentration. In interlaboratory comparisons of pH measurements and in long-term environmental monitoring, it is essential that the absolute accuracy of the measurement can be guaranteed. One way to minimize sources of error would be to make the use of reference electrodes with stable liquid junctions (e.g. free-diffusion liquid junctions (FDJs)) mandatory for such investigations. As this would complicate routine measurements, it has been suggested (6) that FDJs could be used in a "reference" procedure to verify the suitability of other more practical electrode assemblies.

Unfortunately there has been little systematic investigation of the effects of junction geometry size or dynamics on junction performance. Early work (7-9) indicated that errors in potential difference of 1 mV or more (equivalent to 0.02 pH) existed between flowing and quiescent junctions for the system: HCl (10^{-1} mol dm^{-3})- KCl (10^{-1} mol dm^{-3}). Ferguson et al. (10) compared directly flowing and quiescent junctions and found that overall cell potential differences were higher at lower flow rates. These effects were found to be particularly pronounced at ionic strengths of 10^{-1} mol kg^{-1} . More recently Covington, Whalley, and Davison (11-13) have published designs of reference electrode (known here as CWD), based on forming FDJs in T pieces, which can be used in conventional dip cells or in flow cells. Both designs were shown to be superior to most commercial reference electrodes for determining the pH of dilute buffers and lake waters. Hach, Inc., USA, have produced a commercially available reference electrode with a renewable FDJ formed by using a syringe to extrude bridge electrolyte through a small bore tube (2). In this work the performance of liquid junctions with different configurations and dynamic properties has been tested. Most work was undertaken at low ionic strength, 10^{-4} mol kg^{-1} , where liquid junction problems are known to be particularly acute (2, 13, 14). Junctions were formed in T pieces of both Perspex and glass and tested against a previously described (14) "reference" FDJ of simple cylindrical geometry. Additionally, alternative previously reported (11, 15) designs of FDJs were tested against the "reference" FDJ and compared with the performance of the T pieces.

EXPERIMENTAL SECTION

Principles. As it is impossible to measure a single liquid junction potential (1), the performance of a liquid junction was tested by measuring the potential difference between it and a "reference" junction created in a 0.5-mm capillary. Two reference electrode elements, A and B, were connected via a bridge electrolyte of saturated KCl to each liquid junction as previously described (14). The measured emf, E , was therefore composed of the individual potentials of the reference electrode elements, E_R , and junctions, E_J

$$E = E_{RA} - E_{RB} + E_{JA} - E_{JB}$$

With the liquid junctions disconnected and a tap connecting the bridge electrolytes opened, it was possible to bypass the liquid junctions and obtain the bias potential, that is the potential difference between the two calomel reference electrode elements, $E_{\Delta R}$

$$E_{\Delta R} = E_{RA} - E_{RB}$$

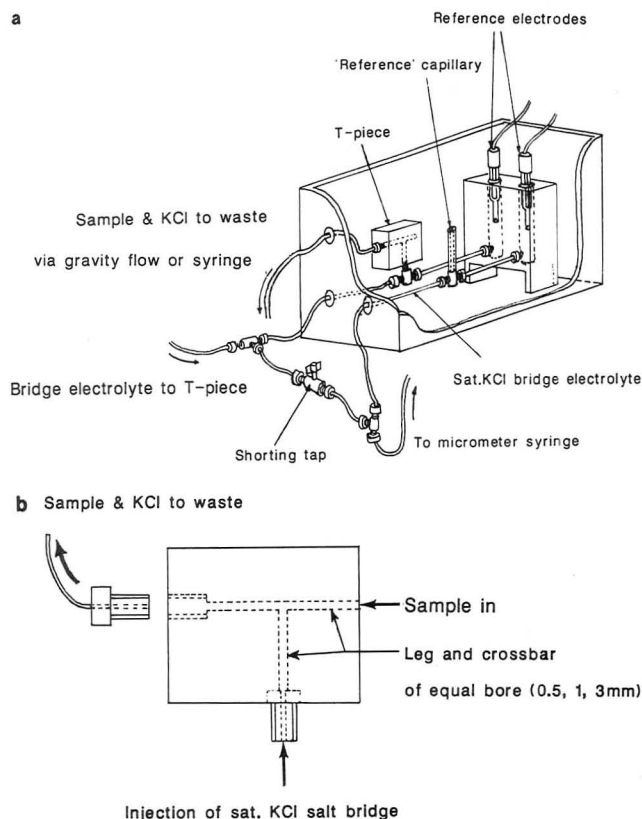


Figure 1. (a) Pictorial representation of the measuring vessel. The tank was filled with sample solution to a level where the capillary was covered. (b) Design of Perspex T piece used throughout this work for flowing and quiescent junctions.

The potential difference due to the liquid junctions, $E_{\Delta J}$, is then the difference between these two measured potentials

$$E_{\Delta J} = E - E_{\Delta R}$$

Practical Arrangement. The measuring cell containing the sample solution consisted of a rectangular glass tank (20 × 15 × 10 cm) which was fitted with a water jacket maintained at $20 \pm 0.1^\circ\text{C}$. T pieces of 0.5-, 1-, and 3-mm bore were machined from Perspex (Figure 1b) or blown from glass capillary. Perspex blocks housing the reference electrodes (Radiometer K4112 saturated KCl) and T pieces and capillary assemblies for the liquid junctions were contained within the tank (Figure 1a) and immersed in the sample solution. PTFE tubing (0.5-mm bore) carried the bridge electrolyte and provided connections to a micrometer syringe, which controlled the level of the liquid junction within the 0.5-mm glass capillary, and to a solution dispensing system used to define the liquid junctions in the T pieces. Three different dispensing systems were used: ganged syringes, a syringe pump (F. T. Scientific Ltd Perfusor VI), and micrometer syringes. The tubing connections and a shorting tap were located outside the cell. Extensive tests involving disconnection of the tap showed that there was no shorting of the circuit when the tap was closed. PTFE tubing was connected to one end of the crossbar of the T pieces so that sample solution could be withdrawn either by a siphoning mechanism (gravity "feed") or by a syringe. In some experiments, to test the performance of alternative renewable FJDs against the "reference" junction, the T pieces were replaced by either the CWD or Hach reference electrodes.

A magnetic stirrer unit under the tank was used to control a 5-cm magnetic follower. Switching on the stirrer could bring about a shift in potential, measured as $E(\text{stirred}) - E(\text{unstirred}) = E_s$, and also introduced high frequency perturbations, the amplitude of which gave E_n , known as the stirring noise. The whole assembly was enclosed in a Faraday cage.

The measuring equipment, emptying and filling the cell, and solution preparation was as previously described (14).

Measurement of the Calomel Bias Potential. The bias potential between the calomel reference elements was measured

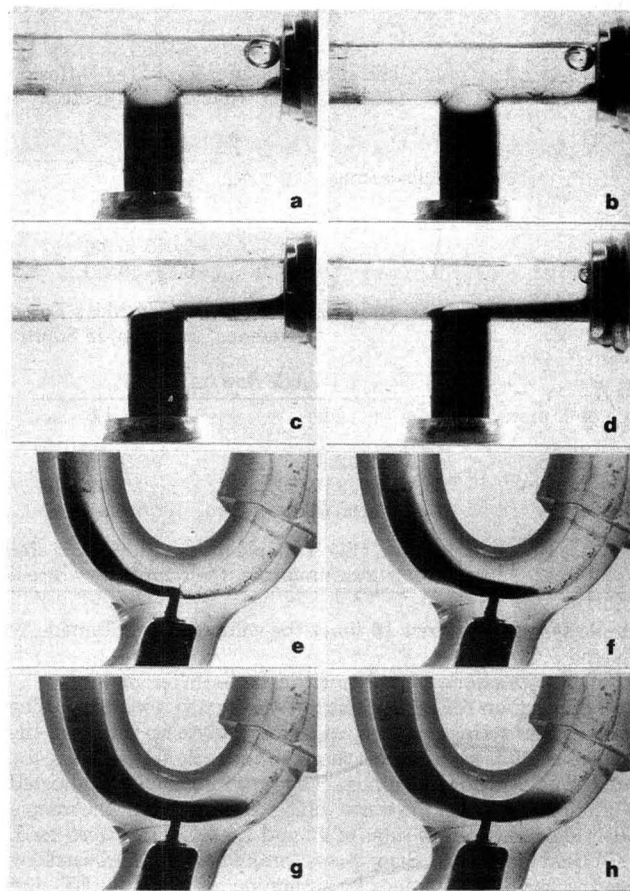


Figure 2. Photographs of a 3 mm bore T piece containing: (a) simple quiescent junction; (b) single flow junction; (c) ganged quiescent junction; (d) dual flow junction; (e)–(h) time-lapse photography performed with the CWD junction after $t = 0$ s (e), $t = 5$ s (f), $t = 15$ s (g), and $t = 25$ s (h). NOTE: The darker liquid at each junction is KCl containing KMnO_4 .

by opening the external shorting tap (Figure 1a) after forming an air bubble in the top of the "reference" capillary and in the crossbar of the T piece.

"Reference" Free-Diffusion Junction. The "reference" junction was formed, as described previously (14), by slowly expelling a bubble from the top of the capillary and withdrawing the newly formed junction to a depth of 5 mm within the capillary. It was allowed to stabilize for 5 min before being used in measurements. Comparison with a pH glass electrode showed that after the initial 5 min the drift in potential difference was $<0.01 \text{ mV min}^{-1}$. Unless otherwise stated this criterion was used to define the response time, R .

Formation of Liquid Junctions in T Pieces. Junctions were formed in several different ways and examined visually by adding KMnO_4 to the saturated KCl and photographing with a high magnification macrolens (Figure 2). In each case, and for each bore of T piece, two measurements were made upon a single day for five consecutive days, in order to examine within- and between-day variation. There were three different configurations of quiescent junctions formed between saturated KCl and $10^{-4} \text{ mol kg}^{-1} \text{ HCl}$.

(a) **Simple Quiescent Junction (SQ).** Two micrometer syringes were connected to the T piece. Bridge electrolyte was first pushed up the leg of the T and then sample was withdrawn along the crossbar.

(b) **Simple Quiescent Withdrawn Junction (SQW).** A simple quiescent junction was formed as in (a) and the junction withdrawn down the leg of the T piece to a depth of approximately 5 mm by a micrometer syringe.

(c) **Ganged Quiescent Junction (GQ).** Ganged, reciprocating syringes designed by Covington et al. (11) were used to form a junction. One syringe, connected to the leg of the T piece, was used to supply bridge electrolyte while the other simultaneously withdrew sample solution along the crossbar. In this work the

Table I

(a) Mean Potential Differences, $\bar{E}_{\Delta J}$, in mV, of Free-Diffusion Junctions of Various Configurations and Bores, Measured against a "Reference" Junction, in Quiescent Solutions of 10^{-4} mol kg $^{-1}$ HCl at 20 ± 0.1 °C

bore of T piece/mm	junction type		
	GQ ^a	SQ ^b	SW ^c
0.5	+0.015 (0.06) ^d	+0.035 (0.04)	-0.022 (0.02)
1	-0.045 (0.03)	-0.057 (0.02)	-0.030 (0.03)
3	+0.134 (0.04)	+0.062 (0.04)	+0.088 (0.05)

(b) Effect of Flow Rate, and Bore of T Pieces upon Mean Potential Differences in mV of Free-Diffusion Junctions, Measured against a "Reference" Junction, in Solutions of 10^{-4} mol kg $^{-1}$ HCl at 20 ± 0.1 °C

bore of T piece/mm	single flow/mL min $^{-1}$		dual flow/mL min $^{-1}$		
	12	1.5	0.2 (12)	0.2 (2)	5 (5)
0.5	+0.062 (0.06) ^d	+0.043 (0.05)	+0.026 (0.03)	-0.017 (0.04)	+0.041 (0.02)
1	+0.009 (0.03)	-0.030 (0.02)	+0.039 (0.02)	+0.021 (0.05)	+0.015 (0.05)
3	-0.108 (0.01)	+0.014 (0.06)	-0.054 (0.02)	-0.024 (0.02)	-0.060 (0.05)

^a GQ is ganged quiescent. ^b SQ is simple quiescent. ^c SW is simple withdrawn. ^d Standard deviations (9 degrees of freedom) are given in parentheses. ^e In dual flow measurements, the sample flow rate is in parentheses.

sample syringe withdrew 10 times the volume of simultaneously injected KCl.

Flowing junctions were formed in three different ways.

(a) Single Flow (SF). The junction was formed initially by using a micrometer syringe to push bridge electrolyte up the leg of the T piece. Sample solution was then continuously flowed along the crossbar using a simple siphon. The flow rate could be adjusted by altering the bore of the waste tubing or the height of the sample collection vessel. Flow rates of 12 and 1.5 mL min $^{-1}$ were used.

(b) Dual Flow (DF). Sample was continuously withdrawn along the crossbar of the T piece by siphoning action as for SF, and at the same time bridge electrolyte was continuously replenished with a syringe pump. Initially, bridge electrolyte was flowed at 0.2 mL min $^{-1}$, while the sample flow rate was varied between 2 and 12 mL min $^{-1}$, further experiments were then performed with both solutions flowing at 5 mL min $^{-1}$.

Dual flow measurements were also made with a 1 mm bore Perspex T piece in high ionic strength solutions (5×10^{-1} mol dm $^{-3}$ NaCl + 10^{-4} mol dm $^{-3}$ HCl). Both bridge electrolyte and sample were flowed at various rates up to 5 mL min $^{-1}$, in order to repeat the work of Ferguson et al. (10). These experiments were performed in triplicate upon a single day.

Effect of T Piece Material upon Junction Performance.

There is the possibility, especially in flowing solutions, that the material of the structure in which the liquid junction is created may affect the measured potential by developing a surface charge. Therefore some additional measurements were made, replacing the Perspex T junction by a 1-mm glass T piece. Only three types of junction were tested: the simple quiescent, single flow (flow rate 12 mL min $^{-1}$), and dual flow (sample flow 12 mL min $^{-1}$, bridge electrolyte flow 0.2 mL min $^{-1}$). Each experiment was performed in triplicate upon a single day using 10^{-4} mol kg $^{-1}$ HCl as the sample solution.

Performance of the CWD and Hach Electrodes. A reference electrode with a renewable FDJ designed by Covington, Whalley, and Davison (11) and previously used for measuring the pH of lake water (6) was tested against the "reference" junction in solutions of 10^{-4} mol kg $^{-1}$ HCl. Ganged syringes were used to renew the junction of the CWD electrode, and duplicate measurements were made on a single day and on four consecutive days.

A Hach electrode (15) was also tested against the "reference" junction. Replicate measurements were performed within a day by using the commercially supplied filling solution containing glycerol and also using saturated KCl, saturated with AgCl, as the bridge electrolyte. Experiments were performed in 10^{-4} mol kg $^{-1}$ HCl solutions and, for each filling solution, five measurements were made upon a single day.

RESULTS AND DISCUSSION

Calomel Bias Potential. The reproducibility of the bias potential between the two calomel electrode elements, which was measured before each experiment, gives an estimate of

Table II. Mean Response Times (min) for FDJs Formed in Perspex T Pieces Using Single Flow and Dual Flow Solutions^a

bore of T piece/mm	single flow/mL min $^{-1}$		dual flow/mL min $^{-1}$		
	12	1.5	0.2 (12)	0.2 (2)	5 (5)
0.5	4	2.6	1	2	1
1	1.5	1	4	1.5	1
3	2	2.4	1	1.5	1.5

^a In dual flow, sample flow rate is in parentheses.

the precision associated with factors other than liquid junctions. The variation in bias potential, measured within each day was 0.01–0.02 mV, while between separate days it was as great as 0.03–0.05 mV. At ambient temperatures (approximately 20 °C in this work) the potential of the K4112 calomel electrode changes by 0.06 mV for each 0.1° change in temperature. Therefore, the small observed drifts in bias potential are appropriate to temperature control to ± 0.1 °C. Potential shifts associated with the liquid junctions are only considered significant if they exceed the bias potential errors.

Configuration of Static Liquid Junctions. Table Ia shows mean potential differences, $\bar{E}_{\Delta J}$, associated with liquid junctions, of different geometric configuration constructed in T pieces of three different bores. Within- and between-day variations were less than or similar to the calomel bias potential drift and therefore insignificant. There is no systematic or significant variation of $\bar{E}_{\Delta J}$ with junction configuration, all but one value lying within 0.1 mV of the "reference" junction. Although the absolute magnitude of $\bar{E}_{\Delta J}$ increased with increasing bore size, the changes in sign and comparable precision for all bores suggests that the trend is not significant.

As response times did not vary significantly with junction configuration, mean response times were calculated for each bore. They were 2.3 min for the 0.5-mm T pieces and 1.5 min for the 1-mm and 3-mm T pieces.

In stirred solutions the stirring noise, E_n , was found to be consistently less than the minimum value measurable from the chart recorder of ± 0.035 mV and independent of junction configuration or the bore of T piece. Shifts due to stirring were always less than 0.05 mV and in most cases 0.2 mV.

Dynamic Liquid Junctions. No significant or systematic variation in $\bar{E}_{\Delta J}$ was observed with change in flow rate or T-piece bore for either dual or single flowing solutions (Table Ib). The magnitude and precision of $\bar{E}_{\Delta J}$ values were similar

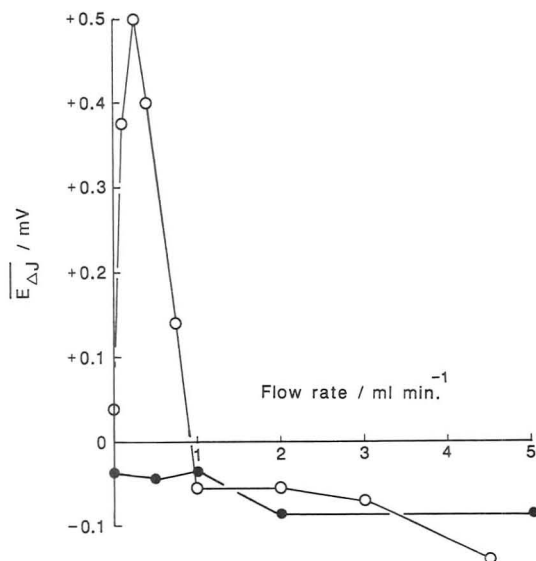


Figure 3. Variation, with flow rate of bridge electrolyte and sample, of the mean potential difference between liquid junctions: (●) this work (5×10^{-1} mol dm $^{-3}$ NaCl + 10^{-4} mol dm $^{-3}$ HCl), (○) Ferguson et al. (10^{-1} mol dm $^{-3}$ HCl). In all cases the flow rates of the two solutions were equal.

Table III. Performance of Junctions Formed in a 1 mm Glass T Piece, in Simple Quiescent, SQ, Single Flow, SF, and Dual-Flow, DF, Configurations^a

junction type	$E_{\Delta J}/\text{mV}^b$	E_s/mV^c	E_n/mV^d	R/min^e
SQ	-0.008	-0.05	$<\pm 0.035$	1
	-0.021	0.00	$<\pm 0.035$	1
	-0.020	+0.05	$<\pm 0.035$	1
SF/12 mL min $^{-1}$	+0.064	-0.05	± 0.035	1
	+0.021	0.00	$<\pm 0.035$	2
	+0.048	0.00	$<\pm 0.035$	2
DF/0.2 (12) mL min $^{-1}$	+0.010	-0.05	$<\pm 0.035$	1
	+0.021	-0.05	$<\pm 0.035$	1
	-0.010	0.00	$<\pm 0.035$	2

^a In the latter case sample flow is in parentheses. Each experiment was performed in triplicate upon a single day, and was measured at 20 ± 0.1 °C on solutions of 10^{-4} mol kg $^{-1}$ HCl. ^b $E_{\Delta J}$ is the potential difference with respect to the "reference" junction. ^c E_s is the shift in potential on stirring. ^d E_n is the noise associated with stirring. ^e R is the response time.

to those observed for quiescent junctions.

Mean response times were usually less than 3 min and independent of flow rate or bore (Table II).

At low flow rates, ca. 1.5 mL min $^{-1}$, the noise due to stirring, E_n , was consistently less than the chart recorder discrimination of ± 0.035 mV. At higher flow rates, the flow of the solution introduced noise, as even in unstirred solutions fluctuations of ± 0.01 mV were observed on the multimeter. Stirring shifts, which were independent of flow rate or T-piece bore, were always less than 0.1 mV and generally ca. 0.05 mV.

To compare our data with those of Ferguson et al. (10) measurements were made over a range of flow rates on a sample solution with an ionic strength of 5×10^{-1} mol kg $^{-1}$. Contrary to previous observations, no significant or systematic change in $E_{\Delta J}$ was observed as the flow rate changed (Figure 3). For the 0 mL min $^{-1}$ data point, junctions were created with ganged syringes because this junction was the stationary analogue of the dual flow configuration (Figure 2).

Liquid Junctions Created in Glass T Pieces. To investigate possible effects of the construction material on liquid junctions, measurements were made on 1 mm glass T pieces in dual flow, single flow, and simple quiescent configurations (Table III). Values of stirring noise, E_n , shift, E_s , and response

Table IV. Performance, in Duplicate on Four Separate Days, of the CWD Electrode Relative to the "Reference" Junction in Solutions of 10^{-4} mol kg $^{-1}$ HCl at 20 ± 0.1 °C

	$E_{\Delta J}/\text{mV}^a$	E_s/mV^b	E_n/mV^c	$E_{\Delta J}/\text{mV}^d$	R/min^e
day 1	+0.538	-0.075	$<\pm 0.035$	+0.548	3
	+0.582	-0.05	$<\pm 0.035$	+0.560	5
day 2	+0.588	+0.15	± 0.035	+0.532	12
	+0.559	+0.175	± 0.035	+0.544	8
day 3	+0.564	-0.100	± 0.035	+0.535	8
	+0.571	-0.175	± 0.035	+0.598	7
day 4	+0.572	+0.05	± 0.035	+0.537	6
	+0.599	+0.05	± 0.035	+0.584	8

^a $E_{\Delta J}$ is the potential difference with respect to the "reference" junction. ^b E_s is the shift in potential on stirring. ^c E_n is the noise associated with stirring. ^d After allowing the potential difference to drift for periods of up to 20 minutes the liquid junction was reformed. ^e The response time, R , is the time taken for the drift of an initially formed junction to be no more than 0.03 mV min $^{-1}$.

Table V. Performance of Hach Electrodes against the "Reference" Junction in Solutions of 10^{-4} mol kg $^{-1}$ HCl at 20 ± 0.1 °C^a

(a) Hach Electrode Filled with Saturated KCl (Saturated AgCl)

$E_{\Delta J}/\text{mV}^b$	E_s/mV^c	E_n/mV^d	R/min^e
+1.028	-0.232	$<\pm 0.035$	4
+0.204	0.000	$<\pm 0.035$	2
+0.211	-0.050	$<\pm 0.035$	5
+0.491	0.000	$<\pm 0.035$	2
+0.602	+0.067	$<\pm 0.035$	2

(b) Hach Electrode Filled with the Commercial Solution of 2.4 mol dm $^{-3}$ KCl (Saturated AgCl) in 40% Glycerol

$E_{\text{measd}}/\text{mV}^f$	E_s/mV	E_n/mV	R/min
+41.972	-0.130	$<\pm 0.035$	5
+42.717	0.00	$<\pm 0.035$	5
+43.716	-0.016	$<\pm 0.035$	12
+43.599	+0.079	$<\pm 0.035$	8
+44.352	+0.024	$<\pm 0.035$	5

^a All measurements were made within a single day. ^b $E_{\Delta J}$ is the potential difference with respect to the "reference" junction. ^c E_s is the shift in potential on stirring. ^d E_n is the noise associated with stirring. ^e R is the response time. ^f E_{measd} is the directly measured potential difference.

time, R , were similar to those observed for the Perspex counterpart, and no significant differences in performance were observed between quiescent or flowing junctions.

Performance of Reference Electrodes with Renewable FDJs. (a) *CWD Electrode.* The potential difference measured after a few minutes between the CWD electrode with renewable FDJ and the reference junction (Table IV) was consistently large ($+0.57 \pm 0.04$ mV). This fairly constant error showed no appreciable day to day variation. Noise due to stirring, E_n , was less than ± 0.05 mV to ± 0.18 mV.

$E_{\Delta J}$ was never completely stable and even after 2 h was still drifting at 0.03 mV min $^{-1}$. Re-forming the liquid junction (Table IV) generally brought $E_{\Delta J}$ to within 0.05 mV of the value measured within a few minutes. Response times for this junction (defined as a drift of 0.03 mV min $^{-1}$) were highly variable.

(b) *Hach Electrode.* A potential difference of +44.3 mV was measured between the Ag/AgCl electrode of the Hach arrangement and the calomel electrode of the "reference" junction when saturated KCl was used as a common bridge electrolyte and filling solution. The accepted potential difference between saturated KCl calomel and silver/silver chloride electrodes is 45 mV (1) indicating that even though only a simple chloridized silver wire is employed in the Hach

Table VI. Differences between the Mean Potential Differences in mV, $\bar{E}_{\Delta J}$, Obtained with Flowing (SF and DF) and Quiescent (SQ and GQ) Junctions of the Same Configuration^a

bore of T piece/mm	$\Delta \bar{E}_{\Delta J}(\text{SF} - \text{SQ})/\text{mV}$		$\Delta \bar{E}_{\Delta J}(\text{DF} - \text{GQ})/\text{mV}$		
	12 mL min ⁻¹ ^b	1.5 mL min ⁻¹	0.2 (12) mL min ⁻¹	0.2 (2) mL min ⁻¹	5 (5) mL min ⁻¹
0.5	+0.027	+0.078	+0.011	-0.032	+0.026
1	+0.066	+0.027	+0.084	+0.066	+0.060
3	-0.170	+0.074	-0.188	-0.158	-0.148

^aSF is single flow (sample flowing only). SQ is simple quiescent. DF is dual flow (both sample and bridge electrolyte flowing). GQ is ganged quiescent. In the (DF - GQ) column sample flow rates are in parentheses. ^bFlow rates.

electrode, the reference element performs well.

$E_{\Delta J}$ varied appreciably (Table Va) over the five measurements. The mean value of $E_{\Delta J}$ was +0.51 mV with a 95% confidence interval of ± 0.42 mV. Stirring shifts, E_s , were also variable, -0.23 to +0.07 mV, but, stirring noise, E_n , was relatively small ($< \pm 0.035$ mV). Measurements with a Hach electrode were never completely stable and the estimated mean response time of 3 min was determined when the potential drift was approximately 0.05 mV min⁻¹.

Replacing the saturated KCl with the commercially supplied glycerol/2.4 mol dm⁻³ KCl/saturated AgCl mixture in the Hach electrode half-cell prevented measurement of bias potentials. Only the directly measured potential difference, E , between the Hach and "reference" junction could be obtained (Table Vb). Opening the shorting tap allowed a liquid junction to form between the different bridge electrolytes and the resultant potential was not reproducible. The mean measured potential difference, E , of +43.27 mV was very variable (95% confidence interval of ± 1.15 mV). The poor junction performance may be due to the glycerol additive changing the structure of the junction or increasing the viscosity of the bridge electrolyte and so reducing ionic mobility (16). Stirring shifts were between -0.13 mV and +0.08 mV, but stirring noise was consistently less than ± 0.035 mV. The measured potential difference was less prone to drift when using the recommended filling solution; over 134 min the average drift was < 0.01 mV. However, response times based on this drift varied considerably.

GENERAL DISCUSSION

Earlier work (14) showed that the "reference" junction used in this work is reproducible to 0.1 mV or 0.002 pH. The variability of the bias potential gives an assessment of other errors as 0.02 mV within a day and up to 0.05 mV between days. As the measured potential differences between junctions were within these limits, there is no significant difference in performance (Table I) between "reference" junctions formed in a cylinder and quiescent and flowing T junctions.

Ganged quiescent junctions are the quiescent analogue of dual flowing junctions and simple quiescent junctions are analogous to single flowing junctions. The performance of these flowing and quiescent junctions can therefore be compared directly. Mean potential differences, $\bar{E}_{\Delta J}$, for quiescent junctions were obtained, by subtraction, from the equivalent data obtained for flowing junctions (Table VI). In all cases the absolute magnitude of $\bar{E}_{\Delta J}$ systematically increased as the bore of the T piece increased. The difference was only appreciably greater than the experimental errors for the 3 mm bore T piece, where it was equivalent to 0.002-0.004 pH. These results indicate that flowing or quiescent FDJs created in 0.5 and 1 mm capillary T pieces would not contribute significantly to any error in measured pH in low ionic strength solutions. Increasing the flow rate of sample and bridge electrolyte through a 1 mm bore T piece did not affect $\bar{E}_{\Delta J}$ significantly. This result conflicts with the work of Ferguson et al. (10) (Figure 3), who observed that the potentials of junctions formed in slowly flowing solutions were different

to those of quiescent junctions. The junctions used by Ferguson et al. (10) were created in 9 mm bore tubing which could have allowed uncontrolled mixing of the bridge electrolyte and sample at low flow rates. Our results indicate that there is no difference between quiescent and flowing junctions formed in 1-mm T pieces, or in a 0.5-mm cylinder for simple binary electrolytes with ionic strength ranging from 10⁻⁴ to 0.5 mol kg⁻¹.

Slight noise which is introduced at high flow rates is insignificant (< 0.001 pH) for practical pH measurement. Response times for all FDJs, except for the CWD and Hach designs, were generally less than 3 min and so should not hamper dip-mode pH measurement of low ionic strength solutions where equilibration times of 2-4 min are usually allowed. However, they may be a limiting factor in designing systems for rapid measurement, perhaps based on flowing junctions.

Changing the material of the T piece from Perspex to glass did not affect the performance of FDJs. Although Perspex and glass appear to be satisfactory, not all materials may be suitable because extraneous potentials may be introduced by the charge on capillary walls.

The CWD electrode with renewable FDJ did not perform as well as the other T pieces, often giving results in quiescent solutions which would contribute an error of 0.01 pH. Other workers (17) have also reported problems when using this design. Time-lapse photography of the solutions in the junction (Figure 2) showed that the waste mixture of KCl and sample, which was denser than the sample, could flow down the perpendicular exit port and create an ill-defined junction in the sample tube rather than at the T piece. The indeterminate nature of the junction probably accounts for the potential drift of 0.03 mV min⁻¹ which amounts to an error of 0.06 pH over a 2-h period. In comparison a T junction used in this work created by ganged syringes typically drifts at a rate of 0.002 mV min⁻¹ which, after 2 h, would contribute a negligible error of 0.004 pH.

Like the CWD electrode, the Hach electrode did not perform as well as the T-piece junctions. Its potential output was never completely stable. With a common bridge electrolyte of saturated potassium chloride, $E_{\Delta J}$ values varied by ± 0.42 mV (± 0.008 pH), well outside errors attributable to the reference junction. The liquid junction is formed at the end of an upturned plastic tube. It is analogous to J junctions, described by Guggenheim (3) as sharp junctions of indefinite type, which were found to vary in potential by several millivolts, and were thought to be unstable owing to the lack of cylindrical symmetry at the junction. Poorly defined junctions, similar to that used in the Hach electrode, were created with a 0.5-mm capillary. When a junction was formed at the tip of the capillary, rather than withdrawing it, the potential output was erratic (Figure 4), as for the Hach electrode. Stirring the solution exacerbated the errors, presumably by introducing uncontrolled mixing due to spillage of the bridge electrolyte and oscillation of the liquid junction.

Although this work has demonstrated that configurational or dynamic variation of FDJs has little effect upon their

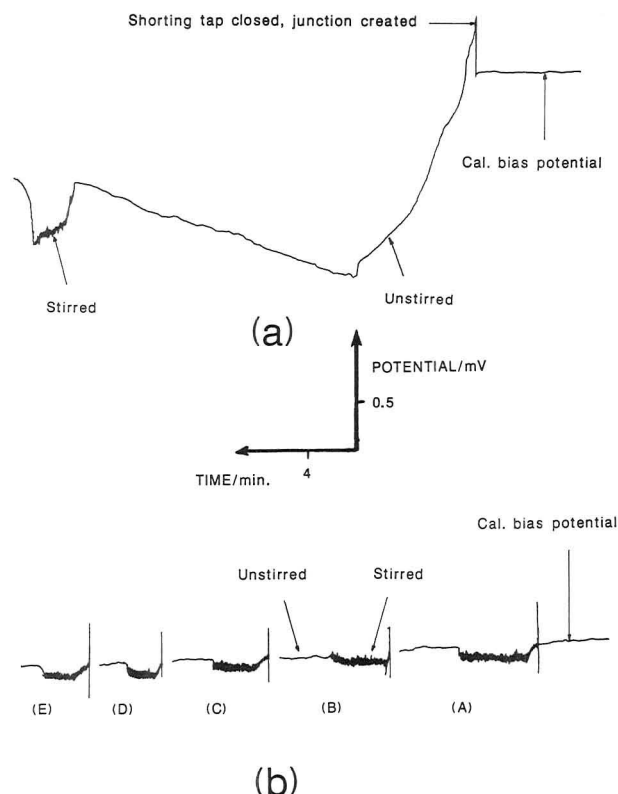


Figure 4. (a) Performance of a liquid junction which was allowed to form at the end of a 0.5 mm capillary. (b) Performance of liquid junctions formed within a 0.5-mm capillary, in five separate solutions of 10^{-4} mol kg^{-1} HCl, at junction depths of (A) 2 mm, (B) 5 mm, (C) 10 mm, (D) 15 mm, and (E) 20 mm.

performance, it would be incorrect to assume that problems are not encountered when using FDJs. The particular problems associated with high impedance measurements, which demand special attention to earth contacts and careful screening from stray electrical fields, are exacerbated when measurements are made in poorly conducting low ionic strength solutions. In this work, where the electrodes and connecting tubes were immersed in the sample solution, poor plumbing of bridge electrolyte could result in unstable, drifting potentials. Even the smallest solution path between sample solution and bridge electrolyte could form separate, ill-defined liquid junctions.

The good performance of flowing junctions is dependent on a smooth flow of solution. When syringe and HPLC pumps were used in place of the gravity-fed syphon to withdraw sample, irreproducible and fluctuating potentials (± 1.5 mV) were observed. Experiments with KMnO_4 showed that this was due to a pulsing action causing a poorly defined junction.

IMPLICATIONS FOR MEASUREMENTS

Free-diffusion junctions formed in T pieces can provide a stable potential in low ionic strength solutions that is indistinguishable from the potential developed by a free-diffusion junction formed in a cylinder. Flowing junctions perform just as well as their quiescent counterparts and, providing the junction is well-defined without any extraneous convective effects, it appears to matter little whether the junction is formed in a cylinder, in a T piece, or along the length of a tube. Evidently the long-held view (3) that cylindrical symmetry is necessary to ensure good junction performance is not true. These general conclusions should be applicable to most solutions of low-ionic strength such as boiler-feed waters, freshwaters and rainwaters and should also apply to moderately high ionic strength solutions of simple inorganic electrolytes. Further work is needed to test their performance in solutions containing organic components which may modify

the structure of the liquid junction (16). Practical pH measurements using FDJs of various design have already been made (6, 11, 12, 18–20). This work has validated the use of such devices and established criteria for future development of more practical pH and ion-selective electrode assemblies based on free-diffusion liquid junctions.

FDJs must be well-defined so that the junction cannot be perturbed in any way. In this sense a flowing junction has some inherent advantages because the diffusion of the separate solutions into one another represents a true steady state. So-called quiescent junctions are in fact continually changing as the two solutions diffuse into one another. Therefore the potential will ultimately drift and the junction is more prone to extraneous convective effects. If the size or geometry of the tubing is outside the limits tested in this work, further verification of the junction will be necessary. Similarly, very fast flow rates can only be used if the assembly is tested against a proven design. By use of simple T or cylindrical junctions, the measurement of the pH of low ionic strength solutions may be performed with a precision of ± 0.001 pH. If the electrodes are calibrated with standard buffer solutions the pH should be interpretable in terms of the hydrogen ion activity to 0.02 pH (21). Poor design will adversely affect the performance as shown by the CWD and Hach junctions, but even these gave results which were better than those commonly found for commercial electrodes with ceramic frit junctions (6). Nevertheless there is a clear need for a well-designed free diffusion junction which can be used for making simple pH measurements in the traditional dip-mode. Encouraging new designs are now emerging (22).

This work was necessary because the definitions of pH (1, 4, 21) do not give guidelines for the type of junction which should be used for a real pH measurement of a solution of unknown pH. Admittedly, a free diffusion junction has been used to compare BS and NBS pH scales. The pH values of a series of buffer solutions, measured against a phthalate buffer using a FDJ, agree well with values of the pH evaluated from cells without liquid junctions (1, 4). The good agreement between the two scales validates the use of a free-diffusion junction for most buffer solutions (4) and recent work has shown that FDJs are suitable for low-ionic strength (11, 12), estuarine water (20), and seawaters (19). In this work we have established some design criteria and in particular have substantiated the use of flowing junctions and other designs which depart from cylindrical geometry. The time may well be appropriate to extend the operational definition of pH so that it explicitly states the type of junction which can be relied upon to produce a good estimate of pH. Such a junction cannot be of the constrained type because it is not feasible to precisely define the geometry, but it could be a FDJ which conforms to some simple design criteria. This would not preclude pH measurements being made with other junction designs but it would provide a standard reference procedure so that measurements made on an unknown solution, such as a natural water, using a commercial electrode with a fritted junction could be checked with a standard, but practical, cell.

ACKNOWLEDGMENT

We thank Professor A. K. Covington for his continued interest and critical comments.

LITERATURE CITED

- (1) Bates, R. G. *Determination of pH*; Wiley: New York, 1964.
- (2) Illingworth, A. J. *Biochem. J.* **1981**, *195*, 259.
- (3) Guggenheim, E. A. *J. Am. Chem. Soc.* **1930**, *52*, 1315.
- (4) Covington, A. K.; Bates, R. G.; Durst, R. A. *Pure Appl. Chem.* **1985**, *57*, 531.
- (5) Stumm, W.; Morgan, J. J. *Aquatic Chemistry*, 2nd ed.; Wiley: New York, 1981.
- (6) Davison, W.; Woof, C. *Anal. Chem.* **1985**, *57*, 2567.
- (7) Roberts, E. J.; Fenwick, F. *J. Am. Chem. Soc.* **1927**, *49*, 2789.
- (8) MacInnes, D. A.; Yeh, Y. L. *J. Am. Chem. Soc.* **1921**, *43*, 2563.

- (9) Chloupek, J. B.; Danes, V. Z.; Danwsova, B. A. *Collect. Czech. Chem. Commun.* **1933**, *5*, 469, 527.
- (10) Ferguson, A. L.; Van Lente, R.; Hitchens, K. J. *Am. Chem. Soc.* **1932**, *54*, 1285.
- (11) Covington, A. K.; Whalley, P. D.; Davison, W. *Anal. Chim. Acta* **1985**, *169*, 221.
- (12) Covington, A. K.; Whalley, P. D.; Davison, W. *Analyst (London)* **1983**, *108*, 1528.
- (13) Covington, A. K.; Whalley, P. D.; Davison, W. *Pure Appl. Chem.* **1985**, *57*, 877.
- (14) Davison, W.; Harbinson, T. R. *Anal. Chim. Acta* **1986**, *187*, 55.
- (15) Ersson, E. K. *Vatten* **1985**, *41*, 266.
- (16) Van den Berg, L. *Anal. Chem.* **1960**, *32*, 628.
- (17) Jones, C.; Marsicano, F.; Williams, D. R. *Sci. Total Environ.* **1987**, *64*, 211.
- (18) Howson, M. R.; House, W. A.; Pethybridge, A. D. *Analyst (London)* **1986**, *111*, 1215.
- (19) Culberson, C. In *Marine Electrochemistry*; Whitfield, M., Jagner, D., Eds.; Wiley: New York, 1981.
- (20) Whitfield, M.; Butler, R. A.; Covington, A. K. *Oceanol. Acta* **1985**, *8*, 423.
- (21) Bates, R. G. *CRC Crit. Rev. Anal. Chem.* **1981**, *10*, 247.
- (22) Dohmer, R. E.; Wegmann, D.; Morf, W. E.; Simon, W. *Anal. Chem.* **1986**, *58*, 2585.

RECEIVED for review February 6, 1987. Accepted June 15, 1987. Financed by the Surface Water Acidification Programme of the Royal Society.

Investigation of pH-Dependent Complex Equilibria at Low Ligand to Metal Ratio by Nonlinear Least-Squares Fit to Linear-Sweep or Cyclic Voltammetric Data

Harald Gampp

Institut de Chimie, Université de Neuchâtel, CH-2000 Neuchâtel, Switzerland

Metal-ligand equilibria can be studied voltammetrically provided the chemical equilibria are rapid and one of the equilibrium species can be reversibly reduced/oxidized. In the case of strong complexation, the use of voltammetry is no longer limited by the need to work with an excess of ligand. Stability constants are straightforwardly determined from data obtained at low ligand to metal ratio by using least-squares and simulation methods. Specifically, the common case of pH-dependent equilibria is discussed, where the experimental data are obtained from voltammetric/pH potentiometric titrations. Synthetic data show the effect of stability constants on peak potentials and currents. As a chemical example, the complexation of copper(II) by oxalate is studied.

Voltammetric techniques are frequently used in order to study metal-ligand equilibria in solution. For the common case of a reversible electrode process and of rapid chemical equilibria, the only effect of complexation is a shift of the voltammetric wave provided the ligand is present in excess over the metal. The basis of the respective methods for determining equilibrium constants is that under these conditions the observed shift of the current-potential curve is a simple function of the concentration of the ligand in the bulk solution and of the stability constants (ref 1 and further references therein). Early applications were restricted to single equilibria (2) and later it was shown that extension to multiple equilibria involving one (3) or several ligands (4) is equally possible. Data evaluation using either graphical (3) or least-squares methods (5-7) is straightforward and a detailed error analysis has been given (8).

However, it will not always be possible to study an equilibrium system in the presence of excess ligand, e.g. because the ligand may not be sufficiently soluble. A situation where it is not desirable to use the ligand in excess occurs in the case of stepwise formation of very stable complexes ML_i ($i = 1, 2, \dots, p$): For ligand to metal ratios greater than p the species ML_p will be formed almost exclusively and only the p th equilibrium could be studied accordingly. Current-potential curves obtained under conditions of nearly stoichiometric or

substoichiometric ligand to metal ratio may have shapes which are different from those expected for reversible systems (1) as has been shown for polarography (9, 10) and cyclic voltammetry (CV) (11, 12).

Recently, Savéant and Xu have presented a theoretical study of the effect of ligand concentration and of the stability constant on linear-sweep voltammograms for the case of a metal ion which is reversibly reduced and which forms a 1:1 complex with a ligand (13). They also showed working curves which allow one to determine the value of the stability constant from individual voltammetric curves.

For the case of a metal ion forming both 1:1 and 1:2 complexes Philp and co-workers reported simulated cyclic voltammograms (11, 12, 14) and differential pulse polarograms (15) and discussed the influence of stability constants and ligand to metal ratio f on both shapes and positions of the current-potential curves. Using a trial-and-error procedure, they were able to estimate stability constants by fitting calculated to experimental cyclic voltammograms (11, 12).

Thus, in the case of multiple equilibria the stability constants do affect the voltammetric curves. The magnitude of this effect depends not only on the values of the stability constants but also on the ligand to metal ratio f . Accordingly, f should be varied in a voltammetric equilibrium study. However, if f is small there is no simple relation between the current-potential curves and the stability constants and the bulk concentrations of metal and ligand (8).

It is the purpose of this paper to show that equilibrium constants can be straightforwardly determined from voltammograms obtained at low ligand to metal ratio f by using a nonlinear least-squares method in combination with a simulation program. Specifically, the common case of a pH-dependent equilibrium system will be discussed where an obvious way to change f consists in varying the pH of a given solution of metal and ligand. As a chemical example, the complexation of copper(II) by oxalate is studied by combined cyclic voltammetric-pH titration.

EXPERIMENTAL SECTION

Cyclic voltammograms were obtained with a potentiostat (Metrohm E506), a signal generator (Metrohm E612), and an x-y recorder (Hewlett-Packard 7040A). A standard three-electrode

arrangement was used with a Pt-coil counter electrode, a saturated calomel (SCE) reference electrode, and a hanging mercury drop working electrode (HMDE, Metrohm).

pH was measured with a combined glass electrode and a pH meter (Metrohm 632); buffers of pH 4.00 and 7.00 (Metrohm) were used for calibration.

A pH-potentiometric titration of oxalic acid (1.48 mM) with NaOH (0.4 M) was carried out and the pK of the ligand was determined by using the program TITFIT (16).

For the CV-pH titrations two different solutions were prepared: (a) $[Cu^{2+}] = 0.182$ mM, $[Ox^{2-}] = 0.191$ mM; (b) $[Cu^{2+}] = 0.241$ mM, $[Ox^{2-}] = 0.124$ mM. In each experiment HNO_3 (0.02 and 0.2 M) was stepwise added to 25 mL of the respective solution in order to vary the pH between 8 and 1. After each addition of acid both the cyclic voltammogram and the pH were measured.

Experiments were carried out in a titration vessel thermostated at 298 K under N_2 in aqueous solution of constant ionic strength ($I = 0.50$ M, KNO_3).

Voltammograms were recorded at 0.1 V s^{-1} scan rate with an electrode surface of 0.014 cm 2 .

Analytical grade chemicals and doubly distilled water were used throughout.

DATA REDUCTION

Simulation of Cyclic Voltammograms. Calculations were made by using the explicit method of Feldberg (17) as outlined in ref 1. For a given set of parameters which define the electrochemical experiment (initial and switching potential, potential step size) and the chemical system (stability constants, total concentrations of metal and ligand, pH), the program calculates the (adimensional) current ψ for each value of the (adimensional) potential ξ .

The following assumptions are made: (1) The free metal ion is reversibly reduced at a planar microelectrode; other electroactive species do not occur. (2) The chemical processes are sufficiently fast that equilibrium is always established. (3) All diffusion coefficients are equal. (4) The pH of the solution does not change during the potential scan, not even near the electrode surface. (5) With the exception of the proton, activities are replaced by concentrations.

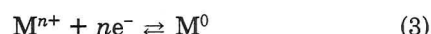
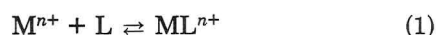
A similar simulation program has been described by Philp and co-workers (11) and more details can be found in their article.

Determination of Stability Constants from CV-pH Titrations. A nonlinear least-squares program was written which requires as input the experimental peak potentials, pH values, and total concentrations of metal and ligand and the conditions of the electrochemical experiment. The peak potentials are converted into adimensional potentials ξ_p (1, 13). The simulation program described above is called as a sub-routine which for a given set of estimated stability constants returns the corresponding calculated peak potentials $\xi_{p,cal}$. The stability constants are refined by applying the Newton-Gauss method using numerical derivatives (18).

Calculations were done on a Hewlett-Packard HP9835 desk computer with 128K memory, equipped with a plotter HP 7225A.

RESULTS AND DISCUSSION

Theoretical Considerations. The effect of stability constants on cyclic or linear-sweep voltammograms obtained at different pH values for a given mixture of metal and ligand will first be discussed for the following system:



It can be described by three thermodynamic parameters, β_{ML} ($= [ML^{n+}] / ([M^{n+}][L])$), K_{HL}^H ($= [L][H^+] / [HL^+]$), and E° . Figure 1 shows the dependence of the (cathodic) peak po-

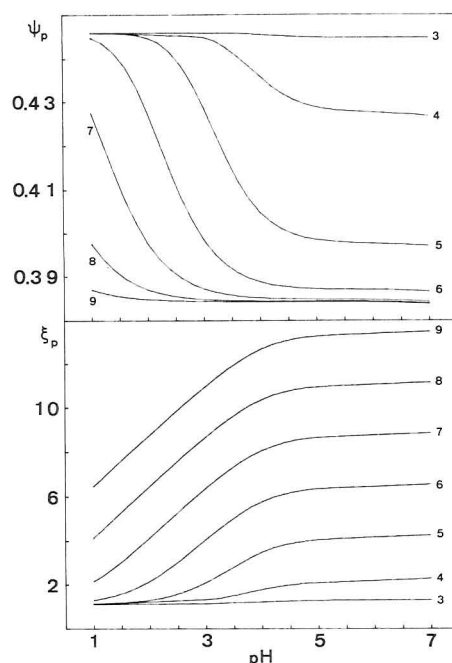


Figure 1. pH dependence of cathodic peak currents (upper part) and potentials (lower part) for the system described by eq 1-3 with $pK_{HL}^H = 4$ and $\log \beta_{ML}$ varied from 3 to 9 ($c_M^0 = c_L^0 = 0.2$ mM).

tentials and peak currents for an equimolar mixture of metal and ligand. In the case of weak complexation the peak characteristics at low pH are as expected for a reversible system, i.e. $\psi_p = 1.1$ and $\xi_p = 0.446$ (1). Clearly, under these conditions most of the ligand is protonated and complexation does not occur.

Increasing pH results in a decrease of ψ_p and in an increase of ξ_p . For $pH \geq 5$ both peak potential and peak current remain almost constant which is due to the fact that at high pH protonation of the ligand becomes negligible and that the concentration of complex ML is practically independent of pH.

The decrease of ψ_p clearly indicates that the shape of the corresponding voltammograms is different from that usually observed for a reversible system (1, 13). The minimum value of ψ_p is 0.384 in perfect accordance with the theoretical value (13). As can be seen from Figure 1 the effect of pH on the peak current is relatively small, in particular when very stable complexes are formed. Thus, the determination of stability constants based on measurements of the peak current only does not seem to be a good approach.

The effect of pH on the peak potentials is relatively large and, moreover, strongly depends on β_{ML} (see Figure 1). The limiting potentials at high pH, $\xi_{p,lim}$, are as predicted by the theory (13)

$$\xi_{p,lim} = 1.16 + \ln(\beta_{ML}c_M^0) \quad (4)$$

It should be noted that the shapes of the curves shown in Figure 1 do not depend on K_{HL}^H and that a variation of this parameter shifts all the curves by the same amount parallel to the pH axis. Thus, from measurements of peak potentials as a function of pH it will be possible to determine β_{ML} as well as K_{HL}^H .

Clearly, in the case of this simple equilibrium system the stability constants can be obtained without using a least-squares procedure, β_{ML} can be calculated from $\xi_{p,lim}$ (eq 4), and K_{HL}^H can be determined by using working curves as given in Figure 1.

For more complicated equilibrium systems the ξ_p -pH curves depend on the total concentrations of metal and ligand and on the set of ligand and complex stability constants. Ac-

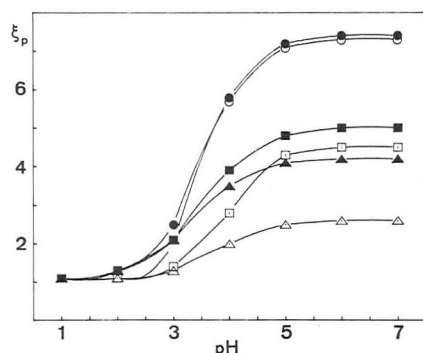
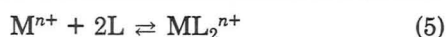


Figure 2. pH dependence of the cathodic peak potentials for the system described by eq 1–3 and 5 with $pK_{HL}^H = 4$, $\log \beta_{ML} = 4$ (open symbols) and 5 (full symbols): $\log \beta_{ML} = 8$ (Δ), 9 (\square), and 10 (\circ) ($c_M^0 = c_L^0 = 0.2$ mM).

cordingly, the use of working curves for determining the thermodynamic parameters will be rather inconvenient and a least-squares fitting procedure is to be preferred. Nevertheless, the calculated curves show some general trends which will be useful in designing an actual CV–pH titration experiment.

For a system described by eq 1–3 and 5 some calculated ξ_p –pH curves are given in Figure 2 ($\beta_{MLL} = [ML_2^{n+}]/([M^{n+}][L]^2)$). Due to the additional formation of a 1:2 com-



plex the limiting peak potentials increase. $\xi_{p,lim}$ depends both on β_{ML} and on β_{MLL} ; the effect of β_{ML} , however, becomes less important as β_{MLL} increases. Whereas β_{MLL} mainly influences $\xi_{p,lim}$, β_{ML} in addition has a marked effect on the curve shape. Increasing values of β_{ML} result in a shift of the inflection point of the ξ_p –pH curves to lower pH values. Again, the effect of β_{ML} becomes smaller with increasing β_{MLL} . However, the influence of β_{ML} can be enhanced by decreasing the ligand to metal ratio and/or the total concentration of metal, i.e. under conditions that disfavor the formation of the 1:2 complex.

This leads to a point of practical interest, namely, the optimum choice of the ligand to metal ratio f . If f is too large, only β_{MLL} can be determined and, in addition, precipitation of the ligand or of a complex may occur. On the other hand, if f is too small, only β_{ML} can be determined (in the extreme case, $f \approx 0$, even this is no longer possible). Moreover, decreasing f leaves increasing amounts of uncomplexed metal which might create additional complications due to the formation of hydroxo complexes (vide infra). Fortunately, in our case of pH-dependent equilibria the choice of a reasonable f is not very critical: By addition of base to a given mixture of metal and protonated ligand the actual value of f changes from 0 ($pH \ll pK_{HL}^H$) to c_L^0/c_M^0 ($pH \gg pK_{HL}^H$). Curves calculated with the parameters used in Figure 2 for $0.5 < c_L^0/c_M^0 < 4$ show that the influence of β_{ML} has its maximum around pH 3, whereas β_{MLL} has its main effect at $pH > 5$. (Clearly, these pH regions are determined by the pK of the ligand.) For $c_L^0 \approx c_M^0$ a variation of β_{ML} or β_{MLL} produces effects of similar magnitude in the respective pH regions. Thus, a reasonable experimental strategy will be to start from a stoichiometric mixture of metal and ligand and to measure voltammograms between pH 2 and 7.

Complexation of Copper(II) by Oxalate. The Cu(II)–oxalate system has been studied by many workers both by potentiometric (19) and by voltammetric methods (4, 11, 20). Although this is a relatively simple equilibrium system where only the complexes $Cu(Ox)$ and $Cu(Ox)_2^{2-}$ are formed, considerably differing stability constants have been reported. For the same conditions ($I = 0.1$ M, 298 K) values range from 4.8 to 6.7 for $\log \beta_{ML}$ and from 9.2 to 10.5 for $\log \beta_{MLL}$ (19, 21).

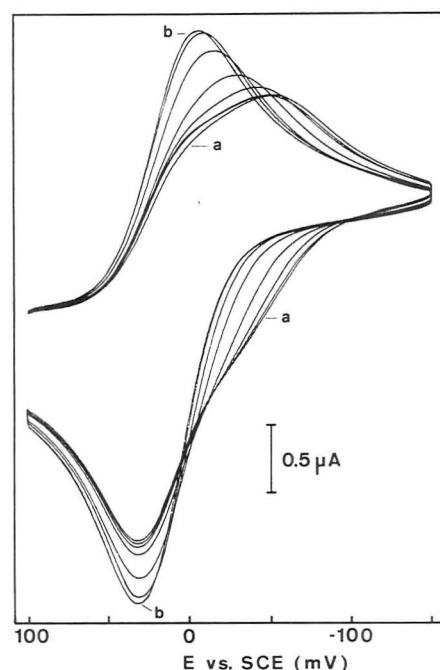


Figure 3. Effect of pH on cyclic voltammograms for the copper(II)–oxalate system. $c_{Cu}^0 = 0.241$ mM, $c_{Ox}^0 = 0.124$ mM, pH varied from 4.85 (a) to 1.43 (b) ($I = 0.5$ M, KNO_3 ; 298 K).

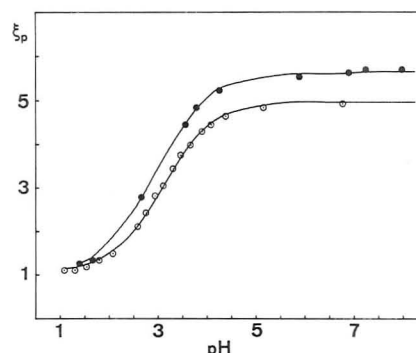


Figure 4. pH dependence of the cathodic peak potentials for the copper(II)–oxalate system: open ($f = c_{Ox}^0/c_{Cu}^0 = 0.51$) and full circles ($f = 1.05$) of radius equal to the standard error of fit; calculated curves, —.

In view of these large discrepancies between the published stability constants, a reinvestigation of the Cu(II)–oxalate system by an alternative method appeared to be called for.

CV–pH titrations were made for ligand to metal ratios, f , of 1.05 and 0.51 (see Experimental Section for details). The total concentrations of metal and ligand were chosen sufficiently small in order to prevent precipitation of cupric oxalate (solubility 0.158 mM at 298 K (22)).

Figure 3 shows the dependence of the cyclic voltammograms on pH for $f = 0.51$. Decreasing the pH leads to an increase of cathodic and anodic peak currents and to a shift of the cathodic peak toward more positive potentials. The voltammograms at high pH are rather broad and look like superpositions of two waves (curve a, Figure 3). With decreasing pH the voltammograms become more narrow, and at $pH < 1$, where no complexation occurs, the shape of the curve is as expected for a reversible two-electron transfer.

From a least-squares fit to the cathodic peak potentials, $\log \beta_{ML} = 5.44 \pm 0.01$ and $\log \beta_{MLL} = 8.99 \pm 0.09$ were obtained. In the calculation the pK values of oxalic acid, 1.04 (21) and 3.68 (determined by potentiometric titration), were kept constant and only the complex stability constants were iteratively refined. The overall standard error of fit is $\sigma_\xi = 0.06$ (corresponding to $\sigma_E = 0.8$ mV) which leads to an excellent

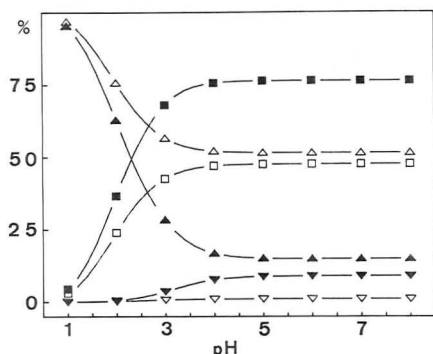


Figure 5. Species distribution for the copper(II)-oxalate system as a function of pH. The results are given as the percentage of the total copper present: Δ , Cu^{2+} ; \square , CuOx ; ∇ , $\text{Cu}(\text{Ox})_2^{2-}$. Open symbols refer to $c_{\text{Cu}}^0 = 0.24$ mM and $f = 0.51$, full symbols refer to $c_{\text{Cu}}^0 = 0.175$ mM and $f = 1.05$ ($\text{p}K_{\text{HLL}}^{\text{H}} = 1.04$, $\text{p}K_{\text{HL}}^{\text{H}} = 3.68$, $\log \beta_{\text{ML}} = 5.43$, $\log \beta_{\text{MLL}} = 9.21$).

fit of the experimental points by the respective calculated curve as can be seen from Figure 4.

From the titration data obtained for $f = 1.05$, $\log \beta_{\text{ML}} = 5.45 \pm 0.02$ and $\log \beta_{\text{MLL}} = 9.19 \pm 0.04$ were calculated ($\sigma_{\xi} = 0.06$). Again, the good fit is evident from Figure 4.

Although the values of the parameters determined from the two independent titrations are in good agreement, the error in the stability constants is different. β_{MLL} is better defined based on data obtained at higher ligand to metal ratio, whereas the opposite is true for β_{ML} . A simultaneous fit to both data sets yields $\log \beta_{\text{ML}} = 5.43 \pm 0.01$ and $\log \beta_{\text{MLL}} = 9.21 \pm 0.02$ ($\sigma_{\xi} = 0.06$ as before). Thus, while the quality of fit and the values of the parameters remain practically unchanged, both parameters are now equally well defined.

The calculated stability constants closely agree with the values given by Philp and co-workers (11), $\log \beta_{\text{ML}} = 5.4$ and $\log \beta_{\text{MLL}} = 9.2$, which were determined by fitting a simulated curve to a single experimental voltammogram. Clearly, this approach has the advantage in that good estimates for the stability constants are obtained in a short time. On the other hand, reliable values of the parameters and unbiased estimates of their confidence limits can only be expected if the data analysis is based on a series of measurements. This is especially important if one studies equilibrium systems where neither the number nor the nature of the complexes is known prior to the analysis. In these cases one can only be sure that the correct chemical model has been found if calculated and experimental titration curves (as the ones shown in Figure 4) do not show systematic deviations (23).

In order to estimate the potential of the present method, it is illustrative to inspect the species distributions shown in Figure 5. Under the conditions of the CV-pH titrations, the maximum bulk concentrations of ML_2 are only 11% ($f = 1.05$) and 2% ($f = 0.51$), respectively. Moreover, the formation of ML_2 occurs almost in the same pH region where ML is formed. Methods like potentiometry or spectrophotometry which are based on measurements of bulk concentrations, would hardly allow one to determine β_{MLL} under these conditions. Surprisingly, from CV-pH titrations both parameters could be determined even from the data for $f = 0.51$, where the complex ML_2 is practically not present in the bulk solution. This is due to the fact that the species concentrations near the electrode surface are different from the respective bulk concentrations if the ligand is not present in large excess over the metal. During the potential scan the free metal ion is reduced and the ligand to (oxidized) metal ratio accordingly increases near the surface of the electrode. As a consequence the concentration of ML_2 increases and β_{MLL} thus affects the voltammogram.

It should be mentioned that the presence of hydroxo com-

plexes was neglected in the calculations for the copper(II)-oxalate system. Actually, the formation of CuOH^+ starts around pH 7 ($\beta_{\text{CuOH}} = [\text{CuOH}^+]/([\text{Cu}^{2+}][\text{OH}^-]) = 10^{6.1}$ (25)). However, under the experimental conditions the concentration of CuOH^+ never exceeds 4% ($f = 0.51$) or 11% ($f = 1.05$), respectively, of the total copper concentration and, even more important, including the additional species does not affect the peak potential at pH ≤ 8 . Simulations show that for pH > 7 the formation of CuOH^+ results in a cathodic shift of the ascending part of the voltammogram (i.e., at potentials that are more positive than the peak potential). The change of the curve shape as a function of pH becomes more important when f is smaller. Decreasing f results in increasing the concentration of Cu^{2+} which is not complexed by oxalate (cf. Figure 5) and, accordingly, in increasing amounts of CuOH^+ . For the lower value of f used in this study (0.51) only at pH ≥ 8 would the effect of the hydroxo complex be sufficient to affect the peak potential.

To conclude, cyclic or linear-sweep voltammetry is a promising tool for studying stepwise metal-ligand equilibria. The method can be applied to any system where chemical equilibria are rapid and where one of the equilibrium species can be reversibly reduced or oxidized. The former restriction to relatively large excess of ligand is no longer necessary which considerably increases the potential of this method for determining stability constants. Equilibrium systems where the use of high ligand concentrations is either not possible (due to low solubility of one of the equilibrium species) or not desirable (due to the predominance of the complex with the maximum number of ligands) can be conveniently studied by voltammetry. Data analysis by using a least-squares procedure is straightforward despite the fact that no simple relation between peak potential and bulk concentration and stability constants can be formulated. In many cases of interest voltammetry will thus become a reasonable alternative to potentiometry or spectrophotometry.

Clearly, information about the chemical system is not only obtainable from a single feature of the voltammetric curves (24). Future work will tell if least-squares fitting to complete voltammograms further improves the data analysis. This might become important when more complicated equilibrium systems are studied.

ACKNOWLEDGMENT

The author wishes to thank R. H. Philp, Jr. (University of South Carolina), for a listing of this simulation program, T. A. Kaden and A. D. Zuberbühler (University of Basel) for allowing use of their computer, and J.-L. Marendaz for technical assistance.

LITERATURE CITED

- (1) Bard, A. J.; Faulkner, L. R. *Electrochemical Methods*; Wiley: New York, 1980.
- (2) Lingane, J. J. *Chem. Rev.* **1941**, *29*, 1.
- (3) DeFord, D. D.; Hume, D. N. *J. Am. Chem. Soc.* **1951**, *73*, 5321.
- (4) Schaap, W. B.; McMasters, D. L. *J. Am. Chem. Soc.* **1961**, *83*, 4699.
- (5) Leggett, D. J. *Talanta* **1980**, *27*, 787.
- (6) Santaballa, J. A.; Blanco, C.; Arce, F.; Casado, J. *Talanta* **1985**, *32*, 931.
- (7) Gampp, H. *J. Chem. Soc., Faraday Trans. 1* **1987**, *83*, 1719.
- (8) Klatt, L. N.; Rouseff, R. L. *Anal. Chem.* **1970**, *42*, 1234.
- (9) Elenkova, N. G.; Nedelcheva, T. K. *J. Electroanal. Chem.* **1976**, *69*, 385.
- (10) Macovschi, M. E. *J. Electroanal. Chem.* **1968**, *16*, 457.
- (11) Killa, H. M.; Mercer, E. E.; Philp, R. H., Jr. *Anal. Chem.* **1984**, *56*, 2401.
- (12) Killa, H. M.; Philp, R. H., Jr. *J. Electroanal. Chem.* **1984**, *175*, 223.
- (13) Savéant, J.-M.; Xu, F. *J. Electroanal. Chem.* **1986**, *208*, 197.
- (14) Spell, J. E.; Philp, R. H., Jr. *J. Electroanal. Chem.* **1980**, *112*, 281.
- (15) Castleberry, A. A.; Mercer, E. E.; Philp, R. H., Jr. *J. Electroanal. Chem.* **1987**, *216*, 1.
- (16) Zuberbühler, A. D.; Kaden, T. A. *Talanta* **1982**, *29*, 201.
- (17) Feldberg, S. W. *Electroanal. Chem.* **1969**, *3*, 199.
- (18) Gampp, H.; Maeder, M.; Zuberbühler, A. D. *Talanta* **1980**, *27*, 1037.
- (19) Brookes, G.; Pettit, L. D. *J. Chem. Soc., Dalton Trans.* **1977**, 1918.

- (20) Killa, H. M. *J. Chem. Soc., Faraday Trans. 1* **1985**, *81*, 2659.
(21) Martell, A. E.; Smith, R. M. *Critical Stability Constants*; Plenum: New York, 1977; Vol. III, p 94.
(22) *CRC Handbook of Chemistry and Physics*, 64th ed.; CRC Press: Boca Raton, FL, 1983; p B-91.
(23) Gampp, H.; Haspra, D.; Maeder, M.; Zuberbühler, A. D. *Inorg. Chem.* **1984**, *23*, 3724.
(24) Oldham, K. B. *J. Chem. Soc., Faraday Trans. 1* **1986**, *82*, 1099.

- (25) Martell, A. E.; Smith, R. M. *Critical Stability Constants*; Plenum: New York, 1982; Vol. V, p 394.

RECEIVED for review April 20, 1987. Accepted July 1, 1987.
This work was supported by the Swiss National Science Foundation (Grant No. 2.838-0.83).

Infrared Studies of the Liquid Crystal *N*-(*p*-Cyanobenzylidene)-*p*-octyloxyaniline Coated on Underivatized and Trimethylsilane-Derivatized Silica

C. J. Hann¹ and R. K. Gilpin*

Department of Chemistry, Kent State University, Kent, Ohio 44242

Diffuse reflectance Fourier transform infrared spectra were acquired for varying amounts of the liquid crystal *N*-(*p*-cyanobenzylidene)-*p*-octyloxyaniline coated on underivatized and trimethylsilane-derivatized silica. Broad, asymmetrical bands were observed in the nitrile stretch region (2190–2290 cm⁻¹). These data can be explained in terms of overlapping higher and lower frequency bands arising respectively from hydrogen-bonded and non-hydrogen-bonded cyano groups. Differences in the distribution of hydrogen-bonded to non-hydrogen-bonded groups varied with coating weight and surface treatment.

Since uniform alignment of liquid crystalline molecules is essential for most display applications (1), techniques to control molecular orientation have been extensively explored. The most popular procedures are either mechanical treatment of the substrate [i.e., etching (2, 3), rubbing (3, 4), or stretching (3, 4)] or physical coating of the substrate with an organic (1, 5–7) or inorganic (8, 9) material. Sometimes a combination of these methods is utilized (2, 10).

Although alignment techniques have progressed to a rather mature state, the boundary ordering mechanism is still a subject of both interest and controversy (11). For mechanically prepared surfaces interfacial alignment is usually attributed to minimization of either elastic energy (4, 12, 13) or interfacial tension (14, 15). Hydrogen bonding (16) and van der Waals forces (17) are factors controlled by chemical modification of the surface. Amphiphilic impurities in the liquid crystals also have been suggested to be an important aligning factor (18–20).

Most of the commonly used characterization techniques provide only qualitative information as to whether the molecules are ordered perpendicular or parallel to the substrate's surface. Infrared dichroism (21, 22), refractive index (23), and microscopy (24) have been used most often for determining the degree of orientational order. However, in most cases information about bulk, not interfacial, properties is obtained.

In a recent review (11), Miyano points out that, despite its long research history, a basic understanding of the boundary ordering mechanism is still lacking due to limited experimental techniques for microchemical characterization of the sub-

strate-liquid crystal interface. In a limited number of studies the interfacial region has been examined. The distances that surface effects are observed have been studied by microscopy (24) and gas chromatography (25, 30).

One of the major causes of display failure is orientational changes resulting from chemical degradation at the interface (1). Increased interfacial stability has been obtained via modification of the substrate with reactive silanes (1). Interestingly, this procedure is similar to procedures used to produce chemically bonded stationary phases for chromatographic applications (31). Hence knowledge and techniques developed in this latter field of study seem to be readily applicable to investigating and controlling the interfacial alignment of liquid crystalline systems.

The earliest descriptions of silane-modified chromatographic surfaces were based almost solely on data generated by the technique itself (32). Recently, however, spectroscopic investigations have been used to probe the microchemical orientation and dynamics of the immobilized ligands (33–38). Nontraditional studies of these systems have been the subject of a recent review (39). For cyanoalkyl-modified silica Fourier transform infrared (FT-IR) spectroscopy has been used to monitor changes in the band shape of the nitrile stretch for varying chain lengths of immobilized cyanoalkyl ligands (36–38). Since the bonding process leads to a nonhomogeneous distribution of attached groups, a two-site interaction model best explains observed changes in the band contour. One ligand population forms hydrogen bonds with free surface silanols while other cyanoalkyl chains are sterically unable to hydrogen bond. Potentially these results are useful in understanding local ordering at the surface for a variety of nitrile-containing molecules (e.g., liquid crystalline systems).

In the current study, trimethylsilane (TMS) was chemically attached to porous silica by replacement of the silanol protons. Subsequently, derivatized as well as underivatized silica were physically coated with varying amounts of the liquid crystal *N*-(*p*-cyanobenzylidene)-*p*-octyloxyaniline (CBOA) and diffuse reflectance FT-IR spectra were acquired from these samples. In most cases a broad asymmetrical absorption band was observed in the nitrile stretch region resulting from the presence of two distributions of cyano groups. These data are similar to those obtained previously for cyanoalkyl-derivatized silica (36–38). The ratio of hydrogen-bonded to non-hydrogen-bonded nitrile groups varies as a function of the amount of sorbed liquid crystal and is different for the

¹ Present address: Loral Systems Group, Akron, OH 44315.

* Author to whom correspondence should be addressed.

derivatized and underivatized silica. These results not only illustrate that surface derivatization can be used to control interfacial molecular orientation of the liquid crystalline coating but also demonstrate that FT-IR can be used to selectively probe the microstereochemistry of the substrate-liquid crystal interface.

EXPERIMENTAL SECTION

Materials. Silica Gel 60 (particle size 0.040–0.063 mm, 230–400 mesh [E. Merck]) was reacted with excess trimethylchlorosilane (Petrarch Systems, Inc.) under toluene reflux conditions (32) to produce the bonded phase. The amount of bound carbon was 5.1%. The silicas were physically coated by first dissolving a given weight of CBOA (Eastman Kodak Co.) in ethyl ether and then adding either 0.2775 or 0.2500 g of derivatized or underivatized silica. The larger amount of derivatized silica was used to obtain the same level of coverage per unit surface area of silica (i.e., to compensate for the weight of the immobilized silane). The mixture was allowed to equilibrate at ambient conditions and then the solvent was removed with a rotary evaporator at 38–40 °C. The coated samples were dried in a vacuum oven at 38 °C for 48 h and then stored in brown bottles in a desiccator. With this procedure samples were coated with between 1 and 80% CBOA.

Spectrometry. Infrared spectra were collected on undiluted samples with a Barnes diffuse reflectance accessory and an IBM Instruments Model IR/32 FT-IR spectrometer equipped with a DTGS detector and operated to give 4-cm⁻¹ resolution. All samples were loaded into 1 cm diameter macrocups which were gently tapped to facilitate settling. Ratios of between 1000 and 10 000 sample scans vs. 300 background scans were used. Expansions of spectra in the nitrile stretch region (2190–2290 cm⁻¹) were automatically zeroed by using the instrument's software. To facilitate comparison of the bands shown in Figures 3 and 4, the data were normalized to full scale.

RESULTS AND DISCUSSION

The purpose of the current study was to examine the effect of surface silanols on the orientation of mesogenic molecules which contain nitrile groups as well as to investigate chemical modification as a means of minimizing hydrogen bonding effects. In order to do this a series of physically coated materials was prepared with varying levels of coverage. Coating thicknesses ranged from less than monolayer coverage of CBOA up to amounts of the liquid crystal which should exceed monolayer coverage by a few layers of sorbed molecules.

Infrared spectroscopy was selected as a means of studying these materials because the nitrile stretch frequency is in a spectral region unobscured by interferences from surface silanols, adsorbed water, and the silica and polysiloxane backbone structures (40). When samples were prepared and run, techniques were avoided that would allow the liquid crystals to come in contact with other surfaces or foreign materials that could perturb their orientation. Thus the use of solvents, pellets, and mulls which are traditional methods for increasing infrared transparency and spectral throughput and decreasing scattering for porous silica were avoided. All spectra were acquired on neat samples using diffuse reflectance techniques.

Data were collected at room temperature. The solid to mesophase transition for CBOA is approximately 73 °C, and at higher coating levels the crystal was in the solid phase under the conditions studied. However, at lower coating levels, which were in many cases below or near monolayer coverage, the solid to mesophase transition should not be a factor. Thus for the most part the orientation and degree of interaction of the sorbed CBOA are the subject of this initial investigation.

A typical spectrum over the total infrared region scanned (4000–400 cm⁻¹) is shown in Figure 1. Expansions of spectra in the nitrile region (2190–2290 cm⁻¹) are shown in Figures 2–4. Broad, asymmetrical bands were observed from most samples. Mori et al. (41) have suggested a graphical method to resolve similar asymmetrical bands observed in the OH

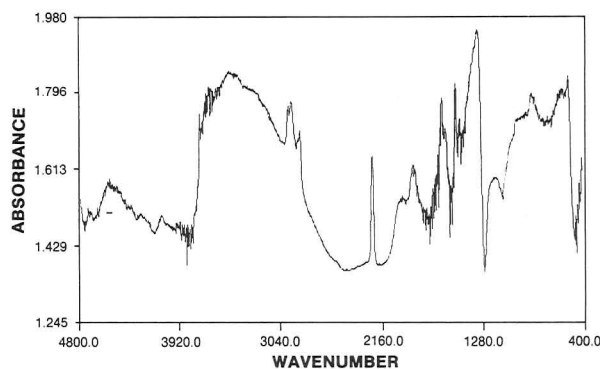


Figure 1. Typical spectrum acquired, 40% CBOA sample on underivatized silica.

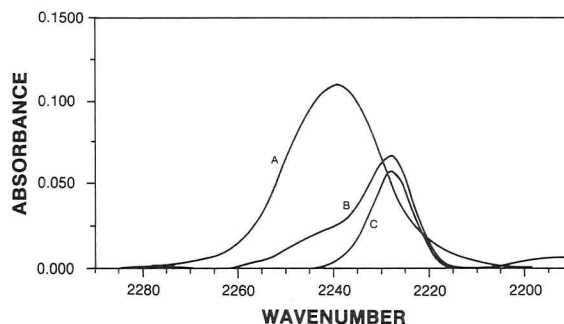


Figure 2. Comparison of the nitrile stretching region for 2% CBOA: (A) underivatized silica, (B) trimethylsilane-derivatized silica, (C) weighted difference.

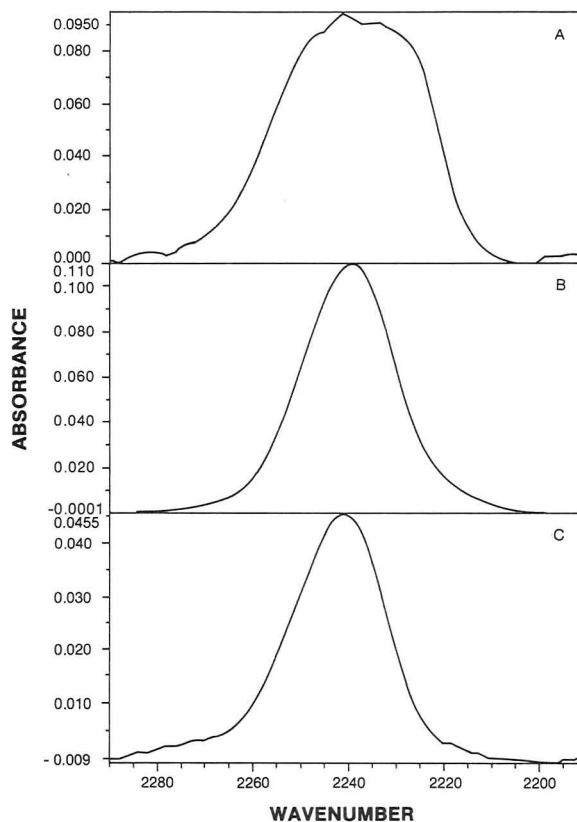


Figure 3. Comparison of the nitrile stretching region for CBOA on underivatized silica: (A) 60% coating, (B) 2% coating, (C) 1% coating.

stretch region of cyanoalkanols dissolved in carbon tetrachloride. High- and low-frequency components were assigned, respectively, to two types of stereoisomers, those that had free hydroxyl groups and those that had OH groups which formed hydrogen bonds with cyano groups. By use of a similar approach, the asymmetrical bands in the current study can be

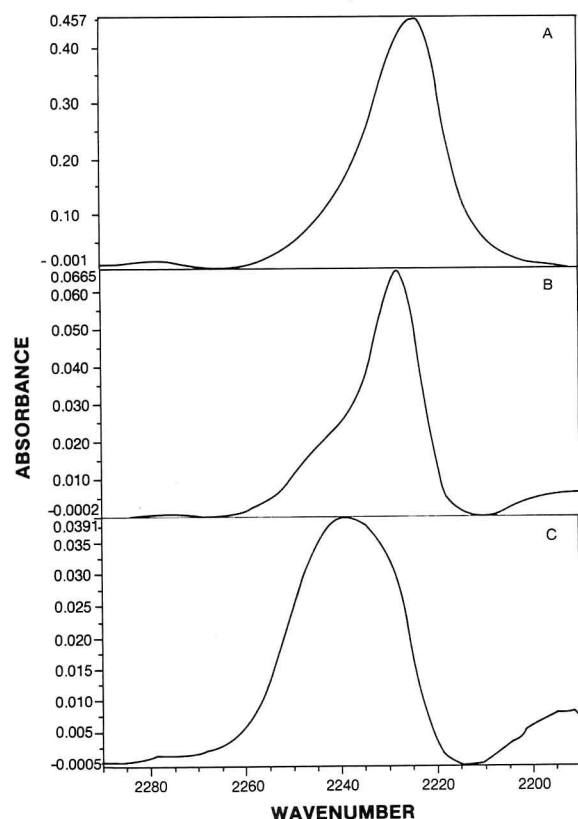


Figure 4. Comparison of the nitrile stretching region for CBOA on trimethylsilane-derivatized silica: (A) 60% coating, (B) 2% coating, (C) 1% coating.

resolved into two symmetrical components centered at 2240 and 2232.5 cm^{-1} . These frequencies represent respectively nitrile groups that form hydrogen bonds with free silanols and nitrile groups that do not hydrogen bond with the substrate. Similarly the current band assignments are consistent with other infrared studies of hydrogen bonding vs. non-hydrogen bonding for cyano groups (36–38, 42, 43).

A broad symmetrical band (Figure 2, band A) was obtained from the 2% CBOA on underivatized silica. This sample is representative of samples with less than monolayer coverage. Under these conditions excess silanols are present which interact strongly with the nitrile groups in the liquid crystal. Also shown in Figure 2 (band B) are data obtained from the sample coated with 2% by weight CBOA on trimethylsilane-derivatized silica (band B). This latter band is skewed at the higher frequency side resulting from a relatively small population of CBOA which hydrogen bonds via the cyano group. The band corresponding to the hydrogen bonded population was scaled and subtracted from the composite band (B) using the system's software (Figure 2, band C). The presence of two peaks suggests a two-site adsorption model (i.e., two conformations for CBOA) in which one population of molecules hydrogen bonds with surface silanols via their cyano groups while another population of CBOA molecules is sterically hindered from forming hydrogen bonds.

Suffolk and Gilpin (36–38) suggested a similar two-site interaction model for various silica-immobilized cyanoalkyl ligands. In their study Fourier self-deconvolution of asymmetrical bands similar to those observed in the current study produced unresolved doublets. A nonuniform distribution of surface immobilized groups was suggested to exist due to nonhomogeneous chemical modification. Ligands bonded in sparsely derivatized areas or at the edges of ligand clusters could form hydrogen bonds with surface silanols while ligands within richly derivatized areas sterically were restricted from forming hydrogen bonds.

In the current study, changes in peak shape for underivatized and trimethylsilane derivatized silica are shown in Figures 3 and 4, respectively. The ratio of free nitrile groups to those which formed hydrogen bonds increased as the coating weight increased for both types of silica. These data are consistent with Rochester's observation that the relative band height for stretching frequencies assigned to hydrogen-bonding and non-hydrogen-bonding Si–OH groups, respectively, increases and decreases as hydrogen bonding between propionitrile and silica increases (43).

At lower coverages the ratio of groups forming hydrogen bonds to free cyano groups is greater for the underivatized silica. This is seen by comparing the nitrile bands from the 1% and 2% levels (bands C and B) shown in Figures 3 and 4. As noted earlier the 2% level on the underivatized silica gave a broad symmetrical band characteristic of hydrogen bonding. However, this was not true for the same level of coverage on the derivatized silica where an asymmetrical band indicative of the presence of both hydrogen-bonded and non-hydrogen-bonded CBOA molecules was observed. At the 1% coating level shown as band C in Figures 3 and 4, band shapes suggest the presence of predominantly hydrogen-bonded nitrile groups for both derivatized and underivatized silicas. These data seem reasonable since a sizable fraction of silanols (about half) on the derivatized surface was replaced with trimethylsilyl groups during bonding (44). Several other levels of coverage were studied (i.e., 5, 7.5, 10, 20, 30, 40, 50, 60, and 80%). At lower levels (up to about 20%) trends were consistent with the above. However, at high coating weights (e.g., 60% as shown in Figures 3A and 4A), peak shapes did not fit the same trends as at lower coverages. Based on the underivatized silica's listed surface area and assuming a planar arrangement of the liquid crystal molecules, multilayers should start to form at about 20% coverage. However, this estimate will vary depending on alignment and available surface area. For a similar system Marciniak and Witkiewicz (45) have reported variations depending on both of these parameters. Each of these may change for the derivatized material. This was noted not only by the current infrared studies but also in differential scanning calorimetry experiments carried out on these same materials. Thermally the solid to mesophase transition was observed at approximately 20% and 40% coverage for the derivatized and underivatized materials, respectively.

CONCLUSION

Spectra from CBOA and related cyano containing liquid crystals adsorbed on silica derivatized with ligands of different blocking abilities are needed to assess the feasibility of controlling orientation via utilization of different bonded ligands. Experiments are now in progress with different liquid crystals coated on silica derivatized with various ligands differing in size, shape, and attached functionality. Infrared, gas chromatographic, and thermal studies are being used to probe the interfacial region.

Registry No. CBOA, 34572-35-5.

LITERATURE CITED

- (1) Kahn, F. J. *Appl. Phys. Lett.* **1973**, *22*, 386.
- (2) Helfrich, W. *Phys. Lett.* **1971**, *35A*, 393.
- (3) Creagh, L. T.; Kmetz, A. R. *Mol. Cryst. Liq. Cryst.* **1973**, *24*, 59.
- (4) Berreman, D. W. *Phys. Rev. Lett.* **1972**, *28*, 1683.
- (5) Haas, W.; Adams, J.; Flannery, J. B. *Phys. Rev. Lett.* **1970**, *25*, 1326.
- (6) Kutty, T. R. N.; Fischer, A. G. *Mol. Cryst. Liq. Cryst.* **1983**, *99*, 301.
- (7) Kutty, T. R. *Mol. Cryst. Liq. Cryst.* **1984**, *102*, 167.
- (8) Janning, J. L. *Appl. Phys. Lett.* **1972**, *21*, 173.
- (9) Uchida, T.; Seki, H.; Shishido, C.; Wada, M. *Mol. Cryst. Liq. Cryst.* **1979**, *54*, 161.
- (10) Margerum, J. D.; Miller, L. J. *J. Colloid Interface Sci.* **1977**, *58*, 559.
- (11) Miyano, K. *Jpn. J. Appl. Phys.* **1985**, *24*, 1379.
- (12) Berreman, D. W. *Mol. Cryst. Liq. Cryst.* **1973**, *23*, 215.
- (13) Nakamura, M.; Ura, M. *J. Appl. Phys.* **1981**, *52*, 210.

- (14) Zisman, W. A. *Adv. Chem. Ser.* **1964**, No. 43, 1.
- (15) Naemura, S. J. *Phys. (Les Ulis, Fr.)* **1979**, 40, 514.
- (16) Dubois, J. C.; Gizard, M.; Zann, A. J. *Appl. Phys.* **1976**, 47, 1270.
- (17) Richmond, P.; White, L. R. *Mol. Cryst. Liq. Cryst.* **1973**, 27, 217.
- (18) Uchida, T.; Ohgawara, M.; Shibata, Y. *Mol. Cryst. Liq. Cryst.* **1983**, 98, 149.
- (19) Ohgawara, M.; Uchida, T. *Jpn. J. Appl. Phys.* **1981**, 20, L75.
- (20) Ohgawara, M.; Uchida, T.; Wada, M. *Mol. Cryst. Liq. Cryst.* **1981**, 74, 227.
- (21) Kirov, N.; Simova, P.; Ratajczak, H. *Mol. Cryst. Liq. Cryst.* **1980**, 58, 285.
- (22) Fernandes, J. R.; Venugopalan, S. *Mol. Cryst. Liq. Cryst.* **1976**, 35, 113.
- (23) Akahane, T.; Tako, T. *Jpn. J. Appl. Phys.* **1979**, 18, 19.
- (24) Price, F. P.; Bak, C. S. *Mol. Cryst. Liq. Cryst.* **1975**, 29, 225.
- (25) Grushka, E.; Solsky, J. F. *J. Chromatogr.* **1975**, 112, 145.
- (26) Sojak, L.; Farkas, P.; Janak, J.; Rang, S.; Eisen, O. *J. Chromatogr.* **1984**, 287, 271.
- (27) Grushka, E.; Solsky, J. F. *Anal. Chem.* **1973**, 45, 1836.
- (28) Witkiewicz, Z.; Suprynowicz, Z.; Dabrowski, R. *J. Chromatogr.* **1979**, 175, 37.
- (29) Rayss, J.; Witkiewicz, Z.; Waksmundzski, A.; Dabrowski, R. *J. Chromatogr.* **1980**, 180, 107.
- (30) Witkiewicz, Z.; Pietrzyk, M.; Dabrowski, R. *J. Chromatogr.* **1979**, 177, 189.
- (31) Gilpin, R. K. *Am. Lab. (Fairfield, Conn.)* **1982**, (March), 103.
- (32) Gilpin, R. K.; Gangoda, M. E. *J. Chromatogr. Sci.* **1983**, 21, 352.
- (33) Miller, M. L.; Linton, R. W.; Bush, S. G.; Jorgenson, J. W. *Anal. Chem.* **1984**, 56, 2204.
- (34) Leyden, D. E.; Kendall, D. S.; Burggraf, L. W.; Pern, F. J.; De Bello, M. *Anal. Chem.* **1982**, 54, 101.
- (35) Lochmuller, C. H.; Colborn, A. S.; Hunnicutt, M. L.; Harris, J. M. *Anal. Chem.* **1983**, 55, 1344.
- (36) Suffolk, B. R.; Gilpin, R. K. *Anal. Chem.* **1985**, 57, 596.
- (37) Suffolk, B. R.; Gilpin, R. K. *J. Chromatogr. Sci.* **1986**, 24, 423.
- (38) Suffolk, B. R.; Gilpin, R. K. *Anal. Chim. Acta* **1986**, 181, 259.
- (39) Gilpin, R. *Anal. Chem.* **1985**, 57, 1465A.
- (40) Kitson, R. E.; Griffith, N. E. *Anal. Chem.* **1952**, 24, 334.
- (41) Mori, N.; Omura, S.; Yamakawa, H.; Tsuzuki, Y. *Anal. Chem.* **1965**, 38, 1627.
- (42) White, S. C.; Thompson, H. W. *Proc. R. Soc. A* **1966**, 291, 460.
- (43) Rochester, C. H.; Tiebilco, D. A. *Chem. Ind. (London)* **1978**, 127.
- (44) Gilpin, R. K.; Burke, M. F. *Anal. Chem.* **1973**, 45, 1383.
- (45) Marciniak, W.; Witkiewicz, Z. *J. Chromatogr.* **1985**, 324, 299.

RECEIVED for review March 23, 1987. Accepted July 7, 1987.
Support from DARPA-ONR Contract N0014-86-K-0772 is acknowledged.

Direct Correlation of Ion and Electron Microscopic Images by Digital Image Superpositioning

Lisa K. Turner, Yong-Chien Ling, Mark T. Bernius, and George H. Morrison*

Baker Laboratory of Chemistry, Cornell University, Ithaca, New York 14853-1301

A method has been developed whereby micrographs obtained from identical sample areas, but by different instrument and detection systems, can be correlated and superimposed upon one another through digital image processing. Various Cr-based steels were analyzed by secondary electron (SE), backscattered electron (BSE), and secondary ion microscopies, and results are presented for a sample of ordinary high-speed tool steel. Digital image superpositioning incorporates an n th-order polynomial ($n \leq 3$) mapping function to implement the spatial transformation and a pixel-filling algorithm to estimate the corrected pixel gray level. By direct correlation of electron and ion micrographs, relative distortions caused by instrumental or operational incongruity have been removed. This methodology enables verification of secondary contrast mechanisms, such as topography, from secondary ion maps. Finally, image correlation has allowed the assessment and correction of image distortion and astigmatism within the stigmatic ion microscope.

Ion microscopy, based on secondary ion mass spectrometry (SIMS), is a microanalytical technique that can generate a spatially resolved, isotopic image of a sample's surface. As in any analytical technique, there exists a great need to extract, from the output, quantitative information that relates signal intensity to sample concentration. In SIMS, however, because secondary ions are generated by physically sputtering atoms from the surface of the sample, properties of the sample, such as topography, crystal orientation (I), and local chemical environment, directly influence secondary ion yields. The contrast of the resulting image can, therefore, be due to factors other than concentration gradients within the sample. Direct quantification of images is prohibited until all of the contrast

artifacts can be identified and removed.

In addition, artifacts in SIMS ion micrographs arise from distortions due to nonoptimal imaging parameters. This becomes very important in the pursuance of high spatial resolution images. In principle, an image should have a one-to-one correspondence with the object space that it represents. The exact correspondence is, however, disturbed by the presence of one or more degradation mechanisms as, for example, astigmatism.

The purpose of the image correlation technique proposed herein is to use the morphological information present in electron microscopic methods to identify and correct artifacts present in SIMS micrographs and thereby obtain true chemical morphology. In addition, the same techniques may be used in a comparative fashion to correct or compensate for instrumental distortions.

Historically, correlative microscopy has been manifested through visual, side-by-side comparison of photomicrographs (2, 3) or by the creation of shift vectors, which represent the translation needed to match unrecognizable or distorted image points (4, 5). For the routine presented in this work, visual comparison extends only as far as coarse recognition, during analysis, of the same sample area under different imaging conditions or from different instruments. Additionally, the sample image itself is not contorted selectively until it coincides with the reference image; rather, a single mathematical function is applied to the entire sample image in order to map out a corrected image. The operation, based on information transmission theory, is continuous and preserves connectivity (6). The method comprised a polynomial function to designate the spatial transformation and an algorithm to correctly define gray-level values for each newly generated pixel. Most recently, a similar correlation algorithm used to correct motion between images has been reported (7). It involves images taken with the same instrument and does not have as rigorous

Table I. Contrast Mechanisms

	primary	secondary
secondary electrons (SE)	topography	shadowing: incomplete collection of SE by detector diffusion: enhanced SE emission at edges generated by diffusely scattered primary electrons material: inclusion of backscattered electrons with low take-off angles within solid angle of the detector voltage: change in SE emission due to local electrostatic fields (charging) type I magnetic: deflection of SE exit angular distribution by external fringing fields in ferromagnetics
backscattered electrons (BSE)	mean atomic number (material)	diffusion: (same as above) topography: specular collection channeling: penetration and exit of electrons relative to lattice planes type II magnetic: deflection of BSE trajectories, within ferromagnetics by magnetic induction
electron induced X-rays	mean atomic number (material)	background: insufficient removal of X-ray continuum from characteristic peak at characteristic energy (especially with energy dispersive detector) detector discrimination
secondary ions	atomic mass	topography: emission of secondary ions at large angles to the surface normal and optical axis channeling: penetration and exit of ions relative to lattice planes charging: deflection of primary ion beam from sample surface caused by charge buildup matrix composition: the variation in ionization probability due to changes in the local chemical environment

a procedure for the selection of control points as the method reported here.

As mentioned previously, the most significant advantage of this fundamental approach to correlation is the ability to decipher the mechanisms responsible for contrast in an ion image. Stigmatic ion microscopy, based upon SIMS, is a microanalytical technique whereby a sample undergoes interaction with an energetic primary beam, usually Cs^+ or O_2^+ , resulting in ejection of secondary ions from the surface. The secondary ions are accelerated and focused through an ion-optical system, energy and mass filtered, and focused onto a microchannel-plate/fluorescent-screen assembly for visual image formation. Subsequently, the image is recorded on 35-mm film or by low-light video camera for direct image digitization. For purposes of quantification, the contrast in an ion image should be the sole result of elemental distribution gradients in the sample; however, because secondary ions are generated by physical sputtering of material, sample inhomogeneities such as topography and crystallographic orientation can also give rise to contrast artifacts within an image. Hence, the extraction of quantitative chemical information from an image without removal of these artifacts, particularly from heterogeneous samples, is a formidable task.

The advent of computer processing allows the elimination of some of these artifacts by mapping a sample image to a reference image. The reference image can be obtained by an alternate microanalytical technique in which the primary contrast mechanism responsible for image formation is the same as that responsible for inaccuracies within the sample image (Table I). The mutualization of these methods yields a wealth of information regarding the sample, and an exemplary microscope would incorporate the lot. Under present commercial limitations, though, the most viable strategy is one in which images from different detectors as well as from different instruments are correlated, allowing elimination of inconsistencies in data and an increase in the reliability of image information.

In the present paper, photomicrographs of secondary ions (SI), secondary electrons (SE), and backscattered electrons (BSE) have been successfully correlated; also presented is a general method whereby an assortment of photomicrographs from different instruments and detection systems may be superimposed.

EXPERIMENTAL SECTION

Ion images were acquired by using a Cameca IMS-3f ion microanalyzer and show a 150- μm -diameter field of view, using a 10- μm contrast aperture. A defocused O_2^+ primary ion beam of 3 μA accelerated to 12.5 keV was used to generate positive secondary ion images. The sample was held at 4.5 keV. Images were recorded on 125-ASA 35-mm film with integration times of under 5 s. A JEOL JSM-35CF scanning electron microscope equipped with an Everhart-Thornley secondary electron detector as well as a split annular solid-state detector for backscattered electron detection was used to compile electron micrographs. Images were recorded on Polaroid Type 52 Polopan film.

The sample, a Cr-based high-speed tool steel with vanadium inclusions, was mechanically polished to optical flatness. SIMS analyses were executed first so as to facilitate feature identification in SE and BSE analyses; i.e., the crater formed was used as a reference mark. Both electron and ion micrographs were rephotographed onto Kodak Technical Pan 2415 35-mm film to roughly equal magnifications. The adjustment of magnification was not critical since the computer program is designed to compensate for modest differences in magnification of the images. The negatives were digitized on a Joyce-Loebl Model 6 microdensitometer. Images were analyzed on a PDP 11/34A mini-computer interfaced to a TRAPIX image processor. The software package utilized was developed in this laboratory (8) (SIMPS, secondary ion mass image processing system), coded in Fortran IV, and operated under the RT-11 operating system.

RESULTS AND DISCUSSION

Image Registration. The impediment in superpositioning a sample image onto a reference image lies in compensation of the distortion arising from the application of different image generating techniques, both with regard to the image generation process, i.e. scanning beams vs. stigmatic optics, and in the dissimilar geometry of the detection devices. Within an individual technique, daily operational performance disparities also result in relative image distortions. Mere translation and rotation of the two images will not result in perfect correspondence. The sample image must first be corrected through application of a mapping function and then reconstructed by use of a pixel-filling algorithm in order to create an image of coincidence.

The correlation program applies three steps toward the construction of a proper image (Figure 1). The first of these is the selection, by the user, of similar features or control points

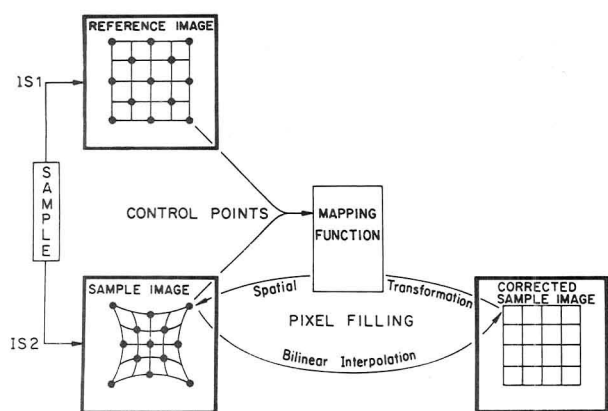


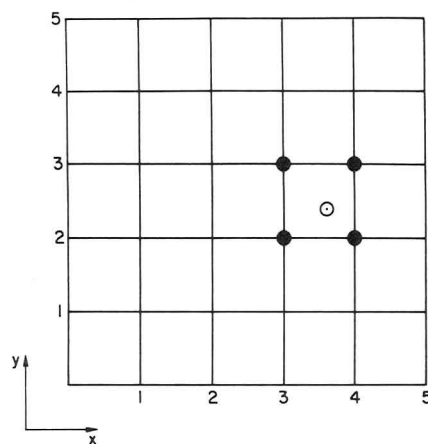
Figure 1. Schematic diagram of image correlation. From an identical sample area, a reference and a sample image are generated by using imaging systems IS1 and IS2, respectively. After the selection of control points from both the reference and the sample image, a mapping function is obtained and applied to define the spatial transformation from the sample to the reference image. The corrected sample image is then filled, pixel by pixel, by finding the corresponding pixel in the sample image. Gray-level values are assigned by using bilinear interpolation.

from both the sample and reference images, rendered in one of three ways: (1) a demarcation area is formed around a central feature and the center of mass is then calculated for the demarcation region; (2) control points are specified in the reference image and a larger area is searched in the sample image to find the best match point by using a correlation coefficient as a figure of merit; (3) a joy stick is used to visually specify control points. The appropriate selection of control points is most critical. Careless selection results in blurring of features in the superpositioned images due to misregistration. In the present experiment, a large number of control points are selected, but only those that are verified independently by all three approaches, and found to be consistent, are used in registration.

The next step toward registration is the application of, in this case, a second-order polynomial to compute the mapping function. From this function, the corresponding pixel location in the sample image is found to fill every pixel location in the corrected image. Each pixel in the output image can be mapped back to a corresponding pixel in the sample image. Hence, the connectivity and continuity of features are assured by the adaptation of the pixel-filling algorithm even if the transformation is nonlinear. Memory space of the PDP 11/34A limits the algorithm to polynomials of degree three, though second-order polynomials are usually sufficient to achieve registration.

Finally, the gray-level value of each of the pixels in the corrected image is duplicated from the corresponding gray level in the sample image. If a pixel lies outside the sample image boundary, a background gray-level value is assigned. For most pixel locations in the corrected image, however, the corresponding coordinates in the sample image are fractional, and pixel duplication is inappropriate. Therefore the gray-level value must be obtained through interpolation. Interpolation may be achieved simply by nearest neighbor resampling. Although relatively fast, this method may produce discontinuity artifacts at the edges of features. Instead, a bilinear interpolation was implemented throughout this work (Figure 2).

Images of vanadium inclusions (Figure 3) illustrate image registration. Here, a BSE image is selected as the reference image because it is sensitive to composition (similar to SIMS), yet subject to less distortion (compared to SIMS). A number of control points are selected and highlighted by the demarcation area (Figure 3a). Notice in the SIMS micrograph



$$I_2 = [G(4, 2) - G(3, 2)] (3.6 - 3) + G(3, 2)$$

$$I_3 = [G(4, 3) - G(3, 3)] (3.6 - 3) + G(3, 2)$$

$$G(3.6, 2.4) = (I_3 - I_2) (2.4 - 2) + I_2$$

Figure 2. Illustration of gray-level estimation using bilinear interpolation. Here, $G(3.6, 2.4)$ depicts the gray level corresponding to pixel location $(3.6, 2.4)$ and is specified by an open circle in the array. Linear interpolation is performed in the horizontal direction for the row above $(y = 3)$ and below $(y = 2)$ to yield two intermediate values, I_3 and I_2 . The corresponding gray level, $G(3.6, 2.4)$, is then found by using a second linear interpolation in the vertical direction at $x = 3.6$.

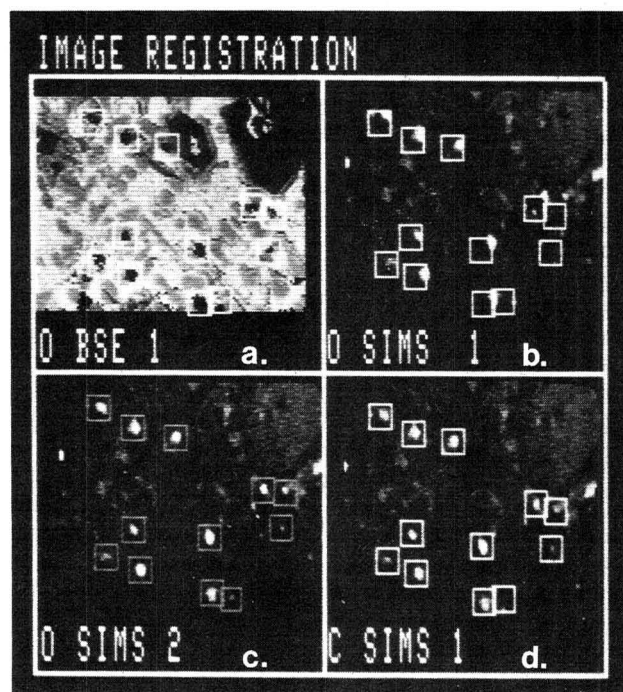


Figure 3. Image registration process. (a) O BSE 1, reference BSE image with 12 control points centered in the type 1 demarcation regions. (b) O SIMS 1, sample SIMS image of $^{51}\text{V}^+$ with type 1 demarcation. Notice that features do not lie at the centers of the demarcation regions. (c) O SIMS 2, sample SIMS image with type 2 demarcation. (d) C SIMS 1, corrected SIMS image of $^{51}\text{V}^+$ after registration is complete. Control points are now centered within type 1 demarcation regions. "O" denotes original image; "C" denotes corrected image. Type 1 and type 2 demarcations are different in location only.

(Figure 3b) the features are displaced from the centers of the demarcation regions defined in the reference image. A separate demarcation is performed on the SIMS image to specify sample control points (Figure 3c). By the use of both sample and reference control points, polynomial mapping is performed on the SIMS image yielding a corrected, superimposable ion image (Figure 3d). The features now reside in the centers of

the demarcation regions. Notice that the mapping has the final effect, on the original SIMS image, of south-west translation of the upper and right edges, and rotation clockwise in order to achieve coincidence. This addresses a recurring difficulty in stigmatic imaging: that reproducibility of an operator's proficiency in tuning the instrument will determine, to a high degree, the quality of the image. Subtle distortions, such as aperture displacement, and incorrect focus are often imperceptible in secondary ion imaging, especially for low signal-to-noise ratios. In SEM operation, at comparable image magnifications, these distortions are more easily compensated.

Astigmatism Correction. Astigmatism arises from irregularities in a lens, which cause portions of the beam pencil to be refracted in a direction not along the optical axis (nonparaxially). Thus, the focusing capability is direction dependent, meaning that distortion may be greater in one direction than in another. The Cameca IMS-3f, as commercially designed, accommodates a stigmator to correct for astigmatism between the secondary magnet and the projection lenses. When digital image superpositioning is performed, however, distortions often remained in the ion images. This was especially evident when attempting to achieve uniform focus of a field of view containing small features of irregular size. Finding that the residual astigmatism was caused by a misalignment of the magnetic and geometric axes within the spectrometer, a combination electrostatic octupole stigmator and cosine deflector was designed and installed (9).

The series of images in Figure 4 demonstrates (1) the extent of residual astigmatism that may be present in an ion image without the incorporation of the octupole lens, and (2) the success of correlation and digital image superpositioning in correcting distortions that may go unnoticed when collecting an ion image.

The images are of the same field of view as in Figure 3, but are maps of $^{52}\text{Cr}^+$ intensity. The dark spots are vanadium inclusions (verified in Figure 3). Figure 4a is taken with the octupole lens in operation, and in comparison to (although not registered with) electron micrographs, the image possesses minimal astigmatism. By comparison, Figure 4b, taken with the octupole lens inactivated, exhibits major distortion in the east-west direction, but only slight distortion in the north-south direction. With Figure 4a as the reference image and Figure 4b as the sample image, Figure 4c is constructed and yields an image in which the spatial distortion caused by astigmatism has been minimized. Notice that the sharpness of detail is not improved in Figure 4c because the algorithm does not create information not already contained in the sample image, but merely corrects for one type of distortion identified. It is evident from Figure 4a, though, that the incorporation of the octupole lens allows for an improvement in the overall image focus. Because features in real samples most often do not have regular spatial relationships to one another, as they do in the Cu grid used for tuning, an operator may record what he believes to be an optimum image, when in fact it suffers from residual astigmatism. Digital image superpositioning can, in cases like this, provide an assessment of the degree to which distortion affects a sample image by correlation with a reference image of low distortion.

Image Superpositioning. The impetus for image correlation is to obtain the capability to superimpose two or more images in order to enhance the information quality of a sample image. By correlation of electron micrographs with ion micrographs, an assessment can be made as to whether the contrast seen in the ion image is due to topography or elemental differences.

In Figure 5, vanadium inclusions in steel are imaged by ion, SE, and BSE microscopes. For publication clarity, a feature map of the SIMS $^{51}\text{V}^+$ image (Figure 5b) is constructed by

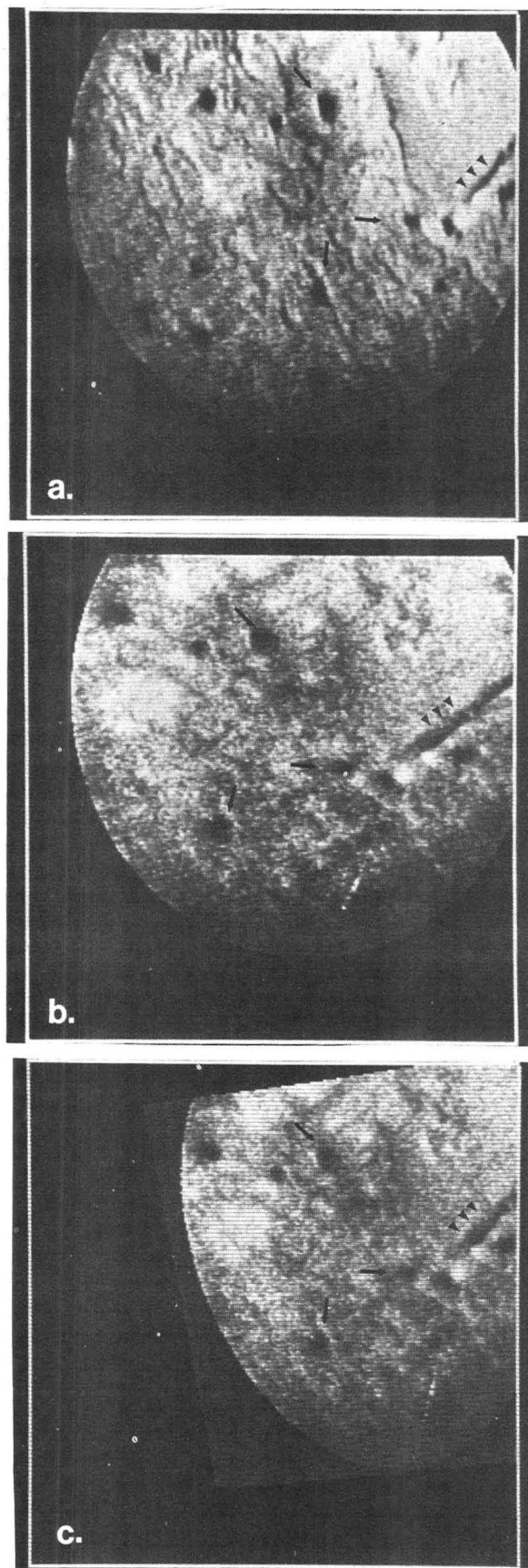


Figure 4. Astigmatism correction: (a) SIMS $^{52}\text{Cr}^+$ image taken with octupole stigmator lens in operation. (b) SIMS $^{52}\text{Cr}^+$ image of same area with lens inoperative. All other instrumental parameters were kept constant. (c) Registered "(b)" image. Image resolution remains as in "(b)" image—information content is retained—but distortion has been removed. Features, marked with arrows, are now spatially correct, relative to one another.

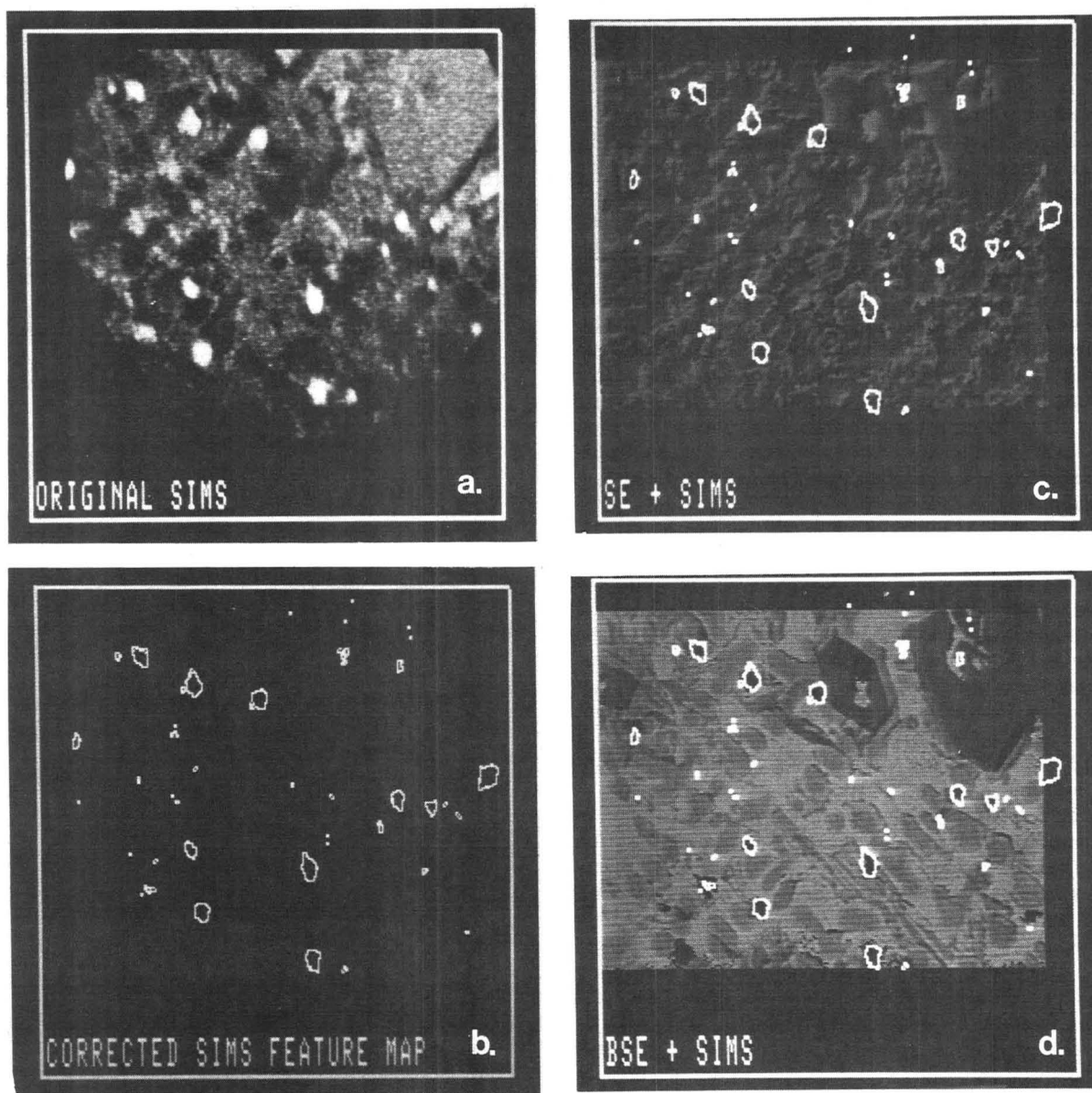


Figure 5. Digital image superpositioning: (a) SIMS $^{51}\text{V}^+$ original image; (b) corrected SIMS $^{51}\text{V}^+$ feature map (see text for details); (c) feature map of $^{51}\text{V}^+$ SIMS image superimposed on SE image; (d) feature map superimposed upon BSE image. SIMS features do not correspond to topographic features in SE image, but to compositional features in BSE image. Notice that for some of the features, the demarcated region does not cover the entire dark regions of the BSE image. This is because BSE has greater information depth than SIMS. Since BSE yield is proportional to the square of the atomic number, the dark features on the BSE image are most probably vanadium inclusions.

reducing the gray-level values into three distinct states—high, medium, and background—corresponding to $^{51}\text{V}^+$ intensity. The reduction is accomplished by using the optimal thresholds generated automatically by decomposing the histogram into three components (10). Only features corresponding to the $^{51}\text{V}^+$ are kept, whereas the other two classes of features are set to zero. A pixel becomes a boundary point if it is determined that any of its four neighboring pixels is zero and is changed to a white pixel. The feature pixels inside the boundary are then set to zero.

Superpositioning of the SIMS feature map upon SE and BSE images, respectively, verifies that the contrast mechanism in the SIMS image is indeed compositional and not topographic. In the SE + SIMS map (Figure 5c) notice that most of the demarcated regions are not homogeneous in gray level, while the same regions in the BSE + SIMS map (Figure 5d) are all homogeneous in gray level. The features of high $^{51}\text{V}^+$ intensity in the SIMS image directly correspond to features on the BSE map that indicate compositional differences within the sample. The SIMS features do not lie over any specific features in the SE image that might indicate topography.

Therefore, digital image superpositioning confirms that topography contributes minimally to the contrast in this SIMS image and that elemental difference accounts for the major mechanism in the formation of this image.

It is interesting to note that the two hexagonal contours in the upper right corner of the images are probably induced by sample topography. Examination of SE and BSE images indicates that these features were created as a result of differential sputtering under ion bombardment, since the sample surface was featureless after polishing and prior to SIMS analysis. In cases such as this, the ion beam induces sample topography. The SIMS image exhibits contrast along the edges of the hexagons. While the features themselves may be of different composition, the edges should not exhibit mass dependence as they appear to in the SIMS image. Digital image superpositioning can be used to ascertain whether the depth of topographic features is great enough to contribute to SIMS image contrast. Previously, the criterion has been determined by using dark-field ion imaging (11). The advantage of digital image superpositioning is that once identified, topographic artifacts may be eliminated completely

through further image processing techniques (demonstrated elsewhere) (11).

CONCLUSION

In an attempt to maximize the analytical capability of the Cameca IMS-3f, correlation via digital image superpositioning has been attained between ion micrographs, which contain predominately isotopic (elemental) concentrations as a function of surface location, and electron micrographs, primarily topographic and compositional in nature. Ion microscopy, in particular, often suffers from secondary image generation mechanisms, which yield contrast not representative of concentration gradients within a sample. The correlation algorithm outlined in this paper has made it possible to directly superimpose photomicrographs of corresponding sample areas in order to ascertain and eventually eliminate some of these interfering contrasts. It cannot, however, identify contrast due to variations in the ionization probabilities caused by the chemical state or chemical environment of the sample.

Additionally, SIMS images taken with and without compensation of astigmatism by an octupole lens system have been correlated. This approach demonstrates the possibility of recording distorted images if (1) no correction of the distortion (for example, the stigmator lens) is implemented, (2) no reference image of low distortion is available, or (3) the shape of the features is not known in advance. Reproducibility of distortion-free images, especially in particle or low-level imaging, is enhanced when digital correlation is utilized. It minimizes systematic errors associated with instrument operation and image tuning.

For ion microscopy, a logical extension of image correlation is the unambiguous correction and subsequent quantification of image features. As in any instrument that spatially reproduces an object, comprehension of the mechanisms involved in image formation is vital. While former methods have subtracted artifact enhanced ion images from raw ion images (11, 12), the objective of the current work is to employ multimicroscopic techniques in a manner consistent with maintaining the desired information content. It is demonstrated that with correlation and superpositioning, image artifacts can be identified and distortions minimized.

While developed for ion microscope image evaluation, it is important to remember that the keystone of this undertaking,

the direct correlation and superpositioning of photomicrographs, is applicable to any and all microscopic techniques and instruments. It presents a method of objectively analyzing images to ensure that the data acquired is that which is actually sought. Since no microscopic method is capable of extracting complete conclusions regarding a sample, it is necessary to exploit assorted techniques in a complementary capacity. This methodology allows for the ready superpositioning of multiple photomicrographs so as to truly extrapolate the contrast of an image to the physical or chemical information concerning the sample.

ACKNOWLEDGMENT

The authors acknowledge John Hunt of the Material Science Center Electron Microprobe Facility for his technical assistance.

Registry No. Chromium steel, 11100-60-0.

LITERATURE CITED

- (1) Werner, H. W. *SIA, Surf. Interface Anal.* **1980**, *2*, 56-74.
- (2) Kupke, K. G.; Pickett, J. P.; Ingram, P.; Linton, R. W.; Shelburne, J. D. *J. Microsc. (Oxford)* **1983**, *131*, RP1-RP2.
- (3) Siklos, L.; Rozsa, M.; Zombori, J. *J. Microsc. (Oxford)* **1986**, *142*, 107-110.
- (4) Newbury, D. E. "Applications of Secondary Ion Mass Spectrometry Image Analysis in Material Science"; presented at the 34th Annual Conference on Mass Spectrometry and Allied Topics, Cincinnati, OH, June 8-13, 1986.
- (5) Bright, D. S. In *Microbeam Analysis 1984*; Romig, A. D., Jr., Goldstein, J. I., Eds.; San Francisco Press: San Francisco, CA, 1984; pp 173-174.
- (6) Castleman, K. R. *Digital Image Processing*; Prentice-Hall: Englewood Cliffs, NJ, 1979; Chapter 8.
- (7) Pickens, D. R.; Price, R. R. *Med. Phys.* **1987**, *14*, 56-61.
- (8) Ling, Y. C.; Bernius, M. T.; Morrison, G. H. *J. Chem. Inf. Comput. Sci.* **1987**, *24*, 86-95.
- (9) Bernius, M. T.; Ling, Y. C.; Morrison, G. H. *J. Appl. Phys.* **1987**, *61*, 1677-1681.
- (10) Velasco, F. R. D. *IEEE Trans. Syst., Man, Cybern.* **1980**, *SMC-10*, 771-774.
- (11) Bernius, M. T.; Ling, Y. C.; Morrison, G. H. *J. Appl. Phys.* **1986**, *59*, 3332-3338.
- (12) Patkin, A. J.; Chandra, S.; Morrison, G. H. *Anal. Chem.* **1982**, *54*, 2507-2510.

RECEIVED for review April 1, 1987. Accepted July 1, 1987. This work was supported through funding from the Cornell Materials Science Center, the National Science Foundation, the Office of Naval Research, and the National Institutes of Health.

Determination of Arsenic, Selenium, and Antimony Using Metastable Transfer Emission Spectrometry

William H. Hood¹ and Thomas M. Niemczyk*

Department of Chemistry, The University of New Mexico, Albuquerque, New Mexico 87131

Metastable transfer emission spectrometry (MTES) has been shown to be an extremely sensitive method for the determination of trace metals. In this communication, we discuss the determination of As, Se, and Sb. The analytes are directly determined from aqueous solution, in contrast to most other atomic spectrometric techniques where a separation/pre-concentration procedure such as hydride generation must be performed to achieve good sensitivity. Detection limits for As, Se, and Sb are found to be 22, 16, and 65 pg, respectively.

The determination of As, Se, and Sb has been the subject of many reports. The high level of interest is due in part to the difficulties encountered when attempting to determine these elements, as well as the fact that all three are of health and environmental concern. Each is acutely toxic to man and animals in large doses. As and Sb have also been shown to exhibit chronic toxic effects at very low intake rates (1). Selenium is an essential trace element for animal nutrition but is toxic at higher levels (2).

Although many methods are available for the determination of these elements, the most commonly used methods involve atomic spectroscopy. Conventional methods of analysis, such

¹Current address: Proctor and Gamble, Cincinnati, OH 45224.

Table I. Vaporization Temperature of As, Se, and Sb

element	electrothermal atomization temp range, °C	boiling point or sublimation temp, °C		
		element	chloride	oxide
As	1200–1400	613	130	312
Se	1600–1750	685	288	345
Sb	1700–1850	1750	283	1550

as direct aspiration of sample solutions into a flame for atomic absorption or a plasma for atomic emission or direct analysis of sample solutions by graphite furnace atomic absorption, suffer from lack of sensitivity and interferences. Indeed, direct determination of Se and Sb in seawater by electrothermal atomic absorption spectroscopy is not feasible due to lack of instrumental sensitivity. Thus, various separation and preconcentration techniques have been developed for the determination of As, Se, and Sb. For the past 10 years, the most widely used of these separation techniques has been hydride generation (3–10). Once adjusted to the proper valence state, the As, Se, or Sb in acidified aqueous samples is reduced to volatile hydrides, AsH_3 , H_2Se , or SbH_3 , using a strong reducing agent and introduced into the spectrometer as the gaseous species. The hydride generation step results in the elimination of many interfering species as well as the preconcentration of the analyte(s) so that the range of applications of the analysis procedure is extended. Authors using the hydride generation technique coupled with graphite furnace atomic absorption spectroscopy or inductively coupled plasma atomic emission spectroscopy have reported absolute detection limits for As, Se, and Sb in the range of 100 pg (11–14). Since the hydride generation results in the concentration of the analyte from samples of significant volume, the relative detection limits achieved using these techniques are quite impressive.

As, Se, and Sb have been determined by using atomic emission spectroscopy with active nitrogen excitation by D'Silva, Rice, and Fassel (15). They used a hydride generation technique to introduce the analytes to a flow of atmospheric pressure active nitrogen that was produced in an ozonizer type discharge. They reported detection limits for the determination of As, Se, and Sb in 1.0-mL samples of 0.1, 5, and 1 ng, respectively. In the work to be discussed here, the active nitrogen was generated in a microwave discharge at low pressure. This results in an active nitrogen flow of significantly different character than that produced in an ozonizer type discharge (16). Further, no preconcentration step was performed in the work discussed here. The samples were directly vaporized into a flow of active nitrogen with an electrothermal vaporizer.

EXPERIMENTAL SECTION

The experiments were carried out in an apparatus consisting of four modules: the sample introduction system, the active nitrogen generation system, the flow cell, and the detection system. The detection system and flow cell are identical with those discussed previously (17).

Sample Introduction. Samples were introduced to the flow cell by electrothermal vaporization into a stream of argon. The argon swept the sample vapor into the flow cell through the innermost of the three concentric flow cell tubes. The electrothermal vaporizer consisted of a tantalum boat powered with a modified Varian CRA-90 programmable power supply (18). Because of the relatively high volatility of As, Se, and Sb and some of their compounds, drying temperatures were kept as low as possible. The drying temperatures were set at 90 °C. No ashing cycle was used in the electrothermal vaporizer temperature program. As can be seen from the data in Table I, some of the compounds likely to be present are very volatile and the use of an ashing cycle would likely result in loss of analyte. The va-

porization cycle thus directly followed the drying cycle. The atomization temperatures used are also listed in Table I. The temperatures were set by use of an optical pyrometer.

Active Nitrogen Generation. Two methods of active nitrogen generation were tested for use in these studies, the microwave discharge and the dielectric discharge. The dielectric discharge used was identical with that previously characterized as producing higher concentrations of the nitrogen metastable species $\text{N}_2(\text{A}^3\Sigma_u^+)$ than the microwave discharge (19). However, in all studies performed with As, Se, and Sb as the analytes, the performance of the system when using the dielectric discharge produced active nitrogen was inferior to that achieved when using the microwave discharge produced active nitrogen. Thus, all data included in this paper have been obtained by using the microwave discharge active nitrogen production system.

Reagents. Matheson UHP nitrogen (99.999% N_2) was used to obtain all data included here, with the exception of the NO background spectrum to be discussed below. The Ar and all chemicals used were reagent grade and all dilutions were performed with distilled deionized water. A Varian Techtron 1000 ppm solution of Se was used to prepare all Se standards. A 1000 ppm As solution was prepared by dissolving 0.3300 g of As_2O_3 powder in 10 mL of 20% NaOH. This solution was acidified by careful addition of 20 mL of 1:1 HNO_3 and then diluted to 250 mL. The 1000 ppm Sb solution was prepared by dissolving 0.500 g of Sb in 25 mL of 1:1 HCl and 1 mL of 1:1 HNO_3 , followed by dilution to 500 mL. All dilutions were prepared fresh for each experiment as needed. The blank solutions were prepared by using identical acid/base solutions as used to prepare the analyte solutions.

Procedures. All measurements were made by pipetting 2.5- μL samples onto the Ta boat, drying the sample, evacuating the system, and initiating the vaporization sequence. The Ta boats used limit the sample size that can be accommodated without significant degradation of precision to 5 μL or less. The detection limits are reported as the amount of analyte needed to produce a signal-to-noise ratio of 2. The signal-to-noise ratios were determined by measuring the standard deviation of at least 10 repeat determinations.

Well Samples. Groundwater samples were obtained from monitoring wells near uranium tailings piles in the Grants, NM, area. The samples were membrane filtered (0.45 μm), acidified with concentrated HNO_3 to a pH <2, and stored in well-rinsed polyethylene bottles. The As and Se concentrations in the samples were determined by use of graphite furnace atomic absorption spectroscopy. The standard procedure used for these determinations calls for a 1:10 dilution of the sample and addition of 0.1% Ni in the form of $\text{Ni}(\text{NO}_3)_2$. This method has been shown to produce accurate and precise results for samples of this type (20). The results reported are based on five determinations.

For determinations in the MTES apparatus the samples were diluted 1:10. The results reported are a minimum of seven determinations.

RESULTS AND DISCUSSION

Active Nitrogen Source. As pointed out in the Experimental Section the performance of the MTES system when determining As, Se, and Sb was superior when using microwave discharge produced active nitrogen relative to the performance when using dielectric discharge produced active nitrogen. The performance evaluation was based on the signal level of the analyte as well as the precision. This result is analogous to that obtained when sulfur- and phosphorus-containing molecules were introduced to the active nitrogen flow (17). Most of the S- and P-containing molecules were volatile species and introduced directly in the gaseous state. Thus, the active nitrogen was responsible for both the atomization as well as the excitation of the analyte species. It has been shown that the flow of active nitrogen produced by the dielectric discharge has almost no nitrogen atoms when the discharge is operated at low pressures (19). In contrast, the active nitrogen produced by the microwave discharge has a high concentration of nitrogen atoms. The nitrogen atoms are the only chemically reactive species in the active nitrogen

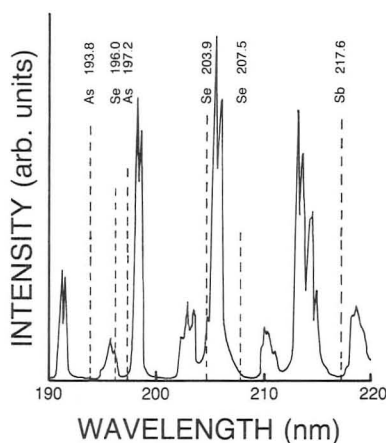


Figure 1. Location of the As, Se, and Sb emission lines relative to the NO γ -band emission between 190 and 220 nm. The intensities of the analytical lines are relative only to the other lines of that analyte.

flow and must be responsible for the break up of any analyte-containing molecules. The lack of nitrogen atoms in the dielectric discharge would account for the very small analyte signals produced when molecular species were introduced to the flow (17).

An analogous situation exists here. A significant fraction of the As, Se, and Sb in the samples analyzed might be expected to be present in volatile compounds that would be vaporized into the cool argon carrier, rather than atomized. Thus, the active nitrogen would have to atomize the analyte-containing molecules prior to the excitation process. Again, the only chemically reactive species in the active nitrogen are nitrogen atoms, and thus it is not surprising that the results obtained by using the microwave discharge produced active nitrogen (high nitrogen atom concentration) would produce superior results when compared to those obtained by using the dielectric discharge produced active nitrogen (low nitrogen atom concentration).

Wavelength Selection. The analyte emission spectrum produced from a MTES plasma is generally fairly simple when compared to the spectrum produced by a high-energy discharge such as the inductively coupled plasma. Thus, the emission spectra of most elements generally contain only a very small number of intense lines. Further, the Wigner spin conservation rule seems to hold very strongly and, for many elements, the resonance line normally used in atomic spectrometric methods to determine that element might not be the most sensitive (18). Finally, the active nitrogen background in the region of the analyte line must be considered.

The most intense atomic emission lines for the elements As, Se, and Sb lie between 190 and 220 nm. In this region of the spectrum, the active nitrogen background is dominated by the NO γ -band system. The NO γ bands are the result of NO and other oxygen-containing impurities in the nitrogen used to produce active nitrogen. The active nitrogen background and the positions of several As, Se, and Sb lines in the 190–220-nm range are shown in Figure 1. Note that the intense NO γ bands were obtained by running the MTES system with the standard grade of nitrogen (99%). The NO γ -band system is more than an order of magnitude more intense than that measured with the UHP nitrogen normally used.

It can be seen from Figure 1 that the most intense lines of As and Sb lie in regions of very low background. However, for Se the situation was not so ideal. The most intense Se emission line at 203.9 nm was found to have significant background overlap. The dominant noise source was background flicker. Thus, a line with significant background overlap resulted in a poor signal-to-noise ratio. The Se line

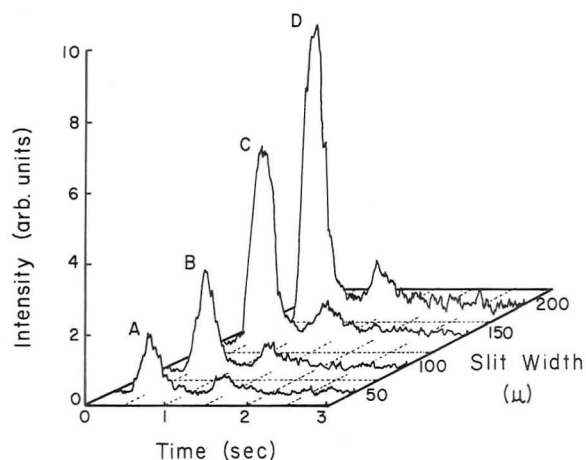


Figure 2. Emission-vs.-time profiles obtained at 207.5 nm for the determination of 20-ng Se samples as a function of monochromator slit width.

at 196.0 nm was somewhat better, but the line at 207.5 nm produced the highest signal-to-noise ratio even though it was less intense.

Operating Conditions. Another factor in the determination of optimum operating conditions was the choice of operating pressure. Both the background and the analyte intensity increased with flow cell pressure. The background intensity increases with increasing pressure at a higher rate than does the analyte signal. Thus, the best signal-to-noise ratio obtained at a particular analyte line is a function of the background intensity at that wavelength and the total operating pressure.

The signal-to-noise ratio for a constant amount of analyte was determined as a function of operating pressure. As discussed above, the analytical lines were chosen to minimize background overlap. Thus, the highest signal-to-noise ratios were obtained at "high" pressure. The microwave discharge does not work well at pressures above approximately 20 Torr, thus the optimum pressure for the determination of As, Se, and Sb was selected to be 18.0 Torr.

The spectral band-pass of the monochromator was also found to have an effect on the signal-to-noise ratio of the measurement if the analyte line was close to a strong background peak. The peaks for As and Sb are sufficiently separated from background signals so that the monochromator band-pass, i.e. slit width, had little effect on the signal-to-noise ratio. The Se line at 207.5 nm was sufficiently close to the background peak at 206 nm, that an optimum slit width was found. This is illustrated in Figure 2 where the output signal for 20-ng Se samples is shown as a function of slit width. The signal-to-noise ratios measured for the indicated slit widths were as follows: A, 38; B, 72; C, 129; and D, 94. Based on these experiments, a slit width of 150 μ m was selected for all determinations.

Blank Signals. Figure 3 shows an example of the emission-vs.-time profiles resulting from samples containing As in amounts ranging from 100 pg to 2.5 ng. Note also that the blank produces a signal corresponding to approximately 50 pg of As. The blank signal was very reproducible, with a precision of better than 10%. The blank signal appeared to be due to As contamination of the reagents or water used to make up the blank solutions. It has been shown that the quality of laboratory environment can contribute to the background signal in many analyte determinations (21). The precision of As determination was found to be approximately 10% at As levels close to the detection limit and approximately 5% at higher As levels.

The emission-vs.-time profiles for Sb and Se appear very similar to those shown for As in Figure 3. The blank signal

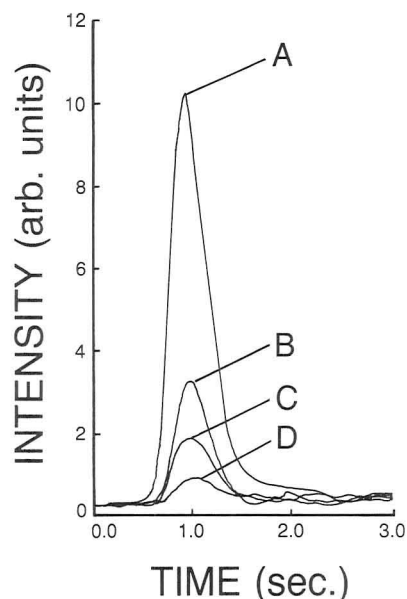


Figure 3. Emission-vs.-time profiles obtained at 193.8 nm from samples containing various amounts of As: (A) 2.5 ng, (B) 500 pg, (C) 100 pg, (D) blank.

Table II. MTES Detection Limits and Linear Ranges for the Elements As, Se, and Sb

element	detection limit, ng	wave-length, nm	linear range (orders of magnitude)
As	0.022	193.8	5.3
Se	0.016	207.5	5.5
Sb	0.065	217.6	4.8

for Se was found to be somewhat less than that seen for As, and the blank for Sb was essentially zero. The fact that the Sb blank averaged to zero is an indication that the blank signals measured for As and Se were not likely to be due to radiation produced by the hot atomizer surface or stray light. Indeed, the blank signals for As and Se were zero at wavelengths just off the analytical wavelengths for those elements. Again, the precision of determination for Sb and Se was approximately 10% near the detection limit and about a factor of 2 better at higher levels. The detection limits for As, Se, and Sb, as well as the linear ranges achieved are shown in Table II.

Matrix Effects. In previous studies involving the determination of metals in solutions containing various matrix constituents, MTES was shown to be relatively free of interference effects (22). Indeed, those interferences that were seen could be assigned to processes affecting the atomization of the analyte rather than something affecting the excitation process. A similar study has been carried out for the analytes As, Se, and Sb, and the results are summarized in Table III. The emission-vs.-time profiles obtained for the determination of 12 ppm As in the presence of varying amounts of NaCl are shown in Figure 4.

At an analyte concentration of 12 ppm, the precision of determination is approximately 5%. Thus, changes in the analyte signal, as shown in Table III, of 5% or less are not significant. The data show, however, that there are significant changes in all cases of 1000 ppm matrix concentration except for the case of As and NaCl. Even in this case, the data shown in Figure 4 indicate that the NaCl has a significant effect on the vaporization of As into the active nitrogen flow. As can be seen in Figure 4, the As emission-vs.-time profile shifts to later times for the 100 and 1000 ppm NaCl solutions.

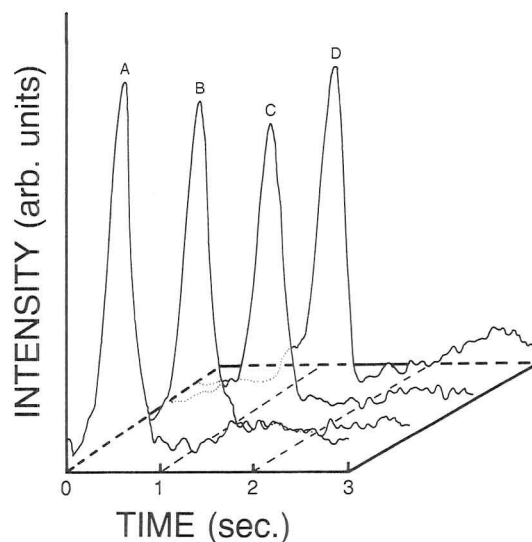


Figure 4. Emission-vs.-time profiles obtained at 193.8 nm from samples containing 12 ppm As and various concentrations of NaCl: (A) distilled water, (B) 10 ppm NaCl, (C) 100 ppm NaCl, (D) 1000 ppm NaCl.

Table III. Percent Changes in the Analyte Signal for Various Levels of Matrix Concentration

	matrix, ppm	As		Sb	Se
		0.25 ppm	12 ppm	12 ppm	12 ppm
NaCl	10	-10	-7	+7	+2
	100	-21	-8	-6	0
	1000	-23	-5	-27	-9
Na ₂ SO ₄	10	-18	0		
	100	-22	-3		
	1000	-43	-8		

Table IV. As and Se Determinations in Well Water Samples

well	As, ppm		Se, ppm	
	AA	MTES	AA	MTES
1	0.32 ± 0.11	0.16 ± 0.11	1.6 ± 0.2	1.4 ± 0.2
2	0.29 ± 0.11	0.17 ± 0.10	1.3 ± 0.1	1.0 ± 0.2
3	0.16 ± 0.09	0.09 ± 0.06	0.6 ± 0.1	0.7 ± 0.1
4	0.41 ± 0.11	0.35 ± 0.15	2.2 ± 0.2	1.9 ± 0.3

The results indicate that physical effects, such as occlusion, are dominating the interference rather than a stoichiometrically dependent chemical effect. As can be seen from the data in Figure 4, there is a significant shift in the peak when going from 10 ppm NaCl to 100 ppm NaCl but no further shift at 1000 ppm NaCl. Occlusion also is reasonable when one considers the vaporization temperatures of the analytes and the matrices. All three analytes are volatile and thus the matrix cannot be vaporized prior to the analyte vaporization. Thus, at heavy matrix concentrations, the analyte would be insulated from the tantalum boat by the matrix and would likely covolatilize with the matrix.

Well Samples. The well water samples contained high total dissolved solids, between 1000 and 6000 mg/L, and thus represent a very challenging matrix. As can be seen from the data presented in Table IV, the results obtained by using the MTES technique agree fairly well with the results obtained by using the standard atomic absorption (AA) technique for Se. The results obtained for As are not in as good agreement. The concentration of As in these samples, after the 1:10 dilution was, however, within an order of magnitude of the detection limit for the technique. Further, the precision of the AA determinations for As was not very good, a factor that

probably also contributed to the lack of agreement noted.

CONCLUSIONS

The MTES system shows very good sensitivity and wide linear dynamic range when applied to the detection of As, Se, and Sb. The absolute detection limits for these elements are superior to those reported for commonly used techniques, such as atomic absorption spectrometry. Indeed, preconcentration techniques, such as hydride generation, are commonly employed when atomic absorption spectrometry is used for the determination. This can result in a great increase in sensitivity. If a preconcentration technique were to be utilized in conjunction with the MTES system, the detection limits might improve significantly. This is an area that should be explored, for a decrease in detection limits for As, Sb, and Se would make MTES an extremely powerful technique that could be applied to many problems where ultratrace determinations of these analytes are important.

LITERATURE CITED

- (1) Luckey, T. D.; Venugopal, B. *Metal Toxicity in Mammals*; Plenum: New York, 1977.
- (2) Levine, R. J.; Olson, R. E. *Proc. Soc. Exp. Biol. Med.* **1970**, *134*, 1030.
- (3) Holak, W. *Anal. Chem.* **1969**, *41*, 1712.

- (4) Braman, R. S.; Justen, L. L.; Foreback, C. C. *Anal. Chem.* **1972**, *44*, 2195.
- (5) Thompson, K. C.; Thomerson, D. R. *Analyst (London)* **1974**, *99*, 595.
- (6) Orheim, R. M.; Bovee, H. H. *Anal. Chem.* **1974**, *46*, 921.
- (7) Fiorino, J. A.; Jones, J. W.; Capar, S. G. *Anal. Chem.* **1976**, *48*, 120.
- (8) Braman, R. S.; Tompkins, M. A. *Anal. Chem.* **1978**, *50*, 1088.
- (9) Andreae, M. O.; Asmode, J.; Foster, P.; Van't Dack, L. *Anal. Chem.* **1981**, *53*, 1766.
- (10) Krivan, V.; Petrick, K.; Welz, B.; Melcher, M. *Anal. Chem.* **1985**, *57*, 1703.
- (11) Sturgeon, R. E.; Willie, S. N.; Berman, S. S. *Anal. Chem.* **1985**, *57*, 6.
- (12) Sturgeon, R. E.; Willie, S. N.; Berman, S. S. *Anal. Chem.* **1985**, *57*, 2311.
- (13) Yamamoto, M.; Yasuda, M.; Yamamoto, Y. *Anal. Chem.* **1985**, *57*, 1382.
- (14) Cutter, G. A. *Anal. Chem.* **1985**, *57*, 2951.
- (15) D'Silva, A. P.; Rice, G. W.; Fassel, V. A. *Appl. Spectrosc.* **1980**, *34*, 578.
- (16) Yang, H. C. Ph.D. Dissertation, University of New Mexico, 1986.
- (17) Hood, W. H.; Niemczyk, T. M. *Anal. Chem.* **1986**, *58*, 210.
- (18) Na, H. C.; Niemczyk, T. M. *Anal. Chem.* **1982**, *54*, 1839.
- (19) Niemczyk, T. M.; Hood, W. H.; Yang, H. C. Pittsburgh Conference and Exposition on Analytical Chemistry and Applied Spectroscopy, Paper No. 1145, New Orleans, LA, March 1, 1985.
- (20) Dreesen, D. R.; Gladney, E. S.; Owens, J. W. *J. Water Pollut. Control Fed.* **1979**, *51*, 2447.
- (21) Adeloju, S. B.; Bond, A. M. *Anal. Chem.* **1985**, *57*, 1728.
- (22) Na, H. C.; Niemczyk, T. M. *Anal. Chem.* **1983**, *55*, 1240.

RECEIVED for review November 24, 1986. Resubmitted June 8, 1987. Accepted June 29, 1987.

Resonance Ionization Spectrometric Determination of Gallium Using an Electrothermal Graphite Atomizer

George Bekov and Vladimir Radaev

Institute of Spectroscopy, USSR Academy of Sciences, SU-142092 Troitsk, Moscow Region, USSR

Jari Likonen, Riitta Zilliacus, Iiro Auterinen, and Eeva-Liisa Lakomaa*

Technical Research Centre of Finland, Reactor Laboratory, Otakaari 3 A, SF-02150 Espoo, Finland

Laser resonance ionization (RIS) after thermal atomization under vacuum has been used in the analysis of low gallium concentrations. The excitation scheme used for gallium is $4p^2P_{3/2} \rightarrow 5s^2S_{1/2} \rightarrow 17p^2P_{1/2,3/2}$, the wavelengths being 403.3 and 430.0 nm, respectively. The 17p state is field-ionized with a pulse of 7.5 kV/cm. Ga samples prepared of different compounds containing the same amount of Ga gave equal analytical signals in all of the cases. The reproducibility was better than 15% when analyzing 27 50- μ L samples of a GaCl₃ solution containing 50 pg of Ga. The calibration curve was linear in the concentration range from 0.1 ng/g to 1 μ g/g. Detection limits of 5×10^7 atoms for pure Ga samples and 3×10^{10} atoms/cm³ in germanium samples were noticed. The comparison measurements between two spectrometers and the electrophysical method gave comparable results for $(6.7-8) \times 10^{15}$ atoms of Ga/cm³ of Ge.

One of the most promising analytical methods effectively developed in recent years is laser resonance ionization spectroscopy (RIS) employing thermal vacuum atomization of the substance to be analyzed. In this method thermally atomized atoms from a graphite crucible are resonantly excited by two or three steps with tunable dye lasers to Rydberg states. These excited atoms are further ionized with an electric field, and ions are detected. The principal advantages of the method

as compared to traditional techniques (atomic absorption analysis, fluorescence spectrometry, etc.) are its high sensitivity, the possibility of detecting practically every atom reaching the laser field (1, 2), and the possibility of the direct analysis of both liquid and solid samples without any appreciable matrix effect (3-5).

It is necessary to carry out intercalibration measurements to further develop the method as well as ensure the reliability of the determinations. Two resonance ionization analytical spectrometers were used in parallel to study the determination of gallium in pure solutions and solid germanium.

Gallium, an element of fairly low crustal abundance, was selected as the object of study. Thus the possibility of the samples being contaminated from environmental impurities could be avoided and there was no call for a special clean room area.

EXPERIMENTAL SECTION

Apparatus. The instruments used for the determination have been described earlier (6). The atomization ovens installed in the vacuum chambers were similar in both installation as well as the ion detectors used.

A schematic drawing of the analytical chamber is shown in Figure 1. For sample evaporation and atomization an electrically heated pyrolytic graphite crucible was used (see Figure 2). The crucibles are transported to the laser laboratory in a specially designed box which is mounted with an airtight connection to the overpressurized cover box under the analytical chamber. The crucible is positioned in the atomizer by means of a manipulator.

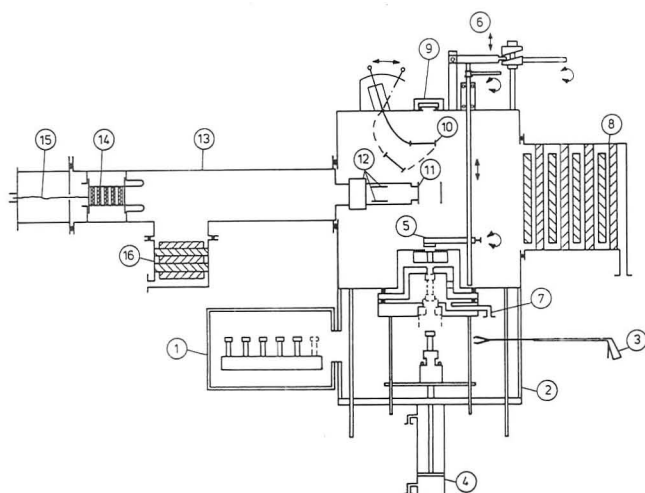


Figure 1. Schematic drawing of the analytical chamber. Details are not to scale, the side of the cubic chamber is 23 cm. Key: (1) transport box for the graphite crucibles; (2) overpressurized cover box for the sample exchange system; (3) manual manipulator for the crucibles; (4) pneumatic piston to move the lower electrode of the atomizer oven; (5) vacuum-tight valve to separate the atomizer from the ionization chamber; (6) manipulators for the above valve; (7) roughing line for the atomizer; (8) turbomolecular pump for the main chamber; (9) window for measuring the oven temperature with an optical pyrometer; (10) beam dump for the atomic beam used for protection of the window; (11) field ionization plates; (12) constant field plates to steer the ions to the detector; (13) time-of-flight tube; (14) ion detector, "venetian blind" type electron multiplier; (15) signal lead from the anode of the electron multiplier; (16) turbomolecular pump for the time-of-flight tube.

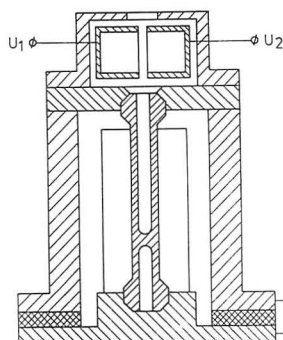


Figure 2. Atomizer with a resistively heated pyrolytic graphite crucible. The length of the crucible is 50 mm and channel diameter 3 mm.

A vacuum-tight valve separates the atomizer from the ionization chamber thus enabling rapid sample exchange while maintaining the main vacuum.

An atomic molecular beam is formed from the sample by heating the crucible. Thermal ions and electrons are prevented from getting into the detection volume by a static electric field in an ion suppressor over the atomizer. As a result, the observed residual thermal ion background at 2500 °C is no more than an ion per second. The collinear laser beams (diameter 2–8 mm) and the atomic beam cross perpendicularly determining the ionization volume. When the atomic beam hits the beam dump and cold chamber walls the gallium atoms are adsorbed.

The laser pulses arrived simultaneously to the excitation volume. The selectively excited atoms were ionized by an electric field pulse of 7.5 kV/cm generated with a laser-triggered spark gap. The electric field arrived along a coaxial transmission line to the electrodes about 70 ns after the laser pulses. The amplitude of the pulse was adjusted to be well above the critical value for the field ionization of the Rydberg levels (7). For the used effective principal quantum number $n^* \approx 14.7$, it is 6.9 kV/cm. The saturation of the field ionization was also verified experimentally.

The energy-level diagram of the Ga atom and its transitions used for excitation is shown in Figure 3.

The dye laser systems in the two spectrometers, designated hereafter I and II, had different power ratings. The two

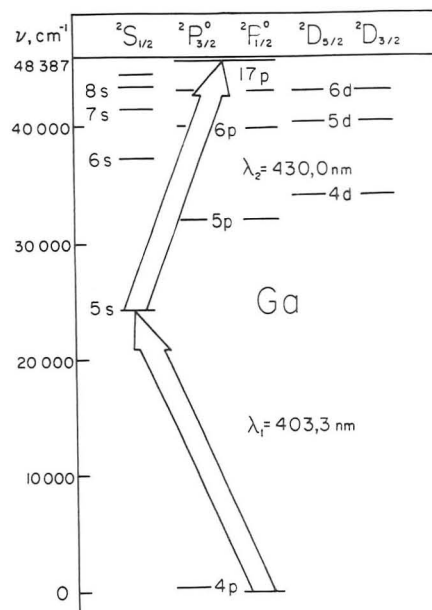


Figure 3. Energy-level diagram of Ga and transitions used for excitation.

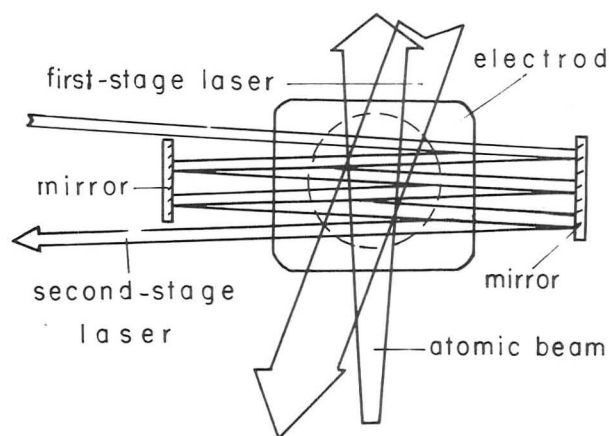


Figure 4. Multipass system.

Hänsch-type dye lasers (line width $\Delta\nu = 1 \text{ cm}^{-1}$) employed in the spectrometer I were pumped with an N_2 laser ($f = 10 \text{ Hz}$, $P_{\text{pulse}} = 0.7 \text{ MW}$, $\tau_p = 10 \text{ ns}$). The near-Gaussian beams had diameters for the first and second excitation steps of 5 and 2 mm, respectively. The fluence of the first-stage excitation laser, $E_1 = 70 \mu\text{J}/\text{cm}^2$, was high enough to saturate the transition $4p^2 P_{3/2} \rightarrow 5s^2 S_{1/2}$, and the laser fluence at the second excitation stage, $E_2 = 3.5 \text{ mJ}/\text{cm}^2$, was lower by a factor of 3 to 5 than that required to saturate the transition $5s^2 S_{1/2} \rightarrow 17p^2 P_{3/2}$. The saturation energies were determined by measuring the analytical signal as a function of pulse energy from a steady atomic flux.

In order to utilize the second-stage laser radiation more effectively and, moreover, to improve the sensitivity of the analysis in spectrometer I, use was made of a multipass system (Figure 4) installed inside the vacuum chamber. The system was comprised of two aluminum mirrors arranged parallel to each other and spaced 10 cm apart. The mirrors were 90% reflective at $\lambda_2 = 430 \text{ nm}$. The second-stage laser radiation was introduced into the multipass system at a small angle, so that it was reflected eight times at each mirror until it left the system. The first-stage laser radiation was introduced into the vacuum chamber from above and counter to the atomic beam at an angle of around 10° to its axis so as to avoid attenuation of the radiation by the film of the evaporated substance deposited onto the top window. The use of the multipass system allowed the sensitivity of the spectrometer to be improved 5 times.

In the other spectrometer (II) the dye lasers (Lambda Physik, FRG, FL2002, $\Delta\nu = 0.2 \text{ cm}^{-1}$) were pumped by an excimer laser (Lambda Physik EMG103E, $f \approx 100 \text{ Hz}$, $P_{\text{pulse}} = 10 \text{ MW}$, $\tau_p = 13 \text{ ns}$) and they delivered enough energy to saturate both the

transitions in a beam with a diameter of up to 8 mm.

Arranged behind the ground electrode was a time-of-flight (TOF) mass filter of the length 0.7 m (I) or 1.0 m (II) which was used to discriminate the signal caused by the background ions from that of Ga^+ ions of masses 69 and 71. This rendered it possible to essentially suppress the nonselective ion background at these masses and to registrate single selective ions. The selectivity of the laser excitation was verified by detuning the second step laser by 5 to 10 line widths which reduced the gallium signal below noise level but did not affect the amount of background ions. When both laser beams were blocked, no gallium or background signal was registrated. The ion background was formed mainly by the photoions produced as a result of interaction between the second-step laser radiation and the matrix components undergoing evaporation. The ions were detected by an electron multiplier (VEU-2, made in the USSR, venetian blind, effective area $16 \times 16 \text{ mm}^2$) with a near-unity efficiency. The ion collection efficiency was measured to be over 70% of the value when the detector was placed close behind the ground electrode.

The signal from the ion detector was amplified with a FET (I) or Plessey 560 (II) preamplifier. The amplified signal was monitored by means of an oscilloscope and processed with a gated integrator (II) (NF Electronic Instruments Mdl BX-531) or a boxcar averager (I) (Princeton Applied Research Mdl 162 with Mdl 164 gated integrator). A minicomputer was used to sum up the total gallium signal from a sample.

The vacuum in the system was maintained by turbomolecular (II) or oil diffusion (I) pumps. The residual pressure in the system was 10^{-4} Pa. During evaporation the pressure in the ionization chamber was not allowed to rise over 10^{-3} Pa. The pressure in the TOF tube was kept at 10^{-4} Pa by a separate pump. Working vacuum condition after sample changing was obtained in 1 min. The heating and cooling procedure took in this case 6 min. Thus the determination time for one dried sample was 7 min. The data interpretation of a sample could be performed simultaneously while the following sample was atomized.

Materials. Gallium stock solutions (10 mg/g) were prepared from metallic Ga. In addition solutions of GaCl_3 , $\text{Ga}(\text{NO}_3)_3$, and $\text{Ga}_2(\text{SO}_4)_3$ were used for standards. High-purity Ge containing calibrated amounts of Ga was used in the experiments. Standard solutions were prepared daily from a 20 $\mu\text{g/g}$ standard by diluting with deionized water. Solutions (5–50 μL) were pipetted with Fintpipettes (Labsystems, Finland) into pyrolytically treated graphite furnaces (Ringsdorf Werk GmbH, FRG) and dried by electric heating (I) or by IR lamp (II) at a temperature below 100 $^\circ\text{C}$. The furnaces were moved into the analytical chamber and the atomization and excitation procedure was started after the vacuum was better than 10^{-3} Pa.

Methods. Thermal atomization and the effect of the temperature on the analytical signal were studied by using different Ga compounds. A temperature distinctly exceeding that needed for the atomization is used in order to clean the crucible for the next sample. This procedure is similar to the practice in graphite furnace atomic absorption spectrometry.

The reproducibility was studied by determining 27 samples of 50 pg of Ga prepared with GaCl_3 .

A calibration curve was determined after analyzing concentrations between 0.1 ng/g and 1 $\mu\text{g/g}$, the sample volume being 5–50 μL . The detection limit of the method was evaluated.

Gallium in high-purity germanium was determined by the direct evaporation of Ge under vacuum. The amount of the Ge samples was 10–20 mg in mass.

RESULTS AND DISCUSSION

Figure 5a shows a typical heating cycle for the crucible, while parts b and c of Figure 5 give the gallium ion signal as a function of time for 5 ng and 50 pg of gallium, respectively. The integral signal was found to be independent of the crucible heating conditions, provided the final temperature was high enough. The analytical signals from GaCl_3 , $\text{Ga}(\text{NO}_3)_3$ and $\text{Ga}_2(\text{SO}_4)_3$ containing equal amounts of Ga were the same in all of the cases. Thus standard Ga solutions can be prepared of different reagents without changing the size of the analytical signal. This does not exclude matrix effects caused by strong anion or cation concentrations present in the solution analyzed

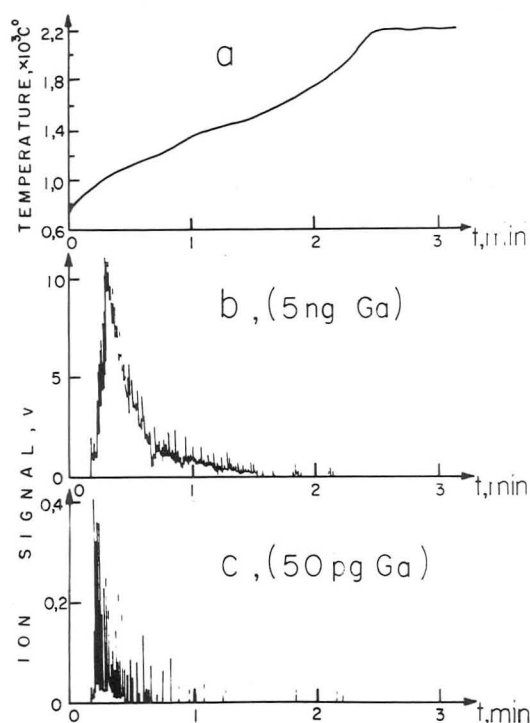


Figure 5. Time dependence of (a) crucible temperature, (b) ion signal for 5 ng of Ga, and (c) ion signal for 50 pg of Ga measured with the spectrometer (I).

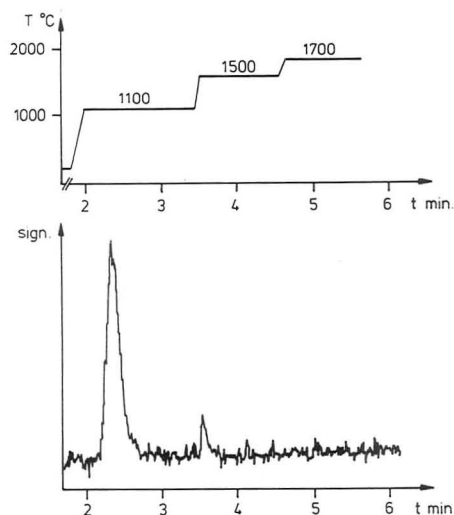


Figure 6. Signal of 90 fg of Ga measured with spectrometer II.

or compounds present in different matrices. The atomization conditions of this method differ from those of graphite furnace atomic absorption spectrometry in that we use vacuum instead of atmospheric pressure and shield gas environment. Reactions with graphite can be expected. The interferences in this case have not yet been widely studied, but the samples have been simple Ge compounds and Ge matrix.

Figure 6 shows the analytical signal of 90 fg of Ga obtained with instrument II. The signal consists of two distinct peaks, which by detuning of the lasers have been found to be gallium. The second peak is probably due to the evaporation of Ga from the colder walls of the crucible, which heat more first when the temperature is increased.

We also investigated the reproducibility of the resonance ionization spectrometry under small-signal conditions. Figure 7 presents a histogram of the results of 27 analyses of 50 μL of a GaCl_3 solution containing 50 pg of Ga, obtained in three successive runs by setup I. The figure also shows a Gaussian curve approximating the experimental distribution obtained.

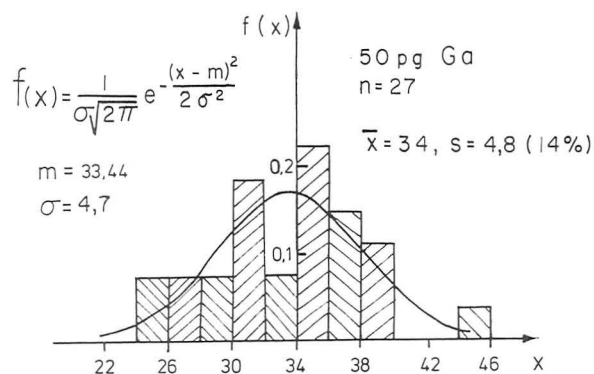


Figure 7. Histogram of 27 determinations with spectrometer I of GaCl_3 solution samples containing 50 pg of Ga.

Mean value of the analytical signal $x = 34$; standard deviation $s = 4.8$ ($\pm 14\%$). Best fit Gaussian distribution mean value $m = 33.44$; variance $\sigma = 4.7$. The standard deviation was less than 15% in the concentration range 0.1 ng/g to 1 $\mu\text{g/g}$ but deteriorated to 60% when concentrations fell below 0.005 pg/g as were used in instrument II. Improvements in the detection electronics and signal registration system are taken to improve the precision of the system.

We found the calibration curve to be linear within the concentration range studied (0.1 ng/g to 1 $\mu\text{g/g}$). By reduction of the heating rate of the crucible, higher concentrations can also be determined, only if care is taken not to have the ion detector saturated.

The detection limit was 2.5×10^{-13} g by setup I. The sensitivity when using setup II was better than that obtained by using setup I, because the former used a more powerful excimer laser for pumping. On the basis of the 90-fg signal (Figure 6) recorded with a gated integrator averaging 32 laser shots per data point, the detection limit expressed as $x_L = \bar{x}_B + 3s_B$ (8) was evaluated to be 5×10^{-15} g. The detection limit is far better than that obtained in neutron activation analysis, 10^{-11} g (9), graphite furnace atomic absorption spectrometry 1.6×10^{-11} g (10), or spark source mass spectrometry 9×10^{-11} g (11). The sensitivity of the analysis can still be increased by enhancing the transport of the atoms to the detection volume and by increasing the laser pulse repetition rate to cover all the atoms released in the atomizer.

Gallium in Germanium. The procedure for the determination of Ga in Ge was the following. Ge samples 10–20 mg in mass were placed in a graphite crucible. Once the crucible was placed in the atomizer and the chamber evacuated, the crucible was heated step by step. At $t \geq 1550^\circ\text{C}$, an appreciable diffusion of Ga atoms from molten germanium ($t_{\text{melt}} \approx 940^\circ\text{C}$) occurred giving rise to a selective ion signal. The optimum temperature for registering the analytical signal was 1650°C . At this temperature the level of the Ga ion signal was suitable for the registration system and the flow of germanium was low enough so that no loss of Ga as a result of its atoms escaping from the crucible in the form of clusters would take place. The signal dropped to zero in 3–5 min, depending on the mass, no more than 1 mg of Ge being lost by evaporation during this time.

The Ga concentration in Ge samples was 8×10^{15} atoms/ cm^3 which was determined by electrophysical methods (12, 13). The analytical signals from the Ge samples and GaCl_3 samples containing the same amount of Ga turned out to be

equal. The concentration determination carried out with spectrometer I by the reference beam technique (14) yielded a value of 6.7×10^{15} atoms/ cm^3 . The reference beam technique is based on the comparison of the ion signals from the atomizer and the reference oven. The flux of gallium atoms from the reference oven, where metallic Ga is placed, can be calculated. The ratios of the ion signals and atom fluxes for the atomizer and the reference oven are equal, because the atoms are ionized and detected under the same conditions. Thus the atom flux from the atomizer can be determined and the amount of element introduced into the crucible with the sample can be obtained. All these facts can be explained only by the complete escape of the impurity from the Ge melt and complete atomization of GaCl_3 as well as the other compounds of Ga under our experimental conditions. Ga can be determined in high-purity germanium in concentrations down to 3×10^{10} atoms/ cm^3 . The reproducibility of the method is good for performing reliable analysis even on concentration levels lower than the parts-per-billion level. The question concerning the total atomization of different compounds will be discussed in a separate paper. The measurements with the two spectrometers, I and II, yielded comparable results for the samples originating from the same Ge piece, 6.7×10^{15} and 8.2×10^{15} atoms/ cm^3 , respectively.

ACKNOWLEDGMENT

The authors are grateful to Vladilen S. Letokhov, Institute of Spectroscopy, USSR Academy of Sciences, and Rainer Salomaa, Helsinki University of Technology, Department of Technical Physics, for helpful discussions.

Registry No. Ga, 7440-55-3; Ge, 7440-56-4.

LITERATURE CITED

- Hurst, G. S.; Payne, M. G.; Kramer, S. D.; Young, J. P. *Rev. Mod. Phys.* **1979**, *51*, 767–819.
- Balykin, V. I.; Bekov, G. I.; Letokhov, V. S.; Mishin, V. I. *Sov. Phys.-Usp.* **1980**, *23*, 651–678.
- Bekov, G. I.; Yegorov, A. S.; Letokhov, V. S.; Radaev, V. N. *Nature (London)* **1983**, *301*, 410–412.
- Bekov, G. I.; Letokhov, V. S.; Radaev, V. S.; Baturin, G. N.; Egorov, A. S.; Kursky, A. N.; Narseyev, N. A. *Nature (London)* **1984**, *312*, 748–750.
- Bekov, G. I.; Letokhov, V. S.; Radaev, V. N. *J. Opt. Soc. Am. B: Opt. Phys.* **1985**, *2*, 1554–1560.
- Bekov, G. I.; Kudryavtsev, Yu. A.; Auterinen, I.; Likonen, J. *Proceedings of the 3rd International Symposium on Resonance Ionization Spectroscopy and Its Applications*, Swansea, Wales, 7–12 Sep. 1986; Hurst, G. S., Morgan, C. G., Eds. Institute of Physics Conference Series Number 84; Institute of Physics: Bristol, 1987; 97–102.
- Bekov, G. I.; Letokhov, V. S.; Mishin, V. I. *Sov. Phys.-JETP* **1977**, *46*, 81–85.
- Analytical Methods Committee *Analyst (London)* **1987**, *112*, 199–204.
- Zilliacus, R., Technical Research Centre of Finland, unpublished work; September 1985.
- Barron, D. C.; Haynes, B. W. *Analyst (London)* **1986**, *111*, 19–21.
- Morrison, G. H. *Tech. Rep. Ser.-IAEA* **1978**, *201*, 201–229.
- Kogan, Sh. M.; Lifshits, T. M. *Izv. Akad. Nauk SSSR, Ser. Fiz.* **1978**, *42*, 1122–1130.
- Andreev, B. A.; Ikonnikov, V. B.; Maximov, G. A.; Shmagin, V. B. *Vysokochistye veshchestva* **1987**, No 1, 138–143.
- Akilov, R.; Bekov, G. I. *Sov. Tech. Phys. Lett.* **1982**, *8*, 225–226.

RECEIVED for review February 24, 1987. Accepted June 25, 1987. The comparisons with the two spectrometers were performed within the framework of a scientific project between the Institute of Spectroscopy of the USSR Academy of Sciences, the Reactor Laboratory of the Technical Research Centre of Finland, and the Helsinki University of Technology. The work of the Finnish group has been partly supported by the Finnish Academy.

Radiotracer Investigation of the Interference of Hydrofluoric Acid in the Determination of Arsenic and Antimony by Hydride Generation Atomic Absorption Spectrometry

Kilian Petrick and Viliam Krivan*

Sektion Analytik und Höchstreinigung, Universität Ulm, Oberer Eselsberg, D-7900 Ulm/Donau, FRG

The influence of hydrofluoric acid on the behavior of arsenic and antimony in hydride generation with NaBH_4 was investigated by means of the radiotracers ^{76}As and ^{124}Sb . Simultaneously, the corresponding extinctions were measured. Up to a concentration of 1% hydrofluoric acid present in hydrochloric acid sample solutions does not affect the hydrogenation of As(III) and Sb(III) . In solutions with higher HF concentration, As(V) forms $[\text{AsF}_5\text{OH}]^-$ ions which do not react with NaBH_4 . After the $[\text{AsF}_5\text{OH}]^-$ ions are hydrolyzed, the interference of hydrofluoric acid can be sufficiently reduced by complex formation with boric acid. Antimony(V) is not hydrogenated in the presence of hydrofluoric acid, which, in addition, seriously hinders the reduction of Sb(V) to Sb(III) . Improved procedures are proposed which allow the elimination of the interference of hydrofluoric acid in both the hydrogenation and the absorption measurement stages and also in the reduction of Sb(V) to Sb(III) in this medium.

Hydride generation atomic absorption spectrometry (AAS) is one of the most important methods for the determination of trace concentrations of arsenic and antimony. However, serious interference problems may occur with analysis of samples that must be decomposed in solutions containing larger amounts of hydrofluoric acid. In addition to various metals and geological samples, this is the case in many environmental samples such as airborne particulate matter, sewage sludge, soil, sediments, and many plant materials.

Welz (1) presented an overview on the interference of hydrofluoric acid for all common hydride-forming elements from which it can be seen that hydrofluoric acid causes detectable interferences in the determination of antimony already at a concentration of 0.0002% and in the determination of arsenic at a concentration of 0.02%. In both cases, the signal depression is strongly increasing with the concentration of hydrofluoric acid reaching about 80% depression at 0.02% HF for antimony and about 50% depression at 1% HF for arsenic. However, no information was given on the valence states of the elements. On the other hand, Janousek (2) did not observe any significant interference by hydrofluoric acid in the determination of arsenic in tungsten and niobium and their alloys after their dissolution in a HNO_3 - HCl -HF acid mixture. In all previous investigations, atomization was achieved at temperatures between 900 and 1000 °C by using a quartz tube.

The aim of the present work was to study the mechanism of the interference of hydrofluoric acid by means of the radiotracer technique complemented by conventional absorption measurements. The main aspect was to distinguish between the interference in the hydride-generation vessel and in the atomization device and to develop improved procedures which eliminate the interference of hydrofluoric acid.

EXPERIMENTAL SECTION

Instrumentation. A Perkin-Elmer MHS 20 mercury/hydride system and a Perkin-Elmer atomic absorption spectrophotometer,

Table I. Operating Parameter for the MHS 20 Using a Quartz Tube (Purge Gas Nitrogen) or Graphite Tube (Purge Gas Argon)

parameter	As	Sb
quartz tube		
purge I	25	20
reaction	10	15
purge II	40	50
graphite tube		
purge I	30 s at 25 °C	30 s at 25 °C
heating up to 2100 °C	45 s	45 s
reaction	10 s at 2100 °C	15 s at 2100 °C
purge II	10 s at 2100 °C	10 s at 2100 °C

Model 400, equipped with electrodeless discharge lamps for arsenic (resonance line, 193.7 nm; slit, 0.7 nm; power, 8 W) and antimony (resonance line, 217.6 nm; slit, 0.2 nm; power, 8 W) were used. Atomizations were performed with a commercially available quartz tube at 900 °C and with a pyrolytically coated graphite tube (special manufacture by Ringsdorf-Werke GmbH, Bonn, FRG) at 2100 °C. The gaseous hydrides were introduced into the tubes via a T connection in the center. The graphite tube was 55 mm long, of 11.5 mm i.d. and 14.5 mm o.d. For its heating, a Perkin-Elmer HGA 70 graphite tube furnace was used. The operating parameters for the spectrophotometer are given in Table I. Deuterium-lamp background correction was used for each measurement. The peak area was recorded during an integration time of 12 s.

The γ -rays of the radiotracers were counted with a well-type NaI(Tl) scintillation detector of 23 cm i.d. and 28 cm length (Bicron, Newbury, CT) coupled with a single-channel analyzer (Berthold, Wildbad, FRG). In each experiment, a counting error <1% was achieved by the choice of an appropriate counting rate and counting time.

Radiotracers and Reagents. The radiotracer ^{76}As was produced by irradiation of $(\text{NH}_4)_3\text{AsO}_3$ in a nuclear reactor. Before use, the tracer was oxidized with an excess of concentrated HNO_3 for 1 h at 95 °C. The completeness of the oxidation was tested according to ref 3. More than 98% of the arsenic was present in pentavalent form.

For the production of $^{122/124}\text{Sb}$, SbCl_3 was irradiated. The antimony tracer was oxidized to pentavalent antimony with a mixture of 2 mL of H_2O_2 (30%) and 2 mL of HCl (32%) for 15 min at 95 °C. The radionuclidic purity of the radiotracers was tested by high-resolution γ -ray spectrometry.

All reagents were of pro analysi grade except hydrofluoric acid which was of "selectipur" grade. They were obtained from Merck, Darmstadt, FRG. Sodium borohydride solutions were prepared from sodium borohydride powder (Riedel de Haen/Seelze, Hannover, FRG) by dilution to 3% (stabilized with 1% NaOH) and filtration. Standard arsenic(V) and antimony(III) solutions (1g/L) were prepared from Titrisol solutions (Merck, Darmstadt, FRG) by dilution. Standard solutions for arsenic(III) and antimony(V) were prepared from "pro analysi" purity grade $(\text{NH}_4)_3\text{AsO}_3$ and SbCl_5 (Merck), respectively. Each experiment was carried out with 50 ng of the analyte element.

Determination of the Radioactivity. The solution to be investigated was spiked with the appropriate radiotracer and the reduction vessel was placed in the well of the detector for counting. The activity was counted before and after each hydride generation.

Table II. Hydride Generation Efficiencies and Absorbances for 50 ng of Arsenic(V) in Different Acid Mixtures.

acid mixture	mode	% residue in reduction vessel	% absorbance	
			quartz tube	graphite tube
1% HF/1.5% HCl	I	23 ± 5	40 ± 20	
1% HF/1.5% HCl/H ₃ BO ₃ ^a	I	2.5 ± 1	80 ± 20	90 ± 5
1% HF/1.5% HCl/H ₃ BO ₃ ^a	II	87 ± 3	10 ± 10	25 ± 30
1% HF/1.5% HCl/H ₃ BO ₃ ^a	III	5.5 ± 1	40 ± 40	90 ± 5

^a These solutions were prepared by dilution of 40% HF and 32% HCl in saturated H₃BO₃ to give a 10 mL reaction volume.

The silicone tube connecting the reduction vessel with the quartz tube was rolled up and placed in the detector well.

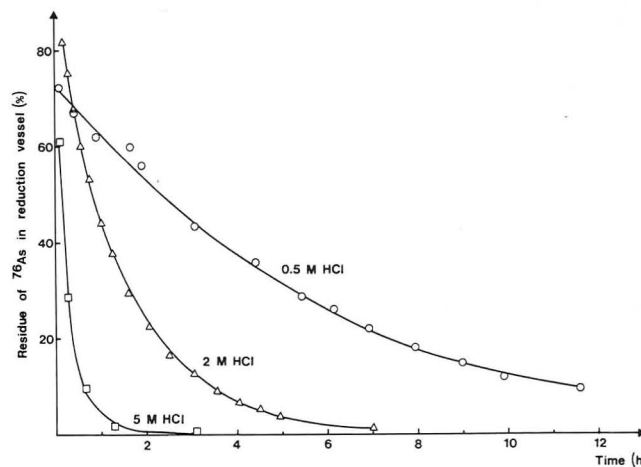
RESULTS AND DISCUSSION

For both investigated elements, no detectable adsorption (<1%) on the vessel walls and the silicone tube connecting the hydride generation vessel with the atomization tube was observed.

Arsenic. By use of a graphite tube for atomization of arsenic at 2100 °C, a temperature high enough to exclude interference by hydrogen fluoride, it was proved that hydrofluoric acid does not hinder the hydride generation from arsenic(III). Up to a concentration of 1%, no significant signal depression (<3%) was observed. In sample solutions obtained by almost all oxidation decomposition procedures, however, arsenic is present in its pentavalent form. So far, no procedure for the prereduction of As(V) to As(III) in the presence of hydrofluoric acid has been described. We developed a method that enables the achievement of hydride generation yields >90% for arsenic(V) and, therefore, did not investigate the common prereduction with KJ in the presence of hydrofluoric acid.

Table II summarizes the results obtained for hydride generation of 50 ng of arsenic(V) from different acid mixtures. They are presented as percentage residue of the analyte element remaining in the reduction vessel and as percentage absorbance of the analyte element, whereby the absorbance measured in 1.5% hydrochloric acid solution was taken with 100% as the basis for comparison. In our recent paper (4), it was proved that hydride generation yields above 99% could be obtained for arsenic(V) from a 1.5% hydrochloric acid solution. The results for percentage residues were obtained from radiotracer experiments and those for absorbances from absorption measurements. In mode I, the acid mixture was prepared first and then the arsenic solution was added. In mode II, the arsenic solution was mixed first with 40% HF and then diluted to 1% HF under contemporary addition of the two other acids. Mode III is the same as mode II except the complete mixture was heated in the hydrogenation vessel for 10 min on the boiling water bath.

The results given in Table II can be explained as follows: Boric acid forms with fluoride complexes which probably do not react with NaBH₄ because of steric hinderance (5). Kolditz and Röhsch (6) showed that, in concentrated hydrofluoric acid, [AsF₆OH]⁻ ions can be formed which are remarkably stable against hydrolysis. It can be assumed that these ions do not react with NaBH₄. At the boiling temperature, however, they hydrolyze rapidly. Furthermore, with free hydrogen fluoride, [AsF₆]⁻ ions are formed that do not hydrolyze at all in aqueous solutions (6). These investigations were carried out at temperatures up to 100 °C. Some modern pressure decomposition methods, however, work at temperatures up

**Figure 1.** Dependence of the hydrolysis of [AsF₅OH]⁻ for three different acid solutions on the time passed between the preparation of the solution (*t* = 0) and the hydride generation.**Table III. Hydride Generation Efficiencies and Absorbances for 50 ng of Arsenic(V) after Antecedent Hydrolysis of [AsF₅OH]⁻ Achieved by Heating the Analyte Solution at 95 °C for 10 min Prior to Hydride Generation**

acid mixture	% residue in reduction vessel	% absorbance	
		quartz tube	graphite tube
0.01% HF/1.5% HCl	1 ± 0.5	60 ± 20	
0.1% HF/1.5% HCl	4.5 ± 0.5	40 ± 20	
0.1% HF/1.5% HCl/H ₃ BO ₃ ^a	1 ± 0.5	60 ± 15	
0.5% HF/1.5% HCl/H ₃ BO ₃ ^a	2.5 ± 1	50 ± 20	94 ± 4
1% HF/1.5% HCl/H ₃ BO ₃ ^a	6 ± 1	50 ± 20	91 ± 3

^a For explanation see Table II.

to 180 °C or even more. In such cases, it is necessary to examine if [AsF₆]⁻ ions are formed.

For the kinetic study of the hydrolysis of [AsF₅OH]⁻ ions, a model "decomposition" solution consisting of 100 µg of As(V) in a mixture of 150 µL of concentrated HNO₃ (65%) and 50 µL of concentrated HF (40%) was prepared and allowed to stand overnight. Then, this solution was diluted with (i) 0.5 M HCl, (ii) 2 M HCl, and (iii) 5 M HCl to 400 mL (1:2000). From each solution, a 10-mL portion was used for hydride generation. The HF concentration in the diluted solutions was 0.005%. In separate experiments, it was ensured that no detectable interference is caused by hydrofluoric acid at this concentration level in the generation of arsenic hydride if arsenic is directly added to the diluted solution prepared before.

Figure 1 shows the dependence of the percentage of arsenic residue remaining in the reduction vessel on the time passed between the dilution of the model solution (*t* = 0) and the hydrogenation. From this figure, a pH dependence of the velocity of hydrolysis of the [AsF₅OH]⁻ ions is evident. This can be explained by the fact that H(AsF₅OH) is a stronger acid than HF (6). Consequently, the determination of arsenic(V) in hydrofluoric acid solutions requires the hydrolysis of the [AsF₅OH]⁻ ions prior to the hydride generation; the necessary hydrolysis duration can be estimated from the diagrams in Figure 1.

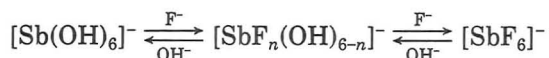
Another easy way for achieving hydride generation yields sufficient for quantitative analysis is to execute the hydrolysis at higher temperatures. Table III gives results for 50 ng of arsenic(V) used in the form of [AsF₅OH]⁻ solution in 10 mL of different acid mixtures which was heated in the reduction vessel at 95 °C for 10 min directly prior to hydride generation.

No improvement could be achieved by prolonging this heating time. No detectable volatilization losses of arsenic were observed.

It can be seen that by addition of boric acid it is possible to extend considerably the HF concentration range for the determination of arsenic in which the interference of hydrofluoric acid remains negligible; at a HF concentration of 1%, the extent of interference reaches 6%. The effect of this interference on the analytical results can further be reduced by the method of standard additions. However, it is necessary to wait with the hydride generation until equilibrium of the hydrolysis is achieved (see Figure 1). Standards must be processed in exactly the same way as samples.

If an uncoated or pyrolytically coated graphite tube is used for atomization at 2100 °C, the interference of hydrogen fluoride in the atomization stage can be reduced to less than 4% (see Table III for data on residues in the reduction vessel and absorbances using graphite tube).

Antimony. Preliminary Experiments. Lange and Askipoulos (7) reported that in diluted hydrofluoric acid the following equilibria of hydrolysis are established for antimony(V):



Kolditz and Sarrach (8) found that in concentrated hydrofluoric acid $[\text{SbF}_6]^-$ ions are formed which, as expected, do not react at all with NaBH_4 . Furthermore, it can be assumed that the equilibrium of hydrolysis for antimony(V) is established much more on the side of the fluorine-containing compounds than in the case of arsenic. Both above references do not report anything about a kinetic hinderance, the occurrence of which, in contrary to arsenic, could not also be observed in any of our experiments.

Some results obtained in preliminary experiments are given below. In the hydride generation of 50 ng of Sb(V) in a mixture of 0.1% HF/3% HCl, antimony remained completely (100%) in the reduction vessel. Since further dilutions to much lower HF concentrations would lead to unacceptable losses in sensitivity, a determination of pentavalent antimony in solutions containing hydrofluoric acid is, in practice, impossible. Complexation with boric acid did not bring any improvement. In order to determine the valence state of the antimony radiotracer, standard solutions of antimony(III) and antimony(V) in 1% hydrofluoric acid were hydrogenated, and for the absorbance measurement, the antimony hydride was atomized in a graphite tube at 2100 °C. Under these conditions, hydrogen fluoride does not interfere with the atomization of the hydride. The results of these experiments showed that antimony(III) is quantitatively hydrogenated, whereas antimony(V) remains quantitatively in the hydride-generation vessel.

In our recent work (4) we showed that even without the presence of hydrofluoric acid the conversion of antimony(V) to antimony hydride is not quantitative, whereby the aging process (condensation of antimony(V) to polyantimonic acids) plays an important role. After hydride generation, 10–50% of the antimony(V) remained in the reduction vessel. On the other hand, if Sb(V) was reduced to Sb(III) according to our procedure recently developed (4) and the resulting solution was made 1% with hydrofluoric acid, the antimony hydride generation efficiency was >99%. This result indicates that there is no interference in the generation of antimony hydride from an antimony(III) solution in 1% hydrofluoric acid.

From the above discussed results, it is evident that in the determination of pentavalent antimony by the hydride generation AAS, a reduction of Sb(V) to Sb(III) prior to the hydride generation is unavoidable—especially in the presence of hydrofluoric acid.

Table IV. Hydride Generation Efficiencies and Absorbances for 50 ng of Antimony(V) in Different Acid Mixtures Obtained by Applying the Improved Reduction Procedure Prior to the Hydride Generation

acid mixture	% residue in reduction vessel	% absorbance	
		quartz tube	graphite tube
0.01% HF/3% HCl/0.05% HNO_3	0.1 ± 0.5	100 ± 7	
0.1% HF/3% HCl/0.5% HNO_3	0.1 ± 0.5	100 ± 7	
0.5% HF/3% HCl/2.5% HNO_3	1 ± 0.5	50 ± 20	
0.5% HF/3% HCl/no HNO_3	25 ± 7		
0.5% HF/4.4% HCl/no HNO_3	0.5 ± 0.5	50 ± 30	99 ± 3
1% HF/6% HCl/no HNO_3	1.5 ± 0.7	30 ± 20	98 ± 3

Also in the case of antimony, no interferences by hydrogen fluoride were observed in the atomization stage if a graphite tube operated at 2100 °C was used instead of quartz tube working at 900 °C. There was no significant difference between results obtained with uncoated and pyrolytically coated graphite tubes.

Reduction of Sb(V) to Sb(III). The reduction of Sb(V) to Sb(III) in the presence of hydrofluoric acid with potassium iodide and with the mixture of potassium iodide/ascorbic acid (4) at room temperature and with potassium iodide at 95 °C was not possible.

In the experiments for an improved reduction procedure, a model "decomposition" solution containing 5 µg of Sb(V) in a mixture of 750 µL of concentrated HNO_3 (65%), and 250 µL of concentrated HF (40%) was used. A portion of 10 µL of this solution containing 50 ng of Sb(V) was diluted with different acid mixtures to 10 mL. Then 0.5 mL of the KI/ascorbic acid solution (5%/5%) was added, and the resulting solution was heated on the boiling water bath for 1 h. As can be seen in Table IV, hydride generation efficiencies near 100% were achieved for all acid mixtures examined. No kinetic hinderance of the establishment of equilibrium was observed.

The comparison of the results obtained with the acid mixtures 0.5% HF/3% HCl/2.5% HNO_3 , 0.5% HF/3% HCl, and 0.5% HF/4.4% HCl indicate that the efficiency of the reduction of Sb(V) to Sb(III) strongly depends on the total acid concentration. When nitric acid was left out, 25% of the antimony remained unreduced. When nitric acid was replaced by an equivalent amount of hydrochloric acid (0.5% HF/4.4% HCl), the residue was again below 1%. With further increase of the hydrochloric acid concentration to 6% and 9%, reduction yields at the same level were obtained. However, at these acid concentrations, ascorbic acid begins to decompose; the accompanying foam formation requires a peak area measurement. With an acid mixture containing 1% HF, 3% HCl, and 5% HNO_3 , because of foam formation, no meaningful measurement was possible. With the mixture 1% HF/6% HCl, in spite of formation of dark brown color during the prereduction and strong foaming during the hydride generation, quantitative yields in both these steps can be obtained. With the hydrofluoric acid concentration of about 1%, however, the upper limit for the above described reduction method is reached. If it is necessary to process any slightly diluted decomposition solutions, e.g., corresponding our 1:10 diluted model solution, nitric acid must be removed prior to the prereduction step.

Registry No. As, 7440-38-2; Sb, 7440-36-0; HF, 7664-39-3; $[\text{AsF}_5\text{OH}]^-$, 25443-48-5.

LITERATURE CITED

- (1) Welz, B. *Atomic Absorption Spectrometry*, 2nd ed.; Verlag Chemie: Weinheim, 1983, p 233.

- (2) Janousek, I. *Fresenius' Z. Anal. Chem.* **1985**, 321, 762.
 (3) Green M.; Kafalas J. A. *J. Chem. Phys.* **1954**, 22, 760.
 (4) Petrick, K.; Krivan, V. *Fresenius' Z. Anal. Chem.* **1987**, 327, 338.
 (5) Jolly, W. L.; Normann, A. D. *Preparative Inorganic Reactions*; Wiley: New York, 1968; p 8.
 (6) Kolditz L.; Röhnsch W. *Z. Anorg. Allg. Chem.* **1958**, 293, 168.

- (7) Lange, W.; Askitopoulos K. *Z. Anorg. Allg. Chem.* **1935**, 223, 369.
 (8) Kolditz L.; Sarrach D. *Z. Anorg. Chem.* **1958**, 293, 132.

RECEIVED for review September 29, 1986. Resubmitted February 1, 1987. Accepted June 29, 1987.

Determination of Boron Isotope Ratios in Geological Materials by Inductively Coupled Plasma Mass Spectrometry

D. Conrad Gregoire

Geological Survey of Canada, Ottawa, Ontario, Canada K1A 0E8

A method for the determination of B isotope ratios in a variety of geological materials is described. Boron isotope ratios are determined with a precision of 0.7% in materials containing as little as 0.5 ppm B. Sample material is leached with HCl in sealed pressure tubes or fused with sodium carbonate. Separation and/or preconcentration of B from matrix elements is accomplished by using Amberlite XE-243, Dowex 50W-X8, or Chelex-100 resins. The use of NASS-1 reference seawater is suggested as a reference material for calculating and comparing isotope shifts for different geological materials. Nonspectroscopic interferences due to the presence of concomitant elements in solution are shown to cause ^{11}B ion count rate suppression at concentrations of Na above 2000 ppm. The presence of excess amounts of concomitant elements causes a matrix-induced mass discrimination effect. Boron isotope ratios ($^{11}\text{B}/^{10}\text{B}$) for the materials studied ranged from 3.91 to 4.18 for basalt and seawater samples, respectively.

The study of boron isotope ratios in nature is of interest to geochemists for a number of reasons. Boron, being a light element, has a proportionately high mass difference between its two naturally occurring isotopes at masses 10 and 11. Boron is known to form volatile compounds and is also mobile in the natural setting. Thus, isotopic shifts are expected to occur in terrestrial rocks. For example, oceanic waters are enriched in ^{11}B by about 5% (1). The ratio of $^{11}\text{B}/^{10}\text{B}$ in terrestrial samples varies between 4.24 and 3.92 (2), whereas a ratio of 3.85 has been reported for meteoritic material (3). Little is known, however, about the relation between boron isotope ratios and mineralization.

The determination of boron isotope ratios has been carried out by a variety of methods including atomic absorption spectrometry (4) and chemical ionization (5) and electron impact (6) mass spectrometry. Because of its high precision, thermal ionization mass spectrometric methods (7-9) have been favored for many applications. Precisions of between 0.2% and 0.3% are typically reported. An important disadvantage of these methods is the time required for sample preparation and isotope ratio determination. The determination of large numbers of samples is often a requirement of geochemical exploration programs, thus excessive analysis time, and hence cost, in many cases precludes the study of boron isotope ratios as part of these investigations.

One of the advantages of inductively coupled plasma mass spectrometry (ICP-MS) over other techniques is its relative speed of analysis. Once prepared in solution form, boron isotope ratios can be determined at the rate of about 1 sam-

Table I. Elan Operating Conditions and Signal Measurement Parameters

rf power	1100 W
plasma gas flow rate	13.0 L/min
auxiliary gas flow rate	2.2 L/min
nebulizer gas flow rate	1.1 L/min
sample uptake rate	1.0 mL/min
sampling orifice to load coil	18 mm
$B = +1.1$ V	$B = +1.1$ V
	$E_1 = -16.2$ V
	$P = -12.3$ V
	$S_2 = -7.0$ V
resolution mode	high
measurement per peak	3
scanning mode	isotope
measurement mode	multichannel
measurement time	5 s
repeats per integration	5
dwell time	300 ms
cycle time	5 s

ple/min. A second advantage rests in the possibility of using less conventional techniques of sample introduction such as laser ablation or electrothermal vaporization.

The measurement of isotope ratios by ICP-MS has been reported in the literature. The majority of papers deal with the determination of Pb (10-17), with a smaller number reporting work on other elements such as Sr (10, 11), Rb (18), U (17, 19), Zn (12), Os (17), and Fe (13). Russ and Bazan (17) determined boron isotope ratios in synthetic solutions and found that the isotope ratios were not altered in the presence of equimolar amounts of Pb or Li. The apparent boron isotope ratio, however, differed by 15% relative to the certified value (SRM 951). Gregoire (20) reported the determination of boron isotope ratios in a variety of geological materials. Boron isotope ratios were determined with a precision of better than 1% in colemanite and anhydrite samples.

The objective of this work was to investigate the possibility of using ICP-MS for the determination of boron isotopes in a wide variety of geological sample types.

EXPERIMENTAL SECTION

Instrumentation. A Sciex (Thornhill, Ontario) Elan Model 250 was used for these studies. The experiments described were done on the Elan 250 after the installation of the new ion lens system. The new ion lens set consists of a three cylinder Einzel lens system, which replaced the ac rods located between the skimmer and the Bessel box lenses. Also, the ring lens positioned immediately behind the skimmer was replaced with a 5-mm-diameter grounded optical stop. This new system was installed by the manufacturer in order to improve signal stability and to reduce instrument susceptibility to effects due to concomitant elements. The new ion lens system reduced the effect of con-

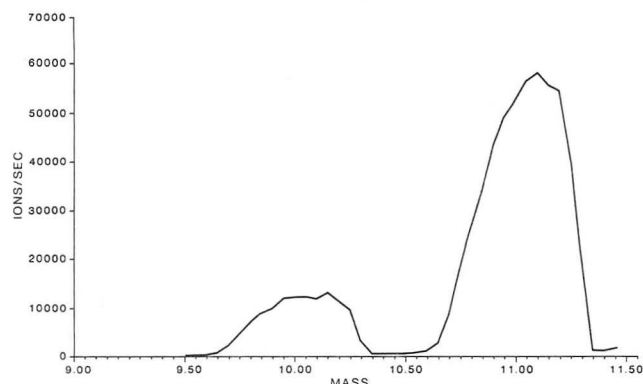


Figure 1. Mass spectrum for a solution of 100 ppb B (SRM 951).

comitant elements by, in some cases, orders of magnitude and also made interference effects immune to changes in ion lens voltage settings (21). A more detailed description of the instrumentation can be found elsewhere (22). The ion lens voltage settings used for this work are listed in Table I.

The long torch supplied with the instrument and a Meinhard C3 concentric glass nebulizer were used. Sample solution uptake rate was controlled with a peristaltic pump (Gilson Minipuls 2). A sampling depth (distance between sampler orifice and rf load coil) of 18 mm was used. The plasma conditions used for the measurement of boron isotope ratios are listed in Table I.

Ion exchange chromatographic columns were fabricated from 10-mL-capacity disposable pipet tips (Oxford, manufactured by Lancer). Column tips were fitted with tygon tubing of sufficiently small diameter to restrict the flow of sample solution to a controlled rate of 1 mL/min. Plugs made from open pore polyurethane foam were used to contain the resin in the columns.

Reagents. All reagents used were reagent grade. Acids were Ultrex grade (J. T. Baker Chemical Co.) with the exception of hydrofluoric acid, which was of reagent grade. Dowex 50W-X8 (Baker) cation exchange resin (20–50 mesh) and Chelex-100 (Bio-Rad Laboratories) chelating resin (50–100 mesh) were used as received and in their hydrogen forms. Amberlite XE-243 (BDH Chemicals) boron specific resin was used without further treatment. Specpure (Johnson Matthey Chemicals) sodium carbonate was used for sample fusions. National Bureau of Standards reference materials 951 (isotopically analyzed boric acid) and 952 (enriched boric acid) were used for calibration purposes. Isotope shifts were calculated relative to NASS-1 seawater reference material (National Research Council of Canada).

Measurement of Boron Isotope Ratios. The isotope ratio program provided with the instrument software was used for the calculation of boron isotope ratios. The parameter settings used are given in Table I. The high resolution mode of signal measurement was used to prevent overlap of the ^{12}C peak on ^{11}B . This occurred mainly when excess carbonate remained in solution following sample preparation procedures utilizing a carbonate flux. Resolution was set at 0.6 u at 10% peak height. Figure 1 is a scan of ^{10}B and ^{11}B of a solution containing 100 ppb boron (SRM 951). No corrections for isobaric interferences were necessary since no other isotopes of any other element exist at mass 10 or 11. As well, with the exception of ^{12}C overlap, no other species originating from water, acids, or plasma gases were found at these masses (23, 24). The formation of boron oxide species was found to be negligible under the experimental conditions used.

Signal measurement was accomplished by using the multi-channel mode. The multichannel mode allows counting times for the m/z of the less abundant isotope to be increased relative to its natural abundance. In this way, the counting statistics for the two boron isotopes were normalized. Three measurements per mass peak were taken for each isotope. The numerical result obtained was the mean of the three values, one taken at the center of the peak and the other two at 0.05 u on either side. All isotope ratios reported are the average of five such determinations.

Nonspectroscopic Interferences. Nonspectroscopic or so-called matrix interferences can pose problems when determining boron isotopes in geological materials. Solutions derived from the fusion or acid digestion of rocks and minerals typically contain

Table II. Effect of Na, Cs, and Pb on the Recovery of ^{11}B ^a Ion Count Rate

molar ratio $\text{M}/^{11}\text{B}$	recovery in the presence of concomitant element (M)		
	Na	Cs	Pb
50			0.88
100		1.00	0.63
200			0.59
300		1.00	0.41
500	1.00		0.26
600		0.67	
1000	1.00	0.43	0.12
1500		0.24	
2000	1.00	0.18	0.05
5000	1.00		
10000	0.97		
15000	0.93		
20000	0.88		

^a 100 ppb boron.

very high quantities of dissolved solids. Dilution of these solutions is generally necessary in order to facilitate their introduction into the plasma. Suppression of analyte ion count rates due to the presence of concomitant elements further complicates the determination of boron because the sensitivity of the technique can be reduced to the point where the determination of traces of boron is not feasible. Thus, knowledge of nonspectroscopic interferences is important in understanding the impact that these might have on a determination and in formulating the steps necessary in order to compensate or correct for these.

Although the nature of nonspectroscopic interferences in ICP-MS is unclear, it is known (21, 25) that the severity of nonspectroscopic interferences is dependent upon both the atomic mass and the degree of ionization in the plasma of the analyte and concomitant elements. The greater the mass and degree of ionization of the concomitant, the greater will be the interference effect. Analytes most susceptible to interferences are those whose atomic mass is small and are also not appreciably ionized in the argon plasma.

Boron is an element which is light and is not completely ionized in the argon plasma. With an atomic mass of 10.81 and a degree of ionization of approximately 58% (26) at 7500 K, it was expected that nonspectroscopic interferences would be serious.

In a separate study (21), this author has reported the effect of plasma conditions on nonspectroscopic interferences. The rf power and the nebulizer pressure were found to be the most important plasma conditions. Depending upon the plasma conditions chosen, the presence of concomitant elements can cause an enhancement, suppression, or no effect on analyte ion count rates. In general, however, analyte ion count rate suppression was observed when the central part of the plasma (position of greatest ion count rate) was being sampled. Thus, although plasma conditions can be used to moderate the effect of concomitant elements, decreases in interference effects were generally coupled with a corresponding decrease in analytical sensitivity. Only under certain circumstances (discussed below) is it advantageous to reduce the analyte sensitivity in order to attenuate nonspectroscopic interferences.

The effect of added Na, Cs, and Pb on the ^{11}B ion count rate is given in Table II. The recovery of the ^{11}B ion count rate is given over a wide range of concomitant to analyte molar ratios. The term recovery is used here to indicate the severity of analyte ion suppression and is defined as the analyte ion count rate obtained for ^{11}B in the presence of concomitant divided by the analyte ion count rate obtained for ^{11}B alone. The experimental conditions used were those given in Table I.

The data in Table II show that the greater the atomic mass of the concomitant element, the greater the analyte suppression. Lead with an atomic mass of 207.2 caused a greater suppressive effect than Cs with an atomic mass of 132.9. Sodium with an atomic mass of only 23.0 caused the smallest suppressive effect of the three elements. A 12% suppression in ^{11}B ion count rate resulted when either 4438 ppm Na (molar ratio, 20 000 to 1) or 95.9 ppm Pb (molar ratio, 50 to 1) were present as concomitant

Table III. Instrumental Mass Discrimination for Boron Stable Isotopes

solution	actual $^{11}\text{B}/^{10}\text{B}$ ratio	measd $^{13}\text{B}/^{10}\text{B}$ ratio
1	4.044	4.208
2	2.714	2.773
3	1.934	1.963
4	1.049	1.046
5	0.568	0.551
6	0.268	0.254

elements. Most of the matrix elements present in a geological matrix are either of low atomic mass (e.g., Na, Ca, Fe) or are not completely ionized in the plasma (e.g., Si, Cl). Simple dilution or separations that use cation exchange resins may be all that are necessary to prepare solutions for B isotope determinations by ICP-MS.

Instrumental Mass Discrimination. Instrumental mass discrimination refers to the resultant effect of mass discrimination processes occurring at the interface, ion lenses, quadrupole mass filter, and detector. In ICP-MS the combined effect from all of these sources is variable and is very dependent on the selection of ion lens voltage. For example, the apparent boron isotope ratio ($^{11}\text{B}/^{10}\text{B}$) for SRM 951 boric acid (certified value: 4.0436) varied from about 3.2 to 4.7 over a broad range of ion lens voltage settings. A different factor to correct for instrumental mass discrimination is necessary for each set of ion lens voltages selected.

The correction factor necessary to convert apparent to actual boron isotope ratios for the experimental conditions given in Table I was determined in the following manner. A series of solutions containing mixtures of NBS SRM 951 and NBS SRM 952 ($^{11}\text{B}/^{10}\text{B} = 0.0532$) were prepared to span the range of boron isotope ratios from 4.0436 to 0.2678. The total boron content of each solution prepared was approximately 150 ppb. The apparent boron isotope ratio was determined for each of these solutions. The calculated and apparent boron isotope ratios for each of these solutions are given in Table III. A linear regression treatment of this data yielded a straight line with a slope of 1.046 with a correlation coefficient of 0.999. The instrumental mass discrimination for the system was determined to be +4.6%. Although the calculated correction factor was reproducible from day to day provided experimental conditions were unchanged, the boron isotope ratio of SRM 951 was determined frequently in order to verify that the correction factor had not changed during the experiment.

Matrix Induced Mass Discrimination. The severity of nonspectroscopic interferences is dependent upon the mass of the analyte. Therefore, for an analyte such as boron, the ion suppression effect should be more severe for the lighter isotope than for the heavier isotope. As mentioned above, the low atomic mass of B, the percentage mass difference between the two stable isotopes, and the relatively low degree of ionization of boron in the argon plasma combined to make B a good candidate for matrix-induced mass discrimination effects. In effect, the presence of an easily ionizable matrix component should (at some concentration) cause the ^{10}B ion count rate to be suppressed to a greater extent than the ^{11}B ion count rate. What should be observed is an increase in the apparent boron isotope ratio with increasing concentration of matrix component.

The effect of added Na (as chloride) on the apparent boron isotope ratio is given in Table IV. For this experiment, a solution containing 150 ppb B (SRM 951) was used. The apparent boron isotope ratio did not change with the addition of Na until a concentration of 3000 ppm was reached. At higher concentrations, the apparent isotope ratio increased sharply with increasing Na concentration. The apparent boron isotope ratio was increased by 8% over the certified value at a Na concentration of 6000 ppm. Since boron isotope ratios are not expected to vary in nature by more than about 5%, it is clear that the presence of concomitant elements could mask completely any real variations in boron isotope ratios present in a series of samples. A comparison of data contained in Table IV with the Na interference data given in Table II indicates that the Na concentration that caused a measurable change in the apparent B isotope ratio was also very close to the Na concentration at which ion count rate suppression began. This is reasonable since the two B isotopes differ in mass by over 10%

Table IV. Matrix-Induced Mass Discrimination Effect for Boron Stable Isotopes

Na/ppm	apparent $^{11}\text{B}/^{10}\text{B}$ isotope ratio
1000	4.044
1500	4.040
2000	4.042
3000	4.124
4000	4.205
5000	4.286
6000	4.367

and their response to the presence of Na would be quite different. Under the experimental conditions used, a total dissolved solids concentration above approximately 1500 ppm should be avoided.

Matrix-induced mass discrimination effects for the light elements could seriously affect isotope ratio determinations as well as analyses carried out by using the isotope dilution method. Both of these techniques rely on the ability to measure accurate isotope ratios. Reduction of the severity of matrix interferences resulting from changes in plasma parameters (21) or sample dilution (25) provide a simple mechanism for avoiding or reducing the possibility of matrix-induced mass discrimination effects. When very low concentrations of B in natural materials are encountered, resorting to preconcentration steps and matrix removal procedures becomes essential.

Separation and Preconcentration of B from Matrix Components. The high solids content of solutions resulting from geological sample digestion/dissolution procedures require the application of B separation procedures prior to the determination of isotope ratios. There are several approaches available to accomplish matrix elimination. These include distillation of the trimethyl ester of boric acid (27), solvent extraction procedures (28–30), and the use of ion exchange resins (31–33).

Distillation procedures are unsatisfactory because these require relatively large volumes of reagents and are time consuming. Solvent extractions from acidic aqueous samples (containing 1% NaCl and 200 ppb B) were not successful. Very low extraction yields were obtained when diethyl ether, isopropyl ether, and ethyl alcohol were used as extractants. When extraction yields were high enough to be of use, excessively high quantities of NaCl were also extracted at the same time.

Ion exchange resins can be used to separate boron from ionic matrix components in two ways. By the use of cation exchange resins, interfering matrix components can be removed from solution while boron is eluted or conversely, B can be selectively removed from solution while matrix components are eluted. The latter technique also can serve as a preconcentration step for materials low in boron. The chemical properties of a boron specific resin (Amberlite XE-243) were discussed in a paper by Kunin and Preuss (34). The resin contains *N*-methylglucamine groups, which complexes boron as borate ion. Matrix components can then be eluted from the resin with ammonium hydroxide. A small quantity of 10% HF is used to convert the borate to the tetrafluoroborate, which is quantitatively retained on tertiary amine groups also located on the resin and which give it a weakly basic anion exchange property. Complexed B is eluted from the column by using 1 M NaOH. To remove Na ion, the eluate is then passed through a column containing a strong cation exchange resin (Dowex 50W-X8) partially loaded with Ca ion. Excess fluoride in solution is precipitated within the column as insoluble calcium fluoride. Columns were prepared from disposable 10-mL Eppendorf pipet tips fitted with small bore tygon tubing to restrict solution flow rates to 1 mL/min. Resin beds were retained within the columns by using plugs made from open-pore polyurethane foam. Details of the experimental procedure used for B separations and the regeneration of columns have been published by other investigators (33–35).

Application of this resin to the separation of boron from materials containing large and trace quantities of boron were successful. Selected results are given below. Great care, however, must be exercised in applying this technique since any excess HF entering the sample introduction system of the ICP can cause high blank values. Hydrofluoric acid leaches boron from com-

ponents such as spray chambers and nebulizers, which are generally made from glass. Use of these columns was also time consuming and thus application of Amberlite XE-243 is recommended only for samples containing less than 0.5 ppm B.

For samples containing boron at concentrations greater than 0.5 ppm, the use of cation exchange or chelating resins such as Dowex 50W-X8 or Chelex-100 is sufficient to reduce matrix concentrations to tolerable levels. Both of these resins were found not to cause any alteration in the boron isotope ratio of a 100 ppb solution of SRM 951. Five milliliters of B solution were equilibrated with an equal volume of resin and allowed to stand for 8 h. Although some B was adsorbed onto the resin or otherwise lost from solution, the isotope ratio did not change from the certified value. Ion exchange resins were used in "batch" form rather than in packed columns in order to save time. Deionized sample solutions were separated from the resin by using a 10-mL Eppendorf pipet whose tip was fitted with a small prefilter made from a 5-mm length of small diameter Tygon tubing packed with a plug of open-pore polyurethane foam. It is essential to ensure that sample solutions do not contain any ion exchange resin beads since these can lodge themselves in the concentric nebulizer causing clogging.

In practice, the use of Chelex-100 chelating resin is recommended since this resin is more selective toward doubly charged ions than is Dowex 50W-X8. Alkaline earth elements are more troublesome than alkali elements primarily because salts of Ca and Mg tend to clog nebulizers to a greater extent. The higher capacity of Dowex 50W-X8, however, makes it more practical to use when large quantities of salt are present such as in solutions derived from fusion melts.

Sample Preparation Procedures. Two procedures were utilized for releasing B from sample material. The first technique was an extraction procedure where up to 5 grams of sample could be used. Sample material ground to -300 mesh was placed in a screw-cap Teflon pressure vessel with a volume of concentrated HCl equivalent in milliliters to the number of grams of sample material used. The mixture was heated in a water bath at 90 °C for 1 h. The mixture was centrifuged and the supernate decanted into a small Teflon vessel. After evaporating the supernate to dryness in order to drive off excess HCl, 5 mL of distilled water was added. Materials rich in iron were treated with a minimum quantity of ammonium hydroxide in order to precipitate iron. After the solution was centrifuged to remove precipitate, the solution was heated on a hot plate to drive off excess ammonia. After the solution was cooled, 3 mL of Chelex-100 resin was added to the solution. The mixture was allowed to stand for 1 h before filtering prior to the determination of B isotope ratios. The removal of excess reagents and the use of ammonium hydroxide contribute to producing sample solutions containing less salt, thus reducing the quantity of chelating resin required in subsequent steps.

The above procedure results in a leaching of acid soluble B and not in the total dissolution of the sample material. Although some of the B trapped in silicates is left behind in the residue, it is unlikely that any mass fractionation of B isotopes would result. In some cases, it may be advantageous to use HCl or milder chemical agents to effect a selective leaching of B from different phases of geological sample materials.

The B isotope ratio relating to the bulk composition of the sample material was obtained via a carbonate fusion of prepared (-300 mesh) sample material. To 100 mg of sample, 400 mg of sodium carbonate was added. In a Pt crucible, the mixture was heated at 900 °C for 20 min. the fused material was dissolved in 10 mL of distilled water. After separation of precipitated silica, the solution was treated with 6 mL of Dowex 50W-X8 ion exchange resin in the manner described above.

For sample material low in boron, each of the above sample preparation techniques can be used prior to preconcentration on Amberlite XE-243 resin. Dissolved fusion melts can be passed directly into the XE-243 column. Solutions obtained from the pressure leaching technique can be added to the resin columns following the acid evaporation step and the addition of water and a small quantity of base.

RESULTS AND DISCUSSION

The determination of B isotope ratios in a wide variety of

Table V. $^{11}\text{B}/^{10}\text{B}$ Isotope Ratios in Geological Materials for Three Different Separation Techniques

	Amberlite XE-243	Dowex 50W-X8	Chelex-100
colemanite 1	4.016 \pm 0.018	4.085 \pm 0.025	
colemanite 2	4.055 \pm 0.048	4.056 \pm 0.050	
tourmaline 1	4.019 \pm 0.043	4.090 \pm 0.050	
tourmaline 2	4.007 \pm 0.059	4.011 \pm 0.030	
anhydrite	4.173 \pm 0.015		4.167 \pm 0.038
gypsum 1	4.128 \pm 0.022		4.148 \pm 0.027
gypsum 2	4.190 \pm 0.055		4.157 \pm 0.016
gypsum 3	4.050 \pm 0.071		4.052 \pm 0.038
gypsum 4	4.034 \pm 0.034		4.058 \pm 0.033

geological materials was carried out. Verification of determined isotope ratios by using reference materials was not possible since none are commercially available. However, the B isotope ratio obtained for some materials can be compared with those obtained from similar samples reported in the literature. There are few reported values of B isotope ratios and these are included for comparison where possible. In all other cases, it was necessary to rely on the determined B isotope ratio of a control substance, which served both as an accuracy check and as a means of calculating values for isotope shifts. The material selected for a control was NASS-1 National Research Council of Canada reference seawater. Seawater contains approximately 5 ppm of B in solution and offers a matrix from which B must be separated before isotope ratios can be measured by ICP-MS. In this way, samples and controls can be subjected to the same sample preparation steps and actual isotope shifts can be calculated relative to the value obtained for the NASS-1 control. The reference seawater is available at a relatively low cost allowing those determining B isotope ratios in natural materials to compare isotope ratio shifts relative to the same material. Isotope shifts were calculated by subtracting the B isotope ratio of NASS-1 from the B isotope ratio of the sample and dividing by the B isotope ratio of NASS-1. Multiplying this factor by 1000 gave the isotope shift in parts per thousand. Apparent isotope ratios were first corrected to actual values (correcting for mass discrimination effects) by using NBS SRM 951 as a calibration standard.

Table V contains data comparing B isotope ratios determined by using the three resins discussed above. Both minerals high in boron (colemanite, tourmaline) and low in boron (anhydrite, gypsum) were studied. Comparison of B isotope ratios obtained for each of the resins compare well with one another. Within experimental error, isotope ratios were the same for each of the resins studied. Thus, no bias was introduced by utilizing different resins for the separation and preconcentration of B from matrix components. A B isotope ratio of 3.995 for colemanite has been reported by Finley et al. (35).

Results were also compared for samples prepared by the acid leach procedure and the carbonate fusion procedure. The data in Table VI show that there is no difference in B isotope ratios where either procedure was used. These data also verify that either Chelex-100 or Dowex 50W-X8 can be used to separate B from the matrix. The principal criterion determining the selection of resin was the capacity of the resin relative to the dissolved salt content of the sample solution. Comparison of B concentrations in leach solutions and solutions derived from the carbonate fusion by ICP-ES indicated that for these samples approximately 35% of the B present was recovered by the acid leach procedure.

In Table VII are given the B isotope ratios for a variety of geological materials. The B isotope ratio of a wood sample

Table VI. $^{11}\text{B}/^{10}\text{B}$ Isotope Ratios Obtained for Acid Leach and Carbonate Fusion Sample Preparation Techniques

sample	$^{11}\text{B}/^{10}\text{B}$ ratio		difference
	acid leach ^a	fusion ^b	
basalt	3.968 ± 0.059	3.987 ± 0.040	0.019
MnO ₂ crust	4.022 ± 0.018	4.040 ± 0.024	0.018
basalt	3.995 ± 0.024	3.989 ± 0.059	0.006
basalt	3.995 ± 0.024	3.990 ± 0.031	0.005
sulfide	3.918 ± 0.024	3.878 ± 0.032	0.040
sulfide	3.944 ± 0.019	3.976 ± 0.036	0.032
sulfide	3.945 ± 0.014	0.964 ± 0.021	0.020
	3.958 ± 0.013	3.975 ± 0.011	0.017

^a Chelex-100. ^b Dowex 50W-X8.**Table VII.** Boron Isotope Ratios in Geological Materials

sample	$^{11}\text{B}/^{10}\text{B}$ ratio	$\delta^{11}\text{B}^a$
oceanic sediment	4.065 ± 0.036	-31.7
	4.027 ± 0.022	-40.7
	4.072 ± 0.029	-30.0
	4.128 ± 0.042	-16.7
	4.074 ± 0.014	-29.5
tin-bearing silicate	4.014 ± 0.025	-40.9
	3.906 ± 0.023	-66.7
	3.942 ± 0.005	-58.1
	3.946 ± 0.022	-57.1
	4.026 ± 0.014	-38.0
serpentinite	4.011 ± 0.007	-39.7
	3.997 ± 0.021	-43.1
	3.967 ± 0.069	-50.3
	4.039 ± 0.041	-33.0
	3.991 ± 0.045	-44.5
basalt	3.949 ± 0.037	-57.5
	3.927 ± 0.028	-62.8
altered hyaloclastite	3.969 ± 0.025	-52.7
	4.024 ± 0.035	-39.6
Mn/Fe oxide mineral	3.982 ± 0.037	-49.7
sulfide	3.982 ± 0.017	-49.7
	3.922 ± 0.065	-64.0
conodont fossil	4.169 ± 0.035	-1.9
alder wood	4.061 ± 0.023	-27.8

^a Relative to NASS-1 reference seawater.

is included because the analysis of organic materials is required in biogeochemical studies. Ashed organic material was leached with dilute HCl and treated with Chelex-100 before determining the B isotope ratio by ICP-MS.

The isotopic shift represented by the δ value in Table VII was calculated from the value of the B isotope ratio obtained for NASS-1 reference seawater. These data show that B isotopes can indeed vary considerably in nature and for the materials listed in Table VII, the ratio ranged from 3.906 to 4.169. This range is greater than that reported by Schwarcz et al. (1) for terrestrial rocks and minerals. The average precision (expressed as a relative standard deviation for three determinations) obtained for the determination of B isotope ratios in geological materials was 0.7%.

The precision of boron isotope ratios determined by ICP-MS is not as good as that obtained by thermal ionization mass spectrometry and thus its application to geological studies will be more limited. However, the sample throughput is high and ICP-MS can serve as a screening technique for evaluating geological systems where boron isotope shifts are expected.

The B isotope ratio determined for NASS-1 reference seawater over a period of several months is given in Table VIII. A mean B isotope ratio of 4.177 was obtained with a relative standard deviation of 0.34%. The B isotope ratio of seawater

Table VIII. $^{11}\text{B}/^{10}\text{B}$ Isotope Ratio of NASS-1 Reference Seawater

1	4.174
2	4.164
3	4.198
4	4.158
5	4.185
6	4.176
7	4.149
8	4.164
9	4.169
10	4.201
11	4.177
12	4.185
13	4.178
14	4.185
15	4.190
mean	4.177 ± 0.014

has been reported to range from 4.02 to 4.07 by Shima (3) and was determined to be 4.208 by Schwarcz et al. (1).

Provided that nonspectroscopic interferences resulting from the presence of concomitant elements can be reduced or eliminated, B isotope ratios in geological and other materials can be determined by ICP-MS with a precision of better than 1%. This precision is sufficient for some geological and geochemical studies since it has been shown that B isotope ratios vary in nature from about 3.91 (basalt) to 4.18 (seawater). Boron isotope ratios of B minerals have already been shown to be an efficient indicator of ore material (36). It remains to be seen if B isotope ratios of other materials can be used as an indicator of mineralization or can be applied to the study of rock and mineral genesis.

A serious concern when B isotopes are determined by ICP-MS is the loss of sensitivity resulting from concomitant elements. More important, however, is the mass discrimination induced by the presence of matrix salts. A too high salt content in the sample solution can be verified by spiking an aliquot of the sample solution with a known amount of ^{11}B . A suppression of the expected ion count rate (compared to a salt-free solution) indicates that a matrix induced mass discrimination effect could affect the accuracy of the result. Separating B from the matrix, changing the plasma conditions so as to reduce the ion suppression effect, or diluting the sample solution are all means capable of eliminating matrix induced mass discrimination.

ACKNOWLEDGMENT

The author is grateful to I. R. Jonasson, W. D. Goodfellow, E. M. Cameron, J. M. Duke, C. E. Dunn, and S. B. Ballantyne for selecting and providing sample material for study and for illuminating discussion on the potential meaning and application of the boron isotope ratio data. K. N. deSilva is thanked for reviewing the manuscript.

Registry No. ^{11}B , 14798-13-1; ^{10}B , 14798-12-0; MnO₂, 1313-13-9; sulfide, 18496-25-8; water, 7732-18-5.

LITERATURE CITED

- Schwarcz, H. P.; Agyel, E. K.; McMullen, C. C. *Earth Planet. Sci. Lett.* **1969**, *6*, 1.
- Handbook of Geochemistry*; Springer Verlag: New York, 1969.
- Shima, M. J. *Geophys. Res.* **1963**, *67*, 911.
- Hannaford, P.; Martin Lowe, R. *Anal. Chem.* **1977**, *49*, 1852.
- Cook, C. J.; Dubiel, S. V.; Hareland, W. A. *Anal. Chem.* **1985**, *57*, 337.
- Mamer, O. A.; Parent, G.; Laporte, R. *Can. J. Spectrosc.* **1985**, *30*, 83.
- Rein, J. E.; Abernathy, R. M. *Talanta* **1972**, *19*, 857.
- Spivack, A. J.; Edmond, J. M. *Anal. Chem.* **1986**, *58*, 31.
- Duchateau, N. L.; Verbruggen, A.; Hendrickx, F.; De Bievre, P. *Talanta* **1986**, *33*, 291.
- Anderson, R. J.; Gray, A. L. *Proc. Anal. Div. Chem. Soc.* **1976**, *13*, 284.
- Gray, A. L. In *Dynamic Mass Spectrometry*; Heydon: London, 1978; Vol. 5, p 106.

- (12) Date, A. R.; Gray, A. L. *Int. J. Mass Spectrom. Ion Phys.* **1983**, *48*, 357.
- (13) Douglas, D. J.; Quan, E. S. K. *ICP Inf. Newsl.* **1984**, *10*.
- (14) Strong, D. F.; Longerich, H. P. *Geosci. Can.* **1985**, *12*, 72.
- (15) Eagles, T. *SCC Workshop on Applications of ICP-MS*, Toronto, 1985.
- (16) Longerich, H. P.; Fryer, B. J.; Strong, D. F. *Spectrochim. Acta, Part B*, in press.
- (17) Russ, G. Price; Bazan, J. *Spectrochim. Acta* **1987**, *42B*, 49.
- (18) Houk, R. S.; Thompson, J. J. *Am. Mineral.* **1982**, *67*, 238.
- (19) Douglas, D. J.; Quan, E. S. K.; Smith, R. G. Presented at the Pittsburgh Conference, 1982; paper 194.
- (20) Gregoire, D. C. *SCC Workshop on Applications of ICP-MS*, Toronto, 1985.
- (21) Gregoire, D. C. *Appl. Spectrosc.* **1987**, *41*, 897.
- (22) Douglas, D. J.; Houk, R. S. *Anal. At. Spectrosc.* **1985**, *8*, 1.
- (23) Vaughan, M. A.; Horlick, G. *Appl. Spectrosc.* **1986**, *40*, 434.
- (24) Tan, S. H.; Horlick, G. *Appl. Spectrosc.* **1986**, *40*, 445.
- (25) Gregoire, D. C. *Spectrochim. Acta, Part B* **1987**, *42B*, 895.
- (26) Houk, R. S. *Anal. Chem.* **1986**, *58*, 97A.
- (27) *Standard Methods of Chemical Analysis*; Nostrand: Toronto, 1962.
- (28) Rynasiewicz, J.; Sleeper, M. P.; Ryan, J. W. *Anal. Chem.* **1954**, *26*, 935.
- (29) Troll, G.; Sauerer, A. *Analyst (London)* **1985**, *110*, 283.
- (30) Mamer, O. A.; Parent, G.; Laporte, R. *Can. J. Spectrosc.* **1985**, *30*, 83.
- (31) Carlson, R. M.; Paul, J. L. *Anal. Chem.* **1968**, *40*, 1292.
- (32) Carlson, R. M.; Paul, J. L. *Soil Sci.* **1969**, *108*, 266.
- (33) Hill, C. J.; Lash, R. P. *Anal. Chem.* **1980**, *52*, 24.
- (34) Kunin, R.; Preuss, A. F. *Ind. Eng. Chem. Prod. Res. Dev.* **1964**, *3*, 304.
- (35) Finley, H. O.; Eberle, A. R.; Rodden, C. J. *Geochim. Cosmochim. Acta* **1962**, *26*, 911.
- (36) Malinko, S. V.; YeLisitsym, A.; Sumin, L. V. *Dokl. Chem. Engl. Transl.* **1982**, *267*, 453.

RECEIVED for review January 8, 1987. Accepted June 9, 1987.
Geological Survey of Canada Contribution No. 50686.

Characterization of Radiation-Induced Damage to Polyadenylic Acid Using High-Performance Liquid Chromatography/Tandem Mass Spectrometry

Anthony J. Alexander and Paul Kebarle

Department of Chemistry, University of Alberta, Edmonton, Alberta, Canada T6G 2E3

Alfred F. Fuciarelli and James A. Raleigh*

Department of Radiobiology, Cross Cancer Institute, Edmonton, Alberta, Canada T6G 1Z2

The application of high-performance liquid chromatography/tandem mass spectrometry (HPLC/MS/MS) to the chemical characterization of molecular products from the irradiation of a model nucleic acid is presented. Polyadenylic acid was irradiated to 1000 Gy in nitrous oxide saturated aqueous solution at neutral pH, a condition resulting primarily in hydroxyl radical attack on the substrate, and then enzymatically hydrolyzed to the mononucleoside level prior to analysis. The radiation-induced molecular products (*R*)- and (*S*)-8,5'-cycloadenosine, 8-hydroxyadenosine, α -adenosine, and adenine were positively identified by comparison of retention times and MS/MS spectra with those of authentic standards. LC peaks corresponding to 8-hydroxyadenine and 4-amino-5-(formylamino)-6-(ribosylamino)pyrimidine were also identified by MS/MS.

The detection of molecular damage in irradiated nucleic acids is a challenging analytical problem. Immunochemical assays for specific radiation-induced molecular products have been developed (1-3) and used in radiation chemical studies (3, 4). Such assays have the ability to measure damage in situ with high sensitivity and good specificity. Recent studies have demonstrated that capillary column gas chromatography/mass spectrometry (5) combined with microderivatization can be utilized to identify a wide variety of products resulting from radiation-induced damage to DNA with very high sensitivity (5-9). The successful coupling of high-performance liquid chromatography and mass spectrometry (HPLC/MS) has opened up an alternative route of analysis for polar and thermolabile compounds which has potential for radiation chemical studies. Recent studies have shown the utility of

HPLC/MS for the analysis of nucleosides present in urine (10) and for the detection of modified nucleosides in enzymatic digests of tRNA (11). However, most HPLC/MS interfaces, including direct liquid introduction (DLI) (12, 13), thermospray (14), ion evaporation (15), and nebulization into an atmospheric pressure chemical ionization (APCI) source (16-18), produce abundant pseudomolecular ions but few fragment ions. Although this is beneficial in terms of overall sensitivity, only limited structural information is obtained.

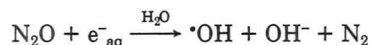
Tandem mass spectrometry (MS/MS) (19, 20) is a means of overcoming this inherent lack of specificity while maintaining good sensitivity. With MS/MS, structurally significant daughter ions are produced by collisionally induced dissociation (CID) of the respective parent ion. In this way additional structural data are obtained and the MS/MS separation stage enables coeluting components to be distinguished and identified. Covey and co-workers (21) have recently demonstrated the advantage gained when a heated nebulizer APCI interface is used in combination with MS/MS for the analysis of drugs in crude equine urine. In the present study a triple quadrupole instrument employing the same type of interface has been used to identify molecular products resulting from radiation-induced damage to polyadenylic acid (poly A). Enzymatic hydrolysis of the polymer to the mononucleoside level preceded the HPLC/MS/MS analysis.

EXPERIMENTAL SECTION

Reagents. Authentic samples of (*R*)- and (*S*)-8,5'-cycloadenosine were obtained from the radiolysis of adenosine 5'-monophosphate (5'-AMP) and 8-hydroxyadenosine was synthesized as described previously (22). Alkaline phosphatase, nuclease P1 (NP1), adenine, adenosine, 2'-AMP, 3'-AMP, 5'-AMP, 2',3'-*O*-isopropylideneadenosine, and polyadenylic acid (poly A) were obtained from the Sigma Chemical Co. (St. Louis, MO) and

used without further purification. The compound, 9- α -ribofuranosyladenine 5'-monophosphate (α -AMP) was a gift of Dr. M. J. Robins (Chemistry Department, University of Alberta). Alkaline phosphatase was used to hydrolyze α -AMP to the corresponding nucleoside. Other chemicals were chromatographic or reagent grade and were obtained from local suppliers.

Irradiation. Irradiations were performed in a Gammacell 220 ^{60}Co - γ radiation source (Atomic Energy of Canada, Ltd.) at a dose rate of 57.4 Gy/min. The total dose was 1000 Gy (1 Gy = J/kg = 100 rad). Solutions of poly A containing 694 $\mu\text{g/mL}$ were made up in distilled water (pH 7.0) which had been purified and deionized before use by passage through a Barnstead three-module NANOpure water purification system (supplied by Fisher Chemical Co.). The 2.0-mL samples of poly A were bubbled with nitrous oxide for 15 min prior to and then throughout the time of irradiation. Nitrous oxide converts aqueous electrons to hydroxyl radicals



(23) thereby maximizing the yield of hydroxyl radicals from water radiolysis. In the presence of nitrous oxide the yield of hydroxyl radicals from water radiolysis, expressed in terms of the G value (molecules produced per 100 eV) is 5.4 (23). The nitrous oxide was scrubbed free of oxygen by passage through a 0.1 M sodium dithionite trap and free of acidic impurities by passage through a 0.1 M sodium carbonate trap.

Hydrolysis of Irradiated Poly A. The irradiated poly A was hydrolyzed with nuclease P1 as described previously (4). Briefly, 0.250 mL of a solution of nuclease P1 containing 7.5 units/mL of enzyme in a buffer of 30 mM sodium acetate (pH 5.3) and 2 mM ZnSO_4 was added to 0.5 mL of poly A solution. This mixture was incubated for 18 h at 37 °C.

The mixture of mononucleotide products was further hydrolyzed to the corresponding nucleosides with alkaline phosphatase. In a typical experiment 0.250 mL of a solution of alkaline phosphatase (25 units/mL of alkaline phosphatase in 0.1 M sodium carbonate/bicarbonate buffer (pH 9.6) containing 0.1 M magnesium chloride) was added to the NP1 digest of the irradiated poly A and the mixture was incubated at 37 °C for 18 h.

Chromatography. A Waters Model 6000A liquid chromatograph pump, a Rheodyne Model 7125 injection valve with a 100- μL sample loop, and a Waters Model 440 fixed-wavelength UV detector (254 nm) were used for the HPLC separation. The HPLC chromatogram was recorded on a chart recorder (Yokogawa, Tokyo, Japan). A reversed-phase Supelco LC-18-S (4.6 mm \times 250 mm) analytical column was used with an eluent of 10% methanol in 0.02 M ammonium formate buffered to pH 4.0 with formic acid. The exit of the UV detector was connected directly to a heated nebulizer LC/MS interface (Sciex, Thornhill, Ontario).

Mass Spectrometry. HPLC/MS and HPLC/MS/MS spectra were obtained with a TAGA 6000E triple quadrupole mass spectrometer (Sciex, Thornhill, Ontario) utilizing an atmospheric pressure chemical ionization (APCI) source. The HPLC effluent was introduced directly into the APCI source via the heated nebulizer at flow rates between 0.8 and 1.0 mL/min. Nitrogen was used as the nebulization gas. Typical operating conditions were as follows: heater temperature, 530 °C; nebulization pressure, 500 kPa; make-up gas flow, 3 L/min. Reagent ions generated from the HPLC effluent in the APCI source are H_4N^+ clusters with water, methanol, and ammonia molecules. Both quadrupoles were tuned (in the mass filter mode) to give a constant peak width at half-height of 0.6 amu. Conventional positive ion mass spectra, starting from m/z 80, were obtained with quadrupole 1 (Q_1) in the mass filter mode and quadrupole 3 (Q_3) in the total ion mode. Daughter ion spectra were generated under standard conditions by use of argon as the collision gas. (Effective target thickness was $\sim 300 \times 10^{12}$ atoms/cm 2 ; collision energy was 50 eV.) In general, the reproducibility of major daughter ions was found to be good. However, significant variations in intensity were often observed for low-intensity daughter ions, particular when the parent ion intensity was also low ($< 5 \times 10^4$ counts/s).

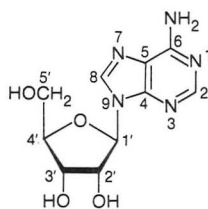
The sensitivity loss under MS/MS conditions, that is, the combination of transmission losses due to having gas in the collision cell and operating Q_3 in the mass resolving mode, was estimated in the following way. Conventional and MS/MS spectra

were recorded for 1 nmol injections of adenosine ($\text{MH}^+ = 268$) while other scan-independent instrumental parameters were held constant. The parent ion intensity obtained, $I(\text{MH}^+)$, was approximately 10^5 counts/s. Daughter and residual parent ion intensities in the MS/MS spectrum of MH^+ were summed to give the total ion yield, $I(\text{D}_T^+)$. For this nucleoside the transmission in the MS/MS mode, $I(\text{D}_T^+)/I(\text{MH}^+)$, was typically 15%.

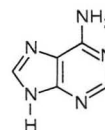
In many of the CID spectra presented (Figures 1b-d, 5, 7a,b, 8, 9, and 10) ions corresponding in mass to M^+ are present. These ions are observed in both the presence and absence of collision gas under MS/MS conditions, i.e. with Q_1 focused on MH^+ and Q_3 mass resolving. Since in the absence of a collision gas only MH^+ and its most abundant metastable ion are generally observed, M^+ must be an instrumental artifact caused by the peak shape of MH^+ .

RESULTS AND DISCUSSION

APCI and CID Mass Spectrum of Adenosine. The APCI spectrum of adenosine (1), the mononucleoside moiety



(1)



(2)

of polyadenylic acid (Figure 1a), reveals that in addition to the protonated molecular ion MH^+ at m/z 268, cleavage of the $\text{C}_1\text{-N}_9$ glycosidic bond in MH^+ accompanied by transfer of a hydrogen atom (24) leads to an intense ion at m/z 136 which will be designated $(\text{BH} + \text{H})^+$, since it probably corresponds to the protonated base adenine (2). Cleavage of the same bond without H transfer and with the charge localized on the sugar fragment leads to (S^+) , m/z 133, as only a very minor ion. This is typical of chemical ionization (CI) spectra of nucleosides in general (10, 24, 25) and can be rationalized on the basis that the proton and thus the positive charge in MH^+ will stay with the higher proton affinity base. In contrast to previously published ammonia CI spectra (24), the ions $(\text{B} + 30)^+$ and $(\text{B} + 44)^+$ corresponding to base plus portions of the sugar were not observed. Probably this is a consequence of the much milder, i.e., less exothermic proton transfer, leading to MH^+ in APCI where the reagent ions are NH_4^+ clusters. The CID spectrum of the MH^+ m/z 268 ion from adenosine, see Figure 1b, contains $(\text{BH} + \text{H})^+$ m/z 136 as the major fragment and a number of lesser intensity fragments all of mass lower than m/z 136. The fragments divide into two groups, those derived from the base and those from the sugar S.

In order to assign the ions originating from the base moiety, a CID spectrum of the $(\text{BH} + \text{H})^+$ m/z 136 ion was obtained (see Figure 1c lower trace). CID of this fragment was found to yield a number of low-intensity ions, which have been tentatively assigned to successive losses of NH_3 and HCN (m/z 119, 109, 92, 65), sequential loss of HCN (m/z 109, 82, 55), and loss of H_2NCN from m/z 109 (m/z 67). These same daughter ions are present in the CID spectrum of the MH^+ m/z 136 ion from an authentic sample of adenine (2). This spectrum, also normalized to the intensity of MH^+ , is shown in the upper part of Figure 1c. Except for minor variations in intensity, the spectra are identical. It is of interest to note that in the electron impact (EI) mass spectrum of adenine the same neutral losses occur in the fragmentation of M^+ (26). The base-derived fragments in the CID spectrum of protonated adenosine (Figure 1b) are therefore m/z 119, 109, 92, 82, 67, 65, and 55. These fragments are of lesser intensity than the sugar derived ions. Other diagnostically useful ions, (B

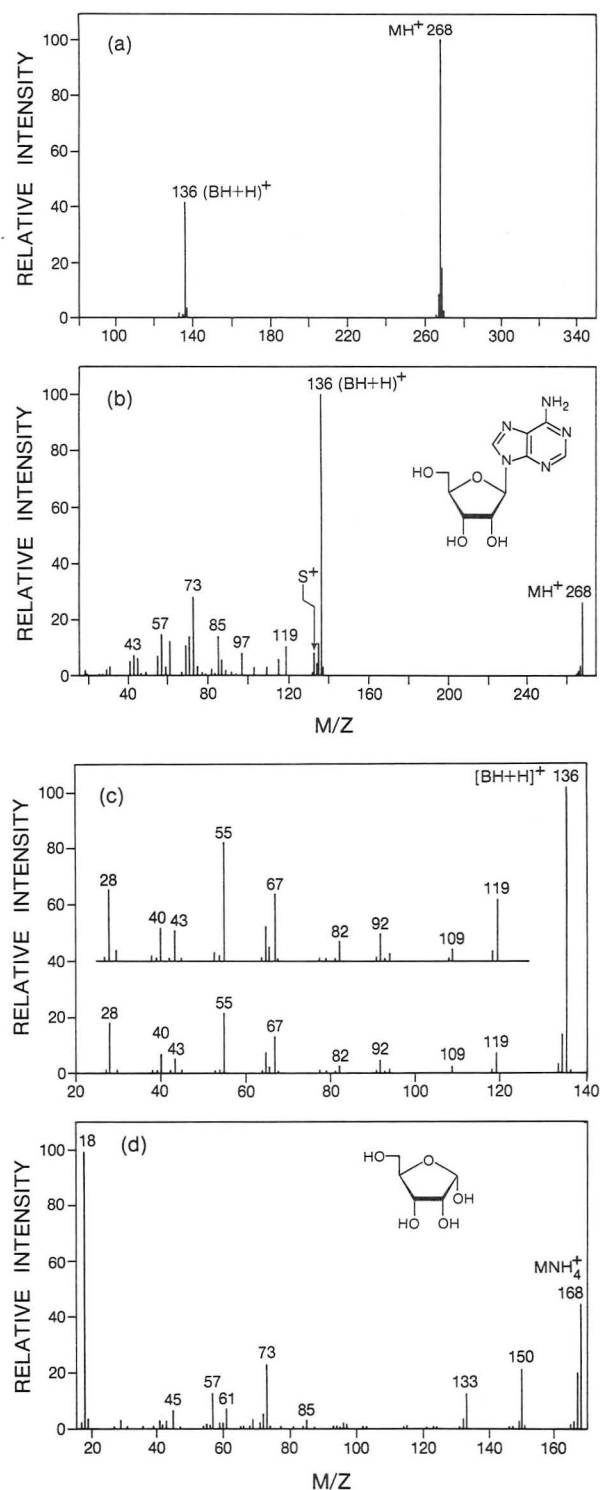


Figure 1. (a) APCI spectrum of adenosine (1) after background subtraction. MH^+ is protonated adenosine, $(BH + H)^+$ is probably protonated adenine. (b) CID spectrum of the MH^+ , m/z 268 ion of adenosine. (c) CID spectrum of the $(BH + H)^+$, m/z 136, ion of adenosine. Upper spectrum shows the CID of MH^+ , m/z 136, from an authentic sample of adenine (2). (d) CID spectrum of the MNH_4^+ adduct ion from D-ribose.

+ 30) $^+$ and $(B + 44)^+$ (24), either were not observed (m/z 164) or were present only at very low intensity (m/z 178) in Figure 1b. One might have expected that with CID, which presumably involves energetic collisions, these ions would be more prominent.

Due to the low intensity of S^+ in the APCI spectrum of adenosine, a CID spectrum could not be obtained. In order to trace the fragments arising from the sugar moiety D-ribose NH_4^+ m/z 168 was collisionally dissociated. Protonated D-

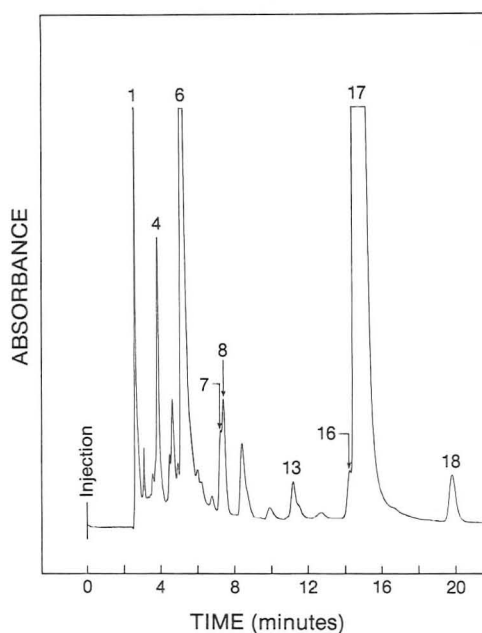


Figure 2. HPLC of a nitrous oxide saturated, enzyme hydrolyzed, solution of poly A irradiated to 1000 Gy at neutral pH. Numbered peaks correspond to compounds for which mass spectra were obtained: peak 1, 4-amino-5-(formylamino)-6-(ribosylamino)pyrimidine; peak 4, (*R*)-8,5'-cycloadenosine; peak 6, adenine; peak 7, 8-hydroxyadenine; peak 8, α -adenosine; peak 13, (*S*)-8,5'-cycloadenosine; peak 16, unconfirmed; peak 17, adenosine; peak 18, 8-hydroxyadenosine. Unlabeled peaks represent unidentified components.

ribose does not form in APCI due to the low proton affinity of the sugar (<207 kcal/mol). The CID spectrum, Figure 1d, contained fragments with nominal masses corresponding to $C_4H_5O_2^+$ (m/z 85), $C_3H_5O_2^+$ (m/z 73), $C_2H_5O_2^+$ (m/z 61), and $C_3H_5O^+$ (m/z 57). Also observed are m/z 150, which is likely to be the $[NH_4^+ - H_2O]^+$ ion, and m/z 133, which corresponds to loss of NH_3 from m/z 150. Some of these ions, m/z 61, 73, and 85, have been previously observed in the methane CI spectra of underivatized sugars (27).

If we now reexamine Figure 1b, the CID spectrum of the MH^+ ion from adenosine, it is apparent that m/z 57, 73, and 85 are fragments of the sugar moiety. Also present are low-intensity ions at m/z 115 and 97. These must also be sugar-derived fragments as they do not occur in the CID spectrum of $(BH + H)^+$ shown in Figure 1c. It is possible that these ions are due to sequential loss of water from S^+ .

APCI and CID Mass Spectra of Radiolysis Products.

Irradiation of nitrous oxide saturated aqueous solutions of poly A, at neutral pH, yields a series of products resulting primarily from hydroxyl radical attack on the polymer (4). Enzymatic hydrolysis of the irradiated poly A yields a mixture of mononucleosides which can be separated by using high-performance liquid chromatography (Figure 2). Chromatography of the enzyme hydrolysate from unirradiated solutions of poly A (data not shown) reveals only the presence of adenosine—the unchanged subunit of poly A. The UV chromatogram shown in Figure 2 was obtained with approximately 130 nmol (in terms of mononucleotide equivalents) of irradiated and hydrolyzed polyadenylic acid injected into the column. Peaks corresponding to the presence of 8-hydroxyadenosine (peak 18), adenine (peak 6), and (*R*)- and (*S*)-8,5'-cycloadenosine (peaks 4 and 13) had been previously identified by cochromatography with authentic samples (4, 28). The known products of radiolysis, quantified in earlier work on the basis of calibration curves using authentic samples (4), are present in the range of 0.66–2.8 nmol. Reconstructed ion chromatograms for these radiation-induced compounds (Figure 3) and APCI mass spectral data (Table I) obtained in the present

Table I. APCI Primary Mass Spectra of Radiolysis Products from Polyadenylic Acid Irradiated in N₂O-Saturated Aqueous Solution at Neutral pH^a

peak no.	compound	MH ⁺	(BH + H) ⁺	(S) ⁺	other ions
17	adenosine	268 (100) ^b	136 (100) ^b	133 (2)	
4 + 13	(<i>R</i>)-&(<i>S</i>)-8,5'-cycloadenosine	266 (100)			164 (7)
18	8-hydroxyadenosine	284 (52)	152 (100)	133 (1)	
6	adenine	136 (100)			
7	8-hydroxyadenine	152 (100)			
1	4-amino-5-(formylamino)-6-(ribosylamino)pyrimidine	286 (22)	154 (100)	133 (1)	196 (23), 178 (19)
8	9- α -ribofuranosyladenine (α -adenosine)	268 (100)	136 (76)	133 (-)	
16		250 (100)	136 (70)		232 (10), 97 (7)

^aRelative intensities (%) are given in parentheses. ^bDetector saturated.

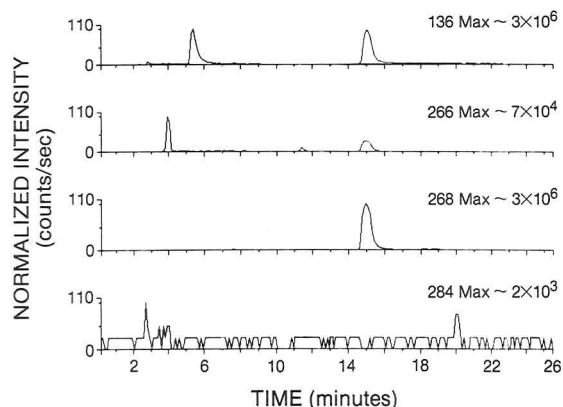


Figure 3. Reconstructed ion chromatograms for peaks corresponding to adenine (MH⁺, *m/z* 136), (*R*)- and (*S*)-8,5'-cycloadenosine (MH⁺, *m/z* 266), adenosine (MH⁺, *m/z* 268), and 8-hydroxyadenosine (MH⁺, *m/z* 284).

work were consistent with the above peak assignments and confirmed that no other coeluting components were present. Due to the high concentration of adenosine, which represented approximately 92% of the total amount of material injected into the column, the ion signals for *m/z* 136 and 268 were saturated at $\sim 3 \times 10^6$ counts/s. The other components, except for 8-hydroxyadenosine, were also detected with good sensitivity. On the basis of the relative amount of 8-OH adenosine present, the MH⁺ ion count for this nucleoside was considerably lower than expected (see later discussion).

Radiation-induced formation of 8-hydroxyadenosine has been observed in irradiated solutions of purine mononucleosides (tides) (4, 22), polyadenylic acid (4, 28), and DNA (1, 5, 7). In the present study, the CID spectrum of MH⁺ obtained from peak 18 in the UV chromatogram (Figure 2) was identical with that obtained from authentic samples of 8-hydroxyadenosine (Figure 4). The fragmentation pattern is similar to that of adenosine in that the major ion is the protonated base at *m/z* 152. Low-intensity ions can be accounted for by assumed successive loss of NH₃ and HCN (*m/z* 135, 125, 108, 81), and sequential loss of HCN (*m/z* 125, 98, 71) from (BH + H)⁺.

Radiation-induced formation of 8,5'-cycloadenosine (see structure X) or its deoxyribose analogue has been observed in irradiated, deoxygenated solutions of purine mononucleosides (tides) (22, 29), polyadenylic acid (3, 4, 28), and DNA (3, 8). The major ions in the MH⁺ CID spectrum of (*S*)-8,5'-cycloadenosine (peak 13, Figure 2), obtained from an irradiated solution of poly A, were identical with those obtained by using an authentic sample (Figure 5). The CID spectrum of the protonated *R* epimer obtained from peak 4 was essentially the same as that of the *S* epimer except for the absence of ions at *m/z* 207 and 82 (data not shown). The relatively high intensity of the MH⁺ ion in the CID spectrum reveals that the intramolecular cyclization between the C₈-C_{5'} carbon atoms leads to greater stability of MH⁺. The possible

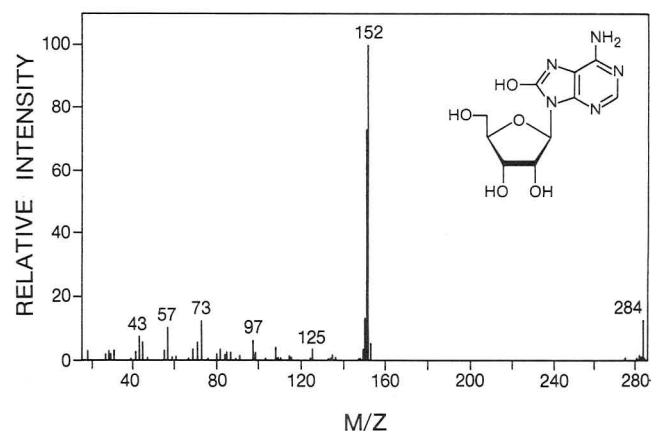


Figure 4. CID spectrum corresponding to peak 18, identified as 8-hydroxyadenosine (MH⁺, *m/z* 284).

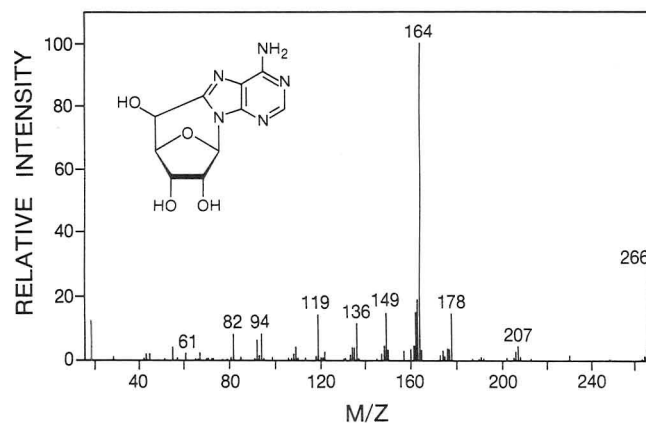
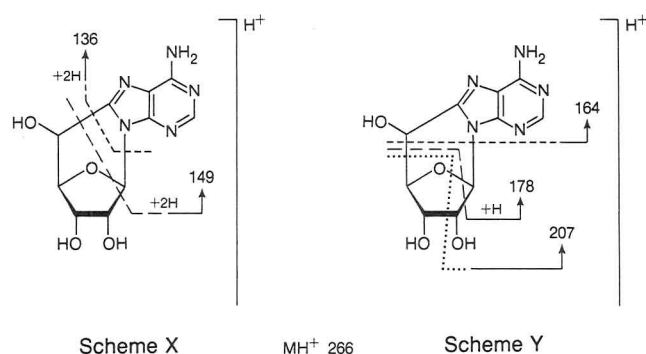


Figure 5. CID spectrum corresponding to peak 13, identified as (*S*)-8,5'-cycloadenosine (MH⁺, *m/z* 266).

fragmentation patterns leading to characteristic daughter ions are illustrated in structures X and Y. Similar bond cleavages



have been proposed to account for the major ions in the EI mass spectrum of (*S*)-8,5'-cycloadenosine-(Me₃Si)₄ (8). Minor ions at *m/z* 248 and 230 can be accounted for by sequential loss of H₂O from *m/z* 266. The search for unidentified ra-

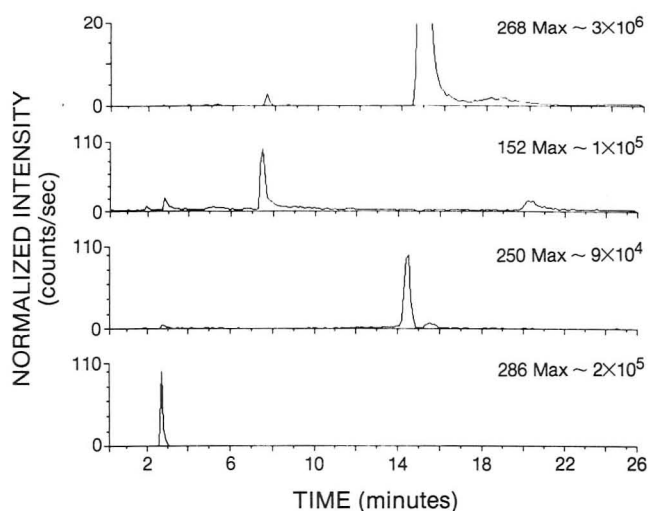


Figure 6. Reconstructed ion chromatograms for peaks corresponding to 4-amino-5-(formylamino)-6-(ribosylamino)pyrimidine (MH^+ , m/z 286), 8-hydroxyadenine (MH^+ , m/z 152), α -adenosine (MH^+ , m/z 250), and adenosine (MH^+ , m/z 268).

diolysis products was initiated by examining the reconstructed total ion chromatogram. Where a local maximum was apparent at the retention time of interest, an APCI spectrum was plotted by averaging the number of scans associated with the ion peak and subtracting an average background spectrum. The background spectrum was obtained by averaging a combination of scans taken just before and after elution of the HPLC peak. A number of extraneous ions, that is, ions which did not maximize at the correct retention time, were often present after background subtraction. The reasons for this are not clearly understood. However, these ions were generally of low intensity and did not complicate the interpretation of the APCI spectrum. The APCI mass spectra of peaks 1, 7, 8, and 16, obtained in this way, are given in Table I. Reconstructed ion chromatograms were also plotted for the ions shown in Table I. In each case the ion maximum obtained coincided with the assigned peak in the UV chromatogram. Such reconstructed ion chromatograms are shown in Figure 6 for the suspected parent ions m/z 152, 250, 268, and 286. Background-corrected spectra were also obtained at retention times of other prominent peaks in the UV chromatogram. However, instead of showing distinct parent or fragment ions, these APCI spectra generally contained a large number of low-intensity ions. This made it very difficult to establish which were the authentic ions originating from the HPLC peak. Even when reconstructed ion chromatograms for the more prominent ions in these spectra were obtained, molecular maxima at the correct retention time could not be found.

The CID spectrum of the m/z ion whose maximum coincides with peak 1, shown in Figure 7, was assigned to 4-amino-5-(formylamino)-6-(ribosylamino)pyrimidine. Formation of this product or its deoxyribose analogue has been observed in irradiated solutions of mononucleosides (tides) (30) and DNA (5, 7, 13). The intense ion at m/z 154 corresponds to $(BH + H)^+$; loss of NH_3 and CO from this ion accounts for the ions at 137 and 126, respectively. The CID spectrum of $(BH + H)^+$, shown in Figure 7b, was identical, except for minor intensity changes, to the CID spectrum of MH^+ derived from an authentic sample of 4,6-diamino-5-(formylamino)pyrimidine. This spectrum, normalized to the intensity of $(BH + H)^+$, is shown for comparison in the upper part of Figure 7b. Cleavage of the glycosidic bond without H transfer and with the charge remaining on the sugar moiety leads to the characteristic ion at m/z 133. Loss of $2H_2O$ from this ion accounts for the ion at m/z 97. The ion at m/z 196 fits the $(B + 44)^+$ fragmentation route previously observed

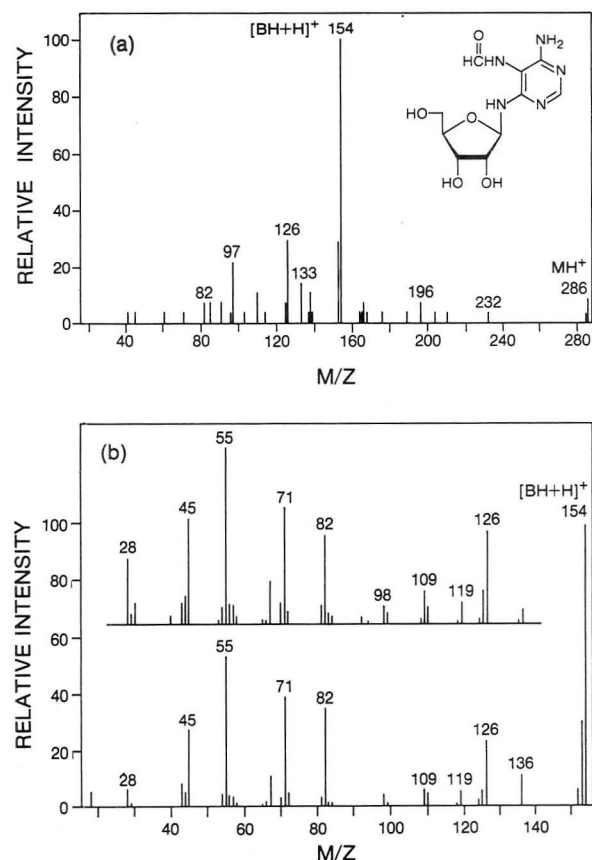


Figure 7. (a) CID spectrum corresponding to peak 1, identified as 4-amino-5-(formylamino)-6-(ribosylamino)pyrimidine (MH^+ , m/z 286). (b) Spectrum of $(BH + H)^+$ corresponding to peak 1. Upper spectrum showed CID of MH^+ , m/z 154, from an authentic sample of 4,6-diamino-5-(formylamino)pyrimidine.

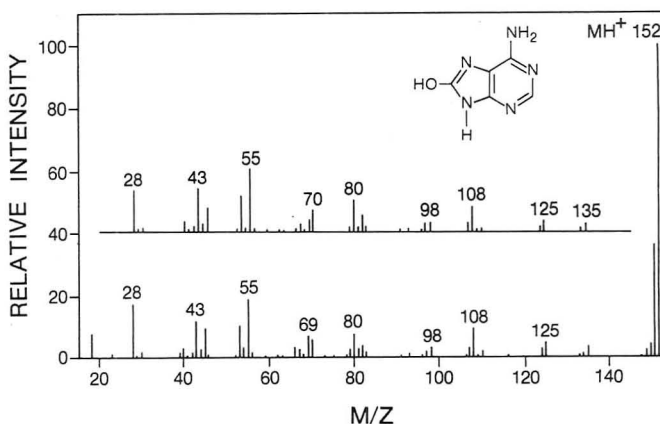


Figure 8. CID spectrum corresponding to peak 7, identified as 8-hydroxyadenine (MH^+ , m/z 152). Upper spectrum shows CID of $(BH + H)^+$, m/z 152, from an authentic sample of 8-hydroxyadenosine.

in CI mass spectra of nucleosides (24).

The CID spectrum of the m/z 152 ion whose maximum coincides with peak 7, shown in the lower part of Figure 8, was assigned to 8-hydroxyadenine. This base has been previously observed in irradiated solutions of DNA (5, 7). Low-intensity ions that can be accounted for by successive loss of NH_3 and HCN (m/z 135, 125, 108, 81) and sequential loss of HCN (m/z 125, 98, and 71) are present. These fragments parallel those produced by CID of protonated adenine, with the expected addition of 16 mass units. A good match was also obtained between this spectrum and a CID spectrum of $(BH + H)^+$ derived from an authentic sample of 8-hydroxyadenosine. For comparison this spectrum, normalized to the intensity of MH^+ is shown in the upper part of Figure 8.

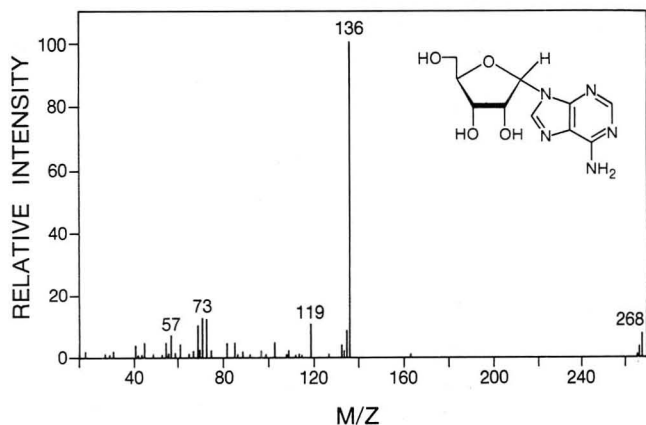


Figure 9. CID spectrum corresponding to peak 8, identified as α -adenosine (MH^+ , m/z 268).

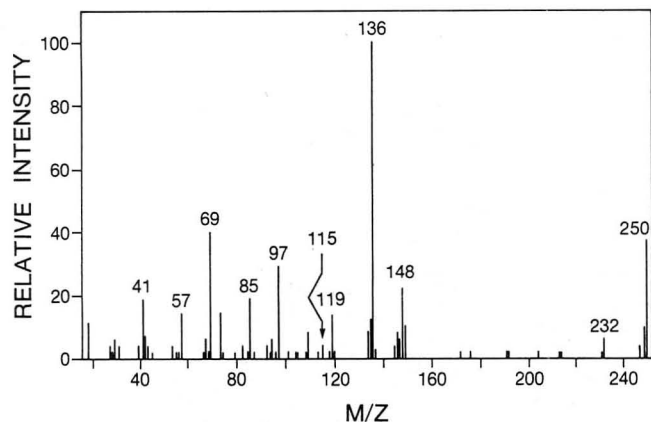


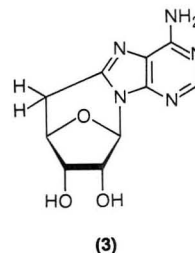
Figure 10. CID spectrum corresponding to peak 16.

The CID spectrum of the m/z 268 ion whose maximum coincides with peak 8, shown in Figure 9, was assigned to 9- α -ribofuranosyladenine (α -adenosine). The intense ion at m/z 136 ($BH + H$) $^+$, together with fragments at m/z 119, 109, 82, and 55, suggest the presence of the unmodified adenine base. In addition the low-abundance ion at m/z 133 indicates that the sugar moiety is unaltered. Other ribose-derived fragments are also present, although the intensity of these ions is somewhat different to that produced by the β -anomer. Authentic material for this compound was available and, except for minor intensity changes, had an identical daughter ion spectrum and retention time (data not shown).

The reconstructed ion chromatogram for m/z 250 (Figure 6) reveals the presence of an intense ion maximum at a retention time of 14.5 min which coincides with peak 16 in the UV chromatogram. In addition to MH^+ at m/z 250 the APCI spectrum contained a prominent ion at m/z 136 which corresponds in mass to the adenine moiety ($BH + H$) $^+$. The CID spectrum of m/z 250 (Figure 10) revealed, in addition to the intense ion at m/z 136, fragments at m/z 119, 109, 92, and 82 which further indicates the presence of an intact adenine base. The lack of the characteristic ribose fragment at m/z 133 and the presence of ions at m/z 115 (modified S) $^+$, m/z 97 (modified S - H_2O) $^+$ are consistent with the possibility that hydroxy radical attack, resulting in elimination of H_2O , has occurred on the sugar. The intensity of the m/z 115 ion would be expected to be low and is similar to that observed for S $^+$ in the CID spectrum of protonated adenosine (Figure 1b). Other sugar-derived fragments are present at m/z 85 and m/z 73 which possibly originate from (S - H_2O) $^+$ for ribose nucleosides rather than S $^+$. It is possible that the fragment m/z 69 arises from elimination of H_2CO involving the C $_5$ carbon to yield the ion C $_4$ H $_5$ O $^+$. The prominent ion at m/z 148 must incorporate adenine together with one of the sugar carbon

atoms. It is conceivable that the C $_1$ carbon atom has become incorporated into a stable linked pyrazine-pyrimidine type ion via a ring-expansion process. The evidence points to a radiolysis product in which the adenine base is intact, while the sugar moiety is damaged in a way consistent with dehydration at the 2' or 3' position. While there are radiolytic precedents for such a process (29, 31, 32), positive identification of the compound appearing as peak 16 awaits further investigation.

In addition to peak 16 there is an isomeric product eluting ~ 1 min later and present at $\sim 10\%$ of its ion intensity. In irradiated samples of 3'-AMP and poly A, UV detection of this peak is masked by the high concentration of adenosine present. A possible candidate for this product is 5'-deoxy-8,5'-cycloadenosine (3) which also exhibits a MH^+ ion at m/z 250. This cyclonucleoside is formed during radiolysis of



(S)-8,5'-cycloadenosine 5'-monophosphate under reducing conditions (31). Reducing conditions are achieved by converting hydroxyl radicals to aqueous electrons by irradiation in the presence of sodium formate. This results in a 2-fold increase in the yield of aqueous electrons from water radiolysis. The major peak in the CID spectrum (not shown) of protonated 5'-deoxy-8,5'-cycloadenosine is m/z 148 which results from C $_4$ -C $_5$ and C $_1$ '-N $_9$ bond cleavage analogous to that observed for (S)-8,5'-cycloadenosine (Figure 5), whereas m/z 136 is only present at low intensity. It is clear from the differences in retention time and CID spectra, together with the fact that m/z 136 is not observed in the APCI spectrum of 5'-deoxy-8,5'-cycloadenosine that peak 16 is not this product. A sample of poly A, irradiated under nitrous oxide and hydrolyzed, was spiked with an enzyme hydrolysate which had been obtained from (S)-8,5'-cycloadenosine 5'-monophosphate irradiated under reducing conditions. The reconstructed ion chromatogram for m/z 250 revealed that 5'-deoxy-8,5'-cycloadenosine coeluted with the unknown peak at 15.5 min. However, the inability to obtain a CID spectrum of m/z 250 for the corresponding peak in irradiated poly A, due to the low quantity of product present, makes it impossible to confirm the presence of 5'-deoxy-8,5'-cycloadenosine.

Detection of Product Damage at Low Radiation Doses. Radiation doses exceeding 10–20 Gy cannot be tolerated by mammalian cells (30). It is therefore of interest to ascertain whether HPLC/MS, based on nebulization into an APCI source, is sensitive enough for the purpose of studying radiation damage at low doses (<10 Gy). A sample of poly A was irradiated under exactly the same conditions as previously employed but to a dose of 10 Gy rather than 1000 Gy. Under these conditions 20 pmol (5 ng) of (R)-8,5'-cycloadenosine and 14 pmol (4 ng) of 8-hydroxyadenosine were calculated to be present on the basis of the calibrated UV absorbance at 254 nm (4). The mass spectrometer was used in the single ion monitoring (SIM) mode, using only Q $_1$ to select the ions of interest.

Considering first the cyclonucleoside product, for which most of the ionization is concentrated in MH^+ , one finds that the LC peak due to 5 ng leads to an MH^+ signal-to-noise ratio of about 3 (see Figure 11). Thus 5 ng may be considered as the detection limit for this type of product. Nucleoside products that do not yield intense MH^+ ions generally have

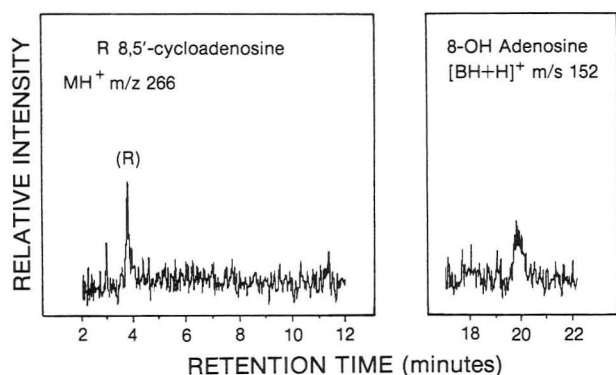
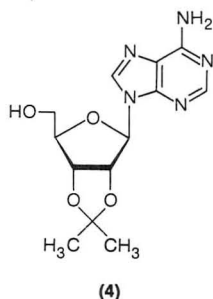


Figure 11. Single ion monitoring (SIM) ion chromatograms for m/z 266 and m/z 152 from a sample of poly A irradiated to a dose of 10 Gy. Other conditions are the same as previously employed.

an intense $(BH + H)^+$ fragment. This is the case for 8-hydroxyadenosine for which 4 ng led to a signal/noise ratio of about 2 at m/z 152. The detection limits are therefore approximately the same for both compounds. These results indicate that this system is not sufficiently sensitive to monitor radiation damage at biologically significant levels. A number of products resulting from DNA irradiated at doses ranging from 0.1 to 10 Gy have been detected by GC/MS/SIM (7–9). Some of these products could be detected at doses as low as 0.1 Gy, but others required a minimum radiation dose of 10 Gy.

Yield of MH^+ under HPLC/APCI Conditions. As previously noted the APCI response, that is, the efficiency of protonation, for 8-hydroxyadenosine was relatively poor (Figure 3). Both the proton affinity and the relative volatility of an analyte would be expected to strongly influence the yield of MH^+ when solutions are directly nebulized into an APCI source. Adenosine has a high proton affinity (>226.6 kcal/mol) (24) and is detected with good sensitivity, comparable to that obtained from other nitrogen-containing bases using APCI (32). Although the site of protonation on nucleosides is not known, the presence of a hydroxyl group on the purine ring is unlikely to reduce the proton affinity significantly (33). However, additional hydroxyl groups, particularly when located on the purine ring, might limit volatility due to more extensive hydrogen bonding. For example, both inosine and guanosine are considerably less volatile than adenosine and ribose nucleosides are less volatile than their 2'-deoxy counterparts (26). Direct comparison of adenosine with 2',3'-O-isopropylideneadenosine (4) and 8-hydroxyadenosine, using



the intensities of MH^+ and $(BH + H)^+$ from 1 nmol injections, revealed that the intensities of these ions were a factor of about 5 times greater for the 2',3'-O-isopropylidene and about 35 times less for the 8-hydroxy derivatives than that for adenosine. The absolute intensity for adenosine (MH^+) was about 10^5 counts/s. The total ionization was essentially constant for each injection indicating that no depletion of the reagent ions had occurred. These trends in overall sensitivity suggest that the presence of a hydroxyl group on the heterocyclic ring, rather than the sugar, affects the efficiency of vaporization

to a greater extent. It is possible that other prominent peaks not identified in the UV chromatogram (Figure 2) are due to radiation-induced products that are less volatile than 8-hydroxyadenosine.

CONCLUSIONS

MS/MS spectra have been used to identify a number of radiolysis products resulting from hydroxyl radical attack on a model nucleic acid. These assignments could not have been made on the basis of the primary APCI spectra alone.

The base-containing fragment of $(BH + H)^+$ is present in APCI spectra of nucleosides but no further ions derived from the base moiety are observed. By comparison the CID spectrum of $(BH + H)^+$ is rich in structural information and can be used to identify the base, modified by hydroxyl radical attack.

The sugar fragment S^+ either is not formed or is of such low intensity (<1%) in APCI that it cannot be reliably used for diagnostic purposes. In the CID spectrum of MH^+ the intensity of this fragment is also low; however, it is consistently present. Furthermore other important diagnostic sugar fragments, at higher yield, are also present. The mass and relative intensities of these ions, together with fragments originating from the base moiety, provide a useful MS/MS "fingerprint".

The greater specificity obtained with MS/MS is often offset by a corresponding loss in sensitivity due to higher transmission losses. In this study about a 10-fold loss in sensitivity was incurred for operation in the MS/MS mode. CID spectra for a number of low yield products were not obtained, either for this reason or because the corresponding parent ions in the primary APCI spectra could not be detected.

ACKNOWLEDGMENT

The authors acknowledge A. M. Hogg for his review of this manuscript and helpful suggestions throughout the course of this study. We thank G. Kennedy for assistance with preparation of the manuscript.

Registry No. 2, 73-24-5; polyadenylic acid, 24937-83-5; (R)-8,5'-cycloadenosine, 62475-47-2; (S)-8,5'-cycloadenosine, 41432-67-1; 8-hydroxyadenosine, 29851-57-8; α -adenosine, 5682-25-7; 8-hydroxyadenine, 21149-26-8; (ribosylamino)pyrimidine, 109637-89-0; hydroxyl, 3352-57-6; nitrous oxide, 10024-97-2.

LITERATURE CITED

- West, G. J.; West, I. W.-L.; Ward, J. F. *Int. J. Radiat. Biol.* **1982**, *42*, 481–490.
- Rajagopalan, R.; Melamed, R. J.; Laspai, M. F.; Erlanger, B. F.; Wallace, S. S. *Radiat. Res.* **1984**, *97*, 499–510.
- Fuciarelli, A. F.; Miller, G. G.; Raleigh, J. A. *Radiat. Res.* **1985**, *104*, 272–283.
- Fuciarelli, A. F.; Shum, F. Y.; Raleigh, J. A. *Radiat. Res.* **1987**, *110*, 35–44.
- Dizdaroglu, M. *Anal. Biochem.* **1985**, *144*, 593–603.
- Dizdaroglu, M. *Biochemistry* **1985**, *24*, 4476–4481.
- Dizdaroglu, M. *J. Chromatogr.* **1986**, *367*, 357–366.
- Dizdaroglu, M. *Biochem. J.* **1986**, *238*, 247–254.
- Dizdaroglu, M.; Bergtold, D. S. *Anal. Biochem.* **1986**, *156*, 182–188.
- Esmans, E. L.; Geboes, P.; Luyten, Y.; Alderweireldt, F. C. *Biomed. Mass Spectrom.* **1985**, *12*, 241–245.
- Edmonds, C. G.; Vestal, M. L.; McCloskey, J. A. *Nucleic Acids Res.* **1985**, *13*, 8197–8206.
- Dedieu, M.; Juin, C.; Arpino, P. J.; Guiochon, G. *Anal. Chem.* **1982**, *54*, 2372–2375.
- Lee, E. D.; Henion, J. D. *J. Chromatogr. Sci.* **1985**, *23*, 253–264.
- Garteiz, D. A.; Vestal, M. L. *LC Mag.* **1985**, *3*, 334–346.
- Iribarne, J. R.; Dziedzic, P. J.; Thomson, B. A. *Int. J. Mass Spectrom. Ion Phys.* **1983**, *50*, 331–347.
- Henion, J. D.; Thomson, B. A.; Dawson, P. H. *Anal. Chem.* **1982**, *54*, 451–456.
- Kambara, H. *Anal. Chem.* **1982**, *54*, 143–146.
- Crowther, J. B.; Covey, T. R.; Silvestre, D.; Henion, J. D. *LC Mag.* **1985**, *3*, 240–254.
- Tandem Mass Spectrometry*; McLafferty, F. W., Ed.; Wiley: New York, 1983.
- Johnson, J. V.; Yost, R. A. *Anal. Chem.* **1985**, *57*, 758A–768A.
- Covey, T. R.; Lee, E. D.; Henion, J. D. *Anal. Chem.* **1986**, *58*, 2453–2460.

- (22) Raleigh, J. A.; Fuciarelli, A. F. *Radiat. Res.* **1985**, *102*, 165-175.
(23) Spinks, J. W. T.; Woods, R. J. *An Introduction to Radiation Chemistry*; Wiley: New York, 1976.
(24) Wilson, M. S.; McCloskey, J. A. *J. Am. Chem. Soc.* **1975**, *97*, 3436-3444.
(25) Esmans, E. L.; Luyten, Y.; Alderweireldt, F. C. *Biomed. Mass Spectrom.* **1983**, *10*, 347-351.
(26) McCloskey, J. A. In *Basic Principles in Nucleic Acid Chemistry*; Ts'o, P. O. P., Ed.; Academic: New York, 1984; Vol I, pp 209-309.
(27) Hogg, A. M.; Nagabhushan, T. L. *Tetrahedron Lett.* **1972**, *47*, 4827-4830.
(28) Fuciarelli, A. F.; Shum, F. Y.; Raleigh, J. A. *Biochem. Biophys. Res. Commun.* **1986**, *134*, 883-887.
(29) Raleigh, J. A.; Kremers, W.; Whitehouse, R. *Radiat. Res.* **1976**, *65*, 414-422.
(30) *Effects of Ionizing Radiation on DNA*; Huttermann, J., Kohnlein, W., Teoule, R., Eds.; Springer-Verlag: Berlin, 1978.
(31) Fuciarelli, A. F.; Alexander, A. J.; Raleigh, J. A., manuscript in preparation.
(32) Sunner, J.; Kebarle, P., submitted for publication in *Int. J. Mass Spectrom Ion Processes*.
(33) Taft, R. W. *Prog. Phys. Org. Chem.* **1983**, *14*, 247-350.

RECEIVED for review December 29, 1986. Accepted June 22, 1987. Financial support of this work was received from the Alberta Heritage Savings Trust Fund and the Alberta Cancer Board. The purchase and operation of the TAGA 6000E triple quadrupole mass spectrometer were made possible by a grant from the Canadian Natural Sciences and Engineering Research Council.

Preconcentration of Trace Metals from Seawater with 7-Dodeceny-8-quinolinol Impregnated Macroporous Resin

Kenji Isshiki,¹ Fumito Tsuji, and Tooru Kuwamoto

Department of Chemistry, Faculty of Science, Kyoto University, Kyoto 606, Japan

Eiichiro Nakayama*

Instrumental Analytical Research Center, Faculty of Science, Kyoto University, Kyoto 606, Japan

7-Dodeceny-8-quinolinol (DDQ) impregnated XAD-4 resin (DDQ resin) was prepared, and its extraction behavior was studied and compared with solvent extraction with DDQ for Ag, Al, Bi, Cd, Cu, Fe, Ga, Mn, Ni, Pb, and Ti. The results demonstrate that the DDQ resin is effective in the preconcentration of those metals from seawater. The column extraction method using the DDQ resin was applied to seawater analysis with satisfactory results being obtained.

Separation and preconcentration are important problems in the determination of trace metals in seawater. Recently, the column extraction technique based on extraction chromatography for the preconcentration of trace metals has been extensively studied (1). This technique has the following advantages: (i) a relatively high concentration factor, and (ii) the ability of treating large volume samples in a closed system to minimize the risk of contamination. These advantages are essential for the preconcentration of trace metals in seawater.

Substances on which ligands are chemically immobilized or impregnated are used for the column extraction. As for ligand-immobilized substances, so called chelating resins, various combinations of functional groups and substrates have been synthesized and examined (2). However, they may suffer from a complicated procedure for synthesis, and there are limitations in the functional groups that can be immobilized. On the other hand, ligand-impregnated substances have advantages in that ligands can be widely selected and impregnated substances can easily be prepared.

In preparing the ligand-impregnated adsorbents, the following properties are required for the ligands: they should be chemically stable, their solubility in aqueous solution should

be sufficiently low, and they should be strongly adsorbed onto the substrates. In addition, for the simultaneous preconcentration of metal ions from seawater, it is desirable that the ligands are capable of forming complexes with as many metals as possible at the natural pH of seawater (ca. pH 8). 7-Dodeceny-8-quinolinol (DDQ) (7-(1-vinyl-3,3,6,6-tetramethylhexyl)-8-quinolinol, the active substance of the liquid ion-exchanger Kelex-100 (3)) is one of the ligands that is expected to satisfy such conditions. Studies on the distribution of DDQ between the aqueous and organic phases (4) have indicated that DDQ has an extraordinarily large distribution ratio, and solvent extraction studies with DDQ (5-10) have indicated that DDQ forms complexes with many heavy metals in the same manner as 8-quinolinol (oxine).

In the present work, a synthesized macroporous resin, Amberlite XAD-4, was used as an adsorbent for DDQ. Prior to the column extraction study, the properties of DDQ in the liquid-liquid extraction were examined with respect to various heavy metals to compare them with those of oxine, and then the properties of the DDQ-impregnated XAD-4 resin in the batch extraction system were examined and compared with those in the liquid-liquid extraction system. Subsequently, the column extraction of the DDQ-impregnated XAD-4 resin was examined and finally applied to seawater analysis.

EXPERIMENTAL SECTION

Apparatus. A Nippon Jarrel-Ash AA-8200 atomic absorption spectrometer was used for all metal measurements by flame atomic absorption spectrometry (FAAS). It was equipped with a Nippon Jarrel-Ash FLA-100 graphite furnace atomizer for measurements by graphite furnace AAS (GFAAS). Aqueous samples were manually injected into a graphite furnace with a Eppendorf Micropipet. A Shimadzu UV-240 spectrophotometer was used for the determination of DDQ, and a Tokyo Iwaki KM Shaker Model V-D was used for shaking separation funnels and glass vials.

All chemical appliances, such as bottles, vials, parts of columns, and tubes, were cleaned before use by soaking in the cleaner (5% solution of Merck Extran MA03) overnight, rinsing with water,

¹Present address: Kochi Women's University, 5-15, Eikokuji-cho, Kochi 780, Japan.

soaking in 4 M hydrochloric acid overnight, rinsing with hot 4 M nitric acid, and rinsing 5 times with water, successively.

Reagents. Kelex-100 (containing DDQ) (Ashland Chemical Co., Columbus, Ohio) was purified according to the procedure of Lakshmanan and Lawson (5). It was purified by shaking a solution in toluene several times with 1 M hydrochloric acid to remove simple oxine derivatives. After the organic phase was washed with water to remove chloride ions, the solvent was evaporated, and the purified DDQ was dried in vacuo over silica gel.

The resins used were purified XAD-4 and XAD-7 (20–50 mesh; Gasukuro Kogyo, Inc., Tokyo, Japan). The XAD resin was gently ground with an acetone-water mixture in a ceramic mortar and sieved with a nylon mesh sifter to obtain 100–200 mesh grains. Then, the resin was soaked in a methanol–4 M hydrochloric acid (1:1) solution overnight, washed with water, and dried in vacuo.

Hydrochloric acid and aqueous ammonia of analytical reagent grade were further purified by rapid isopiestic distillation. Commercial metal standard solutions for atomic absorption spectrometry (1000 mg/L) were used as metal stock solutions. All other chemicals were of analytical reagent grade.

All aqueous solutions were prepared with distilled deionized water, which was further purified by a Millipore Milli-Q water purification system.

Test Solutions. The following test solutions were prepared: A 0.1 M sodium perchlorate solution containing an acetate (pH 1–6) or borate buffer (pH 6–10) was prepared for the pH dependence experiments. Artificial seawater was prepared according to Lyman and Fleming's formula (11) and used after it was passed through a column packed with DDQ-impregnated XAD-4 resin to remove heavy metal impurities and also through a column packed with XAD-4 resin to remove organic impurities including DDQ that had bled.

Seawater samples were collected with a clean sampler (12) at station 1 (35°01'N, 141°46'E) in the adjacent sea of Japan during a cruise of the R.V. *Tansei Maru* (KT-83-21) in December of 1983. They were filtered through a 0.4 μ m Nuclepore filter immediately after collection, acidified to pH 3 with hydrochloric acid, and stored in precleaned polyethylene bottles.

Preparation of the DDQ-Impregnated Resin. The DDQ-impregnated resin (DDQ resin) was prepared by placing an appropriate amount of the dry resin in a beaker and adding 40 mL of acetone containing the required amount of DDQ and 10 mL of concentrated hydrochloric acid. Then, 950 mL of water was gradually added to the mixture, which was stirred with a magnetic stirrer. The DDQ resin obtained was filtered, rinsed with water several times, and stored in water. The impregnated amount of DDQ was determined by measuring the amount of DDQ remaining in the filtrate.

Preparation of Columns. The DDQ resin (0.57 mmol of DDQ/g of resin) was prepared, and 500 mg of the DDQ resin (consisting of 76 mg of DDQ and 424 mg of XAD-4 resin) suspended in water was slurry-packed in a Teflon column (8-mm i.d.) fitted with porous Teflon filters (pore size, 10 μ m) and Teflon stopcocks. The columns were rinsed successively with 4 M hydrochloric acid and water before use. After the completion of each experiment, the columns were rinsed with water and stored for the next experiment.

Procedures. *Liquid-Liquid Extraction of Metals with DDQ.* A 200-mL portion of buffered metal solution and 100 mL of toluene solution of 0.04 M DDQ were equilibrated in a glass separation funnel by vigorous shaking for a tested period. After phase separation, the metal concentration in the aqueous phase was determined by FAAS or GFAAS against the matrix-matched standard solutions. The pH value of the aqueous phase after extraction was taken as the equilibrium pH value.

Distribution of DDQ between the Aqueous Phase and XAD Resins. Hydrochloric acid, 2 M, a buffer solution of pH 8, and artificial seawater were tested. An appropriate amount of DDQ was loaded on 0.4 g of XAD resin, and 50 mL of the test solution was added to the DDQ resin. After equilibrating them by shaking for 15 min, the resin was filtered off. For 2 M hydrochloric acid, dissolved DDQ was determined by measuring the absorbance at 253 nm directly with a spectrophotometer. For the pH 8 buffer solution and artificial seawater, after the filtrate was acidified with 5 mL of hydrochloric acid, dissolved DDQ was extracted in

2 mL of heptane and determined by measuring the absorbance at 247 nm.

Capacity Measurement. The capacity of the DDQ resin was determined for Cd(II), Cu(II), Mn(II), and Ni(II). The conditioned resin, which is prepared by loading 0.57 mmol of DDQ on 1 g of XAD-4 resin, and 100 mL of buffered metal solution containing 1.00 mmol of a single metal ion, which was adjusted at pH 8, were equilibrated by shaking for 2 h. The resin was then filtered off and washed with water. The adsorbed metal was eluted with 50 mL of 2 M hydrochloric acid and determined by FAAS.

Batch Extraction of Metals with the DDQ Resin. Metal ions were tested individually. A 200-mL portion of buffered metal solution and the DDQ resin, which was prepared by loading 0.114 mmol of DDQ on 0.2 g of XAD-4 resin, were equilibrated in a glass vial by vigorous shaking for a tested period. After the resin was filtered off, the metal concentration in the filtrate was determined by FAAS or GFAAS. The pH value of the aqueous phase after extraction was taken as the equilibrium pH value.

DDQ Bled from the Column. Hydrochloric acid, 2 M, the buffer solution adjusted at pH 8, and artificial seawater were chosen as the test solution. A 500 mL portion of the test solution was passed through the DDQ resin column with a peristaltic pump (flow rate, 3.0 mL/min), and DDQ dissolved in the effluent was determined directly by spectrophotometry for 2 M hydrochloric acid or after extracting it into 3 mL of heptane for the buffer solution and artificial seawater.

Recovery of Metal Spikes from Artificial Seawater with the DDQ Resin Column. A 500-mL portion of artificial seawater in which metal ions were spiked, the pH of which was adjusted at pH 8 with a small amount of aqueous ammonia and hydrochloric acid, was passed through the DDQ resin column with a peristaltic pump (flow rate, 3 or 6 mL/min). After the column was rinsed with 20 mL of diluted aqueous ammonia (pH 8), the adsorbed metal ions were eluted by back flushing with 8 mL of 2 M hydrochloric acid (flow rate, 1.0 mL/min). The effluent was evaporated, and the organic residue was decomposed with 0.5 mL of concentrated nitric acid together with 0.25 mL of 30% hydrogen peroxide on a hot plate. The residue was then dissolved in 1 mL of 0.1 M nitric acid, and the metals were determined by GFAAS against aqueous calibration curves. The analytical blanks were measured after each analytical run by passing 8 mL of 2 M hydrochloric acid through the column and treating the effluent in the same way mentioned as above. All of the operations were carried out in a clean box to prevent contamination.

Analysis of Seawater Samples. Samples containing 500 mL of acidified seawater were neutralized and adjusted to pH 8 with aqueous ammonia. Subsequent treatments were the same as those described in the previous paragraph. All concentration and determination procedures were carried out within 1 month after the collection of the samples.

RESULTS AND DISCUSSION

Solvent Extraction. Although much work has been done on the use of DDQ in the liquid-liquid extraction of metal ions, there are few comprehensive studies for a number of metal ions. In the present work, the extraction behaviors of DDQ with various metal ions in liquid-liquid extraction were examined and compared with those of oxine. Table I shows the pH ranges where the metal ions were quantitatively extracted in the organic phase and the time required to achieve the extraction equilibrium for DDQ. Those for oxine reported by Starý (13) are also tabulated in the table. Except for a few metal ions, the extraction behaviors of DDQ were similar to those of oxine, though the time required to achieve extraction equilibrium was longer than that of oxine. In particular, in the extraction of Fe(III), equilibrium was achieved for several hours for DDQ, while it was achieved for only a few minutes for oxine. This is probably due to the lower solubility of DDQ than of oxine in aqueous phase. Also, the results show that almost all metal ions are extracted quantitatively in the organic phase at around pH 8, the natural pH of seawater. Among the metal ions examined, Mg(II) was hardly extracted at all with DDQ in the organic phase. This property is preferable for the preconcentration of trace metals from

Table I. Extraction Behaviors of DDQ and Oxine

metal ion	DDQ (0.04 M in toluene)		oxine ^a (0.10 M in chloroform)	
	pH range ^b	extraction time ^c	pH range ^b	extraction time ^c
Ag(I)	9.0	30 min	<i>d</i>	
Al(III)	6.5–7.5	30 min	4.0–11.0	2–3 min
Bi(III)	3.0–9.0	30 min	3.0–11.0	2–3 min
Cd(II)	6.0–9.0	30 min	6.0–9.5	2–3 min
Cu(II)	1.5–9.0	30 min	2.5–12.0	2–3 min
Fe(III)	2.0–9.0	6.5 h	2.0–10.0	2–3 min
Ga(III)	4.5–9.0	30 min	2.0–12.0	2–3 min
Mg(II)	<i>e</i>		9.0	2–3 min
Mn(II)	8.0–9.0	30 min	8.0–10.0	2–3 min
Ni(II)	3.0–9.0	6.0 h	4.0–10.0	some h
Pb(II)	7.5–9.0	30 min	6.5–10.0	2–3 min
Ti(III)	2.0–9.0	6.5 h	2.0–9.0	1–2 h

^aReference 13. ^bpH range at which quantitative recovery was obtained. ^cExtraction time required to reach extraction equilibrium. ^dRecovery is insufficient at pH 1–11. ^eNot extracted at all at pH 1–9.

Table II. Logarithm of Distribution Ratio of DDQ between Aqueous Phase and XAD Resins^a

resin	aqueous phase	distribution ratio with the following amounts of DDQ loaded			
		0.25 mol/kg	0.5 mol/kg	0.7 mol/kg	0.9 mol/kg
XAD-4	pH 8 ^b	6.7	6.8	6.8	7.0
	ASW ^c	6.5	6.8	6.9	7.2
	HCl ^d	5.4	5.6	5.4	4.3
XAD-7	pH 8 ^b	5.8	6.3		
	ASW ^c	5.9	5.8		
	HCl ^d	3.7	3.7		

^aDistribution ratio, *D*, is defined as $D = [\text{DDQ on the resin (mol/kg)}] / [\text{DDQ in the aqueous phase (mol/L)}]$. ^bBuffer solution of pH 8. ^cArtificial seawater. ^dThe concentration of hydrochloric acid is 2 M.

seawater, which contains a large amount of alkaline-earth metal ions.

Properties of the DDQ Resin. Amberlite XAD-4 resin, which is a styrene-divinylbenzene copolymer, and XAD-7 resin, which is an acrylic ester polymer, have been widely used as adsorbents of organic materials because of their organophilic nature owing to their hydrophobic surface and macroporous structure (14). XAD resins are more stable against acidic or alkaline aqueous solutions and against all organic solvents compared with C₁₈-bonded silica gel, which also has been used as an adsorbent. In the present work, XAD-4 and XAD-7 resins were tested as adsorbent.

Several methods for impregnating water-insoluble reagents into the adsorbents have been applied so far, such as passing the reagent solution through a column packed with the adsorbent (15), soaking the adsorbent in the reagent solution (16), and evaporating the solvent after soaking the adsorbent in the reagent solution (17). In comparison, our procedure has the following advantages: (i) water-insoluble reagents can be adsorbed uniformly onto the adsorbent, (ii) metal impurities in the reagent are removed during the impregnation process because DDQ is loaded on the adsorbent in acidic solution, and (iii) the affinity of the adsorbent for water is not reduced by the impregnation of DDQ.

The distribution of DDQ between the XAD resins and the aqueous solution was investigated for various loading amounts of DDQ. The results are shown in Table II. It was reported that the logarithm of the distribution ratio between 1-octanol and the aqueous phase was 3.0 and 6.5 for 1 M sulfuric acid

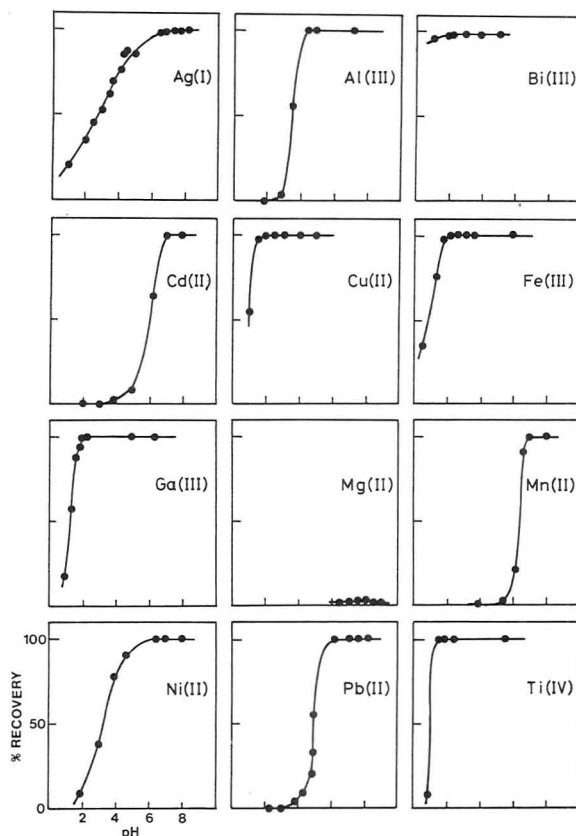


Figure 1. pH dependence of the recovery of metals with the DDQ-impregnated XAD-4 resin. The concentration of metals in the sample solutions is 2 mg/L.

and for the buffer solution of pH 8, respectively (4). In contrast, the distribution ratios for XAD resins are much higher. Especially in the acidic region, the distribution ratio for XAD-4 resin is 2 orders of magnitude higher than that for the organic solvent. This indicates that the effect of the protonation of DDQ on the distribution for XAD-4 resin is less than that for the organic solvent. Also, the results apparently indicate that XAD-4 resin is a more excellent adsorbent for DDQ than XAD-7 resin. Although the specific surface area of XAD-4 resin (784 m²/g) is only 1.7 times larger than that of XAD-7 resin (450 mg²/g) (17), the distribution ratios for XAD-4 are 1 or 2 orders of magnitude higher than those of XAD-7. The difference in the distribution ratio of both resins is probably due to the difference in the hydrophobicity of the surface. Parrish (17) studied the rate of uptake of Cu(II) for various adsorbents on which DDQ are loaded and reported that XAD-7 resin is the most preferable adsorbent for DDQ. He pointed out that the exchange rate is mainly related to the water regain of the resins. However, he did not refer to the distribution of DDQ between the resin and the aqueous phase. In our experiment, XAD-4 resin was found to be superior to XAD-7 resin in its retention of DDQ, which is a significant factor in the extraction efficiency and recycling of the resin. Thus, XAD-4 was chosen as the adsorbent for DDQ.

The capacity of the DDQ resin (0.57 mmol/g) for Cd(II), Cu(II), Mn(II), and Ni(II) was 0.520, 0.550, 0.550, and 0.521 mmol/g, respectively, and the ratio of M:L was ca. 1:1.1 for these metal ions. This suggests that a large part of the metal ions form 1:1 complexes on the resin, which is the same as for other resins (18, 19).

The extraction behaviors of the DDQ resin were examined by the batch method, and the results are shown in Figure 1. The pH dependences of extraction with the DDQ resin are similar to those of liquid-liquid extraction. For almost all of the metal ions examined, except for Fe(III), Ni(II), and Ti(IV),

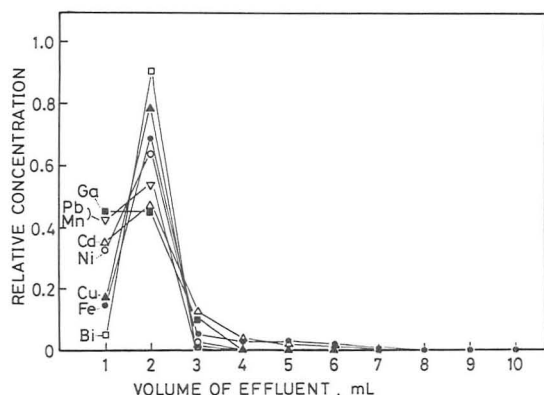


Figure 2. Typical elution curves of metals collected in the column with back flushing. The concentration of metals in the sample solutions is 5 $\mu\text{g/L}$.

Table III. Absolute Analytical Blanks and Detection Limits

metal ion	blank, ^a ng	detection limit, ng/L
Ag(I)	<0.08	0.16
Al(III)	30 \pm 9	54
Bi(III)	<1.5	3
Cd(II)	0.05 \pm 0.01	0.06
Cu(II)	<2.3	4.6
Fe(III)	18 \pm 2	12
Ga(III)	0.8 \pm 0.1	0.6
Mn(II)	<0.8	1.6
Ni(II)	<4.5	9
Pb(II)	0.9 \pm 0.2	1.2
Ti(IV)	<150	300

^aMean and standard deviation of 10 individual analytical runs.

the extraction equilibrium was achieved within 30 min. For these three metal ions, about 2 h was required to achieve equilibrium.

Column Extraction. Some preliminary examinations were carried out for the simultaneous preconcentration of metal ions from seawater by column extraction.

Loss of DDQ in the Column by a Single Analytical Procedure. The amounts of DDQ that bled from the DDQ resin column with 500 mL of 2 M hydrochloric acid, of the buffer solution of pH 8, and of artificial seawater were 1.4×10^{-6} , 8.5×10^{-11} , and 3.0×10^{-9} mol, respectively, which were less than the equilibrium concentrations in the distribution experiments. From these values, the amount of DDQ that bled per one cycle of the analysis is calculated to be 2.54×10^{-8} mol, which is about 0.01% of the total impregnated amount in the column. This shows that the DDQ resin column can be repetitively used without an apparent loss of the complexation capacity of the DDQ resin.

Elution. Hydrochloric acid was used for the elution of the metal ions collected in the DDQ column because reagent of very high purity can be easily obtained by isopiestic distillation. Typical elution curves for individual metal ions obtained when using 2 M hydrochloric acid are given in Figure 2, which shows the relative concentration of metals in each 1-mL portion of the effluent. The first fraction of the effluent apparently indicates that the dead volume of the column is less than 1 mL. Cd(II) and Fe(III) were recovered from the column with 7 mL of the eluent and the others with 3 mL. Therefore, 8 mL of the eluent was used for further experiments.

Analytical Blanks. The absolute analytical blanks per single analysis procedure are shown in Table III. For Ag, Bi, Cu, Mn, Ni, and Ti, the blank values were below the detection limits of GFAAS. For the other metals, the blank values were

Table IV. Recovery of Metal Spikes from Artificial Seawater

metal ion	spiked, ng	found, ^a ng	% recovery
Ag(I)	20	14.6 \pm 1.1	73 \pm 5
Al(III)	400	426 \pm 21	107 \pm 5
Bi(III)	100	100 \pm 2	100 \pm 2
Cd(II)	100	97 \pm 2	97 \pm 2
Co(II)	100	63 \pm 12	63 \pm 12
Cr(III)	100	<1	<1
Cu(II)	100	97 \pm 7	97 \pm 7
Fe(III)	100	98 \pm 5	98 \pm 5
Ga(III)	60	57 \pm 2	95 \pm 4
Mn(II)	100	91 \pm 2	91 \pm 2
Ni(II)	300	290 \pm 12	97 \pm 4
Pb(II)	100	95 \pm 4	95 \pm 4
Ti(IV)	2500	2420 \pm 180	97 \pm 7

^aMean and standard deviation for five individual determinations.

detected with GFAAS, but they were satisfactorily reproducible. Those blanks were almost the same as the sum of the blanks of the reagents, which were added through the whole analysis procedure. In Table III, the detection limits in seawater for the procedure given in the experimental section are also tabulated. These are simply the detection limits obtained by dividing the detection limits calculated from the variation of the analytical blanks (when an analytical blank is below the detection limit of GFAAS, the detection limit of GFAAS is used) by the concentration factor of 500. The detection limit is defined as 3 times the standard deviation of the analytical blank or the fluctuation of the base line of absorption signals from the GFAAS system.

Recovery of Metal Spikes from Artificial Seawater. The efficiency of recovery of spikes from artificial seawater was examined at two different flow rates. At the flow rate of 3 mL/min, satisfactory results were obtained as shown in Table IV. The recovery of Ag(I) was not quantitative, though it was quantitative in the buffer solution, because of the formation of the stable chloro complex. Although Cr(III) and Co(II) were not tested in the liquid-liquid extraction nor in the batch extraction with the DDQ resin, the recovery of Cr(III) and Co(II) was tested here and determined as shown in the table. Cr(III) was not recovered at all. This is due to the inertness of hydrated Cr(III) ion. Co(II) was insufficiently recovered, and the variation of its recovery was larger than that of other metals. This is due to the imperfect dissociation of the inert Co(III) complex which is formed by the oxidation of the Co(II) complex with dissolved oxygen in the same manner as in the solvent extraction (8). At 6 mL/min, the recovery of Al, Bi, Fe, and Mn decreased to 60–80%.

To estimate the effect of coexisting organic materials capable of combining with metals on the recovery of metal spikes from artificial seawater, EDTA and 8-quinolinol-5-sulfonic acid (QSA) were used, although they are not actually present in seawater. Since their ligands form quite stable, water soluble complexes with metals, the resulting complexes are not adsorbed onto XAD-4 resin. The results are shown in Table V. The recovery of metal spikes decreased at more than 10^{-7} M of EDTA and at more than 10^{-4} M of QSA.

Seawater Analysis. Seawaters in the adjacent sea of Japan were analyzed concerning six major metals with the column extraction method. Seawater samples were filtered, acidified to be at pH 3 with HCl on board immediately after the sampling, and then the concentration procedures were carried out within 1 month. Since the storage period was so short, it was considered that there was no apparent loss of the metals determined. The results, which are shown in Table VI, have been calculated on the assumption of 100% recovery

Table V. Effect of Complexing Materials on the Recovery of Metal Spikes

metal ion ^b	% recovery ^a							
	[EDTA], M				[8-quinolinol-5-sulfonic acid], M			
	10 ⁻⁷	10 ⁻⁶	10 ⁻⁵	10 ⁻⁴	10 ⁻⁷	10 ⁻⁶	10 ⁻⁵	10 ⁻⁴
Al(III)	102	100	102	105	102	98	105	82
Bi(III)	80	64	9	7	99	101	91	77
Cd(II)	80	64	<1	<1	102	103	84	75
Cu(II)	77	32	19	26	98	101	103	103
Fe(III)	95	96	89	11	96	95	105	82
Mn(II)	82	67	24	19	100	96	99	100
Ni(II)	99	102	102	85	104	101	100	71
Pb(II)	59	<1	<1	<1	103	95	102	101

^a Single determination. ^b Concentration is 1 µg/L.**Table VI. Analysis of Seawater Samples^a**

depth, m	concentration, ng/L					
	Cd	Cu	Fe	Mn	Ni	Pb
0	10.1	40	230	120	130	310
100	6.7	49	320	99	160	330
200	19	36	540	71	180	750
300	40	39	280	49	220	660
400	38	40	960	99	250	1600

^a Single determination.

of the metals. The concentration factor was 500.

In recent years, much work has been done concerning complexing capacities and conditional stability constants for Cu(II) with organic materials dissolved in seawater. For example, Hirose et al. (20) reported that the complexing capacity, L , is 2×10^{-9} M and the logarithm of the conditional stability constant, $\log K'$, is 11.8, and Buckley and van den Berg (21) reported $L = 1.44 \times 10^{-7}$ M, $\log K' = 9.87 - L = 6 \times 10^{-9}$, $\log K' = 10.7$. These values are larger than $\log K'$ of Cu(II)-EDTA complex ($\log K' = 10.4$). This suggests that a part of the metals that form stable, water-soluble complexes with organic materials dissolved in seawater may not be collected with the DDQ resin column method.

The concentrations for Cd, Cu, Ni, and Mn tabulated in Table VI closely agree with those in the northeast Pacific reported by Bruland (22) (Cd, 0.26–56 ng/kg; Cu, 34–87 ng/kg; Ni, 146–320 ng/kg) and by Landing and Bruland (23) (Mn,

50–200 ng/kg). For Fe, the concentrations are several times higher than those in the northeast Pacific reported by Gordon et al. (24) (Fe, 8.4–145 ng/kg). For Pb, the concentration is more than 25 times higher than that in the northeast Pacific reported by Shaule and Patterson (25) (12 ng/kg). However, it is not clear whether or not the higher concentration of Pb is characteristic in the region where the samples were collected.

ACKNOWLEDGMENT

The authors express their gratitude to E. Yamada for supplying Kelex-100 and to the members of the staff of the Ocean Research Institute, University of Tokyo, and H. Tsubota for their cooperation in the collection of samples.

Registry No. XAD-4, 37380-42-0; Ag, 7440-22-4; Al, 7429-90-5; Bi, 7440-69-9; Cd, 7440-43-9; Cu, 7440-50-8; Fe, 7439-89-6; Ga, 7440-55-3; Mg, 7439-95-4; Mn, 7439-96-5; Ni, 7440-02-0; Pb, 7439-92-1; Ti, 7440-32-6; H₂O, 7732-18-5; 7-dodeceny-8-quinolinol, 59351-71-2; oxine, 148-24-3.

LITERATURE CITED

- (1) Van Grieken, R. *Anal. Chim. Acta* **1982**, *143*, 3.
- (2) Sahni, S. K.; Reedijk, J. *Coord. Chem. Rev.* **1984**, *59*, 1.
- (3) Ashbrook, A. W. *J. Chromatogr.* **1975**, *105*, 151.
- (4) Cote, G.; Bauer, D. J. *Inorg. Nucl. Chem.* **1981**, *43*, 1023.
- (5) Lakshmanan, V. I.; Lawson, G. J. *J. Inorg. Nucl. Chem.* **1973**, *35*, 4285.
- (6) Ashbrook, A. W. *Coord. Chem. Rev.* **1975**, *16*, 285.
- (7) Flett, D. S.; Hartlage, J. A.; Spink, D. R.; Okuhara, D. N. *J. Inorg. Nucl. Chem.* **1975**, *37*, 1967.
- (8) Flett, D. S.; Cox, M.; Heels, J. D. *J. Inorg. Nucl. Chem.* **1975**, *37*, 2197.
- (9) Harrison, G.; Lakshmanan, V. I.; Lawson, G. *J. Hydrometallurgy* **1976**, *1*, 339.
- (10) Yamada, E.; Freiser, H. *Anal. Chem.* **1981**, *53*, 2115.
- (11) Lyman, G.; Fleming, R. H. *J. Mar. Res.* **1940**, *3*, 136.
- (12) Tsubota, H. *Ocean Characteristics and Their Change*; Kajiwara, K., Editor; Kouseisha-kouseikaku: Tokyo, Japan, 1985; pp 225–236.
- (13) Starý, J. *Anal. Chim. Acta* **1963**, *28*, 132.
- (14) Junk, G. A.; Richard, J. J.; Grieser, M. D.; Witiak, D.; Witiak, J. L.; Arguello, M. D.; Vick, R.; Svec, H. J.; Fritz, J. S.; Calder, G. V. *J. Chromatogr.* **1974**, *99*, 745.
- (15) Chwastowska, J.; Mozar, E. *Talanta* **1985**, *32*, 574.
- (16) Lundgren, J. L.; Schilt, A. A. *Anal. Chem.* **1977**, *49*, 974.
- (17) Parrish, J. R. *Anal. Chem.* **1977**, *49*, 1189.
- (18) Vernon, F.; Nyo, K. M. *Anal. Chim. Acta* **1977**, *93*, 203.
- (19) Hoek, P. J.; Reedijk, J. *J. Inorg. Nucl. Chem.* **1979**, *41*, 401.
- (20) Hirose, K.; Dokiya, Y.; Sugimura, Y. *Mar. Chem.* **1982**, *11*, 343.
- (21) Buckley, P. J. M.; van den Berg, C. M. G. *Mar. Chem.* **1986**, *19*, 281.
- (22) Bruland, K. W. *Earth Planet. Sci. Lett.* **1980**, *47*, 176.
- (23) Landing, W. M.; Bruland, K. W. *Earth Planet. Sci. Lett.* **1980**, *49*, 45.
- (24) Gordon, R. M.; Martin, J. H.; Knauer, G. A. *Nature (London)* **1982**, *299*, 611.
- (25) Schaule, B. K.; Patterson, C. C. *Earth Planet. Sci. Lett.* **1981**, *54*, 97.

RECEIVED for review December 10, 1986. Accepted June 22, 1987. This research was supported in part by a grant from the Nissan Science Foundation.

Reversed-Phase High-Performance Liquid Chromatography of Substituted Anilines Utilizing Molecular-Recognizing Ability of Crown Ether: Comparison with Ion-Pair Chromatography

Akimasa Shibukawa, Terumichi Nakagawa,* Atsunori Kaihara, Kumiko Yagi, and Hisashi Tanaka

Faculty of Pharmaceutical Sciences, Kyoto University, Sakyo-ku, Kyoto-shi 606, Japan

Host-guest interaction between crown ether and protonated amino group has been applied to the specific separation of positional isomers of mono- and disubstituted anilines by reversed-phase high-performance liquid chromatography with mobile phase containing 18-crown-6. The retention of these amines on a hydrophobic stationary ligand was enhanced by association with 18-crown-6, and the degree of the enhancement reflected the molecular structure of the guest. The host-guest association constant and the degree of maximum enhancement were evaluated from the experimental values of capacity factor by the use of an equation derived from the equilibria involved in this particular system. The retention and separation of the isomers were characterized in terms of number, position, and functionality of the substituent groups on the aniline ring in comparison with those obtained by conventional ion-pair reversed-phase chromatography.

The selectivity in high-performance liquid chromatography (HPLC) separation can be improved by modification of the interaction between solute and mobile phase and/or stationary phase, especially by incorporation of a second equilibrium system (1) that involves host-guest interaction (2-17). In the previous papers (2-8), the authors have clarified the effect of host-guest interaction between crown ether and amino compounds in reversed-phase HPLC where crown ether was involved as an additive to the aqueous mobile phase (CERPLC). It has been known that 18-membered crown ethers associate with protonated primary amino groups by hydrogen bonding and ion-dipole interaction to form a relatively stable cationic complex in solution (19). Hydration of amino groups in the mobile phase may be weakened by the formation of the complex, so that the retention of the guest on the hydrophobic stationary ligand (e.g. ODS) can be enhanced depending on the stability of the complex and the hydrophobicity of crown ether. According to the model for this particular chromatographic system, we derived the equation that expressed capacity factor of a guest as a function of crown ether and proton concentrations in the mobile phase. The experimental results allowed discussion of the retention behavior, in good agreement with the equation in terms of class, number, and location of amino groups and the chemical structure around amino groups in the guest molecule. Some practical methods for the separation of catecholamines (4), β -lactam antibiotics (3), and amino acids and peptides (7, 8) have been developed by the use of crown ethers.

The present paper deals with the effects of substituent groups on the retention of aniline derivatives in CERPLC, putting emphasis on the molecular recognizing separation of positional isomers of mono- and disubstituted anilines. The discussion is also focused on the comparison between CERPLC and conventional ion-pair reversed-phase liquid chromatography (IPRPLC).

EXPERIMENTAL SECTION

Reagents. 18-Crown-6 was a product of Merck (Darmstadt, FRG). Sodium pentanesulfonate used for ion-pair chromatog-

raphy and triethylamine of analytical reagent grade were purchased from Nakarai Chemicals Co. (Kyoto, Japan). All the guest compounds of analytical reagent grade were obtained from Nakarai Chemicals and Wako Pure Chemical Co. (Osaka, Japan). These reagents were used without further purification. Glass-distilled water and methanol were used to prepare the mobile phase after degassing. Hydrochloric acid of analytical reagent grade was used to adjust the pH of the mobile phase. The analytical column packed with 5- μ m C₁₈ silica (Chemcosorb 5ODSH) was purchased from Chemco (Osaka, Japan).

Measurements of Capacity Factors. A liquid chromatograph (LC-6A, Shimadzu, Japan) equipped with a UV detector (PAD-6A, Shimadzu) was used for the measurements of capacity factors. The operating conditions are given in Table I. The guest materials were dissolved in a small volume of mobile phase or methanol, and the minimum amount required for UV detection was used in order to maintain linearity of the chromatographic system. The capacity factors (k') were calculated from the equation, $k' = (t_R - t_0)/t_0$, where t_R is the retention time of a guest compound averaged over repeated measurements at the top of the elution curve and t_0 is that of a nonabsorbed substance (NaNO₃).

Data Analysis. Nonlinear least-squares fittings were carried out with a PC-9801F microcomputer (NEC, Tokyo, Japan) specially programmed in BASIC (18).

THEORY

In the reversed-phase liquid chromatography where crown ether is contained in the aqueous mobile phase, a sample compound with an amino group may undergo the equilibria shown in Figure 1, where the pH of the mobile phase is low enough to allow complete protonation of amino group and the host-guest interaction is assumed to take place with 1:1 stoichiometry. SH, C, and L represent a protonated guest molecule, host compound (crown ether), and stationary ligand, respectively. The K 's are the association constants specified in Figure 1. By introducing the equilibria in Figure 1 to the capacity factor (k') equation defined as

$$k' = \Phi \frac{[LSH]_s + [LCSH]_s}{[SH]_m + [CSH]_m} \quad (1)$$

we obtain

$$k' = \Phi [L]_s \frac{K_{LSH} + B[C]_m}{1 + K_{CSH}[C]_m} \quad (2)$$

where Φ designates phase ratio (stationary phase/mobile phase), the subscripts "s" and "m" specify stationary phase and mobile phase, and B represents $K_{LCSH}K_{CSH}$, $K_{LCSH}K_{LC}$, or $K_{LCSH}K_{LSH}$.

Since the stationary phase occupied by the guest accounts for a very small part of the total ($[L_T]$)

$$[L_T] \div [L]_s + [LC]_s$$

Therefore

$$[L]_s = [L_T]/(1 + K_{LC}[C]_m) \quad (3)$$

From eq 2 and 3

$$k' = \frac{k'_o + \Phi [L_T] B [C]_m}{(1 + K_{LC}[C]_m)(1 + K_{CSH}[C]_m)} \quad (4)$$

Table I. HPLC Conditions^a

experiment	mobile phase	stationary phase
(A) k' vs. pH profile	H ₂ O/CH ₃ OH = 8/2 (v/v), pH 2.2–5.4 adjusted by HCl, containing 50 μ M triethylamine ^b	Chemcosorb 5DSH (15 cm \times 4.6-mm i.d.)
(B) dependence of k' on [18-crown-6]	H ₂ O/CH ₃ OH = 8/2 (v/v), pH 2.5 adjusted by HCl, containing 0–20 mM 18-crown-6	Chemcosorb 5DSH (15 cm \times 4.6-mm i.d.)
(C) dependence of k' on [C ₅ H ₁₁ SO ₃ Na]	H ₂ O/CH ₃ OH = 8/2 (v/v), pH 2.5 adjusted by HCl, containing 0–10 mM sodium pentanesulfonate	Chemcosorb 5DSH (15 cm \times 4.6-mm i.d.)
(D) separation of methoxyaniline isomers	H ₂ O/CH ₃ OH = 8/2 (v/v), pH 2.5 adjusted by HCl, containing 10 mM sodium pentanesulfonate or 1 mM 18-crown-6.	Chemcosorb 5DSH (15 cm \times 4.6-mm i.d.)
(E) separation of aminocresol isomers	H ₂ O/CH ₃ OH = 8/2 (v/v), pH 2.5 adjusted by HCl, containing 10 mM sodium pentanesulfonate or 2 mM 18-crown-6.	Chemcosorb 5DSH (15 cm \times 4.6-mm i.d.)

^aFlow rate, 0.9 mL/min; detection, UV 220 nm; column temperature, 40 °C. ^bTriethylamine was added to avoid silanophilic effect.

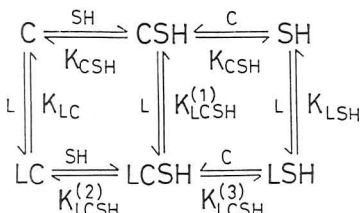


Figure 1. Equilibria involved in reversed-phase liquid chromatography with a crown ether containing mobile phase: SH, protonated amine; C, crown ether; L, hydrophobic stationary phase; K , association constant; K_a , dissociation constant.

where k'_o is the capacity factor of free guest measured without using crown ether. The capacity factor of the host-guest complex (k'_c) is expressed by

$$k'_c = \Phi[L_T]B/K_{CSH} \quad (5)$$

When an anionic ion-pairing agent such as hydrophobic sulfonate is involved instead of crown ether, the following equations in place of eq 4 and 5 are valid:

$$k' = \frac{k'_o + \Phi[L_T]B[I]_m}{(1 + K_{LI}[I]_m)(1 + K_{ISH}[I]_m)} \quad (6)$$

$$k'_I = \Phi[L_T]B'/K_{ISH} \quad (7)$$

where subscript "I" designates the ion-pairing agent and k'_I is the capacity factor of a 1:1 ion pair formed between guest and sulfonate. These equations are conformable to those previously derived according to ion-pair partition theory (20), because of the similarity in modeling of the chromatographic processes. However, the role of crown ether is different from that of the ion-pairing reagent in that the former is a hydrophobic nonelectrolyte, which can participate in stereospecific interactions with organic cations. Equations 4 and 6 predict that the additive exerts opposite effects on the retention of a guest; one is to increase the capacity factor by the complex formation, and the other is to decrease it by competing with the guest in binding to the stationary ligand. Thus, the k' value changes depending on the balance of these effects. The degree of the former effect (retention enhancement effect) depends on the K_{CSH} or K_{ISH} and k'_c or k'_I values. Figure 2 shows the curves of eq 4, where three different values were arbitrarily substituted in k'_c (Figure 2A) and K_{CSH} (Figure 2B), while the other parameters were kept constant. As shown in Figure 2, a larger k'_c value causes a larger increase in k' , and a larger K_{CSH} value causes a more rapid increase in k' , reaching maximum level at a lower concentration of crown ether. This indicates that the solutes, which are hardly separated from each other in the usual reversed-phase mode, can be separated because of the difference in K_{CSH} and/or k'_c value(s). On the other hand, when the additive does not make a complex with the guest but competes with it in binding to

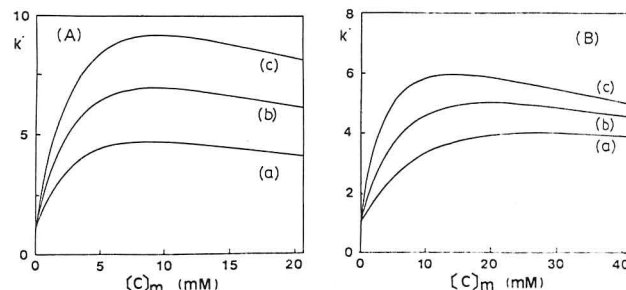


Figure 2. Simulated curves of capacity factor against the concentration of crown ether in the mobile phase at various values of k'_c and K_{CSH} . The simulation is based on eq 4. (A) $k'_o = 1$; $K_{LC} = 50 \text{ M}^{-1}$; $K_{CSH} = 200 \text{ M}^{-1}$; $k'_c = 10$ (line a), 15 (line b), 20 (line c). (B) $k'_o = 1$; $K_{LC} = 20 \text{ M}^{-1}$; $K_{CSH} = 50 \text{ M}^{-1}$; $k'_c = 10$ (line a), 100 M^{-1} (line b), 200 M^{-1} (line c).

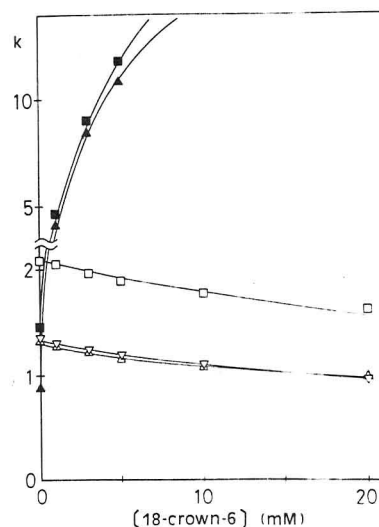


Figure 3. Effect of 18-crown-6 concentration in the mobile phase on the capacity factors of benzylamine (▲), *m*-toluidine (■), *N*-methyl-*m*-toluidine (□), *N,N*-dimethylaniline (▽), and *N,N*-dimethylbenzylamine (Δ). For HPLC conditions, see part B in Table I.

the stationary phase (i.e. $K_{CSH} = K_{ISH} = 0$), the eq 4 and 6 can be simplified to eq 8 and 9, respectively. Apparently, a larger K_{LC} or K_{LI} value causes a larger decrease in k' .

$$k' = k'_o / (1 + K_{LC}[C]_m) \quad (8)$$

$$k' = k'_o / (1 + K_{LI}[I]_m) \quad (9)$$

RESULTS AND DISCUSSION

Estimation of K_{LC} and K_{LI} Values. Figure 3 shows the relationship between capacity factor and concentration of 18-crown-6. The capacity factors of primary amines (benzylamine, *m*-toluidine) were markedly increased by addition of a low concentration (<5 mM) of 18-crown-6, while those of

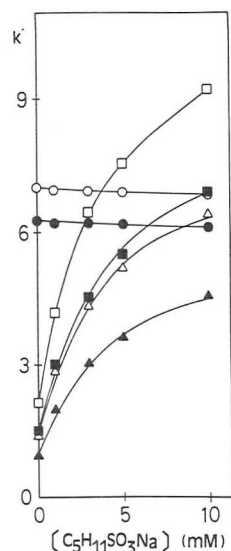


Figure 4. Effect of concentration of pentanesulfonate on the capacity factors of m -toluidine (■), benzylamine (▲), N -methyl- m -toluidine (□), N,N -dimethylbenzylamine (△), phenol (●), and benzyl alcohol (○). For HPLC conditions, see part C in Table I.

secondary amine (N -methyl- m -toluidine) and tertiary amines (N,N -dimethylaniline, N,N -dimethylbenzylamine) were decreased, as expected from eq 8, because the latter two types of amines can scarcely make a stable complex with 18-crown-6 (21). For instance, the capacity factor ratio (k'/k'_0) at 5 mM 18-crown-6 is 12.4 for benzylamine, 7.49 for m -toluidine, 0.91 for N -methyl- m -toluidine, 0.88 for N,N -dimethylaniline, and 0.87 for N,N -dimethylbenzylamine. As a result, the elution order of primary amine and other classes of amines was reversed by a simple modification of the mobile phase with 1 mM 18-crown-6. Such a structure-recognizing ability of 18-crown-6 becomes conspicuous by comparison with the results obtained by IPRPLC (Figure 4). By addition of pentanesulfonate instead of 18-crown-6 at a concentration up to 10 mM, the capacity factors of amines were increased regardless of their class of amino groups, to result in almost the same extent of retention enhancement. For example, the capacity factor ratio at 10 mM pentanesulfonate is 4.60 for m -toluidine, 4.26 for N -methyl- m -toluidine, 4.83 for benzylamine, and 4.58 for N,N -dimethylbenzylamine.

Figure 4 also includes the results of benzyl alcohol and phenol. These data were used for the evaluation of K_{LI} by the simultaneous nonlinear least-squares fittings of eq 9, because the association constants of these compounds with sulfonate (K_{ISH}) are close to zero. The K_{LI} value was thus evaluated to be $2.01 M^{-1}$. Similarly, we calculated the K_{LC} value by fitting eq 8 to the data points for the above-mentioned secondary and tertiary amines in Figure 3 and obtained $K_{LC} = 17.5 M^{-1}$. The K_{LC} and K_{LI} values thus obtained were used for the estimation of the parameters (K_{CSH} , K_{ISH} , k'_c , k'_I , and k'_0) according to eq 4–7.

Retention Enhancement of Aniline and Monosubstituted Anilines. Figures 5, 6, and 7 show, respectively, the dependence of the capacity factors of the isomers of toluidine, methoxyaniline, and aminophenol upon the concentration of 18-crown-6 and pentanesulfonate. The preliminary investigation of k' vs. pH profiles (HPLC condition A in Table I) indicated that these amines were almost completely protonated under the mobile-phase conditions that gave the results shown in Figures 5–7. The series of data points shown in Figures 5–7 were fitted to eq 4 or 6 by the nonlinear least-squares method, using $K_{LC} = 17.5 M^{-1}$ and $K_{LI} = 2.01 M^{-1}$. The curves shown in Figures 5–7 are those best fitted thereby, indicating satisfactory agreement with the experimental values. Table II lists the pertinent values for the parameters.

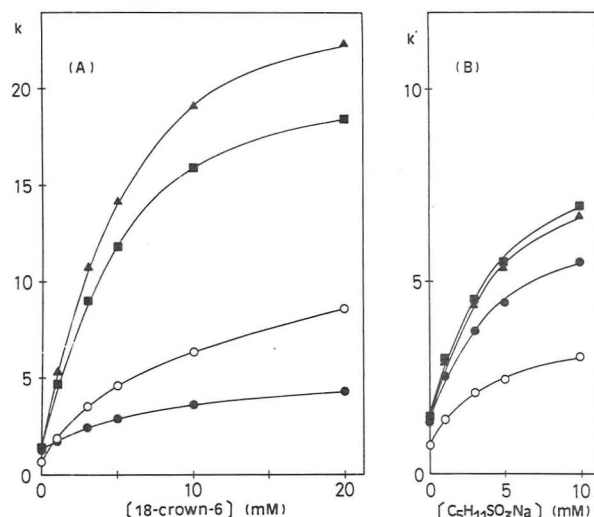


Figure 5. Dependence of the capacity factors of aniline and toluidine isomers on the concentration of 18-crown-6 (A) and pentanesulfonate (B): (○) aniline; (●) o -toluidine; (■) m -toluidine; (▲) p -toluidine. For HPLC conditions, see Table I.

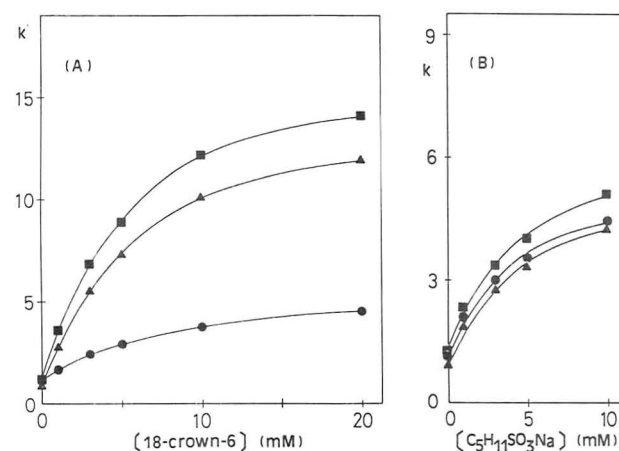


Figure 6. Dependence of the capacity factors of methoxyaniline isomers on the concentration of 18-crown-6 (A) and pentanesulfonate (B): (●) o -methoxyaniline; (■) m -methoxyaniline; (▲) p -methoxyaniline. For HPLC conditions, see Table I.

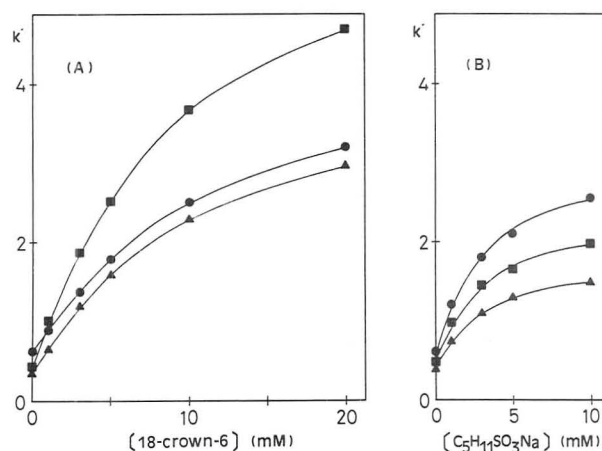


Figure 7. Dependence of the capacity factors of aminophenol isomers on the concentration of 18-crown-6 (A) and pentanesulfonate (B): (●) o -aminophenol; (■) m -aminophenol; (▲) p -aminophenol. For HPLC conditions, see Table I.

The k'_c and k'_I values were calculated from eq 5 and 7, respectively.

In CERPLC, significant selectivity for ortho isomers was observed. The K_{CSH} values of o -toluidine ($48.6 M^{-1}$) and o -methoxyaniline ($56.4 M^{-1}$) were smaller than that of aniline

Table II. Pertinent Values of Parameters in Equations 4–7 for Aniline and Monosubstituted Anilines

	CERPLC				IPRPLC			
	K_{CSH}, M^{-1}	k_o'	k_c'	k_c'/k_o'	K_{ISH}, M^{-1}	k_o'	k_i'	k_i'/k_o'
aniline	75.3	0.74	16.5	22.3	114	0.80	6.03	7.54
<i>o</i> -toluidine	48.6	1.36	10.3	7.57	97.1	1.46	11.7	8.01
<i>m</i> -toluidine	91.1	1.56	37.8	24.2	93.7	1.64	15.2	9.27
<i>p</i> -toluidine	93.2	1.48	45.4	30.7	96.3	1.54	14.6	9.48
<i>o</i> -methoxyaniline	56.4	1.14	10.5	9.21	90.8	1.23	9.68	7.87
<i>m</i> -methoxyaniline	89.1	1.29	29.0	22.5	78.7	1.36	12.0	8.82
<i>p</i> -methoxyaniline	81.8	0.91	25.4	27.9	90.5	1.00	9.47	9.47
<i>o</i> -aminophenol	32.6	0.61	10.0	16.4	128	0.65	4.84	7.45
<i>m</i> -aminophenol	44.8	0.47	12.9	27.4	141	0.53	3.59	6.77
<i>p</i> -aminophenol	39.7	0.35	8.59	24.5	164	0.40	2.60	6.50

(75.3 M^{-1}) indicating that methyl and methoxy groups at the ortho position hindered the access of 18-crown-6 to the amino group and weakened the interaction. This result is consistent with a fact that the association constant between 18-crown-6 and *o*-toluidine in methanol ($\log K_{CSH} = 2.86$) was smaller than that of aniline ($\log K_{CSH} = 3.80$) (21). Furthermore, these ortho-substituent groups suppressed the increase in hydrophobicity expected from the complex formation with 18-crown-6. The k_c'/k_o' values of *o*-toluidine (7.57) and *o*-methoxyaniline (9.21) were only about one-third and two-fifths of the value of aniline (22.3), respectively. This may be because a part of the hydrophobic surface area of the methyl or methoxy groups substituted at the ortho position overlapped with that of 18-crown-6, resulting in the loss of increase in retention onto octadecylsilyl ligand, and weaker association caused less dehydration of the amino group than in case of aniline. On the contrary, substitution of a methyl or methoxy group at the meta or para position brought about increases in both K_{CSH} and k_c'/k_o' values. Consequently, the ortho isomers of toluidine and methoxyaniline can be easily separated by simple modification of the mobile phase with 18-crown-6.

The selectivity of 18-crown-6 to ortho isomer depends on the functionality of the substituent group. The hydroxyl group substituted at the ortho position of aniline caused a large decrease in K_{CSH} (75.3 M^{-1} for aniline to 32.6 M^{-1} for *o*-aminophenol), and unlike in the cases of toluidine and methoxyaniline, K_{CSH} values of *m*- and *p*-aminophenol (44.8 and 39.7 M^{-1} , respectively) were also smaller than that of aniline. In addition, the decrease in k_c'/k_o' value (22.3 for aniline to 16.4 for *o*-aminophenol) was not as conspicuous as in the cases of methyl and methoxy groups. This may be because the ortho hydroxyl group was dehydrated in the mobile phase by the association between the amino group and 18-crown-6. Consequently, the difference in K_{CSH} and k_c'/k_o' values between *o*-aminophenol and the other isomers became smaller than in the cases of toluidine and methoxyaniline. As shown in Figure 7A, the elution order between ortho and meta isomers was reversed and the meta isomer was easily separated by addition of a small amount of 18-crown-6, while the resolution of the ortho and para isomers was not improved markedly even by addition of 20 mM 18-crown-6.

In IPRPLC, the steric effect of the ortho substituent group was not observed. No clear difference was observed in K_{ISH} and k_i'/k_o' values among the three isomers of each of the following: toluidine, methoxyaniline, and aminophenol. Although the k_i'/k_o' values of *o*-toluidine and *o*-methoxyaniline were a little smaller than those of meta and para isomers and the K_{ISH} value of *o*-aminophenol was a little smaller than the values of meta and para isomers, the K_{ISH} values of *o*-toluidine and *o*-methoxyaniline were comparable to those of other isomers and the k_i'/k_o' value of *o*-aminophenol was a little larger than the case of other isomers. Consequently, the

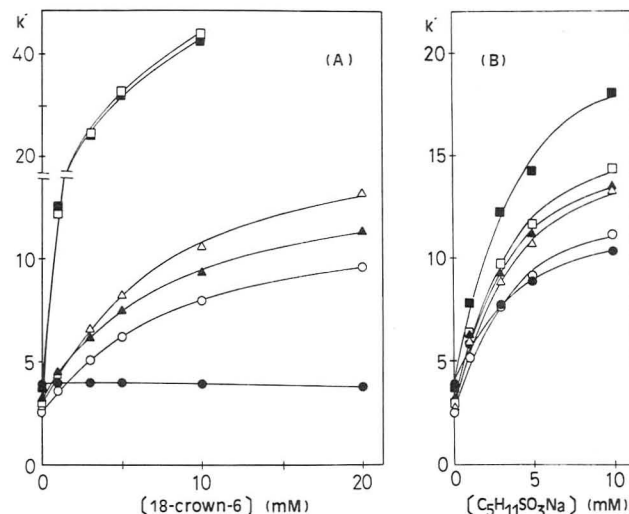


Figure 8. Dependence of the capacity factors of dimethylaniline (DMA) isomers on the concentration of 18-crown-6 (A) and pentanesulfonate (B): (□) 3,4-DMA; (■) 3,5-DMA; (○) 2,3-DMA; (△) 2,4-DMA; (▲) 2,5-DMA; (●) 2,6-DMA. For HPLC conditions, see Table I.

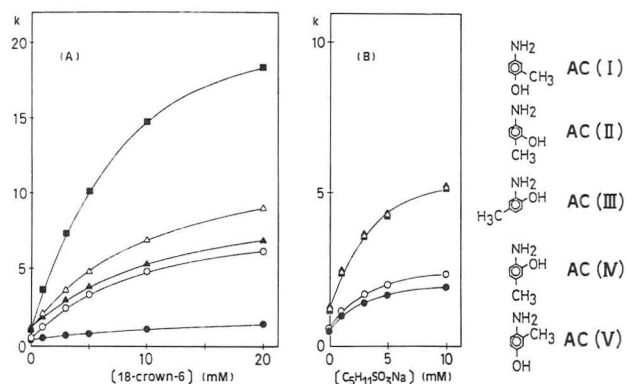


Figure 9. Dependence of the capacity factors of aminocresol (AC) isomers on the concentration of 18-crown-6 (A) and pentanesulfonate (B): (○) AC I; (■) AC II; (▲) AC III; (△) AC IV; (●) AC V. For HPLC conditions, see Table I.

capacity factors of three isomers of these amines increased with the concentration of pentanesulfonate to almost the same extent, and therefore, the elution order did not change as shown in Figures 5B, 6B, and 7B.

It is interesting to note that k_c'/k_o' values of the para isomers of toluidine and methoxyaniline were about 1.3 times larger than those of meta isomers, while k_i'/k_o' values of the para isomers were almost equal to those of the meta isomers. This result indicates that the present method is more effective for separation of meta and para isomers than IPRPLC.

Retention Enhancement of Disubstituted Anilines. Figures 8 and 9 show the dependence of the capacity factors of dimethylaniline (DMA) isomers and aminocresol (AC)

Table III. Pertinent Values of Parameters in Equations 4–7 for Disubstituted Anilines

	CERPLC					IPRPLC			
	$K_{CSH} \text{ M}^{-1}$	k_o'	k_c'	k_c'/k_o'	$k_c'/k_o'_{(calcd)}^a$	$K_{ISH}, \text{ M}^{-1}$	k_o'	k_i'	k_i'/k_o'
3,4-DMA	97.0	3.26	103	31.6	33.3	116	3.26	29.0	8.90
3,5-DMA	98.2	3.98	98.4	24.7	26.3	105	4.09	37.8	9.24
2,3-DMA	50.5	2.63	23.0	8.75	8.21	115	2.75	22.4	8.15
2,4-DMA	49.8	3.02	32.3	10.7	10.4	103	3.15	28.1	8.92
2,5-DMA	50.1	3.33	26.9	8.08	8.21	112	3.46	27.5	7.95
2,6-DMA		(very small change in capacity factor)				101	4.05	20.5	5.06
AC I	48.1	0.53	16.2	30.6	26.6	144	0.59	4.20	7.12
AC II	57.4	1.16	45.3	39.1	37.7	115	1.21	10.5	8.68
AC III	36.1	1.18	20.4	17.3	17.8	122	1.27	10.3	8.11
AC IV	37.8	1.15	26.7	23.2	22.6	123	1.23	10.0	8.13
AC V	16.6	0.43	6.45	15.0	8.32	164	0.50	3.26	6.52

^a Calculated from eq 12.

^a Calculated from eq 12.

isomers upon the concentrations of 18-crown-6 and pentanesulfonate. Figure 9 also shows the structures and abbreviations of AC isomers. The chromatographic conditions are the same as those in Figures 5–7. The preliminary investigation of k' vs. pH profiles (HPLC condition A in Table I) indicated that all of these amines except for 2,6-DMA were protonated completely under the mobile phase conditions employed, and more than 90% of 2,6-DMA should be protonated, because its pK_a value evaluated from the pH profile (22) was 3.66. The data shown in Figures 8 and 9 were fitted to eq 4 and 6 by a nonlinear least-squares method and pertinent values for the parameters were evaluated. The results are shown in Table III. The k_c' and k_i' values were calculated from eq 5 and 7, respectively. The curves in Figures 8 and 9 are those best fitted thereby, indicating satisfactory agreement with the experimental values. Six isomers of dimethylaniline showed almost the same K_{ISH} values, and these values were close to the value of aniline (Table II). The K_{ISH} values of five aminocresol isomers were a little scattered, and no clear dependence on the position and the functionality of the substituent was observed. Furthermore, the k_i'/k_o' values of dimethylaniline and aminocresol isomers were also close to each other except for 2,6-DMA.

On the other hand, the significant effect of the substituent group(s) was observed upon the retention behavior of disubstituted anilines in CERPLC. The results are well-correlated with those of the corresponding monosubstituted anilines. The K_{CSH} and k_c'/k_o' values of 2,3-, 2,4-, and 2,5-DMA and AC III, IV, and V were smaller than those of 3,4- and 3,5-DMA and AC I and II, respectively. The k_c'/k_o' value of AC V, which has a methyl group at the ortho position, was smaller than those of AC III and IV, both having a hydroxyl group at the ortho position. These results coincide well with the results of toluidine and aminophenol isomers. The k_c'/k_o' values of disubstituted anilines having a methyl group at the para position were larger than those of the corresponding *m*-methyl substituted anilines (i.e. 3,4-DMA > 3,5-DMA; 2,4-DMA > 2,3- or 2,5-DMA; AC II > AC I; AC IV > AC III). This fact is agreeable to the above-mentioned relation between *p*- and *m*-toluidines. The K_{CSH} values of five aminocresol isomers were all smaller than the value of aniline, which corresponds to the fact that the K_{CSH} values of three aminophenol isomers were smaller than the value of aniline.

There is a significant difference in the retention behavior of 2,6-DMA between CERPLC and IPRPLC. Figure 8B shows that the capacity factor of 2,6-DMA was enhanced by addition of pentanesulfonate, even though the degree of the enhancement was lower than those of other isomers. Since the K_{ISH} value of 2,6-DMA was almost the same as those of other isomers (see Table III), the weak retention enhancement can be ascribed to its small k_i'/k_o' value. On the other hand, two methyl groups of 2,6-DMA exert significant steric hin-

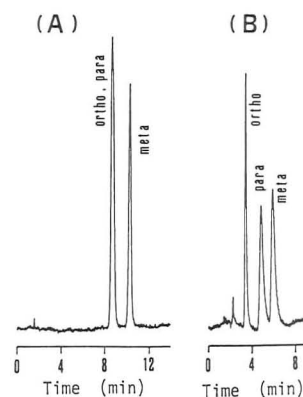


Figure 10. Separation profiles of methoxyaniline isomers in IPRPLC (A) and CERPLC (B). For HPLC conditions, see Table I.

drance in complex formation with 18-crown-6 (21). Therefore the retention enhancement effect was weakened and balanced to the before-mentioned competition effect, resulting in no apparent change in capacity factor.

In order to evaluate the effect of substituent groups on the retention enhancement, it is assumed that the increment of the log k' value ascribable to each substituent group is an additive property. Then

$$\log k_o^{XY} - \log k_o^A = (\log k_o^X - \log k_o^A) + (\log k_o^Y - \log k_o^A) \quad (10)$$

and

$$\log k_c^{XY} - \log k_c^A = (\log k_c^X - \log k_c^A) + (\log k_c^Y - \log k_c^A) \quad (11)$$

where k^{XY} , k^X , k^Y , and k^A represent the capacity factor of *X,Y*-disubstituted aniline, *X*-substituted aniline, *Y*-substituted aniline, and aniline itself, respectively. From eq 10 and 11

$$k_c^{XY}/k_o^{XY} = (k_c^X/k_o^X)(k_c^Y/k_o^Y)/(k_c^A/k_o^A) \quad (12)$$

The k_c'/k_o' values of disubstituted anilines calculated from eq 12, using k_c'/k_o' values in Table II, are also included in Table III. The good agreement between observed and calculated k_c'/k_o' values except for AC V lends the support for the additivity of the contribution of substituent groups to log k' values, although further modification of the equation is, of course, necessary for the accurate retention prediction.

Separation of Positional Isomers of Substituted Anilines. Based on the structure-recognizing ability of crown ether, CERPLC can afford more effective resolution of positional isomers of substituted anilines than the conventional ion-pair chromatography. Figures 10 and 11 show the chromatograms of methoxyaniline isomers and aminocresol isomers, respectively. When the mobile phase ($H_2O/MeOH =$

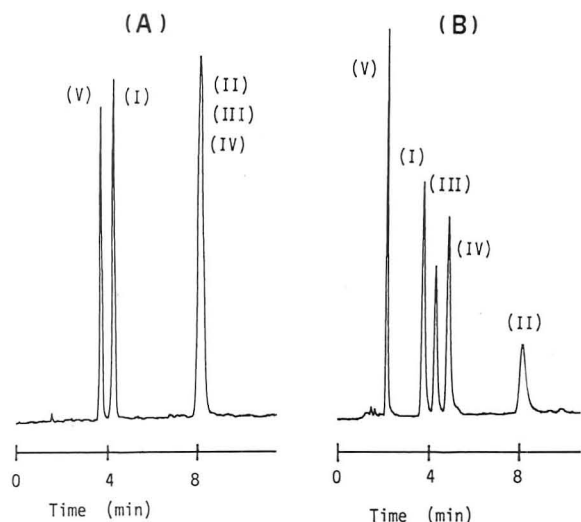


Figure 11. Separation profiles of aminocresol isomers in IPRPLC (A) and CERPLC (B). For HPLC conditions, see Table I.

8/2 (v/v), pH 2.5) contained neither sulfonate nor 18-crown-6, the mutual separations among methoxyaniline isomers, between AC I and V, and among AC II, III, and IV were incomplete. By the addition of 10 mM of pentanesulfonate into the mobile phase, *m*-methoxyaniline was resolved from the other isomers, and AC I and V were separated, whereas the peaks of *o*- and *p*-methoxyanilines and of AC II, III, and IV were not resolved (Figures 10A and 11A). However, addition of 1 mM 18-crown-6 into the mobile phase instead of pentanesulfonate (Figure 10B) resulted in the complete separation of methoxyaniline isomers in a shorter period of time than the result shown in Figure 10A, and addition of 2 mM 18-crown-6 (Figure 11B) resolved five aminocresol isomers in almost the same period of time as shown in Figure 11A.

As for diamino compounds, we reported previously that 24- and 27-membered crown ethers fit *o*-phenylenediamine and 2,3-diaminonaphthalene rather than *m*- and *p*-phenylenedi-

amine and 1,5-diaminonaphthalene, suggesting that two adjacent amino groups were simultaneously anchored to one large cavity, while dibenzo-30-crown-10 fit snugly to 1,8-diaminonaphthalene rather than *o*-diamine compounds (6). The present method can afford structure-recognizing resolution of amino compounds, and the combined use of crown ether with an ion-pair agent (5) provides wider selectivity in controlling retention and separation in reversed-phase HPLC.

LITERATURE CITED

- (1) Karger, B. L.; LePage, J. N.; Tanaka, N. In *High-Performance Liquid Chromatography Advances and Perspectives*; Horvath, C., Ed.; Academic: New York, 1980; Vol. 1, Chapter 3.
- (2) Nakagawa, T.; Mizunuma, H.; Shibukawa, A.; Uno, T. *J. Chromatogr.* **1981**, *211*, 1.
- (3) Nakagawa, T.; Shibukawa, A.; Uno, T. *J. Chromatogr.* **1982**, *239*, 695.
- (4) Nakagawa, T.; Shibukawa, A.; Uno, T. *J. Chromatogr.* **1983**, *254*, 27.
- (5) Nakagawa, T.; Shibukawa, A.; Murata, H. *J. Chromatogr.* **1983**, *280*, 31.
- (6) Nakagawa, T.; Murata, H.; Shibukawa, A.; Murakami, K.; Tanaka, H. *J. Chromatogr.* **1985**, *330*, 43.
- (7) Nakagawa, T.; Shibukawa, A.; Kaihara, A.; Itamochi, T.; Tanaka, H. *J. Chromatogr.* **1986**, *353*, 399.
- (8) Nakagawa, T.; Shibukawa, A.; Kaihara, A.; Tanaka, H. *Nippon Kagaku Kaishi* **1986**, 1002.
- (9) Iwagami, S.; Nakagawa, T. *J. Chromatogr.* **1986**, *369*, 49.
- (10) Wiechmann, M. *J. Chromatogr.* **1982**, *235*, 129.
- (11) Debowski, J.; Sybilska, D.; Jurczak, J. *Chromatographia* **1982**, *16*, 198.
- (12) Debowski, J.; Jurczak, J.; Sybilska, D. *J. Chromatogr.* **1983**, *282*, 83.
- (13) Sybilska, D.; Debowski, J.; Jurczak, J.; Zukowski, J. *J. Chromatogr.* **1984**, *286*, 163.
- (14) Zukowski, J.; Sybilska, D.; Jurczak, J. *Anal. Chem.* **1985**, *57*, 2215.
- (15) Debowski, J.; Sybilska, D. *J. Chromatogr.* **1986**, *353*, 409.
- (16) Gazdag, M.; Szepesi, G.; Huszar, L. *J. Chromatogr.* **1986**, *371*, 227.
- (17) Tanaka, M.; Miki, T.; Shono, T. *J. Chromatogr.* **1985**, *330*, 253.
- (18) Yamaoka, K.; Tanigawara, Y.; Nakagawa, T.; Uno, T. *J. Pharm. Dyn.* **1981**, *4*, 87.
- (19) Cram, D. J.; Cram, J. M. *Science* **1974**, *183*, 803.
- (20) Horvath, C.; Melander, W.; Molnar, I.; Molnar, P. *Anal. Chem.* **1977**, *49*, 2295.
- (21) Izatt, R. M.; Lamb, J. D.; Izatt, N. E.; Rossiter, B. E., Jr.; Chistensen, J. J.; Haymore, B. L. *J. Am. Chem. Soc.* **1979**, *101*, 6273.
- (22) Horvath, C.; Melander, W.; Molnar, I. *Anal. Chem.* **1977**, *49*, 142.

RECEIVED for review March 24, 1987. Accepted July 1, 1987.

Synthesis and Characterization of 2- μ m Wide-Pore Silica Microspheres as Column Packings for the Reversed-Phase Liquid Chromatography of Peptides and Proteins

Neil D. Danielson*¹ and J. J. Kirkland

E. I. du Pont de Nemours and Company, Central Research and Development Department, Experimental Station, Wilmington, Delaware 19898

Silica microspheres have been prepared with wide (200 Å) pores for the high-speed separation of biomacromolecules. These 1–2- μ m particles are synthesized in a narrow particle-size distribution at relatively high yield by significantly modifying the coacervation reaction used to produce Zorbax (Du Pont) chromatography packings. Reversed-phase columns prepared from 2- μ m particles exhibited >130 000 plates/m with good permeability and peak symmetry. Separations of multicomponent peptide and protein mixtures were performed in less than a minute with good recoveries of such solutes.

¹ Permanent address: Department of Chemistry, Miami University, Oxford, OH 45056.

The theoretical desirability of using very small particles (e.g., <3 μ m, sometimes called ultramicroparticles) for the rapid separation of macromolecules is well-known (1). Nevertheless, practical exploitation of this technology has been hampered by the availability of appropriate packing particles and columns. Although the use of short columns packed with 3- μ m spherical silica with 60-Å pores has been reported for separating small molecules (2, 3), similar or smaller-sized particles with wide pores for separating macromolecules were not studied. Pearson (4) has described recovery studies of proteins chromatographed on short columns, some of which were packed with 3- μ m particles. Unfortunately, details of the synthesis procedure for the silica particles or subsequent chromatographic characterization of the columns were not

given. Unger et al. studied the use of totally nonporous 1- μ m silica microspheres as column packings for the HPLC of proteins (5). More recently, the use of 2- μ m pellicular ion-exchange particles for separating protein mixtures in less than a minute has been reported (6). A disadvantage of columns packed with these nonporous particles is that the sample capacity will be limited, compared to totally porous particles of much higher surface area, assuming peak retention and resolution are not sacrificed.

Very small particles packed in short columns should permit the rapid separation of large molecules such as peptides and proteins, due to the greatly improved mass transfer of such solutes, compared to larger particles (1). A report describing the separation of proteins on very short (<1-cm) high-performance liquid chromatography (HPLC) columns suggested that improved resolution should be possible using such columns packed with smaller particles (7). Very fast separations of peptides, proteins, and other biomacromolecular compounds could be important in certain clinical analyses (8) and in applications requiring very rapid control of chemical or enzymatic reactions with such materials.

The objectives of this study were 2-fold. First, a procedure for the reproducible synthesis of 1–2- μ m wide-pore microspheres was needed. Modifications of a synthetic method for porous silica microspheres developed by Iler (9, 10) and Kirkland (11, 12) formed the basis for this part of the study. Second, information on the performance and applicability of such particles for separating biomolecules was desired.

EXPERIMENTAL SECTION

Chemicals. Reagent grade urea, formaldehyde (37%), and nitric acid were used for the synthesis of the silica microspheres. Nalcoag 1060 silica sol (50% SiO₂, 600 Å) was obtained from Nalco Chemical Co. (Naperville, IL). Particle silylation reactions were carried out with tri-*n*-butylchlorosilane (Petrarch, Bristol, PA) or trimethylchlorosilane (Aldrich, Milwaukee, WI) in dry toluene with pyridine (gold label, Aldrich) as the catalyst or acid acceptor (11). Mobile phases were prepared from HPLC grade methanol, acetonitrile, and water from Fisher Scientific (Philadelphia, PA). Trifluoroacetic acid (TFA) was purchased in 1-mL ampules from Pierce Chemicals (Rockford, IL). Peptides and protein samples were obtained primarily from the Sigma Chemical Co. (St. Louis, MO).

Apparatus. Synthesis of the silica packings were carried out with a Neslab (Portsmouth, NH) Ex-300 controlled temperature water bath, a Cole-Parmer (Chicago, IL) 9 × 9 in. magnetic stirrer, and a Beckman 43 pH meter (Fullerton, CA). HPLC experiments were performed on a Du Pont Series 8800 controller, a Du Pont 870 chromatographic pump, a Du Pont column compartment, a Kratos Spectroflow 783 detector (Kratos Analytical, Ramsey, NJ) equipped with a 2.5- μ L flow cell, and a Hewlett-Packard (Palo Alto, CA) 7131A recorder. An injector bypass (13) was installed in the column oven to minimize pressure pulsation during sample injection. All capillary tubing between the injector-column and column-detector was 0.007 i.d. and installed with minimum length to minimize possible extracolumn band-broadening effects. The injector was a Rheodyne (Cotati, CA) Model 7410 equipped with a 1- μ L loop and a Model 7012 loop-filler port. Data were collected on-line and analyzed with a Hewlett-Packard 3357 Laboratory Automation System (LAS).

PROCEDURES

Synthesis of Silica Ultramicrospheres. The reaction used to prepare the particles in this study was a variation of a previously reported procedure (12). Briefly, silica sol of the appropriate diameter is coacervated into spheres by a urea-formaldehyde polymerization process. The polymer then is burned out of the particles, and the resultant cavities between the silica sol particles form the pores of the silica microspheres. Next, these particles are sintered at high temperature for strengthening. The surface of the particles then is fully hydroxylated to permit the desired silanization reaction to

be performed.

Two-micrometer silica microspheres were prepared as follows. Into a 2-L Nalgene beaker containing 1125 mL of distilled water were added 27.5 mL of silica sol and 10.15 g of urea. After the pH of the solution was adjusted to 0.50 with 5.3 N nitric acid, the coacervation reaction was initiated at a temperature of 25 °C by pipetting 12.6 mL of formaldehyde into the stirred solution. The solution was allowed to stir at medium speed for 10–15 min until it developed a milky appearance. The solution was then filtered through flasks fitted with a 1- μ m porosity glass filter and a Gelman 0.3- μ m glass filter, sandwiched in this order. The resultant particles were dried at 110 °C under vacuum overnight. The polymer was burned out of the particles at 540 °C in air for at least 4 h. The particles then were sintered at 850 °C for 3 h to increase their mechanical strength. Finally, the HF hydrolysis procedure described by Köhler and Kirkland for PSM-300 (14) was used to ensure that the surface of the microspheres was fully hydroxylated. Twenty- and forty-gram batches of silica microspheres were prepared with this procedure with a yield of over 85%, based on initial silica sol weight.

Silanization of Silica. To prepare TMS-end-capped C₄ silica, a reflux apparatus was equipped with a 250-mL round-bottom flask and a 30 × 5 cm drying column filled with type 4A spherical molecular sieve. Vacuum was applied to the apparatus, and the glassware was heated with a propane torch to eliminate water. The vacuum was replaced with a dry nitrogen purge, and 8 g of silica was added to the round-bottom flask. Under the nitrogen atmosphere, 60 mL of toluene was percolated through the molecular sieve column into the flask by nitrogen pressure. To this solvent was added 5.6 mL of tri-*n*-butylchlorosilane and 2.5 mL of pyridine. The resultant slurry was refluxed for 72 h at 110 °C under a slow nitrogen purge. After cooling, the slurry was filtered and thoroughly washed with 300 mL each of toluene, methylene chloride, methanol, and acetone. The silica was placed in a vacuum oven and dried overnight at 110 °C.

The same experimental arrangement was used for the end-capping reaction. To 8.0 g of the C₄-modified silica was added 60 mL of dry toluene, 3.0 mL of trimethylchlorosilane (TMS), and 6 mL of pyridine. The mixture was refluxed at 110 °C for 72 h. The silica was washed as previously described and dried in a vacuum oven overnight at 110 °C.

Characterization of Silica Ultramicroparticles. Surface area measurements were carried out by the conventional BET method using a PDP 8M computer-controlled Digisorb 2500 and a manual 2100 surface area analyzer (Micromeritics, Norcross, GA). Pore-size measurements were performed by mercury intrusion with an Autopore 9200 porosimeter (Micromeritics, Norcross, GA). Particle-size distributions were measured with a Digital Particle Analysis System (Du Pont Engineering Physics Laboratory, Wilmington, DE). Elemental analyses were carried out by Microanalysis, Inc., Wilmington, DE.

Packing HPLC Columns. Fines and aggregates were removed from the silica ultramicroparticle preparations with an Andreasson sedimentation pipet (Fisher Scientific, Springfield, NJ). Approximately 6 g of silica was sonicated in acetone and added to the pipet to produce a total slurry of 520 mL. Generally, 40-mL fractions were taken every 5 min and the acetone was allowed to evaporate. After examination by light microscopy, appropriate fractions of the silica particles were then collected and dried under vacuum before use.

For the column packing process, a 50:50 acetone-pentane slurry containing 1.5 g of silica was sonicated and added to the packing reservoir arranged in the downward configuration as described in ref 1. A 1.5- μ m (nominal size) screen backed

Table I. Physical Characteristics of Silica Ultramicrospheres

parameter	sample designation				
	A	B	C	D	E
av particle diameter, μm	1.4	2.6	2.0	1.9	2.0
pore diameter, Å (Hg)	190	200	180	190	175
surface area, m^2/g	58	60	75	64	76
pore volume, mL/g	0.39	0.33	0.39	0.39	0.39
carbon loading, %	1.78	1.94	1.96	1.71	2.27

up by a piece of no. 401 cut-to-size filter-paper disk (Schleicher and Schuell, Boston, MA) was used to maintain the silica particles in the column. First, the column blank (3.3×0.62 cm) was filled with Freon 113 (Du Pont). The silica particles then were suddenly forced into the column at 7500 psi with hexane as the loading or "pusher" solvent (1). The column packing was consolidated by repetitive pressurizations at 5000 psi with methanol until a constant flow rate was reached. The pressure was allowed to bleed off the outlet, and the column was disconnected from the packer. Excess silica particles were carefully scraped off the top face of the column blank, and a compression fitting containing a $1.5\text{-}\mu\text{m}$ stainless-steel screen (but no filter paper) was attached to the column inlet. The use of low-surface-area screens on both ends of the column was deemed especially important because higher-surface-area frits have been reported to adsorb proteins (15).

Protein Recovery. Recovery of proteins from reversed-phase columns of the C_4 -modified silica ultramicroparticles was determined by ratioing the peak area found for the injected protein with and without the column. With the column, a gradient/elution program of 1 min from 70:30% H_2O -acetonitrile (both with 0.1% TFA) to 100% acetonitrile (with 0.1% TFA) was carried out. The column then was replaced with a Teflon capillary tube ($164\text{ cm} \times 0.8\text{ mm}$) whose volume corresponded roughly with the dead volume of the chromatographic column. The mobile phase of 100% acetonitrile with 0.1% TFA was used to solubilize the protein and ensure no adsorption of the protein to the wall of the Teflon capillary by hydrophobic effects.

RESULTS AND DISCUSSION

Physical Characteristics of Silica Microspheres. The spherical particle configuration and relatively narrow particle size distribution of the $2\text{-}\mu\text{m}$ microspheres of Table I (sample B) is illustrated by the scanning electron-micrograph of Figure 1A. An electromicrograph of one of the particles at higher magnification is shown in Figure 1B. The surface roughness is typical of particles made by this process from larger silica sols.

A quantitative particle-size distribution plot for sample C of Table I is shown in Figure 2. The average particle size for this sample was $2.0 \pm 0.9\text{ }\mu\text{m}$, and at least 75% of the particles were in a size range of $1.5\text{--}3.0\text{ }\mu\text{m}$.

Data on the characterization of a variety of silica samples with respect to size distribution, pore size, pore volume, and coverage with bonded C_4 groups are summarized in Table I. Batches of particles ranging from 1.4 to $2.6\text{ }\mu\text{m}$ (samples A and B) were prepared with slightly different reaction conditions. Samples C, D, and E were all prepared under identical conditions, as described in the Experimental Section; good reproducibility of the particles was obtained from batch to batch.

As noted in Table I, the nominal average pore size for all silica samples was about 200 Å , based on mercury intrusion measurements. Reasonable uniformity of the pores throughout the silica particles was indicated by these pore size distribution plots. The surface area values and pore volumes shown in Table I for the silica microspheres are typical of

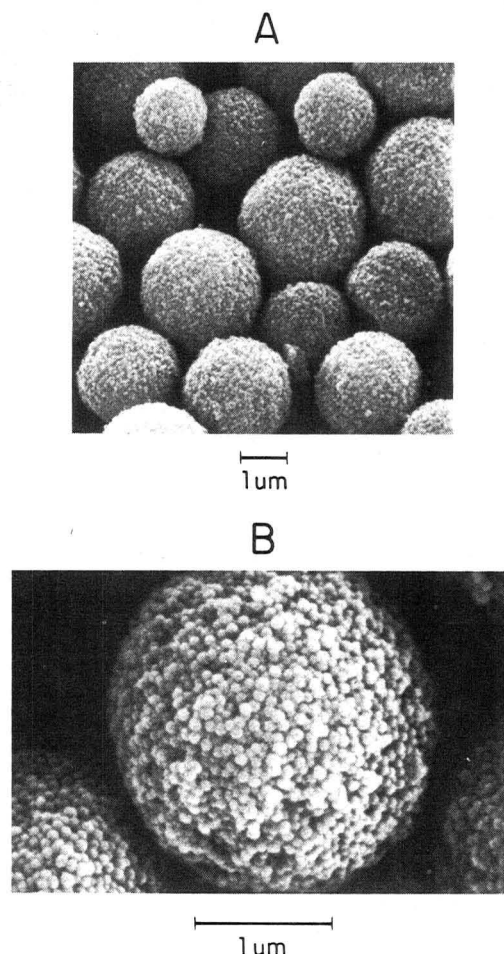


Figure 1. Scanning electron micrograph of silica ultramicrospheres (A). Scanning electron micrograph of single silica particle (B).

NO. PARTICLES/DIA.

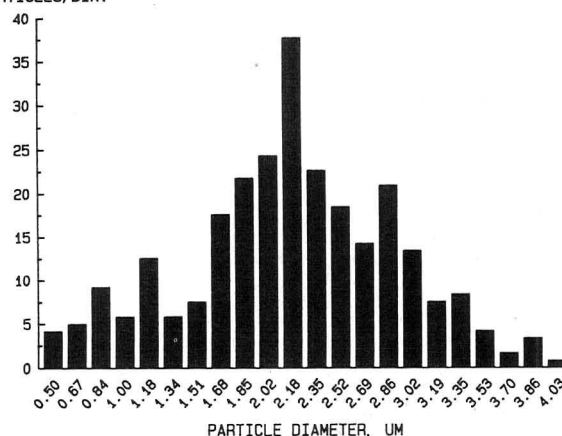


Figure 2. Particle size distribution of sample C. Average size = $2.04 \pm 0.91\text{ }\mu\text{m}$.

wide-pore silica particles (14).

Reversed-phase silica packings were prepared with tributylchlorosilane to create a C_4 -bonded phase. The percent C values for these silicas are somewhat lower than those reported previously for large-particle wide-pore silica (16), since the tributyl group is relatively bulky and, therefore, sterically hindered for reaction with the surface. This bonded-phase group was selected for application in separating peptides and proteins, since it exhibits the desired retention and good stability against degradation in the aggressive trifluoroacetic acid mobile phases of low pH that are widely used in the gradient elution separation of these compounds (17).

Chromatographic Testing. Using a test mixture of small solutes, we studied the efficiency of a $3.3 \times 0.62\text{ cm}$ column

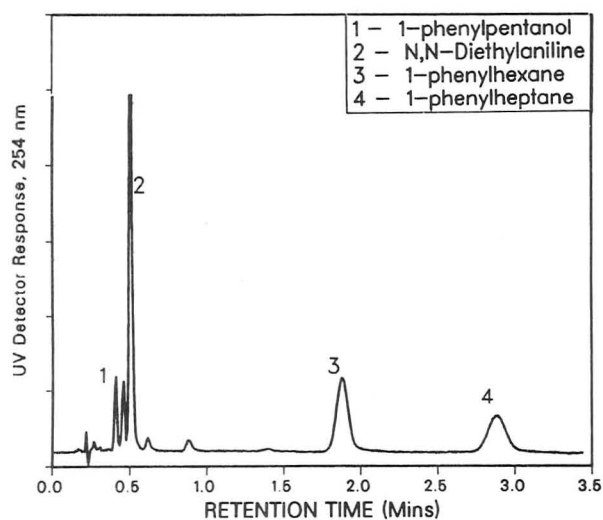


Figure 3. Separation of a test mixture composed of small organic solutes: column, 3.3×0.62 cm; C_4 -modified sample C; mobile phase, 60:40 methanol-water; flow rate, 2.75 mL/min; pressure, 160 bar; 35 °C.

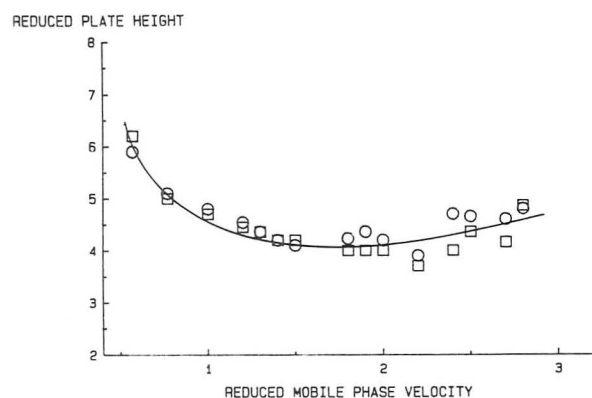


Figure 4. Reduced plate height plot for small molecules. Squares represent phenylhexane ($k' = 6.4$). Circles represent 1-phenylheptane ($k' = 10.1$). Conditions are the same as those in Figure 3.

packed with C_4 -modified silica. Figure 3 shows a representative chromatogram obtained at a flow rate near the HETP minimum for the column. The narrow, symmetrical peak for the basic solute, *N,N*-diethylaniline, is indicative that the silica support has been fully hydroxylated (14); few acidic silanols apparently remain on the support surface. The flow resistance factor (I), ϕ , was calculated to be 1253. This is a reasonable value, considering the very small particles used in the column.

Peak asymmetry values (I) for the 1-phenylhexane and 1-phenylheptane peaks in Figure 3 were satisfactory ($A_s = 1.1$), suggesting that columns prepared with these very small particles are well-packed. These two solutes also were used to generate the reduced plate height vs. the reduced velocity plots shown in Figure 4. To construct this plot, diffusion coefficients of 2.7×10^{-5} cm²/s for 1-phenylhexane and 1-phenylheptane were estimated by the Wilke-Chang equation (18). The plate number for the column in Figure 4 was about 2500 at a mobile phase flow rate of 0.75 mL/min, increases to a maximum of 4000 at 3.25 mL/min, and then decreases to about 3000 at 4 mL/min. The reduced plate height (h) minimum of about 3.5 occurred at the reduced velocity minimum, representing about 130 000 plates/m for this column. This h value compares favorably with the $h = 2-3$ value accepted for "good" HPLC columns made of larger (5- μ m) particles. The reduced-velocity minimum values of 1.5-2.3 observed for this column of ultramicroparticles is typical; a range between 1 and 10 is considered appropriate for most small-particle columns.

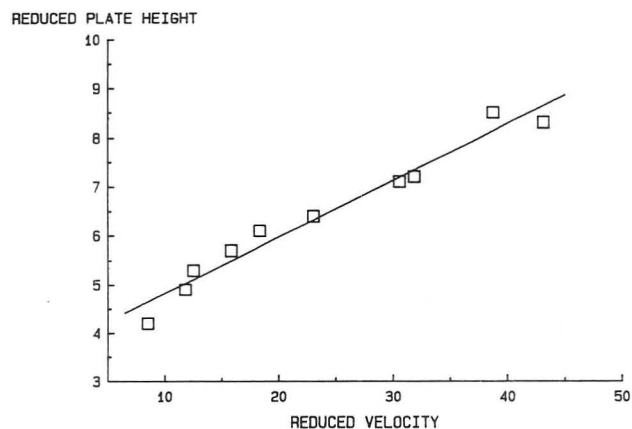


Figure 5. Reduced plate-height plot for insulin ($k' = 9.8$): column, same as for Figure 3; mobile phase, 30:70 acetonitrile-water with 0.1% trifluoroacetic acid (TFA); 35 °C; detection, 220 nm.

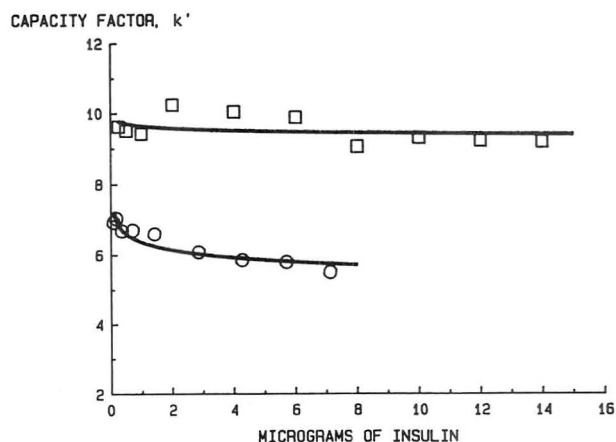


Figure 6. Sample loading of different-sized columns: insulin as the solute; (squares) 33×6.2 mm column, flow rate 3 mL/min; (circles) 33×4.6 mm column, flow rate 1 mL/min; mobile phase, 30:70 acetonitrile-water with 0.1% TFA; 35 °C; detection, 220 nm.

Performance data for the column were fitted to the Knox equation (1), $h = Av^{0.33} + B/v + Cv$. As a result, coefficients $A = 1.17$, $B = 2.71$, and $C = 0.69$ were calculated. For a "good" column, the values $A = 1.0$, $B = 2.0$, and $C = 0.1$ are considered typical of small-particle columns (19). The A and B terms for the ultramicroparticle column are quite comparable; however, the C term is somewhat larger than usual. Larger C terms also were seen by Unger et al. for a column of 1.8- μ m alumina (19), suggesting basic differences in mass transfer for very small particles.

A corresponding reduced plate height vs. mobile phase velocity study was carried out with the protein insulin (molecular weight 6000), as a test solute. To prepare the plot in Figure 5, we calculated the diffusion constant for insulin as 1.5×10^{-6} cm²/s, using the relationship proposed by Staalius et al. (20). The h values in Figure 5 decrease linearly from about 8 to 4 over a reduced velocity range of 50-10. These h values correspond to a plate count change from about 2000 to 3900. Compared to the plot for a small molecule in Figure 4, the higher level of reduced velocity in Figure 5 was anticipated, since the diffusion coefficient of insulin is about a factor of 20 less than that for small molecules. The lower diffusion coefficient for insulin tends to cause the C term of the plate height equation to dominate. Influence of the B term is not observed at the higher flow rates (1-5 mL/min) studied; lower flow rates were not investigated since the main interest in this study was the fast separation of macromolecules.

The effect of sample loading has been studied on both 3.3×0.62 cm and 3.3×0.46 cm columns using insulin as a test compound. The expected loading advantage of using wider

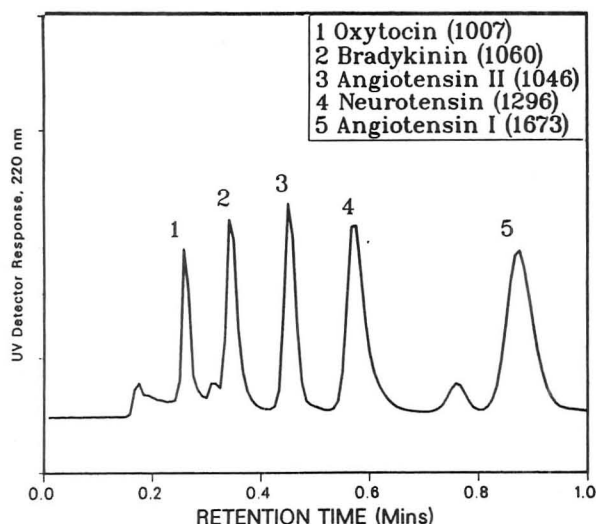


Figure 7. Separation of a peptide mixture: column, same as for Figure 3; mobile phase, 24:76 acetonitrile–water with 0.1% trifluoroacetic acid; flow rate, 4.0 mL/min; pressure, 370 bar; detection, 220 nm; molecular weights as shown.

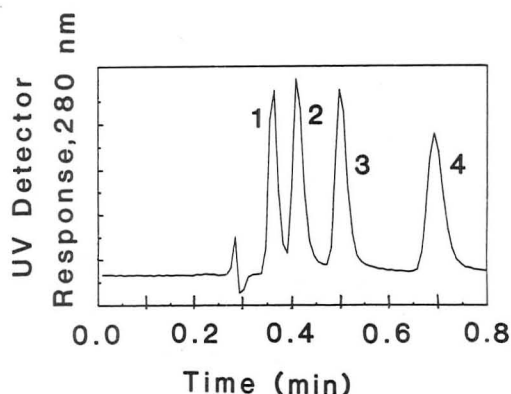


Figure 8. Separation of pentapeptides. Peaks: (1) met-enkephalin, (2) leu-enkephalin, (3) ala-met-enkephalin, (4) ala-leu-enkephalin; approximately 0.67 μ g of each solute injected; mobile phase, 78% 0.2 M NaH_2PO_4 (pH 6)/22% acetonitrile; flow rate, 3 mL/min; pressure, 247 bar; 35 $^\circ\text{C}$; detection, 280 nm.

diameter columns is shown in Figure 6. In these plots of capacity factor k' vs. micrograms of insulin injected, the k' value remains relatively constant for the 0.62 cm diameter column, up to at least 16 μ g of sample. On the other hand, k' values begin to decrease significantly at about 8 μ g for the narrower column. Under the isocratic conditions used, sample loading for this solute was determined to be about 20 μ g/g silica before a 10% decrease in k' is detected. However, larger quantities of proteins (50–100 μ g of each protein) can be injected without a significant degradation in resolution. Still another advantage of using larger column diameters for the very short columns required in this work is that larger peak volumes result. This reduces potential problems of extracolumn effects that could deleteriously broaden the very sharp solute peaks associated with columns of very small particles.

Several examples of peptide and protein reversed-phase separations have been obtained with the C_4 -modified ultramicrospheres. Figure 7 shows the separation of five peptide standards, all containing about 10–15 amino acid groups. Using an isocratic mobile phase and flow rate of 4 mL/min, we separated all the peptides in less than 1 min with base-line resolution. (Other peaks in this chromatogram presumably represent unknown impurities that were present in the peptide standards.) The separation of four enkephalin peptides was accomplished in about 40 s with an isocratic mobile phase, as shown in Figure 8. These pentapeptides vary in structure with respect to only one amino acid group. The apparent

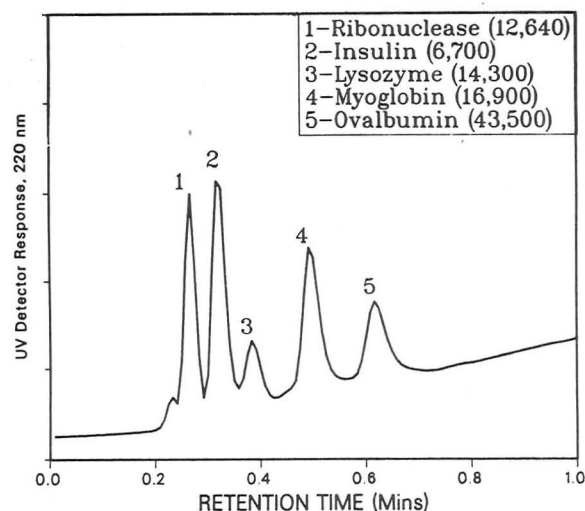


Figure 9. Separation of a five-component protein mixture: column, same as in Figure 3; mobile phase, 25:75 acetonitrile–water to acetonitrile (both with 0.1% trifluoroacetic acid); gradient, 0.3 min; flow rate, 3.3 mL/min; pressure, 340 bar; sample, 2 μ g of each protein, except 0.6 μ g of lysozyme; 35 $^\circ\text{C}$; detection, 220 nm; molecular weight of proteins as shown.

distortion of some peaks in these separations is due to a relatively small number of points taken by the analog-to-digital converter over such a short time period.

As illustrated in Figure 9, a standard protein mixture of ribonuclease, insulin, lysozyme, myoglobin, and ovalbumin was separated in about 50 s with the column of wide-pore ultramicrospheres, using a 0.3-min gradient that was basically in a step-gradient form. Injection of the sample was delayed to take into account the dead volume of the gradient system. We found that this separation was not possible under isocratic conditions. Additional resolution of the components of this mixture was obtained by increasing the gradient time to 2.5 min.

Studies were carried out on the recovery of proteins from the 3.3×0.62 cm columns of C_4 -modified ultramicrospheres. Other work has suggested that higher recoveries of proteins are found for shorter columns of reversed-phase packings operated at higher mobile phase velocities. We used the simple method of comparing peak areas for the protein with and without the column, where an equivalent-volume capillary was substituted. Under these conditions, recoveries of ribonuclease, insulin, lysozyme and myoglobin were 107, 95, 114, and 99%, respectively. While this method of measuring recoveries is subject to some precision error (21), these data clearly demonstrate excellent recovery of these four proteins. Recovery of ovalbumin was only 62%; however, it is well-known that this protein is very hydrophobic and high recoveries are quite difficult unless very short columns are used (4).

Finally, the separation of an eight-component protein mixture ranging in molecular weight from 6000 to 100 000 is shown in Figure 10. A 3-min gradient was required to separate the components of this mixture with almost base-line resolution. We found that the upper cutoff in the molecular weight of proteins permeating the pores of this column was about 200 000. For example, β -amylase (molecular weight 206 000) eluted at about 3 min under the conditions of Figure 10, while higher molecular weight proteins such as urease (molecular weight 480 000) eluted significantly earlier. This 200 000 molecular weight cutoff is reasonable, since for particles with 250-Å pores, the molecular weight permeation range for random coil proteins is about 2000–150 000.

As indicated in other studies (22), the lifetime of reversed-phase columns for peptides and proteins is grossly affected by the low pH (e.g., <2) caused by the 0.1% tri-

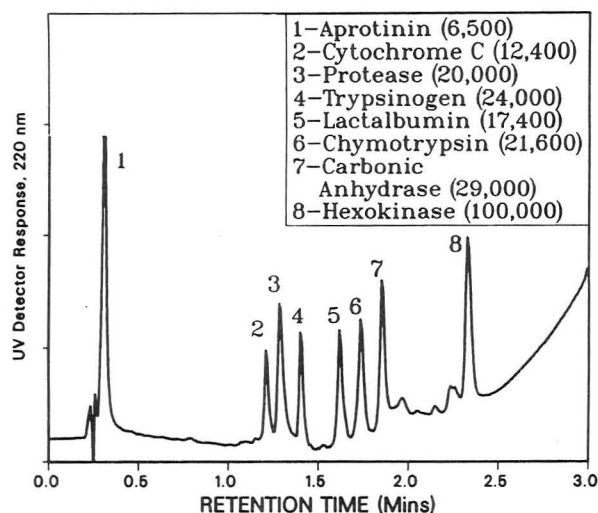


Figure 10. Separation of a eight-component protein mixture: column, same as in Figure 3; mobile phase, as in Figure 9; gradient time, 3.0 min; flow rate, 3.0 mL/min, sample, $\approx 1 \mu\text{g}$ of each protein; detection, 220 nm; pressure, 260 bar; 35 °C; molecular weight of proteins as shown.

fluoroacetic acid typically used in the mobile phase. We also found that, after several months of use, our reversed-phase columns exhibited a significant increase in insulin retention. The difference in k' data shown in Figure 6 was caused by the substantial difference in use with TFA containing mobile phases between the two columns. This observation suggests adsorption of the peptides and proteins on the silica support, caused by probable loss of bonded- C_4 groups on the surface. Research is currently in progress for improving the stability of reversed-phase silica HPLC packings for use with aggressive solvents (e.g., 0.1% trifluoroacetic acid) (23).

ACKNOWLEDGMENT

We gratefully acknowledge the experimental assistance of J. B. Marshall and the helpful discussions with J. L. Glajch. We thank E. E. Carroll for physical measurements on the silica particles.

Registry No. Nalcoag 1060, 7631-86-9; 1-phenylpentanol, 583-03-9; *N,N*-diethylaniline, 91-66-7; 1-phenylhexane, 1077-16-3; 1-phenylheptane, 1078-71-3; insulin, 9004-10-8; oxytocin, 50-56-6; bradykinin, 58-82-2; angiotensin II, 11128-99-7; neurotensin, 39379-15-2; angiotensin I, 9041-90-1; Met-enkephalin, 58569-55-4; Leu-enkephalin, 58822-25-6; Ala-Met-enkephalin, 61370-87-4; Ala-Leu-enkephalin, 64963-01-5; ribonuclease, 9001-99-4; lysozyme, 9001-63-2; aprotinin, 9087-70-1; cytochrome c, 9007-43-6; protease, 9001-92-7; trypsinogen, 9002-08-8; chymotrypsin, 9004-07-3; carbonic anhydrase, 9001-03-0; hexokinase, 9001-51-8.

LITERATURE CITED

- (1) Snyder, L. R.; Kirkland, J. J. *Introduction to Modern Liquid Chromatography*; Wiley: New York, 1979; Chapter 5.
- (2) Dong, M. W.; Gant, J. R. *LC-GC* 1984, 2, 194.
- (3) Stout, R. W.; DeStefano, J. J.; Snyder, L. R. *J. Chromatogr.* 1983, 261, 189.
- (4) Pearson, J. D. *Anal. Biochem.* 1986, 152, 189.
- (5) Unger, K. K.; Jilge, G.; Kinkel, J. N.; Hearn, M. T. W. *J. Chromatogr.* 1986, 359, 61.
- (6) Horvath, C., Separation Science and Biotechnology Seminar, Ft. Lauderdale, FL, Jan 21-23, 1987.
- (7) Moore, R. M.; Walters, R. R. *J. Chromatogr.* 1984, 317, 119.
- (8) Stevens, A.; Morrill, T.; Parlante, S. *Biochromatography* 1986, 1, 50.
- (9) Iler, R. K.; McQueston, H. J. U.S. Patent, 3 855 172.
- (10) Iler, R. K.; McQueston, H. J. U.S. Patent, 4 010 242.
- (11) Kirkland, J. J.; Dilks, C. H., Jr.; E. I. du Pont de Nemours & Co., Wilmington, DE, unpublished work, 1976.
- (12) Kirkland, J. J. *J. Chromatogr. Sci.* 1972, 10, 593.
- (13) DiCesare, J. L.; Dong, M. W.; Gant, J. R. *Chromatographia* 1982, 15, 595.
- (14) Köhler, J.; Kirkland, J. J. *J. Chromatogr.* 1987, 385, 125.
- (15) Sadek, P. C.; Carr, P. W.; Bowers, L. D.; Haddad, L. C. *Anal. Biochem.* 1985, 144, 128.
- (16) Pearson, J. D.; Regnier, F. E. *J. Liq. Chromatogr.* 1983, 6, 497.
- (17) Glajch, J. L.; E. I. du Pont de Nemours & Co., Wilmington, DE, personal communication, 1986.
- (18) Wilke, C. R.; Chang, P. *AIChE J.* 1955, 1, 264.
- (19) Unger, K. K.; Messer, W.; Krebs, K. F. *J. Chromatogr.* 1978, 149, 1.
- (20) Stadalius, M. A.; Gold, H. S.; Snyder, L. R. *J. Chromatogr.* 1985, 327, 27.
- (21) Xindu, G.; Carr, P. W. *J. Chromatogr.* 1983, 269, 96.
- (22) Glajch, J. L.; Kirkland, J. J.; Köhler, J. *J. Chromatogr.* 1987, 384, 81.
- (23) Danielson, N. D.; Glajch, J. L.; Kirkland, J. J.; E. I. du Pont de Nemours & Co., Wilmington, DE, unpublished work, 1986.

RECEIVED for review March 23, 1987. Accepted June 29, 1987. This work was presented at the 10th International Symposium on Liquid Chromatography, San Francisco, CA, May 19, 1986.

Detection Limits with Specified Assurance Probabilities

C. Andrew Clayton,* John W. Hines, and Phyllis D. Elkins

Research Triangle Institute, Research Triangle Park, North Carolina 27709

Traditional methods for determining detection limits are based on achieving protection against false positive conclusions. A preferred approach is to define detection limits so that protection against both false positives and false negatives is assured. This paper offers such a definition of detection limits and describes a theoretical basis for estimating them. The methodology is also appropriate for examining regulatory compliance. The article describes a two-phased experiment, using extractable analytes, that demonstrates the potential applicability of the methodology and validates it empirically. In the first phase, the methodology was employed to arrive at estimates of detection rates as a function of concentration level. Empirical estimates of detection rates were generated in the second phase and compared with those from the first phase: close agreement was found, thus demonstrating not only that the methodology is conceptually sound but also that its implementation in a research laboratory setting is practical.

Chemists for many years have acknowledged the importance of establishing limits of detection for analytical methods. However, the development of more sensitive analytical techniques and recent promulgation of statutory regulations dealing with human or environmental exposure to "low" level chemical health hazards (e.g., ref 1) have served to amplify the need for further examination of procedures used to establish such limits. Traditional techniques for determining detection limits have been concerned only with providing protection against type I errors, or false positive conclusions (i.e., reporting an analyte as present when it is not). They have not considered the corresponding need for similar protection against type II errors, or false negative assertions (i.e., reporting an analyte as not present when it is).

Such traditional techniques persist in many laboratories (2, 3, 4), despite the fact that several authors (e.g., ref 2, 5-12) have pointed out the inadequacy of traditional methods and

have advocated methods that afford adequate protection against both types of errors. For example, in discussing the approach adopted by the International Union of Pure and Applied Chemistry (IUPAC), Long and Winefordner (2) state: "When measurements are made for a sample, the x [concentration] values obtained should follow a normal distribution around a mean value. If a sample were measured to have a mean at the x_L value [the IUPAC detection limit], the distribution of these x values around x_L would...[be such that one-half] of the time the measurement would fall below the x_L value and could not be considered a true signal according to the IUPAC definition." In a similar vein, the *ASTM Standards on Precision and Bias for Various Applications* (10) states: "[If the]...true concentration is equal to the criterion of detection and if all analytical results below the criterion of detection were reported as such, then the probability of discerning the substance would be 0.5 or 50%.... Conversely, the probability of making a type II error and failing to discern the substance would also be 0.5." The literature thus acknowledges that traditional methods of determining detection limits afford protection against type II errors only at moderate levels (i.e., about 50%).

Attempts to redefine limits that have more realistic type II error rates, as we advocate, have generally suffered from one or more of the following deficiencies: (a) the influence of the calibration has been ignored altogether, (b) the measurement error variance has been assumed known (or a large-sample, highly precise estimate of it is assumed available), (c) a simple straight-line calibration with *known* model parameters (slope and intercept) has been assumed, and/or (d) mathematical or logical fallacies have occurred in the development of the detection limit estimators.

The notable exception is the methodology of Burrows (5), which is the methodology that we adopt and demonstrate.

The notion of specifying levels of protection against false positives and false negatives is embedded in statistical concepts of testing hypotheses, rather than in construction of interval estimates from specified type I error criteria. It is curious, therefore, that interval estimation seems to have been the focus of prior work (e.g., ref 6, 8, and 9). Burrows, on the other hand, has shown that detection limits can be defined as a natural consequence of the concept of testing the null hypothesis $X = 0$ vs. alternatives that $X > 0$, where X denotes the true, but unknown, concentration of an analyte in some medium. When specifying the type I error rate and corresponding threshold response value (i.e., that response value used as the decision point for asserting presence or absence of the analyte), the methodology, like traditional methods, considers the derived distribution that holds when the null hypothesis is true. For the linear calibration case in which measurement errors are assumed to follow a Gaussian (normal) distribution with variance independent of concentration level, this distribution is a t distribution with specified degrees of freedom. This assumes that the intercept and slope of the calibration line, and the measurement error variance, have to be estimated. Under the alternative hypothesis, $X > 0$, the appropriate derived distribution is a noncentral t distribution, and detection limits become functions of the corresponding noncentrality parameter. Other techniques involving similar assumptions, such as those cited previously, purport to provide fixed type I and type II error rates but avoid the use of noncentral t probabilities. As pointed out by Burrows, the derivation of such methods must include some type of logical or mathematical fallacy; otherwise such methods "would always be available to circumvent noncentral t distributions when considering power of t tests" (5).

Basic concepts and statistics needed to apply the advocated procedure are described in the next section (see ref 5 for

additional statistical details and a more general theoretical development of the method). Experiments that illustrate and validate the approach are then described in subsequent sections.

THEORY

The advocated method is based upon classical (Neyman-Pearson) statistical theory for hypothesis testing; it assumes that standard calibration procedures are used to provide estimates of all unknown parameters. Whereas calibrations of analyte responses vs. standard concentrations are usually performed for the purpose of *estimating analyte concentrations*, we here assume that *detecting analyte presence/absence* is a primary study goal or requirement. The former purpose implies that the range covered by the standards should encompass all of the concentrations occurring in matrices for which the analytical protocol and calibration results apply. Calibration designs directed solely toward the latter purpose, on the other hand, would cover a narrower range of concentrations—namely, that range over which detectability was considered uncertain. The definitions and methods of this paper presume that a calibration of this latter type will be (or has been) conducted. (This does not imply that an overall calibration design aimed at both purposes should not be considered; on the contrary, efficient use of resources dictates that such a composite calibration design be utilized whenever both of the aforementioned purposes are deemed relevant.)

This section consists of five subsections, entitled as follows: (1) calibration models; (2) estimation of the calibration model; (3) detection limits for linear calibration with known parameters; (4) detection limits for linear calibration with unknown parameters; (5) estimation of detection limits and detection rates for linear calibration. Subsections 1 and 2 contain much material that is available in standard texts; it is reproduced here (a) to document precisely the model and assumptions for which the methodology is applicable and (b) to introduce the mathematical notation needed in later subsections. Subsection 3 considers the concept of detectability within the context of a linear calibration model in which it is assumed (a) that the slope and intercept are known and (b) that the variation of measurement errors (presumed homogeneous over the range of concentrations of interest) is known. One or both of these assumptions is adopted either implicitly or explicitly in most traditional formulations of detection limit determination. A brief discussion of such techniques is included in this third subsection. In subsection 4 we use Burrows' methodology and formally define detection limits and detection rates for the case of a linear calibration model for which the model parameters and error variance are unknown and must be estimated. For this situation, we provide in subsection 5 a simple, four-step procedure for generating detection limit estimates. This final subsection should be useful even to readers unfamiliar with the mathematical statistics contained in the other parts of this section. We nevertheless encourage such readers to read the other subsections, because the concepts presented therein are important and can be understood even without a thorough understanding of the mathematical details.

Calibration Models. The general methodology (5) assumes a calibration model of the form

$$Y_x = \alpha + f(x, \beta) + \epsilon \quad (1)$$

where Y_x is the observed response when the analyte concentration $X = x$, α is the parameter representing the expected background value Y_0 , β is a parameter or vector of parameters, $f(x, \beta)$ is the monotonic function of x with the property $f(0, \beta) = 0$, and ϵ is the observational error for the particular determination, Y_x . Observational errors from different deter-

minations, at the same or different x values, are assumed (i) to be independent, (ii) to be normally distributed, (iii) to have zero mean, and (iv) to have constant variance, σ^2 , at least over the range of concentrations of interest. Clearly, there are cases where distributional assumptions ii and/or iv may not be satisfied; in many such cases, a transformation of observations (e.g., taking logarithms or square roots) can be applied so that these assumptions are tenable on the transformed scale.

The simplest example of model 1 is the straight-line calibration

$$Y_x = \alpha + \beta x + \epsilon \quad (2)$$

For this model, β represents the slope of the line; it can be assumed that $\beta > 0$ without loss of generality in subsequent developments.

Estimation of the Calibration Model. In most applications, the form of function f in model 1 is unknown and a reasonable approximating model form must be inferred from the available observations. Values of parameters α , β , and σ^2 are generally unknown also, and the validity of distributional assumptions concerning ϵ may be questionable. The calibration is carried out by fortifying n "uncontaminated" sample aliquots at m ($\leq n$) different standard concentrations x_1, x_2, \dots, x_m and making n_j determinations at x_j , where

$$n = \sum_{j=1}^m n_j$$

The resulting response measurements, y_i ($i = 1, 2, \dots, n$), are examined via plots against the x_j , and sample averages (\bar{y}_j) and standard deviations (s_j) of the observed responses for each concentration level x_j are computed. Statistical tests of the variance homogeneity assumption are performed; if necessary, transformations of observations are made to stabilize the variances. Various functional forms for f are then examined and their parameters estimated by linear or nonlinear least squares, as appropriate. Adequacy of the candidate models is evaluated and the simplest tenable model is selected. This may involve monotonic transformations of the concentration scale.

In many cases, the straight-line calibration model of eq 2 emerges as a reasonable choice. Henceforth, only this model is considered, although the basic methods of Burrows (5) apply more generally. If transformations are employed, then the symbols X , Y , x , and y used subsequently should be interpreted in terms of these transformed scales.

For model 2, the usual least-squares estimates are applicable

$$\text{estimate of } \alpha: \hat{\alpha} = \bar{y} - \hat{\beta}\bar{x} \quad (3)$$

$$\text{estimate of } \beta: \hat{\beta} = Q_{xy}/Q_{xx} \quad (4)$$

$$\text{estimate of } \sigma^2: \hat{\sigma}^2 = [Q_{yy} - Q_{xy}^2/Q_{xx}]/(n-2) \quad (5)$$

where \bar{y} and \bar{x} are the averages (over all n observations) of responses and of standard concentrations, respectively, and

$$Q_{xx} = \sum_{j=1}^m n_j(x_j - \bar{x})^2 \quad (6)$$

$$Q_{xy} = \sum_{j=1}^m n_j(x_j - \bar{x})(\bar{y}_j - \bar{y}) \quad (7)$$

$$Q_{yy} = \sum_{i=1}^n (y_i - \bar{y})^2 \quad (8)$$

If r subsequent determinations (e.g., $r = 1, 2$, or 3) are made from a "similar" source matrix having unknown concentration $X = x$, and if Y denotes the average of the r responses, then the random variable $(Y - \hat{\alpha} - \hat{\beta}x)$ is, under the stated as-

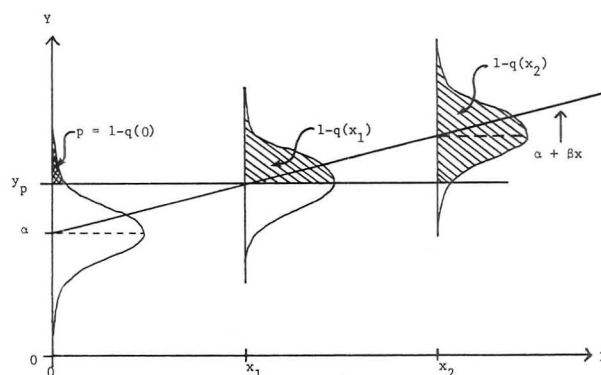


Figure 1. Illustration of how mean observed response, Y , varies with concentration x , for the linear calibration case. Threshold response is y_p . Shaded areas of the Y distributions indicate the detection probabilities.

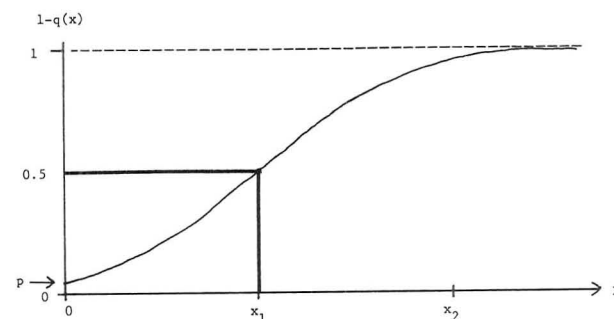


Figure 2. Illustration of how detection probability, $1 - q(x)$, varies with concentration x when using the rule "assert $X > 0$ whenever $Y > y_p$ ".

sumptions, distributed normally with mean zero and variance $\sigma^2 w_x^2$, where

$$w_x^2 \equiv \frac{1}{r} + \frac{1}{n} + \frac{(x - \bar{x})^2}{Q_{xx}}$$

Of particular interest is the case in which the true concentration is zero

$$w_0^2 \equiv \frac{1}{r} + \frac{1}{n} + \frac{\bar{x}^2}{Q_{xx}} \quad (9)$$

This is because detection limits, as subsequently defined, depend on w_0 . For this reason, it is important to consider how the calibration design (which includes location and range of standards, overall sample size n , relative spacings of the standards, and allocations n_j) affects w_0 , as well as how it affects the ability to determine an adequate model form f and how it affects the precision of detection limit estimates. Discussions of these design considerations are given by Clayton et al. (11) and by Clayton (12). It is apparent from eq 9, for instance, that w_0 can be decreased by increasing r or n or by altering the allocation or spacing of the x_j 's so that \bar{x}^2/Q_{xx} decreases.

Detection Limits for Linear Calibration with Known Parameters. To illustrate the basic concepts, we assume that model 2, with $\beta > 0$, is the appropriate calibration model and that α , β , and σ^2 are known. The following detection rule is adopted: "Assert $X > 0$ (i.e., the analyte is present) if $Y > y_p$ " where y_p is a threshold response value chosen so that the rate of false positives (in repeated applications of the rule to blank samples) is fixed at a desired probability level, p . With the stated distributional and model assumptions, this specified protection against type I errors is achieved by choosing

$$y_p = \alpha + \sigma z_p / \sqrt{r} \quad (10)$$

where z_p is the upper 100 p percentage point of the standard

normal distribution (see Figure 1).

When the unknown concentration $X = x$, the detection rate using this rule is given by the probability that the average of the r determinations, \bar{Y} , exceeds y_p

$$\Pr[Y > y_p | X = x] = 1 - q(x) \quad (11)$$

where

$$q(x) = \Pr \left[Z \leq z_p - \frac{\beta x}{\sigma/\sqrt{r}} \right] \quad (12)$$

Here, Z denotes a random variable following the standard normal distribution (mean zero, variance one). Note that $q(x)$, which is the rate of false negatives expected in repeated applications of the detection rule, depends on β/σ , r , and p , as well as x . Also note that the detection rate, $[1 - q(x)]$, is an increasing function of x . It is bounded below by the chosen type I error rate, $p \equiv 1 - q(0)$, and is bound above by 1.

Figure 2 shows this formulation of detection rate as a function of x . Figure 1 illustrates how the detection rule and the (known) calibration line combine to yield the curve of detection rates shown in Figure 2: $[1 - q(x)]$ in Figure 2 corresponds to the area of shaded regions shown in Figure 1. This curve is the power curve for the test of the null hypothesis that $X = 0$ vs. alternatives $X > 0$. It derives directly from classical Neyman-Pearson theory and hence for fixed p and all x , this detection rule yields the minimum false-negative rate, $q(x)$, among all such rules.

The same distributional assumptions are made in most traditional methods for determining detection limits. These traditional approaches use a concentration value like the x_1 value shown in Figures 1 and 2 as a "detection limit". Such a value is derived by inverse interpolation from y_p using the calibration line. In the United States Environmental Protection Agency's "Method Detection Limit" (MDL), for instance, $p = 0.01$ and $r = 1$ are specified, α and β of the calibration function are treated as known quantities, and $\text{MDL} = x_1$ (3). The measurement error variance σ^2 is estimated from several replicate observations at some "low" x value(s). It is clear from Figure 1, however, that if the true analyte concentration of a given source matrix is equal to $x = \text{MDL}$, then repeated applications of the detection rule will yield a false negative rate of 0.50 regardless of protection level p . This difficulty with traditional approaches has been noted previously (e.g., ref 5 and 8); nevertheless, these traditional procedures for determining "detection limits" have continued to receive widespread endorsement and use.

From Figures 1 and 2 and eq 12, it is apparent that the false negative rate can be computed for any $x > 0$. Alternatively, for any fixed rate of false negatives, q , the value $x_d = x_d(p, q)$ corresponding to the lowest concentration for which the rate of detection is at least $(1 - q)$ can be determined. Such a value is inseparable from the detection rule. We define $x_d(p, q)$ as the detection limit with assurance probability $(1 - q)$ for the rule "Assert $X > 0$ whenever $Y > y_p$," with y_p given by eq 10. Then the rate of detection is at least $(1 - q)$ for any analyte concentration exceeding $x_d(p, q)$. The detection limit, for fixed p , q , and r , and known model parameters, is determined from eq 12 to be

$$x_d(p, q) = (z_p + z_q)\sigma/\beta\sqrt{r} \quad (13)$$

For instance, if $r = 1$, $x_d(0.01, 0.01) = 4.652(\sigma/\beta)$ and $x_d(0.05, 0.05) = 3.290(\sigma/\beta)$.

In the case of known α , β , and σ , the detection limit defined by eq 13 is identical with that of Currie (8). When model parameters are unknown, as considered subsequently, this is not the case.

Detection Limits for Linear Calibration with Unknown Parameters. When model 2 applies (with $\beta > 0$), but

α , β , and σ^2 are unknown, eq 3, 4, and 5 are used to provide point estimates of these parameters. We proceed in the manner of the previous subsection by specifying a value of p and adopting the detection rule "Assert $X > 0$ whenever $Y > \hat{y}_p$." In this rule, the threshold level is a random variable since it depends on estimates of α and σ . The prescribed level of false positives in repeated applications of the detection rule is achieved by specifying

$$\hat{y}_p = \hat{\alpha} + w_0 \hat{\sigma} t_p \quad (14)$$

where w_0 is obtained from eq 9 and t_p is the upper 100 p percentage point of Student's t distribution with ν degrees of freedom. If eq 5 is used to estimate σ^2 , then $\nu = (n - 2)$.

Use of the detection rule corresponds to using a t statistic to test the hypothesis that $X = 0$ vs. alternatives $X > 0$. The detection rate, or power of the test, must be obtained from the appropriate noncentral t distribution, rather than the normal distribution used when the parameters were assumed known. With w_0 fixed by the calibration design, the detection rate $[1 - q(x)]$ at concentration x is shown in Appendix A to given by

$$1 - q(x) = \Pr[T(\Delta) > t_p] \quad (15)$$

where $T(\Delta)$ denotes a random variable having a noncentral t distribution with $\nu = n - 2$ degrees of freedom and noncentrality parameter Δ , where

$$\Delta = x\beta/w_0\sigma \quad (16)$$

Alternatively, we can specify $q(x) = q$ and solve eq 15 for $\Delta \equiv \Delta(p, q)$; this permits an analyte concentration $x_d(p, q)$ to be determined, via eq 16, that has specified detection rate $(1 - q)$. Thus

$$x_d(p, q) = w_0 \Delta(p, q) \sigma / \beta \quad (17)$$

is the detection limit associated with the detection rule that achieves assurance probability $(1 - q)$. Some values of $\Delta(p, q)$ for specified p , q , and ν are tabulated by Owen (13) and Burrows (5). A more useful listing for the present application is given here in Table I, which also gives values of t_p , for $p = 0.10, 0.05$, and 0.01 . Note that $x_d(p, q)$ is a parameter; it is not an estimate based on a particular set of observations. As the number of calibration observations, n , increases, the detection limit given by eq 17 approaches that given by eq 13. Apart from the unknown factor (σ/β) , which is analyte- and measurement-specific and which must be estimated, all of the components of eq 17 can be determined for any given calibration design by specifying values for p and q . In practice, it is useful to specify several values of $(1 - q)$ over the range $(p, 1)$ and determine the corresponding values of

$$x_d' = w_0 \Delta(p, q) \quad (18)$$

which are values of x_d expressed as multiples of (σ/β) instead of in original concentration units. Then detection curves such as those shown in Figure 3 can be produced. The particular curves in this figure, which show detection rates $(1 - q)$ as functions of $w_0 \Delta$, were developed for a four-point design with $n = 32$ ($n_1 = n_2 = n_3 = n_4 = 8$) and with standard concentrations $x_1 = 0.0$, $x_2 = 0.2$, $x_3 = 0.8$ and $x_4 = 1.0$ mg/kg.

Figure 3 illustrates an important feature of the advocated methods: such curves can be developed prior to experimentation and the impact of variations in calibration design, as well as various p , q , and r values, can be assessed as a part of the overall experimental plan. Moreover, when parameter estimates for the calibration line become available, threshold response values and estimated detection limits can be projected for calibration designs other than that actually used to obtain the estimates. This allows development of schemes for choosing subsequent calibration designs yielding detection

Table I. Values of t_p and $\Delta(p, q)$ for Selected Degrees of Freedom (ν), Selected Type I Error Rates (p), and Selected Type II Error Rates (q)

ν	t_p values for			$\Delta(0.10, q)$ for			$\Delta(0.05, q)$ for			$\Delta(0.01, q)$ for			
	p	$p = 0.05$	$p = 0.01$	q	$q = 0.05$	$q = 0.01$	q	$q = 0.10$	$q = 0.05$	$q = 0.01$	q	$q = 0.10$	$q = 0.05$
2	1.88562	2.91999	6.96456	3.39898	3.92472	4.93403	4.80923	5.51588	6.88233	10.73647	12.25884	15.21723	
3	1.63774	2.35336	4.54070	3.03785	3.48461	4.33247	3.92821	4.45636	5.46630	6.86300	7.70736	9.33750	
4	1.53321	2.13185	3.74695	2.89243	3.31060	4.10023	3.59994	4.06728	4.95463	5.64011	6.28442	7.52027	
5	1.47588	2.01505	3.36493	2.81469	3.21757	3.97935	3.43174	3.86994	4.69864	5.06784	5.62334	6.68320	
6	1.43976	1.94318	3.14267	2.76648	3.16187	3.90570	3.33014	3.75160	4.54674	4.74177	5.24890	6.21267	
7	1.41492	1.89458	2.99795	2.73371	3.12351	3.85625	3.26231	3.67302	4.44669	4.53276	5.01007	5.91457	
8	1.39682	1.85955	2.89646	2.71000	3.09586	3.82081	3.21389	3.61713	4.37598	4.38794	4.84524	5.71003	
9	1.38303	1.83311	2.82144	2.69206	3.07498	3.79418	3.17762	3.57539	4.32344	4.28190	4.72496	5.56152	
10	1.37218	1.81246	2.76377	2.67802	3.05868	3.77345	3.14944	3.54304	4.28290	4.20101	4.63345	5.44903	
11	1.36343	1.79588	2.71808	2.66673	3.04559	3.75686	3.12693	3.51725	4.25068	4.13732	4.56157	5.36100	
12	1.35622	1.78229	2.68100	2.65745	3.03486	3.74329	3.10853	3.49621	4.22447	4.08590	4.50366	5.29030	
13	1.35017	1.77093	2.65031	2.64970	3.02589	3.73198	3.09323	3.47873	4.20274	4.04354	4.45602	5.23231	
14	1.34503	1.76131	2.62450	2.64313	3.01830	3.72241	3.08029	3.46396	4.18443	4.00804	4.41616	5.18391	
15	1.34061	1.75305	2.60248	2.63748	3.01178	3.71420	3.06921	3.45133	4.16880	3.97787	4.38233	5.14291	
16	1.33676	1.74588	2.58349	2.63257	3.00612	3.70710	3.05961	3.44041	4.15529	3.95191	4.35325	5.10775	
17	1.33338	1.73961	2.56694	2.62827	3.00116	3.70088	3.05122	3.43087	4.14351	3.92934	4.32800	5.07727	
18	1.33039	1.73406	2.55238	2.62448	2.99679	3.69539	3.04383	3.42246	4.13315	3.90955	4.30587	5.05060	
19	1.32773	1.72913	2.53948	2.62110	2.99290	3.69052	3.03726	3.41499	4.12396	3.89204	4.28632	5.02707	
20	1.32534	1.72472	2.52798	2.61807	2.98941	3.68616	3.03139	3.40832	4.11575	3.87645	4.26892	5.00615	
21	1.32319	1.72074	2.51765	2.61534	2.98628	3.68224	3.02610	3.40233	4.10838	3.86248	4.25333	4.98744	
22	1.32124	1.71714	2.50833	2.61287	2.98344	3.67869	3.02133	3.39691	4.10173	3.84989	4.23930	4.97060	
23	1.31946	1.71387	2.49987	2.61063	2.98085	3.67546	3.01699	3.39198	4.09568	3.83848	4.22658	4.95537	
24	1.31784	1.71088	2.49216	2.60857	2.97849	3.67252	3.01303	3.38749	4.09018	3.82810	4.21502	4.94153	
25	1.31635	1.70814	2.48511	2.60669	2.97633	3.66982	3.00940	3.38338	4.08514	3.81861	4.20446	4.92889	
26	1.31497	1.70562	2.47863	2.60496	2.97434	3.66733	3.00606	3.37960	4.08051	3.80991	4.19477	4.91732	
27	1.31370	1.70329	2.47266	2.60336	2.97250	3.66504	3.00298	3.37611	4.07624	3.80189	4.18586	4.90667	
28	1.31253	1.70113	2.46714	2.60188	2.97080	3.66292	3.00013	3.37288	4.07229	3.79449	4.17762	4.89684	
29	1.31143	1.69913	2.46202	2.60050	2.96922	3.66095	2.99748	3.36989	4.06862	3.78762	4.17000	4.88775	
30	1.31042	1.69726	2.45726	2.59922	2.96775	3.65912	2.99502	3.36710	4.06522	3.78125	4.16291	4.87930	
32	1.30857	1.69389	2.44868	2.59690	2.96508	3.65581	2.99057	3.36207	4.05707	3.76976	4.15016	4.86411	
34	1.30695	1.69092	2.44115	2.59486	2.96275	3.65290	2.98667	3.35765	4.05368	3.75971	4.13900	4.85082	
36	1.30551	1.68830	2.43449	2.59305	2.96067	3.65032	2.98321	3.35374	4.04891	3.75082	4.12914	4.83911	
38	1.30423	1.68595	2.42857	2.59144	2.95882	3.64802	2.98013	3.35026	4.04466	3.74292	4.12038	4.82870	
40	1.30308	1.68385	2.42326	2.58999	2.95716	3.64596	2.97736	3.34713	4.04085	3.73585	4.11254	4.81939	
42	1.30204	1.68195	2.41847	2.58868	2.95567	3.64410	2.97487	3.34432	4.03742	3.72948	4.10548	4.81101	
44	1.30109	1.68023	2.41413	2.58750	2.95431	3.64242	2.97261	3.34176	4.03431	3.72371	4.09909	4.80344	
46	1.30023	1.67866	2.41019	2.58642	2.95307	3.64088	2.97055	3.33944	4.03148	3.71847	4.09328	4.79655	
48	1.29944	1.67722	2.40658	2.58543	2.95194	3.63947	2.96866	3.33731	4.02889	3.71368	4.08798	4.79027	
50	1.29871	1.67591	2.40327	2.58452	2.95090	3.63818	2.96693	3.33536	4.02651	3.70929	4.08312	4.78451	
55	1.29713	1.67303	2.39608	2.58254	2.94863	3.63537	2.96317	3.33111	4.02135	3.69975	4.07256	4.77203	
60	1.29582	1.67065	2.39012	2.58090	2.94675	3.63304	2.96034	3.32759	4.01707	3.69186	4.06383	4.76170	
65	1.29471	1.66864	2.38510	2.57951	2.94516	3.63108	2.95741	3.32462	4.01346	3.68521	4.05648	4.75302	
70	1.29376	1.66691	2.38081	2.57832	2.94380	3.62939	2.95516	3.32208	4.01038	3.67954	4.05021	4.74562	
80	1.29222	1.66412	2.37387	2.57640	2.94160	3.62667	2.95151	3.31797	4.00539	3.67037	4.04009	4.73367	
90	1.29103	1.66196	2.36850	2.57491	2.93990	3.62456	2.94869	3.31478	4.00153	3.66328	4.03226	4.72444	
100	1.29007	1.66023	2.36422	2.57372	2.93853	3.62288	2.94643	3.31224	3.99846	3.65764	4.02603	4.71710	
150	1.28722	1.65508	2.35146	2.57016	2.93447	3.61785	2.93970	3.30467	3.98923	3.64085	4.00751	4.69531	
200	1.28580	1.65251	2.34514	2.56839	2.93244	3.61535	2.93636	3.30090	3.98473	3.63254	3.99834	4.68453	

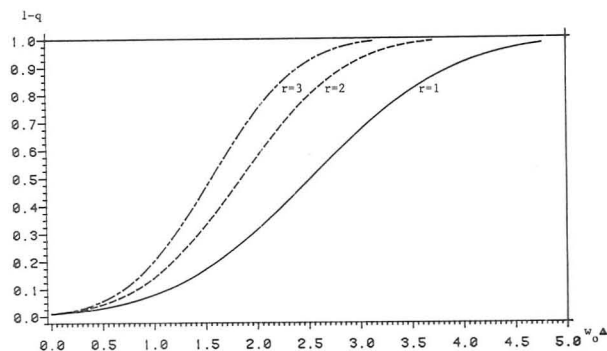


Figure 3. Detection rate curves for a given 32-point design, assuming linear calibration and $p = 0.01$. (See text for explanation of horizontal scale.)

limits that, in expectation, are close to a target detection limit; or if the required design is excessive relative to calibration resources, this provides inferences that target limits are too stringent for that analyte and measurement method. It also permits detection limits from two different calibrations to be compared in an objective fashion. For example, did laboratory A report lower limits of detection than laboratory B because of a more sensitive analytical method (i.e., larger β/σ), a different calibration design, or different choice for p , q , and r ?

Estimation of Detection Limits and Detection Rates for Linear Calibration. Assume now that a calibration over "low" concentrations has been performed according to a prescribed design and that subsequent examination of the response observations (e.g., via plots and appropriate statistical tests) has shown model 2, along with its stated assumptions, to be a tenable model for the analyte of interest. Least-squares estimates $\hat{\alpha}$ and $\hat{\beta}$ and an estimate of the measurement error variance, $\hat{\sigma}^2$, are therefore available. If r and the desired false positive rate (p) and false negative rate (q) are fixed, then the threshold response value and a point estimate of the detection limit can be obtained via the following four-step procedure:

- (1) Compute w_0 , using eq 9.
- (2) Compute the threshold response value, \hat{y}_p , using eq 14. Values of t_p are given in Table I.
- (3) Compute $\Delta(p, q)$, or select an appropriate value from Table I.
- (4) Use eq 17 to compute an estimated detection limit by substituting $\hat{\sigma}$ for σ and $\hat{\beta}$ for β .

Alternatively, rather than fixing q , we can fix r and the type I error rate p and any concentration value x ; then an estimate $\hat{\Delta}$ of the noncentrality parameter can be obtained by substituting $\hat{\beta}/\hat{\sigma}$ for β/σ in eq 16. The estimated detection rate corresponding to concentration x is then obtained by substituting $\hat{\Delta}$ for Δ in eq 15.

Methods for determining interval estimates for $x_d(p, q)$, and for detection rates at specified concentrations x , are discussed by Burrows (5) and by Clayton et al. (11). Appendix B summarizes the results for the detection limit intervals.

EXPERIMENTAL SECTION

An experiment was conducted in two distinct phases that were together designed to demonstrate and validate the advocated methods. Phase I consisted of method calibration as applied to environmental (sediment) samples, estimation of model parameters, and estimation of detection limits having specified assurance probabilities. The statistical analysis performed in this phase of the study illustrates the general procedures required to implement the recommended approach. Phase II of the study, which was used to validate the methodology, involved analysis of sediment samples at selected concentrations. The analytical results were used to generate empirical estimates of detection rates that could then be compared to the theoretical projections derived from phase I.

Table II. Actual Analyte Concentrations Used in Phase I of the Experiment

analyte	target concn, mg/kg		
	0.2	0.8	1.0
2-chloronaphthalene	0.215	0.858	1.07
dimethyl phthalate	0.217	0.867	1.08
hexachlorobenzene	0.200	0.802	1.00
anthracene	0.217	0.870	1.07
phenanthrene	0.210	0.840	1.05
fluoranthene	0.200	0.802	1.00

Sample Preparation. Sediment samples were prepared and analyzed in an identical manner in both phase I and phase II. A single, homogeneous lot of sediment (approximately 1 kg) obtained from a protected drinking-water reservoir (University Lake, Chapel Hill, NC) was used to prepare all sample aliquots. The sediment was stored at 4 °C immediately after collection.

Individual samples consisted of 30-g aliquots of the sediment placed in wide-mouth, 16-oz glass jars fitted with screw caps lined with Teflon. The sediment was homogenized prior to removing each sample aliquot. Sediment samples were fortified by the addition of a 50- μ L aliquot of a standard solution containing six analytes (2-chloronaphthalene, dimethyl phthalate, hexachlorobenzene, anthracene, phenanthrene, and fluoranthene) in acetone. Fortified sediment samples were then stored overnight prior to extraction and analysis. The different fortification levels required in the experiment were achieved by dilution of a single standard solution to appropriate concentrations such that a 50- μ L aliquot of the diluted standard contained the necessary amount of each analyte for the 30-g sediment sample. Nominal and actual sediment fortification levels are shown in Table II. Samples were extracted by use of a sonication procedure described elsewhere (14).

Sample Analysis. Sediment extracts were analyzed by capillary gas chromatography/flame ionization detection with pentadecane as the internal standard. Conditions, procedures, and instrumentation used for sample analysis were identical for both phases I and II, although phase II was initiated about 1 month after completion of the phase I analyses.

Analysis was performed on a Varian Model 3700 gas chromatograph equipped with a homemade splitless/split injector (15) and a flame ionization detector. The Grob "solvent effect" technique (16) was used for the injection of 1.5- μ L volumes of sample with a 60-s initial splitless time. A J&W Scientific DB-1 capillary column (15 m \times 0.25 mm i.d., 0.25- μ m film thickness) was used with a He flow rate of 0.6 mL/min. The split ratio was 80:1 and a makeup gas flow of 35 mL/min (He) was added at the detector inlet. The column temperature was programmed at 5 °C/min from 70 to 220 °C after a delay of 3 min at the initial temperature.

Sample data were collected with a Nelson Analytical Model 4400 data system operating at 2 data points/s. Analyte peaks were confirmed by comparison of sample peak retention times with a standard analyzed with each group of samples. The analytical response of each component was determined as the ratio of analyte peak area to internal standard peak area.

RESULTS AND DISCUSSION

Phase I. The phase I calibration design entailed eight analyses at each of the three fortification levels shown in Table II plus eight analyses of blank (unfortified sediment) samples. Detectability properties of this design are shown in Figure 3. One of the 32 calibration runs was unusable; another was subsequently judged to contain an outlying value for dimethyl phthalate. Hence, $n = 30$ for this analyte and $n = 31$ for all other analytes.

Plots of observed responses against standard concentrations indicated that response variability generally tended to increase with increasing concentration level. A square-root transformation (i.e., $y = \text{square root of peak area ratio}$) provided a simple remedy for achieving homogeneous variation, but plots of transformed responses against standard concentrations were

Table III. Calibration Design Parameters, by Analyte

analyte	<i>n</i>	\bar{x}	Q_{xx}	w_0 values for		
				<i>r</i> = 1	<i>r</i> = 2	<i>r</i> = 3
2-chloronaphthalene	31	0.431 74	2.900 72	1.047 15	0.772 35	0.655 63
dimethyl phthalate	30	0.449 06	2.741 93	1.052 08	0.779 02	0.663 49
hexachlorobenzene	31	0.412 28	2.663 57	1.046 94	0.772 06	0.655 29
anthracene	31	0.433 78	2.918 16	1.047 25	0.772 49	0.655 80
phenanthrene	31	0.425 81	2.830 83	1.047 05	0.772 21	0.655 47
fluoranthene	31	0.412 28	2.663 57	1.046 94	0.772 06	0.655 29

Table IV. Calibration Model Parameter Estimates, by Analyte

analyte	ν^a	$\hat{\alpha}$	$\hat{\beta}$	$\hat{\sigma}$	std error of $\hat{\alpha}$	std error of $\hat{\beta}$
2-chloronaphthalene	29	0.300 676	1.021 72	0.052 883	0.016 429	0.031 05
dimethyl phthalate	28	0.279 346	0.570 02	0.052 519	0.017 170	0.031 72
hexachlorobenzene	29	0.178 793	0.736 51	0.032 441	0.010 055	0.019 88
anthracene	29	0.212 840	1.394 02	0.043 208	0.013 439	0.025 29
phenanthrene	29	0.247 232	1.479 15	0.037 289	0.011 572	0.022 16
fluoranthene	29	0.245 677	1.430 41	0.054 681	0.016 949	0.033 50

^a $\nu = n - 2$ degrees of freedom for $\hat{\sigma}$ (see Table I).

Table V. Threshold Response Values \hat{y}_p , by Analyte, for $p = 0.01$ and 0.05 , and for $r = 1, 2$, and 3

analyte	<i>r</i> = 1		<i>r</i> = 2		<i>r</i> = 3	
	<i>p</i> = 0.01	<i>p</i> = 0.05	<i>p</i> = 0.01	<i>p</i> = 0.05	<i>p</i> = 0.01	<i>p</i> = 0.05
2-chloronaphthalene	0.437 01	0.394 77	0.401 23	0.370 08	0.386 04	0.359 59
dimethyl phthalate	0.415 67	0.373 34	0.380 29	0.348 95	0.365 31	0.338 62
hexachlorobenzene	0.262 41	0.236 50	0.240 46	0.221 35	0.231 13	0.214 91
anthracene	0.324 25	0.289 73	0.295 02	0.269 55	0.282 60	0.260 99
phenanthrene	0.343 36	0.313 57	0.318 13	0.296 16	0.307 41	0.288 76
fluoranthene	0.386 62	0.342 95	0.349 62	0.317 41	0.333 90	0.306 56

clearly not linear. Several transformations of the concentration scale, aimed at producing a linear relationship, were therefore considered. The following transformation was found to be suitable for all analytes:

$$x = \sqrt{x^* + 0.1} - \sqrt{0.1} \quad (19)$$

where x^* was the analyte concentration (mg/kg). With x defined by eq 19 and y defined as the square root of peak area ratio, the straight-line calibration model, model 2, together with its stated distributional assumptions, appeared satisfactory. All subsequent results assume that x and y are so defined.

Table III contains the relevant calibration design characteristics, and Table IV contains the estimates of α , β , and σ , as determined from eq 3, 4, and 5. In practice, a particular false positive rate, p , and a particular r value would have been specified as a part of the detection protocol. For demonstration purposes, results here are given for two p values ($p = 0.01$ or 0.05) and three r values ($r = 1, 2$, or 3 replicate observations). Table V shows the threshold response values, \hat{y}_p , from eq 14, for each combination of these p and r values.

Point estimates of detection limits for given p and q values and for $r = 1$ are shown in Table VI. These are obtained from eq 17 with $\hat{\sigma}/\hat{\beta}$ (from Table III) replacing σ/β . Table VI also gives 95% and 99% interval estimates for $x_d(p, q)$ with $r = 1$. Similar tables for $r = 2, 3, \dots$, can be developed in the same manner. While these tabular results are given in transformed units, they can also be expressed in concentration units (mg/kg) by solving eq 19 for x^*

$$x^* = x^2 + 0.632456x$$

In the first row of Table VI, for instance, the estimated detection limit is 0.194 mg/kg and the 95% and 99% intervals translate to the mg/kg intervals (0.145, 0.288) and (0.134, 0.332), respectively.

Phase II. Apart from the unknown factor σ/β , the advocated methodology enables calculation of a detection rate curve (like Figure 3) for the given calibration design and given r and p values. With the calibration performed, an estimate of σ/β (or of β/σ) is available for each analyte so that estimates of detection rates $[1 - q(x)]$ can be obtained for any x value (or x values can be estimated for different specified q values). For phase II, three distinct concentration levels for each analyte were chosen that would be expected, given the phase I estimates, to have the (approximate) detection probabilities given in Table VII.

Thirty-six aliquots of the reservoir sediment were fortified, 12 each at the low, medium, and high levels. Each of the individual phase II response values, Y , was compared to the predetermined threshold response values (i.e., the \hat{y}_p values corresponding to $r = 1$ in Table V). An observation was considered to yield a "detection" if $Y > \hat{y}_p$, corresponding to application of the detection rule. The count of detections occurring for each analyte and concentration level was then divided by the number of trials (equal to 12 in most cases) to yield an empirical estimate of the detection rate associated with that x^* and p value ($p = 0.01$ or 0.05). The results are summarized in Table VIII.

With the exception of dimethyl phthalate, the results in this table show reasonable agreement between the estimated phase I detection rates and the empirical estimates determined in phase II. Erratic chromatographic performance for dimethyl phthalate was noted throughout the study and was especially severe during phase II (due to diffuse, indistinct chromatographic peaks). The small numbers of trials for each analyte in phase II are responsible for the considerable variation in the empirical estimates of the detection rates; however, because of the phase II design, the projected detection rates from phase I (see Table VII and VIII) are approximately equal for all analytes at each of the low, middle, and high levels

Table VI. Detection Limit Estimation for Selected p and q Values, When $r = 1$

analyte	p	q	detection limit estimate	interval estimates for $x_d(p,q)$			
				coverage = 0.95		coverage = 0.99	
				low	high	low	high
2-chloronaphthalene	0.01	0.05	0.226 01	0.179 07	0.306 84	0.167 21	0.341 08
		0.01	0.264 91	0.209 90	0.359 65	0.195 99	0.399 79
	0.05	0.05	0.182 64	0.144 72	0.247 96	0.135 13	0.275 64
dimethyl phthalate	0.01	0.01	0.220 51	0.174 72	0.299 38	0.163 14	0.332 79
		0.05	0.404 95	0.316 16	0.565 50	0.294 27	0.637 48
	0.05	0.01	0.474 67	0.370 60	0.662 86	0.344 93	0.747 23
hexachlorobenzene	0.01	0.05	0.326 95	0.255 26	0.456 57	0.237 58	0.514 68
		0.01	0.394 74	0.308 19	0.551 24	0.286 85	0.621 41
	0.05	0.05	0.192 30	0.152 53	0.260 53	0.142 45	0.289 29
anthracene	0.01	0.01	0.225 39	0.178 78	0.305 37	0.166 97	0.339 09
		0.05	0.155 40	0.123 26	0.210 54	0.115 12	0.233 79
	0.05	0.01	0.187 62	0.148 82	0.254 20	0.138 99	0.282 26
phenanthrene	0.01	0.05	0.135 36	0.107 60	0.182 61	0.100 54	0.202 32
		0.01	0.158 66	0.126 12	0.214 04	0.117 84	0.237 14
	0.05	0.05	0.109 39	0.086 96	0.147 57	0.081 25	0.163 50
fluoranthene	0.01	0.01	0.132 07	0.104 99	0.178 17	0.098 09	0.197 40
		0.05	0.110 07	0.087 55	0.148 33	0.081 81	0.164 24
	0.05	0.01	0.129 02	0.102 62	0.173 86	0.095 89	0.192 51
	0.01	0.05	0.088 95	0.070 75	0.119 87	0.066 11	0.132 73
		0.01	0.107 39	0.085 42	0.144 72	0.079 82	0.160 25
	0.05	0.05	0.166 89	0.132 51	0.225 68	0.123 78	0.250 34
	0.01	0.01	0.195 62	0.155 31	0.264 52	0.145 08	0.293 43
		0.05	0.134 87	0.107 08	0.182 38	0.100 03	0.202 31
	0.05	0.01	0.162 83	0.129 29	0.220 19	0.120 77	0.244 26

Table VII. Approximate Detection Probabilities Expected for Phase II, Based on Phase I Estimates, for Selected r and p Values

r	p	phase II concn level		
		low	middle	high
1	0.01	0.10	0.35	0.68
	0.05	0.28	0.64	0.89
2	0.01	0.18	0.63	0.93
	0.05	0.42	0.86	0.99
3	0.01	0.25	0.79	0.98
	0.05	0.52	0.94	0.99+

of fortification. It is therefore possible to pool the phase II detection counts over analytes. The results, for $r = 1$, are

shown at the bottom of Table VIII (dimethyl phthalate is excluded). Close agreement between the phase I and phase II rates is evident.

Similar results were obtained for $r = 2$ and for $r = 3$. Within a concentration level, phase II observations were paired sequentially to produce six "observed" mean responses that were compared to the \hat{y}_p values for $r = 2$. A similar grouping was used to produce four means for $r = 3$. Pooling over the five analytes as before yields the results shown in Table IX.

CONCLUSIONS

Traditional methods for determining detection limits usually rely on the assumptions that observed responses are normally distributed and that the variance of these measurements does not depend on concentration level, at least

Table VIII. Comparison of Phase I and Phase II Detection Rate Estimates, for $r = 1$, by Analyte

analyte	phase II fortification level, ppm	(approx) phase I est of detection rate		no. of phase II observations	no. of detections		proportion detected (phase II)	
		$p = 0.05$	$p = 0.01$		$p = 0.05$	$p = 0.01$	$p = 0.05$	$p = 0.01$
2-chloronaphthalene	0.043	0.29	0.10	12	0	0	0	0
	0.086	0.65	0.36	12	6	0	0.50	0
	0.129	0.89	0.67	12	9	7	0.75	0.58
dimethyl phthalate	0.087	0.31	0.11	9	0	0	0	0
	0.173	0.65	0.36	12	0	0	0	0
	0.260	0.87	0.65	11	0	0	0	0
hexachlorobenzene	0.036	0.29	0.10	12	5	3	0.42	0.25
	0.072	0.65	0.37	12	9	5	0.75	0.42
	0.108	0.89	0.69	12	11	8	0.91	0.67
anthracene	0.024	0.28	0.10	12	8	0	0.67	0
	0.047	0.63	0.34	12	12	3	1.00	0.25
	0.071	0.89	0.68	12	12	12	1.00	1.00
phenanthrene	0.019	0.27	0.09	12	4	1	0.33	0.08
	0.038	0.64	0.35	12	3	3	0.25	0.25
	0.058	0.90	0.70	12	11	8	0.92	0.67
fluoranthene	0.030	0.28	0.10	12	0	0	0	0
	0.060	0.64	0.35	12	11	4	0.92	0.33
	0.090	0.88	0.67	12	12	11	1.00	0.92
pooled over 5 analytes (excluding dimethyl phthalate)	low	0.28	0.10	60	17	4	0.28	0.07
	medium	0.64	0.35	60	41	15	0.68	0.25
	high	0.89	0.68	60	55	46	0.92	0.77

Table IX. Comparison of Phase I and Phase II Detection Rate Estimates

	phase II fortifica- tion level	phase I detection rate estimate		proportion detected (phase II)	
		$p = 0.05$	$p = 0.01$	$p = 0.05$	$p = 0.01$
$r = 2$ (30 trials)	low	0.42	0.18	0.33	0.17
	medium	0.86	0.63	0.83	0.67
	high	0.99	0.93	0.97	0.90
$r = 3$ (20 trials)	low	0.52	0.25	0.45	0.25
	medium	0.94	0.79	0.85	0.70
	high	0.99+	0.98	1.00	0.95

over a narrow range of "low" concentrations of interest. The method advocated here relies on these same assumptions; however, it defines detection limits as parameters and offers a statistical procedure for estimating them. Unlike most traditional approaches, the recommended procedure does not treat the calibration curve parameter estimates as known (fixed) quantities. Moreover, it permits the analyst to specify both type I and type II error rates when defining detection limits (and to estimate detection rates at other specified analyte concentrations), whereas traditional methods fix only the type I error rate. The results of this study demonstrate the practicality of the methodology: there is close agreement between the statistical theory and laboratory practice. As pointed out by Burrows (5), methodology for dealing with the problem of determining compliance with a statutory limit is very similar to that advocated here for defining and estimating detection limits. The results of the study therefore also indicate that such methodology can be practical for formulating and handling the compliance testing problem.

ACKNOWLEDGMENT

The authors thank Peter M. Burrows of Clemson University and John Warren of the United States Environmental Protection Agency for their helpful suggestions and comments.

APPENDIX A. DERIVATION OF EQUATION 15

Let Z be a random variable having standard normal distribution and let S_v be a random variable, independent of Z , such that vS_v^2 has a χ^2 distribution with v degrees of freedom. For a given constant Δ , the random variable $T(\Delta) = (Z + \Delta)/S_v$ is distributed according to a noncentral t distribution with v degrees of freedom and noncentrality parameter Δ .

Let \sim denote "distributed as". At concentration $X = x$, $(Y - \hat{\alpha}) \sim (\beta x + \sigma w_0 Z)$, independently of $\hat{\sigma} \sim \sigma S_v$. Let Δ be defined by eq 16. Then

$$\begin{aligned} \Pr[\text{detection}|X = x] &= \Pr[Y > \hat{y}_p|X = x] \\ &= \Pr[Y - \hat{\alpha} > \hat{\sigma} w_0 t_p|X = x] \\ &= \Pr[\beta x + \sigma w_0 Z > \sigma w_0 t_p S_v] \\ &= \Pr[(\Delta + Z)/S_v > t_p] \\ &= \Pr[T(\Delta) > t_p] \end{aligned}$$

as given by eq 15.

APPENDIX B. INTERVAL ESTIMATES FOR DETECTION LIMITS

Define

$$\hat{\delta} = \hat{\beta} \sqrt{Q_{xx}} / \hat{\sigma}$$

and

$$W = w_0 \Delta(p, q) \sqrt{Q_{xx}}$$

Also define δ_- and δ_+ such that the following are satisfied:

$$\Pr[T(\delta_-) < \hat{\delta}] = 1 - \gamma/2 \text{ and } \Pr[T(\delta_+) < \hat{\delta}] = \gamma/2$$

where $0 < \gamma < 1$. Then the interval

$$(W/\delta_+, W/\delta_-)$$

furnishes an interval estimate for the detection limit $x_d(p, q)$, with coverage probability $1 - \gamma$.

LITERATURE CITED

- (1) Cairns, T.; Rogers, W. M. *Anal. Chem.* **1983**, *55*, 54A-57A.
- (2) Winefordner, J. D.; Long, G. L. *Anal. Chem.* **1983**, *55*, 712A-724A.
- (3) Glaser, J. A.; Foerst, D. L.; McKee, G. D.; Quave, S. A.; Budde, W. L. *Environ. Sci. Technol.* **1981**, *15*, 1426-1435.
- (4) Ingle, J. D. *J. Chem. Educ.* **1974**, *51*, 100-105.
- (5) Burrows, P. M. *Technometrics*, in press.
- (6) Oppenheimer, L.; Capizzi, T. P.; Weppelman, R. M.; Mehta, H. *Anal. Chem.* **1983**, *55*, 638-643.
- (7) Altshuler, B.; Pasternack, B. *Health Phys.* **1963**, *9*, 293-298.
- (8) Currie, L. A. *Anal. Chem.* **1968**, *42*, 849-855.
- (9) Hubaux, A.; Vos, G. *Anal. Chem.* **1970**, *42*, 849-855.
- (10) American Society for Testing and Materials *ASTM Standards on Precision and Bias for Various Applications*, 2nd ed.; American Society for Testing and Materials: Philadelphia, PA, 1985; pp 210-213.
- (11) Clayton, C. A.; Hines, J. W.; Hartwell, T. D.; Burrows, P. M. "Demonstration of a Technique for Estimating Detection Limits with Specified Assurance Probabilities"; Research Triangle Institute Technical Report 2757/05-01F, Environmental Protection Agency Contract No. 68-01-6826; Research Triangle Institute: Research Triangle Park, NC, 1986.
- (12) Clayton, C. A. "Calibration Designs for Detecting Presence or Absence of Analytes"; Research Triangle Institute Technical Report 3079/10-01F, Environmental Protection Agency Contract No. 68-01-6826; Research Triangle Institute: Research Triangle Park, NC, 1986.
- (13) Owen, D. B. *J. Am. Statistical Assoc.* **1965**, *60*, 320-333.
- (14) Office of Solid Waste and Emergency Response, U.S. Environmental Protection Agency *Test Methods for Evaluating Solid Waste—Physical/Chemical Methods*, SW-846, 3rd ed.; U.S. Environmental Protection Agency: Washington, DC, 1986; Method 3550: Sonication Extraction.
- (15) Hines, J. W.; Erickson, M. D.; Newton, D. L.; Moseley, M. A.; Retzlaff, L. M.; Pellizzari, E. D. *HRC CC, J. High Resolut. Chromatogr. Chromatogr. Commun.* **1982**, *5*, 52-53.
- (16) Grob, K.; Grob, K., Jr. *HRC CC, J. High Resolut. Chromatogr. Chromatogr. Commun.* **1978**, *1*, 53-64.

RECEIVED for review January 5, 1987. Accepted June 25, 1987. This work was supported by the Statistical Policy Branch, Office of Standards and Regulations, U.S. Environmental Protection Agency, under Contract Number 68-01-6826. This article does not necessarily reflect the views of the Agency, and no official endorsement should be inferred.

Three-Component Self-Modeling Technique Applied to Luminescence Spectra¹

Ya-Ping Sun, Donald F. Sears, Jr., and Jack Saltiel*

Department of Chemistry, Florida State University, Tallahassee, Florida 32306-3006

It is shown that the selection of pure component spectral coefficients is improved when additional applicable constraints are imposed. The method is demonstrated first for a two-component system (the phosphorescence and delayed fluorescence of benzophenone) and then extended to three components. It is first shown that it succeeds in reproducing theoretical curves used to construct an artificial three-component input matrix and then it is applied to resolve experimental spectra composed of the fluorescence of two conformers of *trans*-1,2-di(2-naphthyl)ethene (DNE) and a background spectrum dominated by Raman emission at the excitation wavelength region.

The combination of principal component analysis with the self-modeling technique, first proposed by Lawton and Sylvestre (1), has been used extensively in recent years (2-6). Modification of the original procedure and additional resolution conditions have been used to enhance the decomposition of relatively complicated two-component systems (7-9). In addition several investigators have attempted in various ways to extend the basic concepts of the Lawton and Sylvestre approach to three- or multicomponent systems (10-15). The extension most directly stemming from the concepts applied to two-component systems is that introduced recently by Borgen and Kowalski (16). In this extension, outer and inner limit coefficient lines were sought by applying the condition of nonnegative pure component vectors for the former and observed response vectors for the latter. Geometric considerations in three-dimensional vector space were then used to reduce the possible pure component limit regions for a three-component system. The method successfully reproduced three components from simulated data (16), but no experimental applications to real data were reported.

In this paper we describe a specific and relatively explicit extension of the self-modeling technique which, though based upon the concepts of Lawton and Sylvestre, employs more stringent experimental conditions in seeking the pure component coefficients. The application of the method will be illustrated first for a two-component system and then extended to simulated and real three-component systems.

EXPERIMENTAL SECTION

Materials. Benzophenone (Fischer, Certified Reagent) was twice recrystallized from hexane and then triply sublimed before use. The *trans*-1,2-di(2-naphthyl)ethene was provided by F. B. Mallory, C. W. Mallory, and C. A. Buser (9). The synthesis and purification will be described in a forthcoming paper. Carbon tetrachloride was purchased from Mallinkrodt (SpectrAR) and distilled prior to use while methylcyclohexane (MCH) from Baker (Photrex) was used as received. Benzophenone solutions of 1.04×10^{-2} M in CCl_4 and DNE solutions of $(5.0\text{--}9.0) \times 10^{-6}$ M in MCH containing 0.0-1.0 M CCl_4 were used. All sample solutions were deaerated by several freeze-thaw cycles at ca. 1.0×10^{-5} Torr.

Data Collection. All luminescence measurements were made with a Hitachi/Perkin-Elmer MPF-2A fluorescence spectrophotometer equipped with a 150-W Xe arc source and a Hamamatsu R106UH photomultiplier tube. Fluorescence intensities were recorded at each 0.5-nm interval directly on a CompuPro 816/286 microcomputer equipped with an I/O Technology A/D/A converter board. The scan rate was 200 nm/min. Instrumental noise consisted primarily of a 60-Hz sine wave, 0.10 V root mean square. Signals at λ_{max} ranged between 3.5 and 10.0 V. Emission spectra were not corrected for nonlinear instrumental response.

Sample chamber temperatures were maintained to within $\pm 0.1^\circ\text{C}$, using a Haake FN constant temperature circulator monitored with an Omega Engineering Model 199 RTD digital thermometer. The temperature was monitored immediately above the light beam path. Benzophenone spectra were recorded in quartz electron paramagnetic resonance (EPR) tubes inserted into a cylindrical quartz compartment through which the coolant traveled (methanol or distilled water) to ensure uniform sample temperature over a wide temperature range (-2.4 to 85.2°C). Dry N_2 was used to flush the sample compartment and minimize condensation on sample cell and instrument optics.

Data Analysis. DNE calculations involved the use of 30 fluorescence spectra (five duplicates for each of six $[\text{CCl}_4]$) and one excitation wavelength Raman scattered light spectrum containing 150 points each (340-489 nm). Benzophenone calculations involved the use of 90 total luminescence spectra representing 18 temperatures containing 120 data points each (370-608 nm). Principal component analysis calculations were carried out on a Control Data Corp. Cyber 760 computer.

RESULTS AND DISCUSSION

Introductory Considerations. Suppose \mathbf{Y} is a $m \times n$ experimental data matrix such that each row vector corresponds to a normalized experimental spectrum, \mathbf{S}_i , with n elements composed of the linear superposition of k pure spectra, and the m ($m \geq k$) different row vectors correspond to spectra measured by systematically changing experimental conditions that control the relative contribution of the pure spectra. The value k can be determined by carrying out principal component analysis on the second moment matrix \mathbf{M}

$$\mathbf{M} = \mathbf{Y}' \cdot \mathbf{Y} \quad (1)$$

where \mathbf{Y}' is the transpose of \mathbf{Y} . The analysis leads to

$$\mathbf{M} = \mathbf{C}_1 \cdot \mathbf{V} \quad (2)$$

where \mathbf{C}_1 is diagonalized and \mathbf{V} is the eigenvector matrix. Theoretically, only k nonzero diagonal elements are expected in \mathbf{C}_1 , which define the k significant eigenvectors (rows) in \mathbf{V} . Practically, significant eigenvalues are found by comparing the relative magnitude of all diagonal elements in \mathbf{C}_1 . These comprise an $m \times k$ matrix, \mathbf{A}_1 , known as the combination coefficient matrix, which multiplied by the $k \times n$ eigenvector matrix \mathbf{V} regenerates the initial spectral input matrix

$$\hat{\mathbf{Y}} = \mathbf{A}_1 \cdot \mathbf{V} \quad (3)$$

Basic Concepts for Two-Component Systems. For a two-component system, $k = 2$, \mathbf{A}_1 has only two columns, α and β , and \mathbf{V} consists of two rows, the eigenvectors $\hat{\mathbf{V}}_\alpha$ and

¹ This paper is dedicated to Professor Ernst Fischer on the occasion of his 65th birthday.

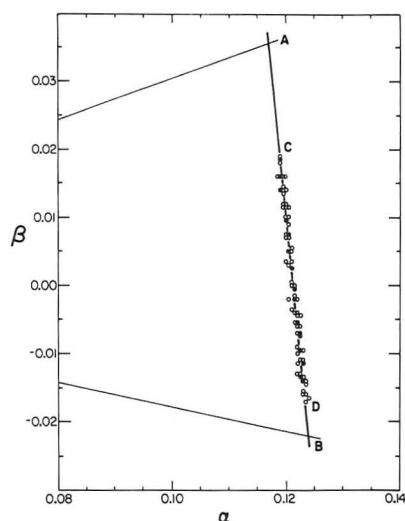


Figure 1. α , β plot for benzophenone luminescence spectrothermal matrix, -2.4 to 85.2 °C. The normalization line is drawn through the points.

\bar{V}_β . Accordingly, each normalized experimental spectrum in \mathbf{Y} is related to a pair of coefficients (α_i , β_i)

$$\bar{S}_i = \alpha_i \bar{V}_\alpha + \beta_i \bar{V}_\beta \quad (4)$$

The plot of the coefficients in two-dimensional α , β space is expected to be linear and to be coincident with the normalization line defined by the eigenvectors

$$\alpha \left(\sum_{j=1}^n V_{\alpha j} \right) + \beta \left(\sum_{j=1}^n V_{\beta j} \right) = 1 \quad (5)$$

where $V_{\alpha j}$ and $V_{\beta j}$ are j th elements of \bar{V}_α and \bar{V}_β , respectively. All experimental spectra are also combinations of two unknown pure-component spectra \mathbf{A} and \mathbf{B} , which could be obtained from eq 4 if the corresponding coefficients (α_a , β_a) and (α_b , β_b) were known. These pure-component coefficients are expected to fall on the outer extremes of the normalization line, eq 5, and therefore represent the limits of the α , β line.

In order to define possible regions for the two limits, Lawton and Sylvestre applied two constraints: (a) that \mathbf{Y} have no negative elements and (b) that the unknown pure-component spectra \mathbf{A} and \mathbf{B} have no negative elements either (1). The first constraint forces the two limits outside of the two ends of the segment of the line defined by the coefficients (α_i , β_i) corresponding to the experimental spectra in \mathbf{Y} . However, the second constraint requires that the farthest acceptable points on the α , β line are those for which each of the two resultant spectra has its first very small negative value. The acceptable regions for the pure components now comprise the two segments at each end of the α , β line between the limiting values thus obtained and the outermost experimental coefficients. This is illustrated on an actual α , β plot (Figure 1) obtained by treating a matrix of benzophenone luminescence spectra in CCl_4 in the -2.4 to $+85.0$ °C temperature range (17). The spectra consist of mixtures of phosphorescence and thermally activated delayed-fluorescence (18, 19). The line sections AC and BD in Figure 1 correspond to acceptable regions for the pure component coefficients when using the above constraints and correspond to sets of spectra consisting of positive luminescence intensities only.

When, as is often the case, the pure component spectra do not overlap over the entire wavelength range, there is at least one wavelength where \mathbf{A} has zero intensity and \mathbf{B} is positive and at least one wavelength where the reverse applies. Under this third constraint the unknown pure components are expected to be uniquely defined by the coefficients corresponding to points A and B in Figure 1 as was recognized by Lawton and Sylvestre (1).

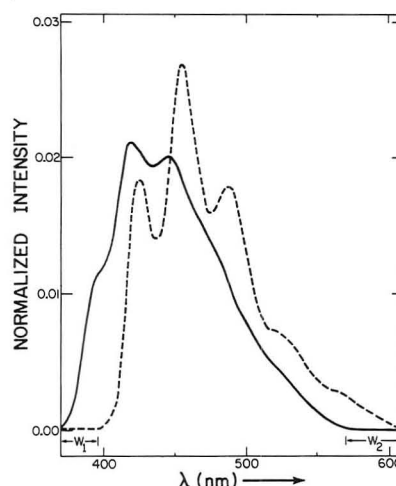


Figure 2. Pure-component benzophenone emission spectra: delayed fluorescence (—); phosphorescence (---).

In formal mathematical treatments, the first two constraints are emphasized since they are generally applicable. Practically, however, these result in wide regions of acceptable pure component coefficients and large uncertainties in calculated pure component spectra. To achieve a unique definition of the pure component spectra it is important to find and apply as many additional constraints as possible for each specific problem. For example, in the case of benzophenone luminescence, for which the origin of the $S_0 \rightarrow S_1$ transition is at higher energy than that for the $S_0 \rightarrow T_1$ transition, the origin of delayed fluorescence is expected to occur at shorter wavelengths than that of the phosphorescence, and the third constraint mentioned above is obviously applicable.

In practice, the three constraints cannot be applied blindly. Experimental spectra include instrumental noise and/or systematic errors stemming from inexact background subtraction, which often lead to discontinuities in the eigenvectors (or even to third eigenvectors, see next section). In some instances it is precisely these irregularities in the eigenvectors which define erroneous limits in the α , β plot. Let us consider Figure 1 in more detail. As we move up from point C by small increments along the normalization line, we obtain a series of spectra with increasing contributions from component A (the fluorescence spectrum in Figure 2) and decreasing contributions from component B (the phosphorescence) as expected from the lever rule. Eventually we will reach the point that corresponds to pure-component spectrum A. When this happens, intensities corresponding to the W_2 wavelength region in Figure 2 should either vanish or have negligibly small negative values. Since fractional contributions are independent of λ , an accurate estimate of α_a , β_a (point A in Figure 1) can be found by simultaneously seeking several zero or very small negative intensities in the W_2 wavelength region. Similarly, α_b , β_b (point B in Figure 1) can be found by setting the same constraint on region W_1 in Figure 2. The spectra shown in Figure 2 were obtained in this way. The advantage of selecting the wavelength region that will define a spectrum and then requiring that several points in that region reach the base line nearly simultaneously is that the possibility that the pure-component α , β values will be reached prematurely due to expressions of noise in the eigenvectors is avoided. In our experience, by going beyond the first negative intensity point, stable spectral solutions are achieved, which are independent of the number of negative points sought in the regions where the spectra do not overlap. A prior knowledge of the precise width and location of the regions W_1 and W_2 is not essential to the application of the method. Actually in the benzophenone case the result was achieved by seeking small negative intensities separately in the first and second

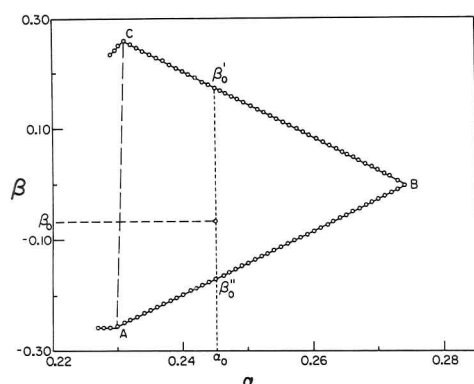


Figure 3. Projection of the coefficient triangle for the simulated three-component system in Figure 4 on the α , β plane.

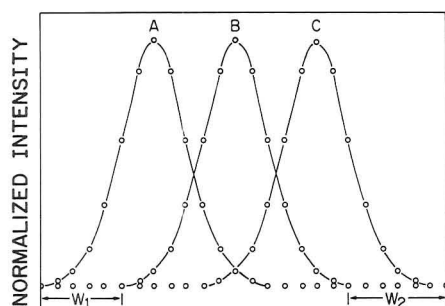


Figure 4. Assumed (solid lines) and recovered (open circles) pure-component spectra.

halves of the wavelength range. Of course, once coefficients for the pure-component spectra are selected, the location and extent of W_1 and W_2 regions become obvious.

Resolution of Three-Component Systems. The above considerations apply to three-component systems. With $k = 3$, the eigenvector matrix consists of three eigenvectors, \bar{V}_α , \bar{V}_β , and \bar{V}_γ , which define a normalization plane in α , β , and γ space

$$\alpha \left(\sum_{j=1}^n V_{\alpha j} \right) + \beta \left(\sum_{j=1}^n V_{\beta j} \right) + \gamma \left(\sum_{j=1}^n V_{\gamma j} \right) = 1 \quad (6)$$

on which all combination coefficients α_i , β_i , and γ_i ($i = 1, \dots, m$) must fall. The rows of \bar{Y} are given by

$$\bar{S}_i = \alpha_i \bar{V}_\alpha + \beta_i \bar{V}_\beta + \gamma_i \bar{V}_\gamma \quad (7)$$

If the pure component spectra are designated as **A**, **B**, and **C**, then

$$S_i = x_{ia}A + x_{ib}B + x_{ic}C \quad (8)$$

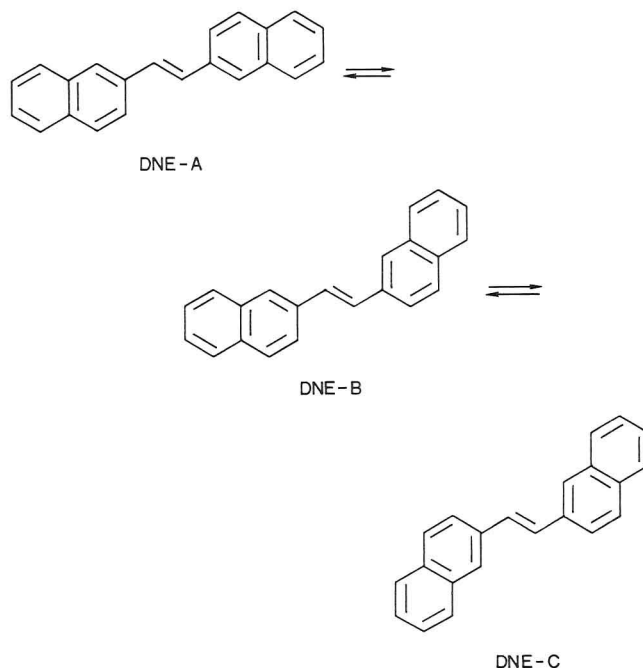
also holds with x_{ia} , x_{ib} , and x_{ic} all positive or zero and $x_{ia} + x_{ib} + x_{ic} = 1$. The x_i 's are fractional contributions of each pure component for the i th experimental spectrum.

By analogy to three-component phase diagrams, all $(\alpha_i, \beta_i, \gamma_i)$ points representing S_i 's fall within a triangle in the normalization plane. The corners of the triangle correspond to the coefficients for each of the three pure-component spectra and its sides correspond to the three combinations of two-component mixtures. Figure 3 shows the α , β plane projection of such a triangle obtained by solving a simulated matrix composed of combinations of the three idealized spectra in Figure 4. The points A, B, and C correspond to pure-component spectra and points on the lines AB, BC, and AC are mixtures of only the two indicated components.

The simulated matrix was constructed by using composite spectra containing at least 0.2 of each component ($x_{ia}, x_{ib}, x_{ic} \geq 0.2$, eq 8) in Figure 4. Treatment of this matrix as described above generates a set of coefficients $(\alpha_i, \beta_i, \gamma_i)$ that fall on the normalization plane defined by the three eigenvectors (eq 6). We now describe our procedure for finding the three points

on the normalization plane that correspond to the pure component coefficients. We begin by projecting the "experimental" coefficients on the α , β plane. This defines a region within an, as yet, unknown triangle in that plane. We now take advantage of the fact that the individual pure component spectra do not overlap over the entire spectral region. Reference to Figure 4 shows that the spectral wavelength region W_1 (corresponding to the onset of real spectra) contains no intensity contributions from spectra B and C, while the region W_2 (the tail part of real spectra) contains no contributions from spectra A and B. By selecting a point (α_0, β_0) in the α , β plane that is roughly in the center of the region defined by the "experimental" coefficients we ensure that our starting point is within the triangle in Figure 3 and corresponds to a spectrum with all intensities positive. We now hold one of the variables α or β constant, say $\alpha = \alpha_0$, and step to higher and lower β values away from β_0 , calculating spectra at each step (note that, when α and β are known, γ is defined by the normalization plane—eq 6) until we obtain spectra containing one or more very small negative intensities. Since only component A contributes to intensities in region W_1 , the resulting point β_0' that leads to a spectrum with very small negative intensities in W_1 must fall on line BC in Figure 3 and corresponds to a spectrum with $x_a = 0$. Similarly, β_0'' is attained when very small negative intensities are found in region W_2 , and corresponds to a point on line AB in Figure 3 and a spectrum with $x_c = 0$. By stepping away from α_0 and repeating the above procedure at each step, we obtain the two curves with linear portions along BC and AB, which cross at point B, thus defining the coefficients for the central component. Since all combinations of A and C have positive intensities throughout the spectral region, the procedure of seeking negative intensities *anywhere* does not generate points along line AC. What is generated instead is a curve that represents negative contributions of component B. Points A and C are readily found because they represent turning points where this curve joins the sides of the triangle. This is illustrated for the simulated matrix in Figure 3. As shown in Figure 4, excellent recovery of the simulated spectra is achieved.

We now describe an application of this method to the resolution of real experimental spectra. It is well established (9, 20, 21) that *trans*-1,2-di(2-naphthyl)ethene, DNE, exists in solution as a mixture of three freely interconverting conformers. Rotation about the aryl-vinyl bonds is frozen out



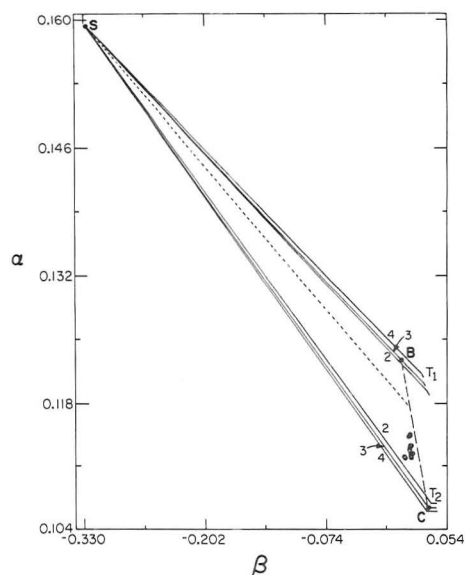


Figure 5. Projection of the coefficient triangle for the DNE-B, DNE-C, and scattered Raman light three-component system on the α , β plane. The points correspond to experimental spectra and lines 2, 3, and 4 correspond to two, three, and four negligibly small negative intensities in calculated spectra, respectively (see text).

in the lowest excited singlet state and fluorescence spectra of DNE consist of a superimposition of the fluorescence spectra of the three noninterconverting conformers. The absorption spectrum of A occurs at somewhat shorter λ than those of B and C, and excitation at the onset of DNE's absorption spectrum, at 366 nm, gives a combination of B and C fluorescence spectra in addition to scattered Raman light centered at 366 nm. B and C fluorescence is differentially quenched by CCl_4 in methylcyclohexane (20). Thus a spectral input matrix can be obtained whose rows correspond to spectra for different $[\text{CCl}_4]$ (concentrations up to 1.0 M were employed). Attempts to treat background-corrected spectra as a two-component system did not give satisfactory results due to imperfect cancellation of the Raman line as reflected in the appearance of a third eigenvector having its shape. We, therefore, constructed a matrix consisting of background uncorrected spectra and included the background as a row of the matrix. Applying the procedure described for the simulated matrix gives the two sets of closely spaced sides for the triangle corresponding to the second, third, and fourth negligibly small negative intensities, Figure 5. The intersections of the lines coincide at the point labeled S which corresponds to the coefficients for the scattered light component. The two sets of turning points are labeled T_1 and T_2 , respectively. The three ST_1 lines were determined by stepping α to higher values and monitoring the tail region of the spectrum and the ST_2 lines were determined by stepping α to lower values and monitoring the onset spectral region. Lines corresponding to the first negative intensity were disregarded because they were found immediately on stepping and were considered to reflect noise in the spectra. The impact of noise is also demonstrated by the dashed line in Figure 5, which was obtained by stepping α to higher values while monitoring the onset spectral region for negative intensities. Clearly, false triangles are obtained when the onset and tail regions are not monitored separately.

Since the three turning points on each side are closely clustered, each represents a possible solution for a pure component spectrum. Selecting the middle lines we define points T_1 and T_2 in Figure 5 which, according to the procedure described for the simulated three component spectra, represent possible limits for the spectra of DNE-B and DNE-C, respectively. However, visual inspection shows that the

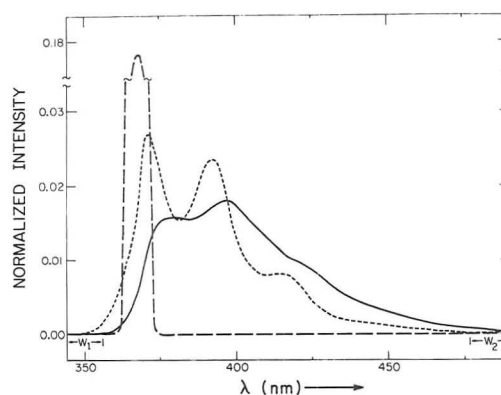


Figure 6. Pure-component spectra for the DNE system: DNE-B fluorescence, (---), DNE-C (—), and scattered Raman light at $\lambda_{\text{exc}} = 366$ nm.

spectrum predicted by the coefficients at T_1 are still somewhat affected by component S. The most likely reason for not finding the exact turning points is again experimental noise. Since line ST_1 represents combinations of two components only, the limit for DNE-B was refined by stepping along the ST_1 line. This is analogous to stepping the limits along the normalization line of a two component system. Triangle SBC represents the final result and corresponds to the normalized pure component spectra shown in Figure 6. Examination of the onset and tail spectral region reveals the presence of W_1 and W_2 segments, which are needed for our approach to succeed.

As pointed out above, noise in experimental spectra often leads to noise in the eigenvectors, which, if not recognized, may control the first few small negative spectral intensities and lead to incorrect triangles. The DNE case demonstrates the need to examine several solutions in the regions of the turning points. The problem is facilitated as soon as two triangle sides are defined because, if the turning points do not give the true pure component spectra, the limits can be refined by proceeding as if two separate two component systems were involved.

Generally speaking, in our applications of the above method to two and three spectral component mixtures, we find that the appearance of the resolved spectra is not very sensitive to small changes in the choice of the limit coefficients. Thus, the different limits associated with different numbers of negative intensities, e.g. the inner and outer triangle sides in Figure 5, usually give very similar spectra. However, the calculated fractional contributions, x_i 's, of the components in the experimental spectra depend very sensitively on the choice of limits. In real chemical problems, relationships between experimental parameters and the x_i 's often exist which provide additional constraints and can be very useful in further refinement of the selection of pure component coefficients. For example, in the case of benzophenone luminescence, the van't Hoff relationship relates fractional coefficients to the temperature.

A few remarks concerning Vandeginste and co-workers' modification of the Lawton and Sylvestre method and its application to three component curve resolution in liquid chromatography and multiwavelength diode array detection (14, 15) are in order. Two modes were employed in treating data matrices. In the Q mode, rows corresponded to UV-vis absorption spectra of eluent at different elution times, whereas in the R mode the input matrix was transposed so that its rows represented elution profiles for individual wavelengths. In both modes coefficients corresponding to experimental curves were transformed to polar coordinates and the search for pure component coefficients was carried out in a θ - ϕ plot. In performing this task the first two constraints of Lawton and

Sylvestre were assumed explicitly. Lawton and Sylvestre's third constraint, on which our method is based, was assumed implicitly, since selection of "estimated pure spectra" coefficients was made along the outer limit coefficient lines (16). It is not surprising that the method was more successful when the data were treated in the R mode rather than in the Q mode, because in the examples described the third constraint was generally valid for the elution profiles but not for the absorption spectra. Matrices of combinations of three partially overlapping elution curves resemble our simulated matrix, Figure 4, and can obviously be treated simply and directly by our method.

The method described in this paper can be extended to systems with larger numbers of components, provided that Lawton and Sylvestre's third constraint holds, although we expect that practical applications will be very difficult.

Registry No. DNE, 2753-11-9; benzophenone, 119-61-9.

LITERATURE CITED

- (1) Lawton, W. H.; Sylvestre, E. A. *Technometrics* **1971**, *13*, 617.
- (2) Macnaghtan, D., Jr.; Rogers, L. B.; Wernimont, G. *Anal. Chem.* **1972**, *44*, 1421.
- (3) Aartsma, T. J.; Gouterman, M.; Jochum, C.; Kwiram, A. L.; Pepich, B. V.; Williams, L. D. *J. Am. Chem. Soc.* **1982**, *104*, 6278.
- (4) Osten, D. W.; Kowalski, B. R. *Anal. Chem.* **1984**, *56*, 991.
- (5) Nicholson, J. C.; Meister, J. J.; Patil, D. R.; Field, L. R. *Anal. Chem.* **1984**, *56*, 2447.
- (6) Saltiel, J.; Eaker, D. W. *J. Am. Chem. Soc.* **1984**, *106*, 7624.
- (7) Sylvestre, E. A.; Lawton, W. H.; Maggio, M. S. *Technometrics* **1974**, *16*, 353.
- (8) Metzler, D. E.; Harris, C. M.; Reeves, R. L.; Lawton, W. H.; Maggio, M. S. *Anal. Chem.* **1977**, *49*, 864A.
- (9) Saltiel, J.; Sears, D. F., Jr.; Mallory, F. B.; Mallory, C. W.; Buser, C. A. *J. Am. Chem. Soc.* **1986**, *108*, 1688.
- (10) Ohta, N. *Anal. Chem.* **1973**, *45*, 553.
- (11) Meister, A. *Anal. Chim. Acta* **1984**, *161*, 149.
- (12) Sasaki, K.; Kawata, S.; Minami, S. *Appl. Opt.* **1984**, *23*, 1955.
- (13) Delaney, M. F.; Mauro, D. M. *Anal. Chim. Acta* **1985**, *172*, 193.
- (14) Vandeginste, B.; Essers, R.; Bosman, T.; Reijnen, J.; Kateman, G. *Anal. Chem.* **1985**, *57*, 971.
- (15) Vandeginste, B. G. M.; Leyten, F.; Gerritsen, M.; Noor, J. W.; Kateman, G.; Frank, J. J. *Chemometrics* **1987**, *1*, 57.
- (16) Borgen, O. S.; Kowalski, B. R. *Anal. Chim. Acta* **1985**, *174*, 1.
- (17) Saltiel, J.; et. al., unpublished results.
- (18) Saltiel, J.; Curtis, H. C.; Metts, L.; Miley, J. W.; Winterle, J.; Wrighton, M. J. *Am. Chem. Soc.* **1970**, *92*, 410.
- (19) Brown, R. E.; Singer, L. A.; Parks, J. H. *Chem. Phys. Lett.* **1972**, *14*, 193.
- (20) Matthews, A. C.; Sakurovs, R.; Ghiggino, K. P. *J. Photochem.* **1982**, *19*, 235.
- (21) Castel, N.; Fischer, E. J. *Mol. Struct.* **1985**, *127*, 159.

RECEIVED for review February 24, 1987. Accepted June 25, 1987. This work was supported by NSF Grant CHE 84-00706.

Photoacoustic Immunoassay Using Sensitivity Size Dependency for Determination of Turbid Solutions

Takehiko Kitamori* and Kazumichi Suzuki

Energy Research Laboratory, Hitachi, Ltd., Hitachi, Ibaraki 316, Japan

Tsuguo Sawada and Yohichi Gohshi

Department of Industrial Chemistry, Faculty of Engineering, University of Tokyo, Bunkyo-ku, Tokyo 113, Japan

A remarkable size dependency for sensitivity, which was considered to originate in dependence on absorption cross section, was observed in determinations with photoacoustic spectroscopy on 0.1–5.0 μm uniform polystyrene latex turbid solutions. A resonant increase in sensitivity appeared at a cross-sectional size coinciding with the excitation beam wavelength. Photoacoustic immunoassay using the size dependency of sensitivity was proposed. In this method, antibody/antigen coated latex particles agglutinated due to an immunoreaction and the size of the agglutinations were controlled to be the same as the excitation wavelength. The agglutinations in a mixture of unreacted latex particles were selectively determined by photoacoustic spectroscopy and the antigen/antibody concentration was obtained. With a rheumatoid factor and denaturated γ -globulin coated 0.2- μm polystyrene latex particles, the principle behind photoacoustic immunoassay was proved and a determination limit of 9.8×10^{-5} IU/mL was obtained. This value was at least 3 orders better than results obtained by conventional turbidimetry.

Photoacoustic spectroscopy (PAS) has been applied to liquid samples by using a direct coupling method in which a piezoelectric element is directly coupled to the liquid samples

as a sensitive photoacoustic (PA) signal detector (1, 2). This method is quite sensitive for optical absorption and has been applied to trace analysis in parts-per-trillion (pg/mL) to sub-part-per-trillion levels (3, 4). Trace analysis with PAS can be applied not only to true solutions but to turbid and colloidal solutions which are light scattering materials (5, 6). Oda et al. (5) have shown the sensitivity of PAS, that is the slope of the calibration curve, is independent of particle size, because the PA signal magnitude is proportional to the optical energy absorbed by the solution and is not affected by light scattering. They showed that two calibration curves for a precipitated BaSO_4 mixture of 6–20 and 0.5–6 μm particles overlapped each other when the 514.5-nm lasing line of an Ar laser was used for the excitation beam. However, in the present study, a remarkable size dependence of sensitivity is found when the particle size is in a region close to that of the excitation beam wavelength. Reasons that explain both independence and dependence of the sensitivity on size are investigated and reported herein.

On the other hand, the latex agglutination method has been developed to improve the sensitivity of turbidimetric immunological determinations (7). In this method, latex micro-particles which are coated by antibody/antigen are added to the sample, and they agglutinate with each other due to an immunoreaction, allowing the antigen/antibody to be determined on the basis of turbidimetric analysis or particle

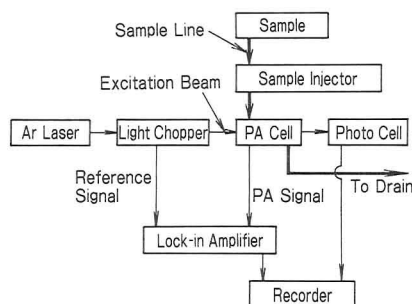


Figure 1. Block diagram of the PAS system.

counting of the agglutinations. The detection limit of this immunoassay method is 2 to 3 orders lower in comparison with the ordinary turbidimetric immunoassay without latex microparticles in which precipitates of antigen-antibody reactants are determined (8). In general, however, the lower determination limit, which is set by the detection limit of the turbidimeter, is still 1 to 2 orders higher than radioimmunoassay (RIA) and enzyme immunoassay (EIA) and is about 2 orders higher than that needed for determination of some kinds of cancer and tumor marker proteins such as carcinoembryonic antigen (CEA) and hormones which are at subnanogram-per-milliliter concentrations (9, 10).

Then, in this report, we propose a photoacoustic immunoassay (PIA) which determines the latex agglutinations with PAS using the sensitivity dependence on particle size. In this novel method, the size of the latex agglutinations is controlled to lie within the highest sensitivity region of PAS. The agglutinations in the mixture of untreated latex microparticles prepared in a nonsensitive size region are selectively determined. The principle of PIA is verified by using the rheumatoid factor (RF) as a sample antigen.

EXPERIMENTAL SECTION

Reagents. All reagents were spectral or biochemical grades. Ultrapurified water was prepared by filtration with reverse osmotic membranes, ion-exchange filters, and membrane filters to remove particulate impurities. Particulate impurities larger than 0.1 μm were almost completely removed. Water conductivity was about 18 M Ω /cm.

Monodispersed polystyrene latex particles of uniform size (0.10, 0.22, 0.33, 0.50, 0.80, 1.0, 2.0, 3.0, and 5.0 μm , Nissin EM Co., Ltd.) were prepared by stepwise dilution from 0.2% (w/w) standard stock solutions. First, the concentration of the samples were roughly diluted to 0.1–1.0 ppb, and then, after filtering 100-mL portions of the respective samples, the exact concentration and particle size of each sample were calibrated by counting and observing particles on the filters through a scanning electron microscope (SEM).

Stock solutions of 21, 42, and 84 IU/mL RF were prepared by dissolving freeze-dried RF into ultrapurified water. (The international unit, IU, for RF is defined by WHO, the World Health Organization. This unit is the measure for activity of immunoreaction and is not related to weight concentration, because the existence ratio of active and nonactive RF is not constant. The quantity of RF in serum of a healthy body is about 10–14 IU/mL (11).) Denaturated γ -globulin coated polystyrene latex particles and glycine buffered saline, which contained bovine serum albumin and Tris buffer, were made up with the "IATROACE RF reagent I" kit (IATRON). Denaturated γ -globulin was used as an antibody of RF in the present experiment, while it is an antigen in a living body. The size of the latex particles was 0.2 μm .

Apparatus. A block diagram of the PAS system is shown in Figure 1. The excitation beam was the 488-nm lasing line of the Ar laser, and the beam power was 1.8 W. The excitation beam was modulated at 181 Hz with a light chopper. The PA cell shown in Figure 2 was a cylindrical direct coupling cell and was a flow type so that the sample could be exchanged easily. However, to reduce the noise level, the PA signal was measured while the flow was stopped. The cell was set in a stainless steel case to shield it from electromagnetic noise sources.

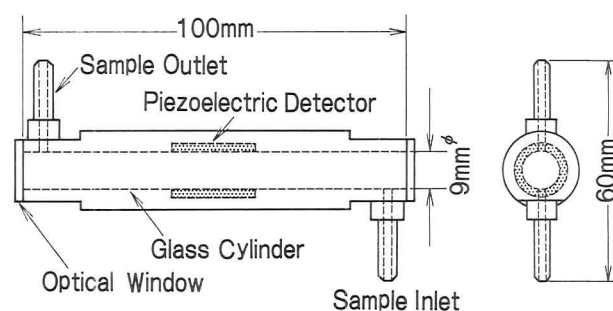


Figure 2. Side and front view of the cylindrical direct coupling PA cell.

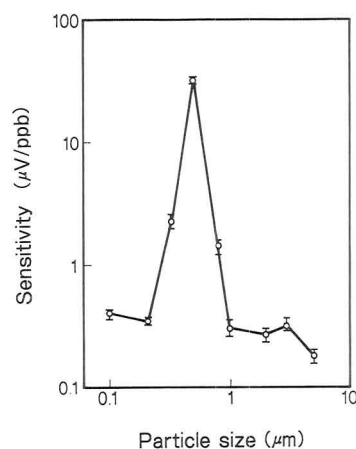


Figure 3. Size dependence of PAS sensitivity. Sensitivity was obtained as the slope of the calibration curves for each size.

A double-beam absorption spectrophotometer was used for turbidimetry.

Procedure 1. For each particle size, the PA signal magnitude at four concentrations of the polystyrene latex turbid solutions in the range of 0.1–1.0 ppb was measured, and calibration curves were obtained as regression lines. The sensitivity of PAS, that is, the slope of the calibration curves, was calculated for each particle size.

Procedure 2. After 3.5-mL portions of glycine buffered saline were added to the RF solutions of 30 μL and a blank solution, they were kept at 37 $^{\circ}\text{C}$ for 5 min, and a 1-mL portion of 0.03% (w/w) polystyrene latex particle reagent was added to each solution. The immunoreaction progressed sufficiently at the chosen temperature after an additional 5 min. After the immunoreaction, each solution was diluted by 1/20000, resulting in agglutination turbid solutions corresponding to RF concentrations of 10^{-3} IU/mL. The calibration curve of RF was subsequently obtained by PAS.

Turbidity of the agglutination turbid solutions for which RF concentration was of 10^{-1} IU/mL order was measured with a double-beam spectrophotometer.

RESULTS AND DISCUSSION

The size dependence of sensitivity obtained by procedure 1 is shown in Figure 3. The error bars were statistically obtained as the standard deviations for the determination of the particle number densities by SEM observation. The sensitivity remarkably depends on the size between 0.3 and 0.8 μm , while such behavior is not conspicuous below 0.2 μm or above 1.0 μm . The maximum sensitivity appears at 0.5 μm where the particle size coincides with the excitation beam wavelength.

The physical meaning of this size dependence of the sensitivity is not clear at present. However, it seems to be caused by a size dependence of the absorption cross section of the particles, which is due to dielectric loss accompanied by light scattering. Figure 4 shows the size dependence of the PA signal magnitude per one particle, which is obtained by dividing the experimental values in Figure 3 by the particle

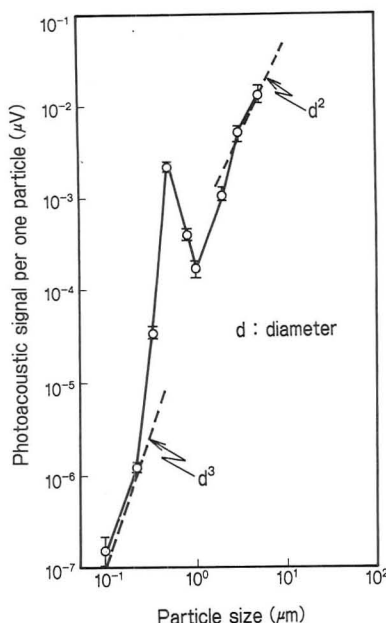


Figure 4. Size dependence of the PA signal magnitude per one particle. The signal magnitude was proportional to the absorbed optical energy; hence the vertical axis was proportional to the absorption cross section of the particles.

number in 1 ppb polystyrene turbid solutions of corresponding sizes. The error bars also indicate statistical error as shown in Figure 3. The PA signal magnitude per one particle is proportional to the absorbed optical energy per one particle, that is, the absorption cross section of the particles. For particle sizes below $0.2 \mu\text{m}$ in Figure 4, the PA signal per one particle is proportional to the third power of the size. This corresponds to the dependence of the absorption cross section on the volume of the scattering body, which is described by using Rayleigh's approximation for a scattering body small compared to the wavelength (12). In the particle size region between 0.3 and $0.8 \mu\text{m}$, the PA signal magnitude varies and it has a peak at the particle size coinciding with the wavelength of the excitation beam. This behavior seems to show a change in absorption cross section to accompany resonance scattering (13) which appears in the particle size region near the excitation beam wavelength. Beyond $1.0 \mu\text{m}$, the PA signal magnitude per one particle asymptotically approaches a quadratic dependence on the particle size. This tendency shows the size dependence of the absorption cross section to accompany light scattering by a particle large compared to the wavelength of the excitation beam. In this size region the absorption cross section is proportional to the geometrical cross section of the scattering body (14). Therefore, from these characteristics of the PA signal magnitude per one particle, the physical meaning of the size dependence of the sensitivity shown in Figure 3 is considered to originate in the size dependence of the absorption cross section of the particles. Further theoretical and quantitative discussion on this size dependence of the sensitivity based on Mie scattering theory will be presented in a subsequent report.

From the above discussion, the following inference can be drawn. A particulate sample has two types of optical absorption. The first is a photon absorption process based on excitation between electronic energy states. This absorption process is unique for the material and is identical for both bulk and particulate states. Hence, the quantity of absorbed optical energy is proportional to the quantity of material in the medium, that is, the material concentration, and the absorbance of the turbid solution is independent of size. The second absorption process is the absorption of the excitation beam as an electromagnetic wave due to dielectric loss accompanied

by light scattering. This process is unique for particulate samples. Most of the optical energy absorbed by both processes is converted to thermal energy and it contributes to generation of PA signals. Under the experimental conditions used by Oda et al. (5), the size of the BaSO_4 precipitates was several times larger than the excitation beam wavelength, and optical absorption of the first type was considered to be dominant. Hence it was stated that sensitivity of PAS for BaSO_4 turbid solutions was independent of size. On the other hand, under the present experimental conditions, optical absorption of the second type is dominant, and PAS sensitivity remarkably depends on size.

By use of the size dependence of sensitivity shown in Figure 3, microparticles for which the size coincides with the wavelength of the excitation beam can be specifically determined with PAS. In the present application of this determination method to immunoassay, latex particle agglutinations of about $0.5 \mu\text{m}$, which are in a mixture of unreacted $0.2\text{-}\mu\text{m}$ latex particles and variously sized agglutinations, are selectively determined. The calibration curve obtained with procedure 2 shows a good linearity for RF concentrations of 1.1×10^{-3} , 2.1×10^{-3} , and 4.2×10^{-3} IU/mL and the blank. The determination limit of RF, defined as double the standard deviation, is obtained as 9.8×10^{-5} U/mL. The coefficient of the relative standard deviation is 0.6% at 1.1×10^{-3} IU/mL for three determinations; hence the reproducibility is confirmed. On the other hand, the determination limit obtained with turbidimetry is 1.6×10^{-1} IU/mL. Therefore, RF can be determined with PIA and the determination limit is at least 3 orders lower than that of the conventional immunoassay using turbidimetry with the latex agglutination method. Further, from the obtained results, PIA is expected to be roughly 1 to 2 orders more sensitive than RIA and EIA (15, 16), and it is anticipated as being applicable to determination for trace tumor and cancer marker antigens, such as α -fetoprotein, basic protein, and CEA (17–21). In addition, no unsealed radioisotopes are used in PIA, and this is advantageous for medical mass screening.

In this report, the possibility of PIA was demonstrated with samples prepared with 20000 dilutions. However, though the lower limit of the determination depends highly on the background levels in the ultrasensitive determination with PAS (4), suppression of the background originating in unreacted latex particles was not examined in the present immunoassay procedure based on a prescription for turbidimetry with a spectrophotometer. In the present experiments, the background level of $8.4 \mu\text{V}$ was a relatively large value in comparison with the slope of the calibration curve $0.42 \mu\text{V}/(10^{-3} \text{ IU/mL})$, even though $0.42 \mu\text{V}$ was distinguishable from the noise level, 4 nV , of the present PAS system (3). Therefore, further study for background reduction by optimizing the immunoassay procedure, applying a double-beam method (22), developing a selective filtration technique of unreacted particles, etc., will be required before the practical application of PIA to clinical examinations is possible.

ACKNOWLEDGMENT

The authors are pleased to acknowledge K. Yasuda, Y. Nomura, and M. Hayashi of Naka Works, Hitachi, Ltd., for sample preparations and useful discussions.

LITERATURE CITED

- (1) Lahmann, W.; Ludewig, H.; Welling, H. *Anal. Chem.* **1977**, *49*, 549.
- (2) Oda, S.; Sawada, T.; Kamada, H. *Anal. Chem.* **1978**, *50*, 865.
- (3) Kitamori, T.; Fujii, M.; Sawada, T.; Gohshi, Y. *J. Spectrosc. Soc. Jpn.* **1985**, *34*, 359.
- (4) Kitamori, T.; Suzuki, K.; Sawada, T.; Gohshi, Y.; Motojima, K. *Anal. Chem.* **1986**, *58*, 2275.
- (5) Oda, S.; Sawada, T.; Moriguchi, T.; Kamada, H. *Anal. Chem.* **1980**, *52*, 650.
- (6) Nomura, M.; Oda, S.; Sawada, T. *J. Photoacoust.* **1982**, *1*, 121.
- (7) Singer, J. M.; Plotz, C. M. *Am. J. Med.* **1956**, *21*, 888.

- (8) Cambiaso, C. L.; Leek, A. E.; De Steenwinkel, F. J. *Immunol. Methods* **1977**, *18*, 33.
 (9) Hirai, H.; *Cancer Res.* **1977**, *37*, 2267.
 (10) Albertsen, P. C.; Chang, T. S. K. *J. Clin. Immunoassay* **1983**, *6*, 51.
 (11) Anderson, S. G.; Bentzon, M. W.; Houba, V.; Krag, P. *Bull. W. H. O.* **1970**, *42*, 311.
 (12) See, for example, Landau, L. D.; Lifshitz, E. M. *Electrodynamics of Continuous Media*; Sykes, J. B., Bell, J. S. Translators; Pergamon: New York, 1960; p 303.
 (13) Van de Hulst, H. C. *Light Scattering by Small Particles*; Wiley: New York, 1957; p 267.
 (14) Van de Hulst, H. C. *Light Scattering by Small Particles*; Wiley: New York, 1957; p 110.

- (15) Addison, G. M. *J. Clin. Pathol.* **1972**, *39*, 326.
 (16) Asakawa, H.; Mori, W. *J. Jpn. Soc. Clin. Pathol.* **1984**, *32*(suppl), 347.
 (17) Nishi, S.; Hirai, H. *Gann Monogr. Cancer Res.* **1973**, *14*, 79.
 (18) Ishii, M. *Scand. J. Immunol.* **1978**, *8*(suppl. 8), 611.
 (19) Gold, P.; Freedman, S. O. *J. Exp. Med.* **1965**, *121*, 439.
 (20) Hirai, H. *Cancer Res.* **1977**, *37*, 2267.
 (21) Kodama, T. *Cancer* **1979**, *44*, 661.
 (22) Sawada, T.; Oda, S. *Anal. Chem.* **1981**, *3*, 539.

RECEIVED for review February 9, 1987. Accepted June 30, 1987.

Improvement in the Definitions of Sensitivity and Selectivity

Gerhard Bergmann, Birgit von Oepen, and Peter Zinn*

Lehrstuhl fuer Analytische Chemie, Ruhr-Universitaet Bochum, 4630 Bochum 1, West Germany

New definitions of sensitivity and selectivity of a multicomponent analysis are presented. An algorithm is developed that relates analytical precision to the noise of the measured spectra, provided that the corresponding sensitivities and selectivities are known. These expressions are derived from a system of linear equations by using the Gaussian rule of error propagation. The algorithm allows for prediction of the standard deviation of concentrations in multicomponent analysis. The new definitions are confirmed by simulated spectra and by IR spectrometric investigations.

There are different mathematical approaches for spectroscopic multicomponent analysis. Some of these methods are difference spectroscopy, factor analysis and regression methods (1-3).

The selection of analytical wavelengths becomes more and more important in the case of overdetermined systems. One criterion for wavelength selection is the selectivity (4, 5). Expressions like selectivity, sensitivity, detection limit, and precision are defined by Kaiser (6). Junker and Bergmann use distension and sensitivity as criteria for wavelength selection (9). Other authors describe the use of selectivity and related criteria for evaluating analytical procedures (5, 7, 8).

The method described in this article makes the attempt to predict statistical expressions like the standard deviation of the concentration by knowledge of functional expressions like sensitivity and selectivity.

THEORY

Precision, sensitivity, and selectivity are important criteria for evaluating an analytical method. The precision of an analytical method can be expressed in terms of the standard deviation $\sigma(c_k)$ with respect to the concentration c_k of component k . The standard deviation will increase with the noise of the analytical signal. It will decrease with growing sensitivity of the method with respect to the components. Kaiser (6) defined the sensitivity H_{ik} of component k at wavelength i as a partial differential quotient of the absorbance y_i and β_k , where β_k is the product of c_k and the cell path length l .

According to Beer's law the sensitivity becomes

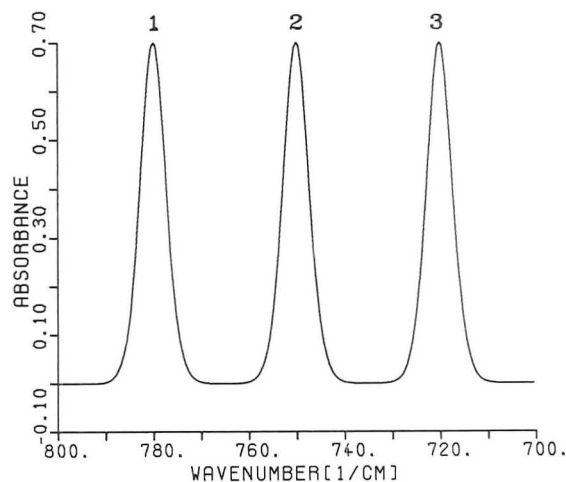


Figure 1. Three-component system, $\bar{\epsilon}_1 = \bar{\epsilon}_2 = \bar{\epsilon}_3 = 1.0$.

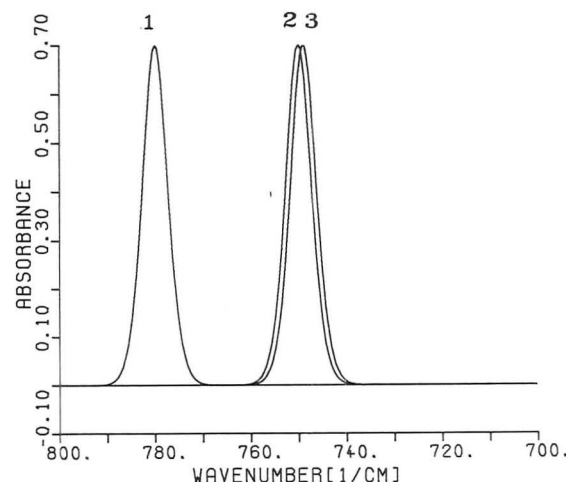


Figure 2. Three-component system, $\bar{\epsilon}_3 = \bar{\epsilon}_2 = 0.26$ and $\bar{\epsilon}_1 = 1.0$.

$$H_{ik} = \partial y_i / \partial \beta_k = x_{ik}$$

In this case the sensitivity is equal to the molar absorption coefficient x_{ik} . For multicomponent analysis Kaiser defined

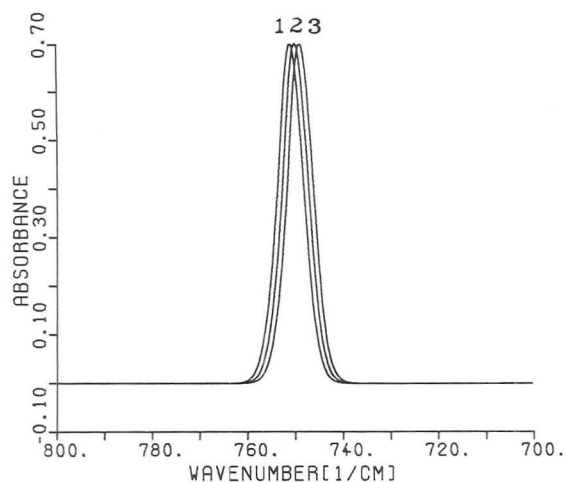


Figure 3. Three-component system, $\bar{\epsilon}_1 = \bar{\epsilon}_3 = 0.098$ and $\bar{\epsilon}_2 = 0.070$.

the total sensitivity H_T as the determinant of the design matrix \mathbf{X} .

$$H_T = \det \mathbf{X}$$

Modifications to this definition of the total sensitivity have been presented by Junker and Bergmann (9), including one that allows for overdetermined measurements

$$H_T = (\det \mathbf{X}^T \cdot \mathbf{X})^{1/2}$$

where \mathbf{X}^T is the transpose of \mathbf{X} .

In multicomponent analysis the standard deviation is also affected by the selectivity $\bar{\epsilon}$ of one component with regard to the others. Kaiser defined the selectivity $\bar{\epsilon}$ as the minimal ratio of the sensitivity of one component to the sum of the others.

$$\bar{\epsilon} = \min_{i=1 \dots n} \frac{|H_{ii}|}{\sum_{k=1}^n |H_{ik}| - |H_{ii}|} - 1$$

Additionally Zinn (10) proposed the definition of partial sensitivities and partial selectivities. According to his definition partial sensitivity H_k of component k summarizes the sensitivities of one component at each analytical wavelength i . Partial selectivity $\bar{\epsilon}_k$ is a comprehensive expression that describes the selectivity of the component k at each analytical wavelength according to the other components. As a result the analytical error of each component depends on the partial sensitivity, selectivity, and the noise of the measured signal.

NEW DEFINITIONS OF SENSITIVITY AND SELECTIVITY

One condition for spectroscopic multicomponent analysis is the additivity of absorbance according to Beer's law. For a multicomponent system Beer's law may be expressed in matrix form:

$$\mathbf{Y} = \mathbf{X} \cdot \beta$$

with \mathbf{Y} = vector of measured signals, \mathbf{X} = matrix of absorption

Table I. Comparison of the Experimental and Estimated Analytical Error of Simulated Two-Component Systems (Component 1 = ν_1 , ν_2 ; Component 2 = ν_3) with Variable Selectivities and Sensitivities

	wavenumber, cm ⁻¹	$\bar{\epsilon}_k$	H_k , L/(mol·cm)	10 ⁴ $\sigma(c_k)$, mol/L		$\sigma(c_k)_{\text{exptl}} / \sigma(c_k)_{\text{est}}$
				exptl	est	
ν_1	810	1.0	3695	0.818	1.156	0.708
ν_2	780					
ν_3	750	1.0		1.617	1.798	0.899
ν_1	810	0.999	3695	1.351	1.162	1.162
ν_2	780					
ν_3	770			1.942	1.662	1.165
ν_1	810	0.936	3695	0.987	1.224	0.806
ν_2	780					
ν_3	775			1.046	1.755	0.596
ν_1	810	0.881	3695	1.157	1.375	0.841
ν_2	780					
ν_3	776			2.136	1.971	1.083
ν_1	810	0.705	3695	1.744	1.645	1.060
ν_2	780					
ν_3	778			2.491	2.358	1.056
ν_1	810	0.618	3695	1.305	1.852	0.705
ν_2	780					
ν_3	779			2.724	2.949	0.924
ν_1	800	0.618	3695	2.122	1.955	1.085
ν_2	780					
ν_3	779			3.206	2.803	1.144
ν_1	790	0.620	3771	1.910	1.806	1.058
ν_2	780					
ν_3	779			3.234	2.643	1.224
ν_1	785	0.585	4386	1.480	1.726	0.857
ν_2	780					
ν_3	779			2.466	2.937	0.840
ν_1	782	0.440	4990	2.314	2.015	1.148
ν_2	780					
ν_3	779			4.371	3.903	1.120
ν_1	781	0.357	5111	2.314	2.349	0.985
ν_2	780					
ν_3	779			4.601	4.659	0.987

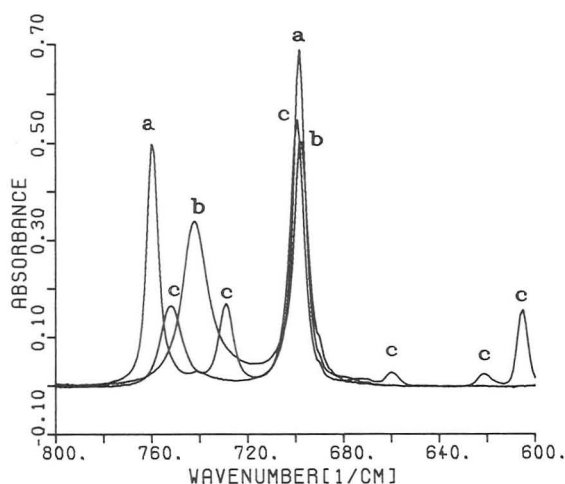


Figure 4. Components of a three-component system with cumene (a), *n*-propylbenzene (b), and triphenylmethane (c).

coefficients, and β = vector of the product of concentrations and cell path length.

Premultiplication of both sides by the transpose of the matrix \mathbf{X} leads to a symmetrical information matrix \mathbf{J} .

$$\mathbf{X}^T \mathbf{Y} = \mathbf{X}^T \mathbf{X} \beta = \mathbf{J} \beta$$

If the formula of the cumulative errors given by Gauss is applied to this system of equations, the standard deviation $\sigma(\beta_k)$ can be computed (11) by the residuals σ_R of the signal vector \mathbf{Y} and the diagonal elements q_{kk} of the covariance matrix $\mathbf{Q} = \mathbf{J}^{-1}$.

$$\sigma(\beta_k) = q_{kk}^{1/2} \sigma_R$$

For a one-component system ($k = 1$) the covariance element q_{kk} becomes

$$q_{11} = \frac{1}{\sum_i x_{i1}^2} = \frac{1}{H_1^2}$$

where $H_1 = (\sum_i x_{i1}^2)^{1/2}$ defines the partial sensitivity. This definition is equivalent to the one developed by Junker and Bergmann for a one-component system.

On the premises that all components contribute additively to the measured absorbance and that the sensitivity of one component is independent of the others, this definition is also valid for multicomponent systems

$$H_k = (\sum_i x_{ik}^2)^{1/2}$$

To split the influence of q_{kk} on the error propagation it is convenient to extend q_{kk} with the partial sensitivity:

$$q_{kk} = \frac{1}{H_k^2} \sum_i x_{ik}^2 q_{kk} = \frac{1}{H_k^2} \frac{1}{\Xi_k^2}$$

where

$$\Xi_k = \frac{1}{(\sum_i x_{ik}^2 q_{kk})^{1/2}}$$

is the definition of the partial selectivity of component k in the mixture.

The value of the partial selectivity can vary between 0 and 1. For $\Xi_k = 1$ the evaluation of one component is fully selective. The error in multicomponent analysis corresponds to the error in one-component systems under the same conditions. In the case of $\Xi_k = 0$ the quantitative determination of the concentration of component k is impossible. The information matrix \mathbf{J} is singular. In this case the spectrum of

Table II. Comparison of the Experimental and Estimated Analytical Error of Simulated Three-Component Systems with Variable Selectivities

		wavenumber, cm ⁻¹	Ξ_k	10 ⁴ $\sigma(c_k)$, mol/L		$\sigma(c_k)_{\text{exptl}} / \sigma(c_k)_{\text{est}}$
				exptl	est	
a	ν_1	810	1.0	4.119	3.847	1.077
	ν_2	780	1.0	1.878	1.924	0.976
	ν_3	750	1.0	1.846	1.924	0.959
b	ν_1	790	0.999	4.660	4.042	1.158
	ν_2	780	0.999	2.274	2.012	1.15
	ν_3	750	1.0	2.107	2.010	1.048
c	ν_1	785	0.902	4.567	4.445	1.027
	ν_2	780	0.902	2.300	2.223	1.034
	ν_3	750	1.0	2.247	2.004	1.121
d	ν_1	783	0.678	6.066	5.725	1.060
	ν_2	780	0.678	3.010	2.863	1.052
	ν_3	750	1.0	1.744	1.942	0.898
e	ν_1	781	0.259	15.753	15.032	1.048
	ν_2	780	0.259	7.961	7.516	1.059
	ν_3	750	1.0	1.942	1.945	0.998
f	ν_1	781	0.258	16.785	15.334	1.095
	ν_2	780	0.258	8.557	7.672	1.115
	ν_3	770	0.996	1.926	1.985	0.970
g	ν_1	781	0.226	17.705	17.439	1.015
	ν_2	780	0.214	9.462	9.214	1.027
	ν_3	775	0.787	2.403	2.503	0.960
h	ν_1	781	0.176	28.515	23.848	1.195
	ν_2	780	0.147	17.108	14.303	1.196
	ν_3	777	0.462	5.021	4.550	1.104
i	ν_1	781	0.099	40.104	43.982	0.912
	ν_2	780	0.051	38.103	41.731	0.913
	ν_3	779	0.099	20.364	21.990	0.926

the component k is very similar to the second or to a linear combination of the other components.

In general the following equation is valid for multicomponent analysis in spectroscopy. According to Beer's law the relation between the standard deviation of the concentration $\sigma(c_k)$ and the residuals σ_R of the absorbance vector is

$$\sigma(c_k) = \frac{1}{l} \frac{1}{H_k} \frac{1}{\Xi_k} \sigma_R$$

This equation is satisfied on the assumption that Beer's law is valid, that all components contribute additionally to the measured signal, that the noise of the analytical signal is constant at all wavelengths, and that there is no base-line shift.

In the case of two- and three-component systems partial selectivities Ξ_1^{II} and Ξ_1^{III} with respect to component 1 can be expressed as

$$\Xi_1^{\text{II}} = (1 - r_{12}^2)^{1/2}$$

$$\Xi_1^{\text{III}} = \left(\frac{1 - r_{12}^2 - r_{13}^2 - r_{23}^2 + 2r_{12}r_{13}r_{23}}{1 - r_{23}^2} \right)^{1/2}$$

with

$$r_{kj} = \frac{\sum_i x_{ik} x_{ij}}{(\sum_i x_{ik}^2 \sum_i x_{ij}^2)^{1/2}} = \text{correlation between}$$

absorption coefficients of k with j

Figures 1–3 show simple three-component systems, which serve to illustrate the formula for the partial selectivity. Similar problems are often investigated in practice. In the case of Figure 1 the bands of the components do not overlap.

Table III. Comparison of the Experimental and Estimated Analytical Error of Simulated Four-Component Systems with Variable Selectivities

		wavenumber, cm ⁻¹	Ξ_k	10 ⁴ $\sigma(c_k)$, mol/L		$\sigma(c)_{\text{exptl}}/\sigma(c)_{\text{est}}$
				exptl	est	
a	ν_1	830	1.0	1.599	2.147	0.744
	ν_2	790	0.999	1.258	1.213	1.037
	ν_3	760	0.999	1.395	1.237	1.128
	ν_4	730	1.0	2.833	2.451	1.156
b	ν_1	830	1.0	2.491	2.033	1.225
	ν_2	790	0.998	1.258	1.150	1.093
	ν_3	770	0.998	1.157	1.172	0.987
	ν_4	740	1.0	2.366	2.320	1.019
c	ν_1	830	1.0	1.744	2.165	0.846
	ν_2	790	0.579	1.926	2.111	0.912
	ν_3	785	0.579	1.942	2.152	0.902
	ν_4	755	1.0	2.539	2.471	1.028
d	ν_1	820	0.999	2.206	2.090	1.055
	ν_2	790	0.579	2.340	2.039	1.148
	ν_3	785	0.579	2.327	2.078	1.119
	ν_4	755	1.0	2.668	2.386	1.118
e	ν_1	810	0.998	2.220	2.002	1.108
	ν_2	790	0.578	1.795	1.953	0.919
	ν_3	785	0.479	1.878	1.990	0.944
	ν_4	755	1.0	2.366	2.283	1.036
f	ν_1	800	0.811	1.926	2.447	0.787
	ν_2	790	0.471	1.709	2.379	0.718
	ν_3	785	0.511	1.709	2.230	0.766
l	ν_4	755	1.0	2.063	2.266	0.910
g	ν_1	795	0.328	5.278	6.581	0.802
	ν_2	790	0.199	5.120	6.119	0.837
	ν_3	785	0.295	3.658	4.215	0.868
	ν_4	755	1.0	2.746	2.467	1.113
h	ν_1	792	0.329	6.166	6.168	1.000
	ν_2	790	0.168	7.299	6.848	1.066
	ν_3	788	0.247	5.358	4.730	1.133
	ν_4	758	1.0	2.429	2.381	1.047
i	ν_1	791	0.318	6.111	6.260	0.976
	ν_2	790	0.203	5.515	5.527	0.998
	ν_3	789	0.204	5.024	5.608	0.896
	ν_4	759	1.0	1.926	2.271	0.848
k	ν_1	791	0.310	6.283	6.955	0.903
	ν_2	790	0.144	7.357	8.477	0.868
	ν_3	789	0.108	10.352	11.548	0.896
	ν_4	788	0.348	5.955	7.063	0.843

Each band is associated with one component. In Figure 1, the three-component system with one band for each component is fully selective. The correlation coefficient between all bands of the components is 0, and the partial selectivity Ξ_k of each component $\Xi_k = 1$. In Figure 2 the selectivity of component 1 equals 1 and the selectivity of the two other components $\Xi_3 = \Xi_2 = 0.26$. The illustrated system is fully selective for one component and only partially selective for the other components. The last, Figure 3, illustrates the almost complete overlap of the three bands. The partial selectivities of components 1 and 3 are $\Xi_1 = \Xi_3 = 0.098$; the selectivity of component 2, the bands of which are almost completely overlapped, is $\Xi_2 = 0.070$. The shapes of the chosen bands are arbitrary and serve as examples. The definitions of selectivity and sensitivity are not confined to isolated bands and may be applied to any real spectra.

EXPERIMENTAL SECTION

The experiments were carried out with a Perkin-Elmer infrared spectrophotometer, Model 983. KBr plates served as an absorption cell with a cell path length of 100 μm . Cyclohexane served as a solvent for different mixtures of components. The subsequent

Table IV. Concentrations in mol/L of Experimentally Investigated One-, Two- and Three-Component Systems with Cyclohexane as Solvent

One-Component Systems	
cumene	0.2062
<i>n</i> -propylbenzene	0.2164
triphenylmethane	0.0852
Two-Component Systems	
cumene	0.1899, 0.1989
<i>n</i> -propylbenzene	0.0782, 0.2095
toluene	0.1467
phenanthrene	0.0780
Three-Component Systems	
cumene	0.1368
<i>n</i> -propylbenzene	0.1408
triphenylmethane	0.0671
<i>o</i> -xylene	0.1205
<i>m</i> -xylene	0.2576
<i>p</i> -xylene	0.2509

analysis was performed on a Digital Equipment microcomputer, Model PDP 11/34. Furthermore, the simulations of spectra based on Gauss-Cauchy product functions were carried out on the same computer. Spectra of mixtures were generated by adding the spectra of the pure components point by point. The wavenumber range of all investigated spectra was from 800 to 600 cm^{-1} with an interval of 1 cm^{-1} .

SIMULATION OF MULTICOMPONENT ANALYSIS AND EXAMINATIONS OF THE DEVELOPED ALGORITHM

The numerical investigation of the developed algorithm was realized with spectra of two-, three-, and four-component systems. The spectra were generated as mixed Gauss-Cauchy-product functions. The investigated wavenumber section was 800–600 cm^{-1} with a wavenumber interval of 1 cm^{-1} . Noise was added to the simulated spectra by using normally distributed random numbers. The simulation of noisy spectra and the computation of the corresponding concentrations were repeated 50 times to calculate the standard deviation of the concentration $\sigma(c_k)_{\text{exptl}}$. The estimated standard deviation of the concentration $\sigma(c_k)_{\text{est}}$ was determined by using the proposed algorithm. Tables I–III compare the results of the simulations and calculations for two-, three-, and four-component systems.

The sensitivity as well as the selectivity were varied for the simulated spectra. This could be done by decreasing the wavenumber difference between the bands of the components. It can be seen from the tables that the quotient of estimated and experimentally determined standard deviation is about 1 in all cases. Small deviations from the quotient 1 result from the employed noise function. As a result the algorithm seems to be correct. The relation between errors in analysis on the one hand and selectivity, sensitivity, and noise of the analytical signal on the other hand is described correctly. The algorithm allows the prediction of the standard deviation of the concentration in synthetic multicomponent systems.

EXAMPLES OF EXPERIMENTALLY INVESTIGATED MULTICOMPONENT SYSTEMS

One-, two-, and three-component systems were investigated for verifying the practicability of the developed algorithm for real multicomponent systems. Solutions of cumene, *n*-propylbenzene, and triphenylmethane formed the compounds of three one-component (Figure 4) systems. The two-component systems consisted of different concentrations of cum-

Table V. Comparison of the Experimental and Estimated Analytical Error of Experimentally Investigated Multicomponent Systems

	σ_R	H_k , L/(mol-cm)	Ξ_k	$10^4 \sigma(c_k)$, mol/L		$\sigma(c_k)_{\text{exptl}} / \sigma(c_k)_{\text{est}}$
				exptl	est	
One-Component Systems						
cumene	0.002 25	634	1.0	6.1	3.5	1.7
<i>n</i> -propylbenzene	0.002 21	574	1.0	7.4	3.9	1.9
triphenylmethane	0.001 65	1626	1.0	2.9	1.0	2.9
Two-Component Systems						
cumene	0.002 75	634	0.746	6.2	5.8	1.1
<i>n</i> -propylbenzene	0.002 75	574	0.746	8.0	6.4	1.3
cumene	0.002 52	634	0.746	6.4	5.3	1.2
<i>n</i> -propylbenzene	0.002 52	574	0.746	9.5	5.9	1.6
toluene	0.005 8	1388	0.989	21.4	4.2	5.1
phenanthrene	0.005 8	3084	0.989	6.3	1.9	3.3
Three-Component Systems						
cumene	0.002 0	634	0.631	13.7	5.0	2.7
<i>n</i> -propylbenzene	0.002 0	574	0.634	8.4	5.5	1.5
triphenylmethane	0.002 0	1627	0.549	9.0	2.2	4.0
<i>o</i> -xylene	0.005 9	1539	0.999	8.4	3.8	2.2
<i>m</i> -xylene	0.005 9	916	0.999	17.2	6.4	2.7
<i>p</i> -xylene	0.005 9	988	0.999	19.3	6.0	3.2

ene and *n*-propylbenzene and also toluene and phenanthrene. Cumene, *n*-propylbenzene, and triphenylmethane as well as *o*-, *m*-, and *p*-xylol served as compounds of three-component systems. Cyclohexane served as the solvent in all cases. Table IV shows the concentrations of the investigated multicomponent systems. The mixtures cover a selectivity range of 0.5–1.0. Measurements were repeated 15 times. The evaluation was carried out in the same way as for the simulated spectra. Table V describes a part of the results. It shows that even for experimental investigations the estimated analytical error is within the same order of magnitude. In all cases the estimated analytical error $\sigma(c_k)_{\text{est}}$ seems to be smaller than the experimental analytical error $\sigma(c_k)_{\text{exptl}}$. This is expected, because the postulated constancy of σ_R is not satisfied in practice. σ_R is a function of the wavenumber, so that $\sigma(c)_{\text{exptl}}$ is increased by systematic errors. Nevertheless it may be stated that the estimated standard deviation $\sigma(c_k)_{\text{est}}$ can be seen as the lowest limit for the experimentally verified analytical error under given experimental conditions.

The theoretical correlation does not account for base-line shift, calibration errors, and any chemical interfering between the components, solvent effects, etc. These systematic effects

add also to the standard deviation $\sigma(c_k)_{\text{exptl}}$. In general it may be said that the more scrupulously the analysis and calibration are performed, the more accurately the analytical error can be predicted.

LITERATURE CITED

- (1) Antoon, M. K.; Esposito, L. D.; Koenig, J. L. *Appl. Spectrosc.* **1979**, *33*, 351–357.
- (2) Rasmussen, G. T. *Anal. Chim. Acta* **1978**, *103*, 2–3.
- (3) Brown, C. W.; Koenig, J. L. *Anal. Chem.* **1982**, *54*, 1472–1479.
- (4) Ebel, S.; Glaser, E.; Abdulla, S.; Steffens, U. *Fresenius' Z. Anal. Chem.* **1982**, *313*, 24–27.
- (5) Boef, G. D.; Haloricki, A. *Pure Appl. Chem.* **1983**, *55*(3), 553–558.
- (6) Kaiser, H. *Fresenius' Z. Anal. Chem.* **1972**, *260*, 252–260.
- (7) Fujiwara, K.; McHard, J. A.; Foulk, S. J.; Bayer, S. *Can. J. Spectrosc.* **1983**, *25*, 18.
- (8) Frans, S. D.; Harris, J. M. *Anal. Chem.* **1985**, *57*, 2680–2684.
- (9) Junker, A.; Bergmann, G. *Fresenius' Z. Anal. Chem.* **1974**, *272*, 267–275.
- (10) Zinn, P. Dissertation, Bochum, 1979.
- (11) Draper, N.; Smith, H. *Applied Regression Analysis*; Wiley: New York, 1981.

RECEIVED for review December 29, 1986. Accepted July 1, 1987.

Parametric Mode Operation of a Hyperbolic Penning Trap for Fourier Transform Mass Spectrometry

D. L. Rempel, E. B. Ledford, Jr., S. K. Huang, and M. L. Gross*

Department of Chemistry, University of Nebraska, Lincoln, Nebraska 68588

The first known use of a parametrically excited hyperbolic Penning trap (cell) in Fourier transform mass spectrometry is described in this paper. The use of this trap builds upon the cylindrical cell of Lee, Wanczek, and Hartmann in which symmetry was used to solve a problem, namely, that of magnetron sidebands in the mass spectrum. Some of the symmetries of the hyperbolic Penning trap are reviewed en route to developing a mass calibration law, which is fundamentally different than the cubic trap mass calibration law. The calibration law is tested at a magnetic field of 1.2 T by using 1,1,1,2-tetrachloroethane major fragment ions and a new pulse excitation method. The results of a comparison with a similar experiment for the cubic trap show a reduced sensitivity to space charge effects. Other advantages and some disadvantages of the hyperbolic Penning trap that are discussed are high order harmonic-free spectra, low ion cloud distortion, image charge displacement sensitivity to magnetron radius, and pulse excitation induced *z*-mode ejection.

The first experimental demonstration of Fourier transform mass spectrometry (FTMS) was performed with a static ion trap (cell) of rectangular geometry (1). The static ion traps employed in FTMS make use of static electric and magnetic fields according to a principle first exploited by Penning (2) and are to be distinguished (3) from the Paul trap (4), which uses an inhomogeneous rf electric field for ion confinement. The conceptual simplicity of rectangular cells, particularly those of cubic geometry (5), and the ease with which they are constructed have led to their widespread use in FTMS. The conceptual simplicity, however, is superficial; the physics of rectangular analyzer cells is actually quite complicated. The rotation frequency of an ion is known to vary with position inside any static ion trap with planar electrodes (6-10). This is a feature not anticipated by the often used idealized ion motion equations that are based on the assumption that the electric trapping fields are quadrupolar. Also, it has been observed that space charge effects in cubic cells degrade mass measurement accuracy (11).

Alternate cells have been designed with the purpose of achieving improved performance. One example is the rectangular cell introduced by Hunter, Sherman, and McIver (12). This cell, which is used with a superconducting solenoid magnet, is elongated in the direction of the magnetic field. The result is less perturbation of ion frequency associated with electric trapping fields and a larger storage volume for ions compared to the cubic cell.

A different approach to cell design was described by Lee, Wanczek, and Hartmann (13). They constructed a three-electrode cylindrical cell with an off-center electron beam for the purpose of suppressing sidebands in ion resonance mass spectra. The salient features of this design are cylindrical symmetry about the *z*-axis (parallel to the magnetic field) and excitation and trapping fields that have identical spatial forms. Their effort represents an attempt to improve performance

by introducing a greater degree of symmetry into the cell design. However, the use of flat trapping plates causes ion rotation frequency to vary with ion position in the cell. This problem can be avoided if the trap electrodes are designed to produce accurately the ideal quadrupolar electric trapping field. This can be accomplished through the use of electrodes that are hyperbolas of revolution consisting of two "end caps" and one "ring" electrode (see Figure 1A). Such a cell was described by Byrne and Farago (14).

One way to adapt a hyperbolic cell geometry to the FTMS experiment is to cut the ring electrode into quadrants, as was done by Van Dyck and Schwinberg to measure cyclotron frequencies of protons and electrons (15). In this configuration, the quadrants of the ring electrode function in a manner analogous to that of the excitation and receiver plates of a cubic cell. However, the "antenna fields" in this cell are not simple. Closed form solution of the frequency/mass relation is possible only by considering the fundamental harmonic of the charge displacement (*vide infra*), as is the case for the cubic trap. Furthermore, the charge displacement is expected to be dependent on ion position in a fashion similar to that of the cubic cell (16).

In this paper we describe a new use for a hyperbolic cell incorporating features that avoid the segmenting of the ring electrode. This is accomplished by combining the hyperbolic cell geometry and the ion formation/excitation scheme of Lee, Wanczek, and Hartmann (13). In this configuration, the electron beam is offset from the center of the cell because ions formed along the *z* axis cannot be excited in a cell comprised of either an unsegmented hyperbolic or a cylindrical ring electrode. The cyclotron modes of ions offset from the *z* axis are excited by applying the appropriate excitation waveform between the ring and end caps, using a bridge circuit similar to that of McIver's (17) (see Figure 1). After the excitation, the ion image current induced on the ring electrode is detected.

Ion excitation in this hyperbolic cell is fundamentally different than excitation in rectangular cells. Because the excitation waveform is superimposed on the trapping voltage, a term that is regarded as a *parameter* of the system, the excitation can be termed *parametric* (18). As will be apparent from the discussion of the equations describing ion motion during excitation, the excitation modulates the coefficient of a term containing dependent variables. The superposition of excitation and trapping voltages simply multiplies the ion position coordinates, and as a result, the system of equations is linear but *not* generally time invariant (19). On the other hand, the excitation voltage for rectangular cells appears in a forcing term of the *idealized* equations of motion, and this term does not depend on the ion position. For rectangular cells, the idealized system of equations is linear and time invariant, but as implied earlier, the idealized system of equations may not be adequate for demanding experiments.

After the excitation, the system equations are time invariant as well as linear if the hyperbolic ring electrode is at ground potential (see Theory). Thus, the equations of motion for ions in the hyperbolic cell and in the idealized cubic cell are essentially the same. Because a characteristic equation for the

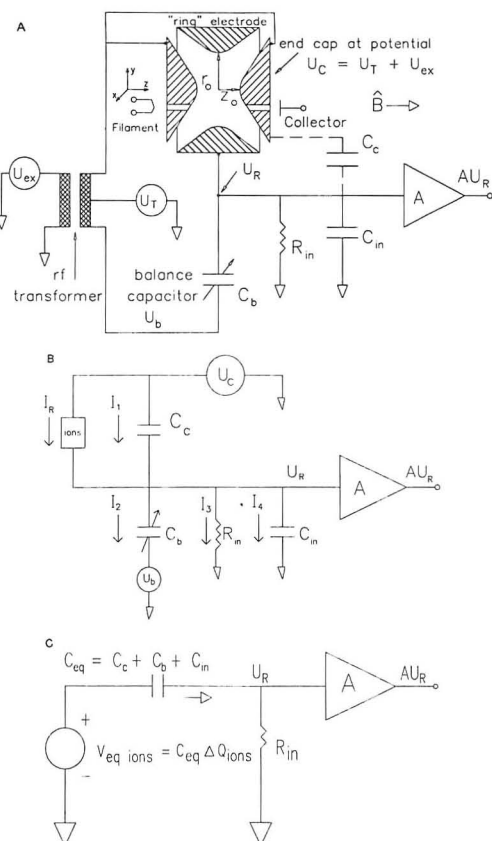


Figure 1. A. Hyperbolic penning trap imbedded in a balanced bridge network. B. Schematic abstracted from Figure 1A to a form suitable for signal analysis. C. Thevenin equivalent of B with the balance condition $I_1 = I_2$. The schematic shows the ion signal as an equivalent voltage $V_{eq\ ions}$.

ion frequencies can be written without regard for the initial condition of the ion trajectory, the ion mode frequencies in both hyperbolic and idealized cubic cells are independent of the location of the ion in the trap.

We also present in this paper the derivation of the calibration law for assigning masses of ions in a hyperbolic cell operated in the parametric excitation mode. Unlike the derivation of the mass calibration law for the cubic cell, the relation between ion motion frequencies and the induced image current frequencies for the hyperbolic cell must be incorporated explicitly. This occurs because these two frequencies are different in the hyperbolic cell. For rectangular cells, the connection between ion motion and image current is usually taken for granted, and the image current frequencies are taken to be identical with the ion motion frequencies. We find that calculations are simplified if the image charge displacement is considered in lieu of the image current. The relationship of the image charge displacement and the preamplifier input voltage can be understood by considering the Thevenin equivalent of the circuit seen by the preamplifier input. The initial and final points of the derivation of the equivalent circuit are given in parts B and C, respectively, of Figure 1 for the convenience of the interested reader.

The use of the hyperbolic trap as reported here has a number of symmetries that are not found in other traps including the cylindrical cell described by Lee, Wanczek, and Hartmann (13). (Recall that the term symmetry denotes invariance with respect to a transformation that can be other than geometrical.) These symmetries result from the identical spatial forms of the excitation and trapping fields (as also applies to the cell described in ref 13) and the linear spatial dependence of these fields. These symmetries are identified in this paper (see Theory).

Finally, we present an experimental test of the mass calibration law and show that parts per million errors are obtained and, more importantly, that the errors depend less on space charge in the hyperbolic cell than in the cubic cell (11). The test of the mass calibration law was performed with a high amplitude, short duration excitation waveform referred to as a "pulse" in this paper. A second excitation consisting of a fixed frequency waveform turned on for an interval of time was used for another comparison with the cubic cell (20). This second waveform is called "rf burst" in ref 17 and in this paper. These two waveforms are viewed by us as being the most tractable in the parametric excitation of the hyperbolic Penning trap.

THEORY

For the discussion of the theory that is to follow, we shall assume a constant and uniform magnetic field, $\vec{B} = B\vec{k}$, parallel to the z axis of a Cartesian coordinate system. An ion is confined in a Penning trap with electrodes conforming to equipotential surfaces of a quadrupolar potential (eq 1) to give the linear electric field in eq 2. In eq 1 and 2, U_T is the

$$U(x,y,z) = [U_T + U_{ex}(t)](r_0^2 - x^2 - y^2 + 2z^2)/(r_0^2 + 2z_0^2) \quad (1)$$

$$\vec{E}(t) = -\nabla U = 2[U_T + U_{ex}(t)](x\vec{i} + y\vec{j} - z\vec{k})/(r_0^2 + 2z_0^2) \quad (2)$$

trapping potential, $U_{ex}(t)$ is the excitation waveform as a function of time, and r_0 and z_0 are shown in Figure 1A. Also, the unit vectors \vec{i} , \vec{j} , and \vec{k} are in the directions of the x , y , and z axes, respectively. For a discussion of electrode shape, see ref 21. The ion motion is described in the general case (but without consideration for space charge effects or collision damping) by the Lorentz force equation (3) (22) with the ion velocity written out in eq 4. Here, q is the charge on the ion

$$\frac{d\vec{v}}{dt} = \frac{q}{m}[\vec{E}(t) + \vec{v} \times \vec{B}] \quad (3)$$

$$\vec{v} = \frac{dx}{dt}\vec{i} + \frac{dy}{dt}\vec{j} + \frac{dz}{dt}\vec{k} \quad (4)$$

and m is the ion's mass. Implicitly, the virtual ground assumption (17) is taken to be valid insofar as effects due to image charge induced on the trap electrodes do not influence the ion motion.

Now consider the time for which $U_{ex} \neq 0$. This circumstance would be applicable to the excitation and ejection events of the FTMS time sequence. The potential $U(t)$ is separable in that we can write eq 5, where terms are defined by eq 6 and 7. This together with the fact that the magnetic

$$U(t) = U_r(t) + U_z(t) \quad (5)$$

$$U_r(x,y,t) = [U_T + U_{ex}(t)](r_0^2 - x^2 - y^2)/(2z_0^2 + r_0^2) \quad (6)$$

$$U_z(z,t) = [U_T + U_{ex}(t)](2z^2)/(2z_0^2 + r_0^2) \quad (7)$$

field is uniform and parallel to the z axis allows us to rewrite eq 3 as decoupled linear eq 8 and 9. In the absence of space

$$\frac{d^2x}{dt^2} = \frac{q}{m} \left\{ [U_r + U_{ex}(t)][2/(2z_0^2 + r_0^2)]x + B \frac{dy}{dt} \right\} \quad (8)$$

$$\frac{d^2y}{dt^2} = \frac{q}{m} \left\{ [U_r + U_{ex}(t)][2/(2z_0^2 + r_0^2)]y - B \frac{dx}{dt} \right\}$$

$$\frac{d^2z}{dt^2} = \frac{q}{m} \{ [U_T + U_{ex}(t)][-4/(2z_0^2 + r_0^2)]z \} \quad (9)$$

charge effects, the decoupling of the radial motion from the z motion in the general case allows for identical radial ion

trajectories independent of the z motion (as long as the ions do not hit an electrode, of course). This is a symmetry *during the time of excitation* which is not achieved for any other static ion trap configuration known to the authors. Note also, eq 8 and 9 are linear but not generally time invariant since $U_{\text{ex}}(t)$ multiplies x , y , and z .

The hyperbolic Penning trap was analyzed by Byrne and Farago (14) for $U_{\text{ex}} = 0$. This circumstance would be applicable to the detection event of the FTMS experiment time sequence. The linear time invariant system of equations that result have been analyzed numerous times under various conditions (17, 22–29), so we shall simply state the form of the solutions in eq 10 and 11, where r_z , r_c , and r_m are complex

$$z = \text{Re}(r_z e^{\lambda_z t}) \quad (10)$$

$$x + iy = r_c e^{-\lambda_c t} + r_m e^{-\lambda_m t} \quad (11)$$

numbers indicative of the initial z , cyclotron, and magnetron mode displacements, respectively, and $i = (-1)^{1/2}$. The frequencies are given by eq 12 through 14 with symbols defined in eq 15 and 16. The symbol m_c refers to the critical mass

$$\lambda_z = i2[qU_T/m(2z_0^2 + r_0^2)]^{1/2} \quad (12)$$

$$\lambda_c = (i\omega_c/2)(1 + [1 - m/m_c]^{1/2}) \quad (13)$$

$$\lambda_m = (i\omega_c/2)(1 - [1 - m/m_c]^{1/2}) \quad (14)$$

$$\omega_c = qB/m \quad (15)$$

$$m_c/q = B^2(r_0^2 + 2z_0^2)/8U_T \quad (16)$$

(11). Because the equations of motion are linear and time invariant, the unexcited Penning trap exhibits a unique symmetry in comparison to other cells: the frequencies of ion motion are invariant with respect to the initial conditions of the ion trajectory. This fact can also be verified by noting that the solutions for the ion position coordinates given by eq 10 and 11 are parameterized by frequencies in eq 12 through 14, which do not depend on the initial position and velocity of the ion.

The theory for the ion-induced signal for the hyperbolic trap is only slightly more complicated than the simplest rectangular trap signal theory, which uses the infinite parallel receiver plate approximation. From Smythe (30), the charge induced on a conductor by the presence of a charge, q , is given in eq 17, where U'_{ion} is the potential at the position of the charge

$$Q_{\text{ion}} = -q(U'_{\text{ion}}/U) \quad (17)$$

that would occur if the conductor were raised to the potential U' in the absence of the charge. For the ring electrode, the quotient in eq 17 expands as shown in eq 18. The term

$$U'_{\text{ion}}(x,y,z)/U' = (2z_0^2 + x^2 + y^2 - 2z^2)/(r_0^2 + 2z_0^2) \quad (18)$$

“antenna field” as used in this paper is the gradient of this quotient. By noting from the equivalent circuit shown in Figure 1C that only changes in charge are important because the effect of the constant charge component will be filtered out at the preamplifier input, we compute a charge displacement, ΔQ_{ion} , in eq 19 by dropping constant terms that

$$\Delta Q_{\text{ion}}(x,y,z) = q(x^2 + y^2 - 2z^2)/(2z_0^2 + r_0^2) \quad (19)$$

would appear when eq 18 is substituted into eq 17. The sign of ΔQ_{ion} is opposite Q_{ion} to conserve charge in the input circuit. Thus, in Figure 1C, the signal, $V_{\text{eq ion}}$, is given by eq 20. For

$$V_{\text{eq ion}}(x,y,z) = qC_{\text{eq}}[(x^2 + y^2)/(2z_0^2 + r_0^2)] - 2qC_{\text{eq}}z^2/(2z_0^2 + r_0^2) \quad (20)$$

a reasonable design, the time constant, $\tau_{\text{in}} = C_{\text{eq}}R_{\text{in}}$, is large

compared to $1/2\pi f$ for the signal frequencies, f , of interest so that $V_{\text{eq ion}}$ is essentially transmitted to the amplifier without modification. Because z does not appear in the first term with x and y and x and y do not appear in the second term of eq 20 with z , the signal voltage contributions of the radial and z motions are independent of the z and radial displacements, respectively, giving a symmetry unique to this use of the hyperbolic Penning trap.

To obtain a mass-frequency relationship for mass calibration, we substituted the solutions for the ion position coordinates given in eq 10 and 11 into eq 20 and then considered the form of the radial contribution to the signal as given in eq 21, where the most interesting frequency is expanded in

$$x^2 + y^2 = |r_c|^2 + |r_m|^2 + 2\text{Re}(r_m^* r_c e^{-\lambda_c t}) \quad (21)$$

eq 22. In eq 21 and 22, the star denotes complex conjugation.

$$\lambda_s = \lambda_m^* + \lambda_c = i\omega_c[1 - m/m_c]^{1/2} \quad (22)$$

It is important to note in eq 22, the signal frequency, λ_s , is different than the frequency, λ_c , normally associated with the cyclotron motion of the ion. This is different from the case of the cubic trap where these two frequencies are the same. Because of this difference, the mass calibration law for the hyperbolic trap will be different than the mass calibration law for the cubic. The signal frequency, λ_s , is imaginary by eq 22 so we write eq 23, where ω_s would be the angular frequency

$$\lambda_s = i\omega_s \quad (23)$$

observed in the frequency spectrum. After squaring and rearranging terms in eq 22, we have eq 24 in a form suitable for use as a calibration law (eq 24).

$$\omega_s^2 = (q/m)^2 B^2 - (q/m)8U_T/(r_0^2 + 2z_0^2) \quad (24)$$

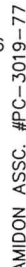
EXPERIMENTAL SECTION

Cell Construction. Hyperbolic cell electrodes were machined on a hand-operated engine lathe from 304H stainless steel to have a geometry given by $r_0 = 0.0127$ m (0.500 in.) and $z_0 = 0.00635$ m (0.250 in.) (Figure 1A). The electron beam was admitted to the cell through a 0.00159-m diameter hole offset radially from the z axis at $1/2 r_0$ to allow the largest possible cyclotron orbit between the z axis and the ring electrode.

Electronics. The cell was incorporated into a capacitance bridge circuit (Figure 1A). A balanced rf transformer formed half of the bridge and provided a means for applying the excitation waveform to the cell. The other half of the bridge was comprised of the cell capacitance and a balance capacitance, C_b , adjusted to minimize conductance of excitation signal to the amplifier input with no ions in the cell (26). The preamplifier was the differential FET input amplifier normally supplied with the Nicolet FTMS 1000. One of the differential inputs was shorted to ground for these experiments.

The rf transformer possesses a 40 turn secondary winding with a center tap and is connected as indicated in Figure 1A. Together with C_b and the stray capacities of the connection and end caps, the inductance of the secondary forms a resonant circuit. An auxiliary two-turn winding in the transformer was connected to a variable resistive load to adjust the damping of the resonant circuit as shown in greater detail in the right hand side of Figure 2. A third winding is a four-turn, center-tapped primary. The transformer was mounted in an Amidon Associates Model PC-3019-77 ferrite pot core.

Two excitation waveforms were used for the work in this paper. The waveforms were applied by using the rf transformer in two different ways. The pulse waveform described in detail along with eq 25 and 26 was employed for the exact mass study. The pulse was formed by switching currents at the transformer primary while making use of the variable damping to control the pulse shape, as described below. The other excitation waveform used for the remainder of the work was a rf burst applied at the observed ion signal frequency. This was accomplished by connecting the output of the excitation amplifier normally supplied with the Nicolet



27

Number of Ions. The number of ions was measured by using a previously reported method (11).

Signal and Data Processing. The experiment was operated in the mixer mode to cover the frequency interval from 165 to 135 kHz, which includes signals from ions of nominal mass 117 through 135 of 1,1,1,2-tetrachloroethane. Between 10 and 25 time domain transients were coadded prior to Fourier analysis. A 32 K data buffer was used to store the signal averaged transients. Observation time was approximately three times (32) the time constant for exponential decay of ion image signals (33, 34), and no zero filling was employed (35).

Single precision floating point computations (30 bit mantissa) were used throughout the study. To ensure that this precision was adequate and to test for ill-conditioned numerical computations (36), synthetic spectra with fictitious spectral peaks of precalculated mass were submitted to the mass calibration software (written in the Nicolet-supplied BASIC). Noise traces digitized by the ADC were added to synthetic spectra in order to determine the sensitivity of numerical procedures to random error in the raw data. In all cases, mass measurement accuracy on synthetic spectra was in the range of 2 ppb, which indicated that the numerical procedures and single precision computations, in particular, are sound.

Each spectrum required 30–120 s of time domain signal averaging, so that a set of four successive spectra were acquired in 2–8 min. Over this time period, the magnetic field drifted slightly. To help compensate for field drift, it was assumed that the frequency of a given peak would change from one spectrum to the next by the same amount; that is, that frequency drift was linear with time. For each peak, a least-squares line through a plot of center frequency vs. spectrum number was computed. The slope of this plot indicates the amount of frequency drift that occurred over a set of four trials. Frequency drifts on the order of 0.02–0.1 Hz/spectrum were observed, from which it was concluded that the magnetic field was sufficiently stable to permit comparison of theory and experiment to 1 ppm or less. Frequency values submitted to the mass calibration software were corrected for the small drifts that were detected.

Protocol. The mass calibration procedures were the same as previously reported (11) except that a mass calibration formula of the form given in eq 27 was used (see eq 24). To place the law in context, a historical summary of mass calibrations in ion cyclotron resonance and FTMS is presented in Table I.

$$f^2 = a/m^2 + b/m \quad (27)$$

RESULTS AND DISCUSSION

Accurate Mass Measurement. For this portion of the study, the pulse excitation waveform was used. The wide-band

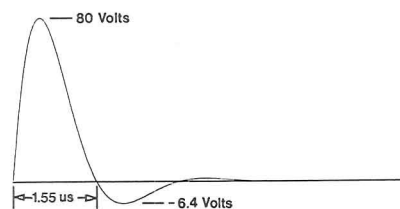


Figure 3. Pulse waveform used for ion excitation in the accurate mass measurement study: $T = 1.55 \mu\text{s}$, $V_p = 80 \text{ V}$, and $V_m = -6.4 \text{ V}$.

Table I. Proposed Mass Frequency Relations

$f = a/m$	
$f^2 = a/m^2 + b/m$	Beauchamp-Armstrong (1969) (24)
$f^2 = a/m^2 + b/m + c$	Ledford et al. (1980) (37)
$f_{\text{sideband}} = a/m$	Alleman et al. (1981) (38)
$f = a/m + c$	Francel et al. (1983) (39)
$m = a/f + b/f^2$	Ledford, Rempel, and Gross (1984) (11)
$f^2 = a/m^2 + b/m$	this work (for hyperbolic cell)

frequency, EI spectrum of 1,1,1,2-tetrachloroethane shown in Figure 4 is typical. Test of the mass/frequency relation revealed mass measurement accuracy on the order of 2 ppm and precision of about 1 ppm (Figure 5). Some errors are systematic, however, as indicated by the fact that the error bars representing single standard deviations over four trials often did not cut the zero error line. Similar results were obtained with a cubic analyzer cell operated with a low number of stored ions (11).

Mass measurement errors were found to be much less sensitive to space charge than were the measurement errors on the same ions in a cubic analyzer cell operated under comparable conditions. Changing the number of ions that were formed by the electron beam from 41 000 to 650 000 did not appreciably change the magnitude of the errors. We interpret this to mean that the systematic nature of the errors is due to some effect other than space charge. For comparison, a cubic analyzer cell operated under similar conditions proved much more sensitive to space charge effects (11). The cubic cell also produced systematic mass measurement errors not associated with space charge effects when the number of stored ions was kept below 20 000 (11).

A possible contribution to systematic errors at low number of ions is magnetic field inhomogeneity induced by the stainless-steel electrodes. Magnetic field inhomogeneity was suspected when it was discovered that the frequency of the signal from benzene ions of m/z 78 varied with orbit size, a result not in accord with theory. Similar experiments with the N_2 radical cation of m/z 28 showed even more pronounced dependence with orbit size. It was postulated that a radial magnetic field gradient accounted for the observed frequency shifts. To test this, the vacuum envelope was opened and the ring electrode removed from the cell. With the nominal magnetic field strength set at 1.2 T, a Hall probe inserted between the end caps revealed a variation of $2 \times 10^{-4} \text{ T}$ as the probe was moved from the z axis toward the position formerly occupied by the ring electrode.

Up to this point, we have considered only pulse excitation because of its apparent simplicity and wide mass range. Another excitation to consider is a rf burst to excite parametrically the resonances of the ion motion. A rf burst of a frequency equal to the observed signal frequency produces essentially a Lorentzian peak. The best resolution was achieved while excitation amplitudes of 0.77 V peak-to-peak (p-p) or less as measured on the end caps of the cell were used.

Varying the duration of the 0.77 V p-p rf burst produces a linear increase in the complex area (40) of the benzene molecular ion peak for excitation times up to about 600 μs , after which the signal falls to zero (40). This result compares

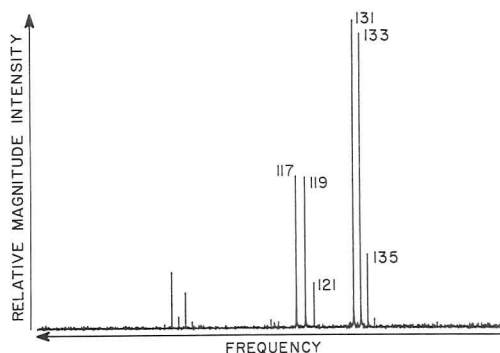


Figure 4. Frequency spectrum of 1,1,1,2-tetrachloroethane obtained by using the hyperbolic trap and exciting with the pulse shown in Figure 3; $p = 3.8 \times 10^{-7} \text{ Torr}$, filament potential = -59.4 V , and other conditions given in the Experimental Section. The abscissa is linear in frequency.

with a linear increase in complex area of the peak for excitation times up to 1100 μs in a similar experiment with a 1.54 V p-p rf burst applied across the plates of a 2.54-cm cubic cell. For the hyperbolic cell experiment, the magnitude mode resolution decreased slowly from approximately 70 K for short excitation times (ca. 150 μs) to about 40 K for longer excitation times ($>600 \mu\text{s}$). This is in marked contrast to the behavior of the cubic cell. As the ion orbit size in a cubic cell was increased again by changing the duration of the rf burst, the resolution increased by a factor of 3 from 10 to 30 K. These experiments were conducted at the same indicated pressure of $2 \times 10^{-7} \text{ Torr}$, and the results are consistent with similar data reported by Marshall et al. (41).

Other Comparisons with Cubic Cell. The charge displacement due to an ion oscillating in a hyperbolic penning trap has three terms (see eq 21). By inspection, two of these terms make a spectral contribution at zero frequency, whereas the remaining term makes a contribution at high frequency. Under conditions in which collisional damping is significant, we would expect these spectral contributions to change only by broadening. Because the low-frequency signals are not normally observed due to electronic filtering, only one peak due to the radial motion of ions is observed for each mass. In contrast, spectral contributions occur at odd harmonics in the cubic cell because of the practical inability to realize ideal uniform antenna fields (16, 42). In particular, third harmonic peak intensities 10% of fundamental peak intensities have been experimentally observed under optimal tuning conditions and with the use of rf burst excitation (16). In principle, the hyperbolic cell used in the mode described in this paper offers a realizable design that gives uncomplicated spectra.

In theory, the hyperbolic analyzer cell, when used in the parametric mode, is free from another problem encountered with the cubic cell; namely, distortion of the ion cloud by the nonuniform excitation electric field. In the cubic cell, the radius of the cyclotron orbit following excitation is strongly dependent upon the amplitude of oscillation along the z axis (parallel to magnetic field) (16). This results in ion cloud distortion. In the hyperbolic cell, this dependence should be largely removed because the equations of axial and radial motion during excitation are decoupled. We believe that distortion of the ion cloud will make treatment of the dependence of mass measurement error on space charge much more difficult.

One complication of the hyperbolic cell may be in studies that rely on quantitative peak intensity information as a function of time (e.g., ion kinetic studies). This complication arises because image charge displacement in the hyperbolic cell varies in proportion to the magnetron displacement of the trapped ion (see eq 19 and 21). As a result, some knowledge of the shape of the ion cloud is needed to determine the

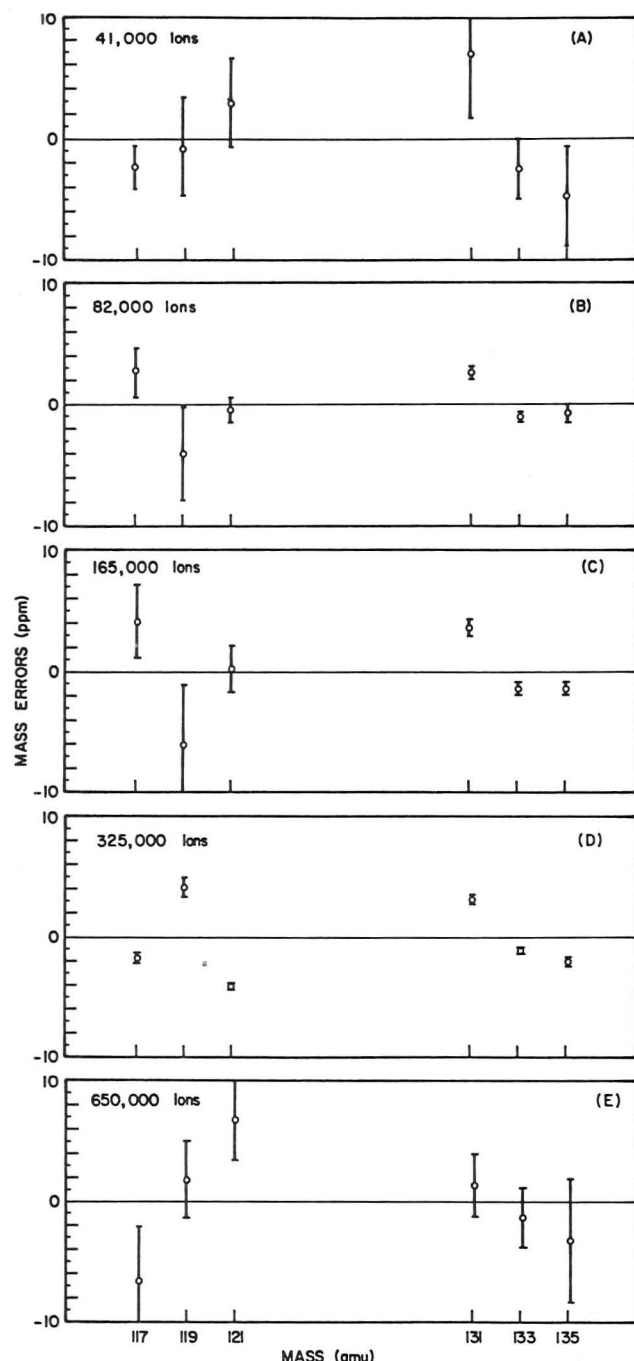


Figure 5. Variation of experimental mass measurement errors as a function of the number of initially formed ions. Mass measurements were of the six ions in the spectrum shown in Figure 4 and were taken at 1.2 T. The errors represent the differences between the actual masses and those calculated with the fitted calibration law.

number of ions associated with a given signal intensity. On the other hand, the sensitivity to the magnetron distribution of ions might provide an opportunity to test diffusion theories (27). Although the dependence of the image current amplitude on magnetron displacement may complicate some experiments, the lack of dependence on z -axial displacement should be an improvement over the cubic cell.

Whereas impulse excitation of the hyperbolic cell produces usable, wide-band ion signals and simplifies the theoretical treatment of excitation, it is believed that this form of excitation can excite the z -axial mode sufficiently to eject some ions from the cell. This ion ejection may contribute to an unexpected sharp tuning behavior with respect to trap voltage and impulse amplitude, which was observed in the course of this study. This is consistent with the observation that tuning behavior is much improved with narrow-band rf burst exci-

tation. It should be recalled that inadvertent excitation of the z -axis mode is observed with the cubic cell (43).

Registry No. 1,1,1,2-Tetrachloroethane, 630-20-6.

LITERATURE CITED

- (1) Comisarow, M. B.; Marshall, A. G. *Chem. Phys. Lett.* **1974**, *25*, 282.
- (2) Penning, F. M. *Physica (Amsterdam)* **1936**, *3*, 873.
- (3) Wineland, D. J.; Itano, W. M.; Van Dyck, R. S., Jr. *Adv. At. Mol. Phys.* **1983**, *19*, 135.
- (4) Paul, W.; Osbergerhaus, O.; Fischer, E. *Forschungsber Wintsch. Verkehrsministeriums Nordrhein-Westfalen No. 415*. Fischer, E. *Z. Phys.* **1959**, *156*, 1. Wuerker, R. F.; Goldenberg, H. M.; Langmuir, R. V. *J. Appl. Phys.* **1959**, *30*, 441.
- (5) Comisarow, M. B. *Int. J. Mass Spectrom. Ion Phys.* **1981**, *37*, 251.
- (6) Woods, I. B.; Riggan, M.; Knott, T. F.; Bloom, M. *Int. J. Mass Spectrom. Ion Phys.* **1973**, *12*, 341.
- (7) Knott, T. F.; Riggan, M. *Can. J. Phys.* **1974**, *52*, 426.
- (8) Bloom, M.; Riggan, M. *Can. J. Phys.* **1974**, *52*, 436.
- (9) Riggan, M.; Woods, I. B. *Can. J. Phys.* **1974**, *52*, 456.
- (10) Hartmann, H.; Chung, K.-M.; Baykut, G.; Wanczek, K.-P. *J. Chem. Phys.* **1983**, *78*, 424.
- (11) Ledford, E. B., Jr.; Rempel, D. L.; Gross, M. L. *Anal. Chem.* **1984**, *56*, 2744.
- (12) Hunter, R. L.; Sherman, M. G.; McIver, R. T., Jr. *Int. J. Mass Spectrom. Ion Phys.* **1983**, *50*, 259.
- (13) Lee, S.-H.; Wanczek, K.-P.; Hartmann, H. *Adv. Mass. Spectrom.* **1980**, *88*, 1645.
- (14) Byrne, J.; Farago, P. S. *Proc. Phys. Soc.* **1965**, *86*, 801.
- (15) Van Dyck, R. S., Jr.; Schwinberg, P. B. *Phys. Rev. Lett.* **1981**, *47*, 395.
- (16) Rempel, D. L.; Huang, S. K.; Gross, M. L. *Int. J. Mass Spectrom. Ion Proc.* **1986**, *70*, 163.
- (17) McIver, R. T.; Ledford, E. B., Jr.; Hunter, R. L. *J. Chem. Phys.* **1980**, *72*, 2535.
- (18) Nayfeh, A. H.; Mook, D. T. *Nonlinear Oscillations*; Wiley: New York, 1979; p 258.
- (19) Zadeh, L. A.; Desautels, C. A. *Linear System Theory: The State Space Approach*; McGraw-Hill: New York, 1963.
- (20) Marshall, A. G.; Roe, D. C. *J. Chem. Phys.* **1980**, *73*, 1581.
- (21) Knight, R. D. *Int. J. Mass Spectrom. Ion Phys.* **1983**, *51*, 127.
- (22) Allis, W. P. In *Handbuch Der Physik*; Flügge, S., Ed.; Springer-Verlag: Berlin, 1956; pp 383-444.
- (23) Harrison, E. R. *Am. J. Phys.* **1959**, *27*, 314.
- (24) Beauchamp, J. L.; Armstrong, J. T. *Rev. Sci. Instrum.* **1969**, *40*, 123.
- (25) Sharp, T. E.; Eyer, J. R.; Li, E. *Int. J. Mass Spectrom. Ion Phys.* **1972**, *9*, 421.
- (26) McIver, R. T., Jr.; Hunter, R. L.; Ledford, E. B., Jr.; Locke, M. J.; Franci, T. J. *Int. J. Mass Spectrom. Ion Phys.* **1981**, *39*, 65.
- (27) Franci, T. J.; Fukuda, E. K.; McIver, R. T., Jr. *Int. J. Mass Spectrom. Ion Phys.* **1983**, *50*, 151.
- (28) Jeffries, J. B.; Barlow, S. E.; Dunn, G. H. *Int. J. Mass Spectrom. Ion Proc.* **1983**, *54*, 169.
- (29) Dunbar, R. C.; Chen, J. H.; Hays, J. D. *Int. J. Mass Spectrom. Ion Proc.* **1984**, *57*, 39.
- (30) Smythe, W. R. *Static and Dynamic Electricity*, 3rd ed.; McGraw-Hill: New York, 1968; p 35.
- (31) Ledford, E. B.; Rempel, D. L.; Gross, M. L. *Int. J. Mass Spectrom. Ion Proc.* **1984**, *55*, 143.
- (32) Marshall, A. G. *Anal. Chem.* **1979**, *51*, 1710.
- (33) Schockley, W. J. *Appl. Phys.* **1938**, *9*, 635.
- (34) Comisarow, M. B. *J. Chem. Phys.* **1978**, *69*, 4097.
- (35) Comisarow, M. B.; Melka, J. D. *Anal. Chem.* **1979**, *51*, 2198.
- (36) Ralston, A.; Rabinowitz, P. *A First Course in Numerical Analysis*; McGraw-Hill: New York, 1978.
- (37) Ledford, E. B., Jr.; Ghaderi, S.; White, R. L.; Spencer, R. B.; Kulkarni, P. S.; Wilkins, C. L.; Gross, M. L. *Anal. Chem.* **1980**, *52*, 463.
- (38) Alleman, M.; Kellerhals, H.; Wanczek, K. P. *Chem. Phys. Lett.* **1981**, *84*, 547.
- (39) Franci, T.; Sherman, M. G.; Hunter, R. L.; Locke, M. J.; Bowers, W. D.; McIver, R. T., Jr. *Int. J. Mass. Spec. Ion Proc.* **1983**, *54*, 189.
- (40) Huang, S. K.; Rempel, D. L.; Gross, M. L. Presented at the 32nd Annual Conference on Mass Spectrometry and Allied Topics, San Antonio, TX, May 27-June 1, 1984.
- (41) Wang, T.-C. L.; Marshall, A. G. *Int. J. Mass Spectrom. Ion Proc.* **1986**, *68*, 287.
- (42) Nikolaev, E. N.; Gorshkov, M. V. *Int. J. Mass Spectrom. Ion Proc.* **1985**, *64*, 115.
- (43) Huang, S. K.; Rempel, D. L.; Gross, M. L. *Int. J. Mass Spectrom. Ion Proc.* **1986**, *72*, 15.

RECEIVED for review August 11, 1986. Resubmitted April 13, 1987. Accepted July 2, 1987. This work was supported by the National Science Foundation (Grant CHE-8018245 and CHE-8620177) and the National Institutes of Health (Grant GM30604-02). Much of this work was presented at the 31st Conference on Mass Spectrometry and Allied Topics (Boston, MA), May 1983.

CORRESPONDENCE

Mixed-Mode Column Thermospray Liquid Chromatography/Mass Spectrometry

Sir: Thermospray liquid chromatography/mass spectrometry (LC/MS) typically involves the use of reversed-phase columns and volatile buffer salts such as ammonium acetate (1-3). However, these simple reversed-phase conditions may not provide sufficient separations of mixtures of ionic or neutral and ionic compounds (4). Ion-pair reagents such as alkylsulfonates may provide improved chromatographic results (4) but these nonvolatile salts are not compatible with the thermospray ion source (1).

We have developed a strategy for thermospray LC/MS analysis of mixtures that contain ionic compounds that are not separated by simple reversed-phase chromatography. This approach utilizes a commercially available mixed-mode hydrophobic ion-exchange HPLC column that simulates ion-pair separations (5, 6). The column incorporates C-4 alkyl and phenylsulfonate functionalities bound to a silica support. A mobile phase of ammonium trifluoroacetate (1 M, pH 2.5) and methanol (75:25) provides good chromatographic results with this column and is volatile under the thermospray conditions.

In order to demonstrate the general utility of this strategy, we have chosen to examine a mixture of the active ingredients in common cold remedies (Table I). These compounds are present in the acidic mobile phase as a mixture of neutral and ionic species. Separation of some of these compounds by ion-pair high-performance liquid chromatography (HPLC) has been previously reported (7).

EXPERIMENTAL SECTION

Reagents. Phenacetin (1), guaifenesin (3-(2-methoxyphenyl)-1,2-propanediol, 2), phenylephrine (3), norephedrine (4), and ephedrine (5) were obtained from Aldrich Chemical Co. Ammonium hydroxide (Mallinckrodt, Inc.), trifluoroacetic acid (Fisher Scientific), and methanol (Burdick and Jackson) were purchased and used without further treatment. Water was obtained from a Millipore Milli-Q purification system.

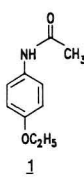
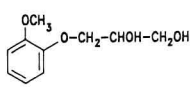
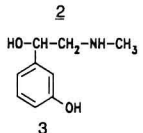
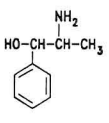
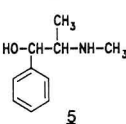
Instrumentation. The HPLC system consisted of a Perkin-Elmer Series 4 solvent delivery system, a Rheodyne 7126 injector with a 50- μ L loop, an RP-SCX column (5- μ m particle size, 100-Å pore size, 4.6 mm \times 25 cm; ES Industries, Marlton, NJ), and an LDC Spectromonitor III UV detector which was equipped with a max-N high-pressure cell (LDC). The exit line from the detector was connected directly to a thermospray interface (Vestec Corp., Houston, TX) which was fitted to a Finnigan 3000 mass spectrometer. On-line data reduction was performed by a Finnigan INCOS data system. The discharge mode of ionization was employed (2, 4). The temperatures for the thermospray interface were $T_1 = 115^\circ\text{C}$, $T_2 = 195^\circ\text{C}$, and block = 350°C .

Procedures. The mobile phase was a 75:25 mixture of 1 M ammonium trifluoroacetate and methanol. The ammonium trifluoroacetate solution was prepared by diluting 160 mL of trifluoroacetic acid and 188 mL of concentrated ammonium hydroxide to 2 L with water (pH 2.5). The chromatographic flow rate was 0.5 mL/min. Sample injections consisted of ca. 1 μ g of each component.

RESULTS AND DISCUSSION

Good separation of the components of a mixture of 1-5 was achieved by use of the mixed-mode column (Figure 1). In the acidic chromatographic mobile phases, phenacetin (1) and guaifenesin (2) are neutral solutes, while phenylephrine (3),

Table I. Thermospray LC/MS Data for Compounds 1-5 (Ionization Mode: Discharge On)

compound	mol wt	relative intensity		
		(M + H) ⁺	(M + NH ₄) ⁺	(M + H - H ₂ O) ⁺
 1	179	100 (<i>m/z</i> 180)		
 2	198	8 (<i>m/z</i> 199)	100 (<i>m/z</i> 216)	
 3	167	100 (<i>m/z</i> 168)		11 (<i>m/z</i> 150)
 4	151	100 (<i>m/z</i> 152)		12 (<i>m/z</i> 134)
 5	165	100 (<i>m/z</i> 166)		4 (<i>m/z</i> 148)

norephedrine (4), and ephedrine (5) are protonated species. The order of elution of phenacetin (1) and norephedrine (4) from the mixed-mode column were reversed in comparison to ion-pair HPLC with pentanesulfonate or hexanesulfonate reagents (7).

The detection of compounds 1-5 was achieved by thermospray MS with discharge-on ionization (2, 4). Quasi-molecular (M + H)⁺ ions were observed for all of the solutes (Table I). No fragmentation was observed for compounds 1 or 2. An (M + H - H₂O)⁺ ion of low intensity was observed for compounds 4 and 5 which contain benzylic alcohol groups.

The choice of mobile phase composition and concentration was somewhat arbitrary. Other volatile salts such as ammonium acetate should also be satisfactory, but they were not investigated. The 0.05-0.1 M salt concentrations which are normally used for reversed-phase thermospray LC/MS were too low for acceptable chromatography of the model compounds with the mixed-mode column. No attempt was made to determine the minimum ionic strength which was required for acceptable chromatographic results. An ionic strength of 1 M was chosen because this concentration was assumed to represent an approximate upper limit for the requirements of the mixed-mode column. The present mobile phase did not cause any problems with the thermospray vaporizer.

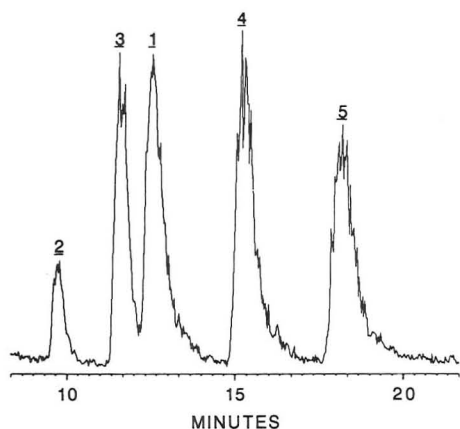


Figure 1. Reconstructed ion chromatogram of a mixture of compounds 1-5.

However, the vacuum line between the thermospray source and the rough pump was found to clog with salt after a few hours of operation. Therefore, the HPLC column flow rate was limited to 0.5 mL/min.

CONCLUSION

Mixed-mode column thermospray LC/MS (discharge ionization) appears to offer an alternative approach to the analysis

of mixtures of ionic or neutral and ionic compounds which are not well separated by simple reversed-phase HPLC.

Registry No. 1, 62-44-2; 2, 93-14-1; 3, 59-42-7; 4, 700-65-2; 5, 299-42-3; ammonium trifluoroacetate, 3336-58-1.

LITERATURE CITED

- (1) Garteiz, D.; Vestal, M. *LC Mag.* **1982**, 334.
- (2) Voyksner, R.; Haney, C. *Anal. Chem.* **1986**, 57, 991.
- (3) Covey, T.; Lee, E.; Bruins, A.; Henion, J. *Anal. Chem.* **1986**, 58, 1451A.
- (4) Snyder, L.; Kirkland, J. *Introduction to Modern Liquid Chromatography*; Wiley: New York, 1979; Chapter 11.
- (5) Crowther, J.; Hartwick, R. *Chromatographia* **1982**, 16, 349.
- (6) Floyd, T.; Cicero, S.; Fazio, S.; Raglione, T.; Hus, S.; Winkle, S.; Hartwick, R. *Anal. Biochem.* **1986**, 154, 570.
- (7) Bidlingmeyer, B. *J. Chromatogr. Sci.* **1980**, 18, 525.

¹ Current address: Finnigan-MAT, Rockville, MD.

John R. Lloyd¹
Mary Lou Cotter
David Otori
Alan R. Oyler*

Research Laboratories
Ortho Pharmaceutical Corporation
Raritan, New Jersey 08869-0602

RECEIVED for review March 11, 1987. Accepted June 29, 1987.

AIDS FOR ANALYTICAL CHEMISTS

Automated Sample Cell Cleaner

D. E. Bautz and J. D. Ingle, Jr.*

Department of Chemistry, Oregon State University, Corvallis, Oregon 97331

The majority of spectrophotometric and spectrofluorometric measurements are made on solutions in 1 cm path length sample cells. Many analytical procedures are based on monitoring the formation of an absorbing or fluorescing product by reaction of the analyte with suitable reagents. To simplify the procedure and to increase sample throughput, the sample and reagent solutions can be added to and mixed in a sample cell that is secured in a sample-cell holder. Addition of samples and reagents with automatic pipets (e.g., Eppendorf) or automatic syringe injectors has proved to be simple and rapid (1). Normally, one evacuates the contents of the cell with a vacuum aspirator and rinses several times with a blank solution from a wash bottle to prepare the cell for the next sample or standard. In continuous flow analysis systems, the sample flow cell is cleaned between sample plugs by the carrier stream without operator attention.

With rapid and often automated addition of samples and reagents to the sample cell and microcomputer-based data acquisition, calculations, and reporting, we find that the emptying and cleaning of the sample cell between measurements is the most time-consuming and tedious step during the analytical measurement. To address these limitations, a microcomputer-controlled cell cleaner was designed to perform the function of cell cleaning. This device allows spectrometric measurements with a conventional cell to be performed in a more automated fashion and frees the operator for more important tasks.

The actual size of the cell cleaning system is small enough to be placed adjacent to or directly on top of the instrument

Table I. Instrumental Components

component	model	source
three-way solution valve and pneumatic activator	30520	Dionex, Sunnyvale, CA
solid-state relays	7052-04-B04-F	Grayhill, LaGrange, IL
three-way air valve	MBD-002	Skinner, New Britain, CT
pump	Lab pump junior	Fluid Metering, Inc., Oyster Bay, NY

containing the sample cell. The cell cleaner was used here to clean a fluorometric cell containing quinine sulfate (QS) and the resulting blank signal was measured as an indicator of the completeness of cleaning.

INSTRUMENTATION

A schematic of the cell cleaning device is shown in Figure 1 and the components are specified in Table I. A glass capillary tube (0.125 in. i.d.) is glued along an inside edge of the sample cell with the bottom end of the tube located ≈ 1 mm above the bottom of the cell. The other end of the capillary tube is connected with 0.125 in. i.d. Teflon tubing to the common input port of a three-way solution valve. The other two ports are connected to a pump and to vacuum. The pump is turned on and off by switching the ac power to the pump with a solid-state relay (SSR1) controlled by TTL logic

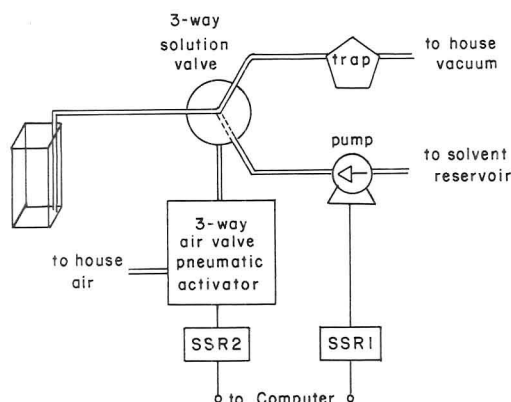


Figure 1. Schematic of the automated cell cleaning device.

signals. The three-way solution valve position is controlled by a pneumatic activator. Another solid-state relay (SSR2) controls a three-way air valve and allows either high-pressure air (60 psi) or the atmosphere to be connected to the three-way valve activator. The three-way solution valve and activations circuitry are mounted in one box and SSR1 is mounted to the pump.

To activate the sample cell cleaner, a logic 1 (+5 V) signal is applied to the control input of SSR2. This switches the position of the three-way solution valve so that the capillary is connected to vacuum. When the control signal to SSR2 is logic 0 (0 V), the three-way solution valve is connected to the pump. The rinse cycle occurs when a logic 1 signal is applied to the control input of SSR1. Normally the inlet of the pump is connected to the blank solution and the flow rate through the capillary tube is approximately 25 mL/min.

Any microcomputer with I/O capability can be used to provide the appropriate logic signals to activate the SSR's. In this case, two I/O lines from port B of the 6522 I/O chip on a Rockwell AIM-65 microcomputer are employed (these I/O lines can source several milliamperes). A short machine language program was written to change the signals on the I/O lines at the appropriate times to evacuate the cell and then fill the cell with blank solution (≈ 2.5 mL). The number and duration of the evacuation and filling (rinse) steps can be set to any desired values. The software was designed to make it easily adaptable for use as a subroutine in a larger data acquisition program.

EXPERIMENTAL SECTION

Reagent grade chemicals were used throughout the study. Solutions were prepared from deionized water from a Millipore Milli-Q system fed by house deionized water. The blank solution was 0.05 M H_2SO_4 . The test solutions were 100 $\mu\text{g/mL}$ QS and 50 ng/mL QS in 0.05 M H_2SO_4 .

A standard 1-cm cell was placed in a spectrofluorometer that has previously been described (1). A magnetic stirring bar in the sample cell was operated continuously. The excitation monochromator wavelength and spectral band-pass were set to 365 and 17 nm, respectively. The fluorescence emission was isolated with an interference filter with maximum transmission at 450 nm and a 20-nm half-width.

To evaluate the performance of the cleaning device, the following procedure was used. First, 2.5 mL of a 50 ng/mL solution of QS was added to the sample cell and the fluorescence signal

was recorded. Next the cell-cleaning program was initiated with a 5-s evacuation step followed by a 12-s blank filling step. The blank signal was measured. The evacuation, filling, and measurement steps were repeated until the blank signal reached a constant level (i.e., the variation in sequential blank signals was random and limited by the blank noise).

The same sequence of measurements was repeated with manual evacuation and rinsing of the cell. A wash bottle containing the blank solution and a disposable pipet attached to a vacuum aspirator were used for cleaning. Approximately the same volume of rinse solution was used to attempt to duplicate the conditions used for the automated procedure.

RESULTS AND DISCUSSION

With a 50 ng/mL QS test solution, it takes three evacuation/filling steps to achieve a constant blank signal with either the automated or manual cell cleaning procedure. After one evacuation/filling cycle, approximately 95% of the QS is removed. The second cycle removes approximately 99% of the initial QS test solution. In another study using a 100 $\mu\text{g/mL}$ QS test solution, the number of evacuation/filling cycles necessary to reach a stable blank signal was determined to be eight for the automated method and six for the manual method. Apparently, the efficiency of removal of the contents of the sample cell for one evacuation/filling cycle is not as good as with manual operation. This may be due to the use of the same tubing for both rinsing and evacuation. Small droplets or a film of the previous contents of the sample cell may adhere to the inside of the tube and be flushed back into the sample cell during the next rinse cycle.

For routine measurements, the computer was programmed to carry out a cell-cleaning sequence consisting of a 5-s evacuation step followed by three rinse/evacuation cycles. The duration of each rinse step was 12 s. Each evacuation step was 5 s except for the final evacuation step. Here the duration was increased to 8 s to ensure complete evacuation of the sample cell. Repetitive measurements of the fluorescence signal from a 50 ng/mL QS test solution were made. Between each measurement, the above automated cell-cleaning sequence was implemented and a blank measurement was obtained. The relative standard deviation in the net fluorescence signal was 0.6% and was essentially the same as obtained with an equivalent manual procedure.

With manual or automatic cell cleaning, an adequate number of rinse cycles must be used to obtain reliable measurements. The total time for the three-cycle automated cell cleaning sequence is 60 s. This is slightly longer than the time required for an equivalent manual rinsing sequence (approximately 30–40 s). However, the operator is free to prepare for the next analysis during the automated cleaning sequence and the cell-cleaning procedure is performed in an identical fashion for all samples. The time for filling the sample cell is the rate-limiting step. This time could be decreased by using a higher rinse solution flow rate.

LITERATURE CITED

- (1) Wilson, R. L.; Ingle, J. D., Jr. *Anal. Chem.* **1977**, *49*, 1060–1065.

RECEIVED for review January 16, 1987. Accepted July 1, 1987. Acknowledgment is made to the NSF (Grant No. CHE-84-01784) for partial support of this research.

Selective Separation of 2,3,7,8-Tetrachlorodibenzofuran by High-Resolution Gas Chromatography and by Alumina Column Liquid Chromatography

Maximilian Swerev and Karlheinz Ballschmiter*

Analytische Chemie, Universität Ulm, Oberer Eselsberg, D-7900 Ulm, Federal Republic of Germany

The identification and quantitation of 2,3,7,8-tetrachlorodibenzofuran (2,3,7,8-T4CDF) (F 83) are still problems. Since 2,3,7,8-T4CDF (F 83) is a compound whose determination is demanded in the GefStoffV (1) (German Dangerous Material Directive), it is necessary to quantitate 2,3,7,8-T4CDF (F 83) without any interference from other congeners, especially 2,3,4,8-T4CDF (F 80). This problem can be very demanding when analyzing PCDF mixtures derived from technical mixtures of polychlorobiphenyls (PCB's) or PCB fires.

In the literature only two methods are described to achieve this separation but both of them have distinct disadvantages:

The use of an OV 225 column (2), whose upper temperature limit of 225 °C excludes the analysis of the higher PCDD/F homologues.

The use of a column switching system with coupled columns together with medium-resolution mass spectrometry (3-5). This method suffers from the problem of determining the retention time windows for the cutting, which are influenced by unavoidable matrix effects.

Besides OV 225 no single gas-chromatographic column exists that can resolve 2,3,7,8-T4CDF (F 83) completely from all other T4CDF's (6-10). Even on isomer-specific cyanopropyl phase columns the separation from 2,3,4,8-T4CDF (F 80) is difficult.

We have now investigated whether the combination of the capillary columns SP 2331 + DB 17 (3-5) can be used without prefractionation of the sample on a packed column. As a second approach an alumina fractionation was developed, analogous to the specific 2,3,7,8-T4CDD separation described by Hagenmaier et al. (11), which permits the separation of 2,3,7,8-T4CDF (F 83) from the other T4CDF's.

It could be shown that either the use of the coupled columns SP 2331 + DB 17 or the alumina fractionation makes the selective determination of 2,3,7,8-T4CDF (F 83) possible without any interferences from other T4CDF isomers. However there are limitations to the determination of other congeners of the 2,3,7,8 class.

EXPERIMENTAL SECTION

High-Resolution Gas Chromatography with Mass Selective Detection (HRGC-MSD). The HRGC-MSD used was a HP 5970 B-MSD. The capillaries used were as follows: 60 m of SP 2331 (Supelco, Sulzbach, FRG), 0.25-mm i.d., 0.2- μ m d.f.; 30 m of SP 2331 (Supelco), 0.25-mm i.d., 0.2- μ m d.f.; 12.5 m of DB 17, J&W (ICT, Frankfurt, FRG), 0.25-mm i.d., 0.25- μ m d.f. Conditions were as follows: carrier gas, He; splitless injection; injector temperature, 260 °C; temperature program, to 180 °C held for 5 min, 2 °C/min to 270 °C, held there for 15 min. The DB 17 column preceded the nonbonded SP 2331 column. This sequence minimizes the change in selectivity caused by bleeding from the first column.

Fractionation by Al₂O₃ Adsorption Chromatography. Basic Alumina B-Super I (ICN, Eschwege, FRG), 50-200 μ m, was used as received. A glass column (20 \times 1 cm) was packed with 2.5 g of basic alumina and 2 g of anhydrous Na₂SO₄ just prior to use. The sample was dissolved in 1-2 mL of hexane and applied to the column. The first fraction was eluted with 25 mL of hexane/CH₂Cl₂ 80/20 (v/v), and the second fraction eluted with 25 mL of hexane/CH₂Cl₂ 50/50 (v/v).

RESULTS AND DISCUSSION

With isomer-specific capillaries, e.g. cyanopropyl phases such as SIL 88 or SP 2331, it is not possible to separate

Table I. Systematic Numbering of the Tetrachlorodibenzofurans (T4CDF) (12)

no.	structure	no.	structure
49	1,2,3,4	68	1,3,6,7
50	1,2,3,6	69	1,3,6,8
51	1,2,3,7	70	1,3,6,9
52	1,2,3,8	71	1,3,7,8
53	1,2,3,9	72	1,3,7,9
54	1,2,4,6	73	1,4,6,7
55	1,2,4,7	74	1,4,6,8
56	1,2,4,8	75	1,4,6,9
57	1,2,4,9	76	1,4,7,8
58	1,2,6,7	77	1,6,7,8
59	1,2,6,8	78	2,3,4,6
60	1,2,6,9	79	2,3,4,7
61	1,2,7,8	80	2,3,4,8
62	1,2,7,9	81	2,3,6,7
63	1,2,8,9	82	2,3,6,8
64	1,3,4,6	83	2,3,7,8
65	1,3,4,7	84	2,4,6,7
66	1,3,4,8	85	2,4,6,8
67	1,3,4,9	86	3,4,6,7

2,3,4,8-T4CDF (F 80) completely from 2,3,7,8-T4CDF (F 83) on a routine basis. Figure 1 shows two chromatograms of the ion 305.9 amu of the T4CDF's of a fly ash extract on an SP 2331. The first chromatogram was obtained from a new column and the second one after the capillary had been in use for a few weeks. The new capillary is able to separate F 83 from F 80. After a short time of use the selectivity of the capillary has changed so that the separation of F 83 from F 80 is no longer possible although the chromatography is still satisfying. Some compounds also start to coelute while separations of other compounds now become possible.

The numbering of the compounds follows a recently published systematic numbering of all PCDF's (12). Table I summarizes the systematic numbering for the T4CDF's. The identification of the T4CDF's on SP 2331 was done by using standards, which have been prepared in our laboratory, literature data, pattern comparison with SIL 88 and SP 2330, and studies of structure/retention relationships. On the combined DB 17/SP 2331 column the identification was done by using standards and comparing the elution patterns, which have been obtained by successively reducing the additional length of DB 17, thus analyzing the influence of tuning the selectivity on the retention (13).

In order to improve the separation the same combination of two columns (60 m of SP 2331 + 12.5 m of DB 17) was used, which was reported to separate F 83 from F 80 (3-5). Figure 2 shows chromatograms of T4CDF standards on this column combination. F 83 and F 80 are well resolved. The solution of the two T4CDF isomers 2,3,4,8-T4CDF (F 80) and 2,3,4,6-T4CDF (F 78) was obtained by pyrolysis of 2,2',3,4,5,5'-hexachlorobiphenyl, PCB 141, at 400 °C for 15 h. In Figure 2.2 where 1,2,7,8-T4CDF (F 61) and 2,3,7,8-T4CDF (F 83) were added to this solution, a base line separation is achieved.

The question of whether or not there are underlying interferences from other T4CDF isomers was also investigated. For this purpose an alumina fractionation was developed which can separate 2,3,7,8-T4CDF from the other T4CDF's. It is known that some 2,3,7,8-class congeners are the latest

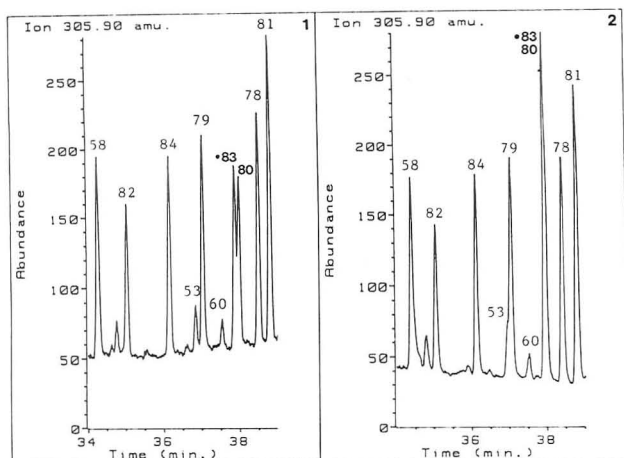


Figure 1. HRGC/MSD (SP 2331, 60 m; 305.9 amu). Separation of 2,3,7,8-T4CDF (F 83) from 2,3,4,8-T4CDF (F 80): (1) on a new capillary; (2) after 2 weeks. Only major compounds are numbered.

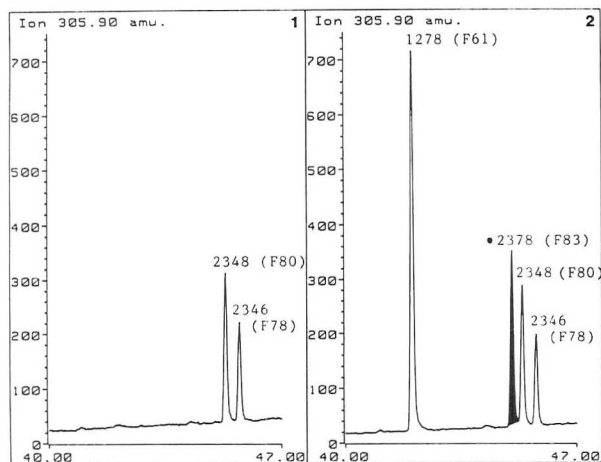


Figure 2. HRGC/MSD (SP 2331, 60 m + DB 17, 12.5 m; 305.9 amu). Separation of F 83 from F 80 on coupled columns: (1) F 80 and F 78 from pyrolysis of 2,2',3,4,5,5'-hexachlorobiphenyl, PCB 141; (2) addition of F 61 and F 83.

eluting ones on basic alumina (11, 14). This property has been used to separate 2,3,7,8-T4CDD (D 48) completely from all other congeners (11). As 2,3,7,8-T4CDF has the same substitution pattern among the PCDF's that 2,3,7,8-T4CDD among the PCDD's has, the elution behavior of 2,3,7,8-T4CDF on basic alumina was studied. The aim was to separate 2,3,7,8-T4CDF at least from all other T4CDF congeners.

The result of the fractionation on Alumina B-Super I is shown in Figure 3, which displays a chromatogram of the original solution and one obtained from the first fraction, which now is free from 2,3,7,8-T4CDF. The pattern of the T4CDF's is the same, only F 83 is missing. No other isomer appears at this position. The same solutions chromatographed on an SP 2331 are shown in Figure 4. Here the same ratio of F 83/F 80 is obtained. The recovery rates for all congeners are greater than 95%, which is within the injection error. They were determined by the use of standard solutions and fly ash extract.

An application of the coupled columns is the determination of polychlorodibenzofurans, particularly 2,3,7,8-T4CDF (F 83), in Clophen A 60, a technical mixture of PCB's. In contrast to fly ash, where the ratio of F 83/F 80 normally lies between 60/40 and 40/60, the ratio of F 83/F 80 shows large variations in PCB extracts. As the separation of compounds is not only a function of the resolution but also of the relative concentrations of these compounds it is impossible to quantitate 2,3,7,8-T4CDF correctly. Even with new isomer-specific capillaries the resolution of F 83/F 80 is too low to get a good

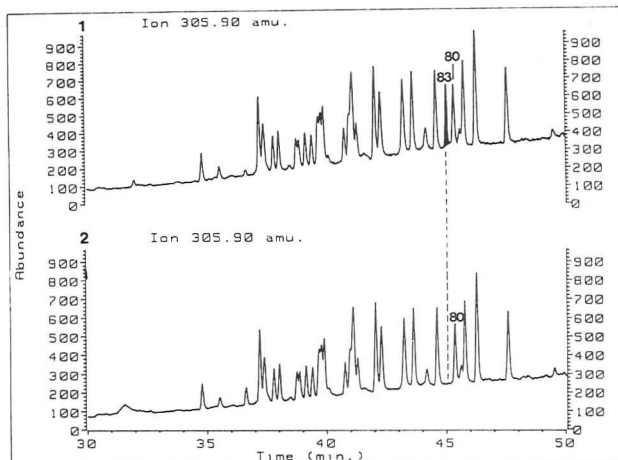


Figure 3. HRGC/MSD (SP 2331, 60 m + DB 17, 12.5 m; 305.9 amu) of the T4CDF's: (1) fly ash extract; (2) first alumina fraction with hexane/CH₂Cl₂ (80/20) as the eluate.

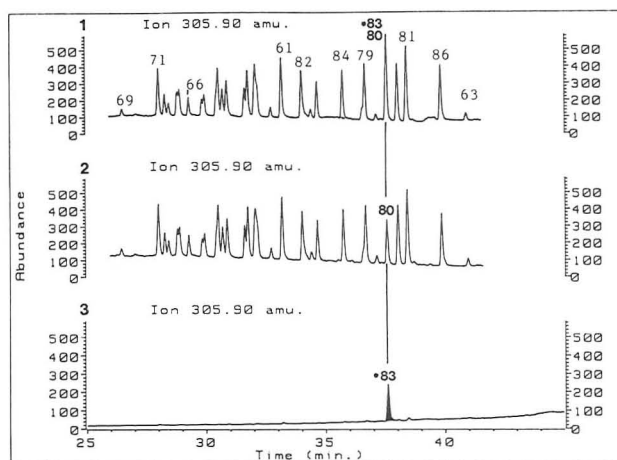


Figure 4. HRGC/MSD (SP 2331, 60 m; 305.9 amu) of the T4CDF's: (1) fly ash extract; (2) first alumina fraction with hexane/CH₂Cl₂ (80/20) as the eluate; (3) second alumina fraction with hexane/CH₂Cl₂ (50/50) as the eluate.

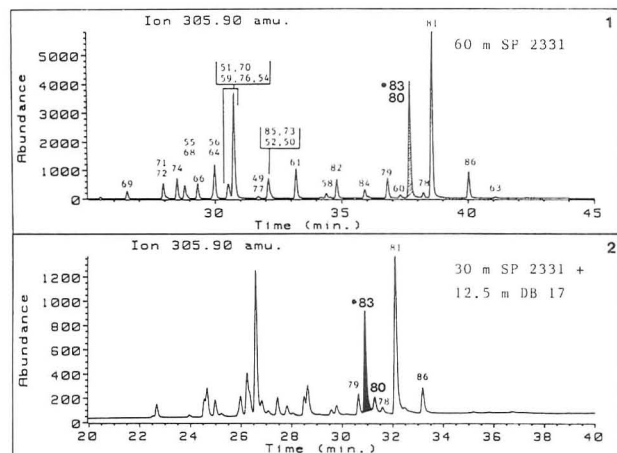


Figure 5. HRGC/MSD (305.9 amu) of the T4CDF's of a Chlophen A 60 extract: (1) SP 2331, 60 m; (2) SP 2331, 30 m + DB 17, 12.5 m.

separation when one component dominates. When the selectivity changes with time this separation cannot be performed, although the basic chromatography is still good (Figure 5.1). The coupled columns show that the ratio of F 83/F 80 is 85:15 (Figure 5.2). 2,3,7,8-T4CDF (F 83) is a major component of this mixture. The same results have been obtained when using 60 m of SP 2331 instead of 30 m of SP 2331 in combination with 12.5 m of DB 17. F 83 was completely

separated from F 80 and no other T4CDF isomer coelutes with 2,3,7,8-T4CDF.

The question of whether or not this column combination allows the separation and determination of the other congeners that cannot be separated by isomer-specific capillaries was also investigated. Of special interest was the determination of the 2,3,7,8-class congeners with this combination. We observed difficulties in the determination of several congeners of the 2,3,7,8-class through interferences with other congeners. 1,2,3,6,9-P5CDD (D 53) coelutes with 1,2,3,7,8-P5CDD (D 54) if we use more than 4.5 m of DB 17. There exist no difficulties in the determination of the three 2,3,7,8-substituted H6CDD's (D 66, D 67, D 70), the two 2,3,7,8-substituted H7CDF's (F 131, F 134), and 1,2,3,4,6,7,8-H7CDD (D 73). 1,2,3,7,8-P5CDF (F 94) still coelutes with 1,2,3,4,8-P5CDF (F 89) as it does on isomer-specific capillaries and an interference from 1,2,3,4,6-P5CDF (F 87) is observed, depending on the additional length of DB 17. 1,2,3,4,7,8-H6CDF (F 118) still cannot be separated from 1,2,3,4,7,9-H6CDF (F 119) and 1,2,3,4,8,9-H6CDF (F 120) interferes with 2,3,4,6,7,8-H6CDF (F 130), depending on the additional length of DB 17. For experimental details, see ref 13.

The combination of the capillaries SP 2331 + DB 17 (30/60 m + 12.5 m) is able to separate 2,3,7,8-T4CDF (F 83) from 2,3,4,8-T4CDF (F 80) without interferences from other T4CDF congeners. This is of special importance for samples with great differences in the 2,3,7,8-/2,3,4,8-T4CDF ratio, for instance technical mixtures of PCB's. The durability of the column combination is about the same as SP 2331 alone. One advantage is the possibility of rinsing the DB 17 column with solvents to remove dirt from the column head.

On basic alumina 2,3,7,8-T4CDF (F 83) can be separated from all other T4CDF isomers. This separation is sometimes impossible to perform cleanly because of matrix effects on the fractionation. Depending on the type of matrix an elution of some T4CDF congeners in the second alumina fraction or a partial elution of 2,3,7,8-T4CDF in the first fraction is observed. Experience shows that its use in the accurate analytical routine is difficult and requires the use of isotopically labeled 2,3,7,8-T4CDF for the control of the fractionation and accurate quantitation. If both methods are combined the

accurate quantitation of 2,3,7,8-T4CDF can be done.

ACKNOWLEDGMENT

We thank J. Andersson for critically reading the manuscript.

Registry No. 2,3,7,8-T4CDF, 51207-31-9; 1,2,3,4-T4CDF, 24478-72-6; 1,2,3,6-T4CDF, 83704-21-6; 1,2,3,7-T4CDF, 83704-22-7; 1,2,3,8-T4CDF, 62615-08-1; 1,2,3,9-T4CDF, 83704-23-8; 1,2,4,6-T4CDF, 71998-73-7; 1,2,4,7-T4CDF, 83719-40-8; 1,2,4,8-T4CDF, 64126-87-0; 1,2,6,7-T4CDF, 83704-25-0; 1,2,6,8-T4CDF, 83710-07-0; 1,2,6,9-T4CDF, 70648-18-9; 1,2,7,8-T4CDF, 58802-20-3; 1,2,8,9-T4CDF, 70648-22-5; 1,3,4,6-T4CDF, 83704-27-2; 1,3,4,8-T4CDF, 92341-04-3; 1,3,6,7-T4CDF, 57117-36-9; 1,3,6,8-T4CDF, 71998-72-6; 1,3,6,9-T4CDF, 83690-98-6; 1,3,7,8-T4CDF, 57117-35-8; 1,3,7,9-T4CDF, 64560-17-4; 1,4,6,7-T4CDF, 66794-59-0; 1,4,6,8-T4CDF, 82911-58-8; 1,4,7,8-T4CDF, 83704-29-4; 1,6,7,8-T4CDF, 83704-33-0; 2,3,4,6-T4CDF, 83704-30-7; 2,3,4,7-T4CDF, 83704-31-8; 2,3,4,8-T4CDF, 83704-32-9; 2,3,6,7-T4CDF, 57117-39-2; 2,3,6,8-T4CDF, 57117-37-0; 2,4,6,7-T4CDF, 57117-38-1; 2,4,6,8-T4CDF, 58802-19-0; 3,4,6,7-T4CDF, 57117-40-5; Chlophen A 60, 11096-99-4.

LITERATURE CITED

- (1) GefStoffV vom 26/8/1986; BGBl. I, p 1470.
- (2) Schäfer, W. Thesis, Ulm, 1986.
- (3) Ligon, W. V.; May, R. J. *J. Chromatogr.* **1984**, *294*, 77-86.
- (4) Ligon, W. V.; May, R. J. *J. Chromatogr.* **1984**, *294*, 87-98.
- (5) Ligon, W. V.; May, R. J. *Anal. Chem.* **1986**, *58*, 558-561.
- (6) Kuroki, H.; Haraguchi, K.; Masuda, Y. *Chemosphere* **1984**, *13*, 561-573.
- (7) Mazer, T.; Hileman, F. D.; Noble, R. W.; Brooks, J. J. *Anal. Chem.* **1983**, *55*, 104-110.
- (8) Rappe, C.; Marklund, S.; Kjeller, L.-S.; Bergqvist, P.-A.; Hansson, M. *Chlorinated Dioxins and Dibenzofurans in the Total Environment II*; Keith, L., Rappe, C., Choudhary, G., Eds.; Butterworth: Boston, MA, 1985.
- (9) Bell, R.; Gara, A. *Chlorinated Dioxins and Dibenzofurans in the Total Environment II*; Keith, L., Rappe, C., Choudhary, G., Eds.; Butterworth: Boston, MA, 1985.
- (10) Ballschmiter, K.; Buchert, H.; Class, T.; Krämer, W.; Magg, H.; Munder, A.; Reuter, U.; Schäfer, W.; Swerev, M.; Wittlinger, R.; Zoller, W. *Fresenius' Z. Anal. Chem.* **1985**, *320*, 711-717.
- (11) Hagenmaier, H.; Brunner, H.; Haag, R.; Kraft, M. *Fresenius' Z. Anal. Chem.* **1986**, *323*, 24-28.
- (12) Ballschmiter, K.; Buchert, H.; Niemczyk, R.; Munder, A.; Swerev, M. *Chemosphere* **1986**, *15*, 901-915.
- (13) Swerev, M.; Ballschmiter, K. *Fresenius' Z. Anal. Chem.* **1987**, *327*, 50-51.
- (14) Swerev, M.; Ballschmiter, K., unpublished results.

RECEIVED for review January 29, 1987. Accepted June 9, 1987.

Ultraviolet-Visible Absorption Spectra of Biological Molecules in the Gas Phase Using Pulsed Laser-Induced Volatilization Enhancement in a Diode Array Spectrophotometer

Liang Li and David M. Lubman*

Department of Chemistry, The University of Michigan, Ann Arbor, Michigan 48109

Numerous studies have appeared recently in the analytical literature of various forms of high-powered, monochromatic laser excitation spectroscopy for gas-phase analysis of molecules. Such techniques include laser-induced fluorescence (1-3), laser-induced dispersed fluorescence (4), laser absorption (5), and laser multiphoton ionization (6, 7) experiments. These techniques are often combined with the supersonic jet technique in order to produce rotationally cold molecules. At room temperature the spectra of most large polyatomic molecules consist of a broad unresolvable congestion of rotational lines so that one cannot take advantage of the monochromatic nature of the laser light for exact identification. However, the sharp spectral features (<0.2 Å) obtained under jet ex-

pansion conditions makes this an excellent technique for enhancing selectivity for chemical analysis. These experiments though require some prior knowledge of the general gas-phase absorption contours of the molecules under study. For reasonably volatile compounds or molecules that are stable upon heating, UV-vis absorption spectrophotometers can be used to obtain the broad gas-phase contours. It is important to know not only the general region in which the molecule absorbs but especially the onset of absorption, since this will generally be near the origin band. This is important for analysis in jet experiments where identification often depends on the position of several sharp absorption bands near the origin. The approximate position of these bands can often

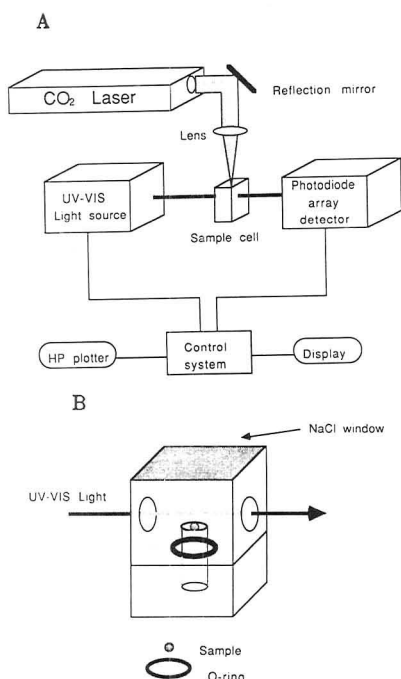


Figure 1. (A) Schematic diagram of the LIVE/UV-vis spectroscopic setup. (B) Sample holder and containment cell for laser-induced volatilization.

be guessed within several nanometers based upon the UV-vis gas-phase absorption taken in a standard spectrophotometer under thermal conditions.

This method has worked well for compounds with sufficient vapor pressure upon heating that do not undergo significant decomposition. However, the gas-phase absorption of most nonvolatile and thermally labile molecules is unknown. Since these include significant classes of biological and pharmaceutical compounds, a method of obtaining the absorption spectra of these molecules is critical if these methods are to be systematically extended to these molecules. Although the liquid-phase spectra of these molecules provide a general absorption contour solvent shifts may be significant depending on the solvent used. Considering the bandwidth of the laser excitation (1 cm^{-1}), even a solvent shift as small as 5–10 nm may be considered as significant. In this short aid, we therefore present a method of obtaining gas-phase absorption spectra of small labile molecules of biological significance by using a combination of pulsed laser-induced volatilization enhancement (LIVE) and a diode array spectrophotometer.

EXPERIMENTAL SECTION

The experimental setup is shown in Figure 1. A pulsed CO₂ laser ($10.6\text{ }\mu\text{m}$) is used to induce desorption of neutral species in the light path of commercial UV-vis spectrophotometer (Hewlett-Packard 8450A) with a photodiode array detector. This device allows us to record the whole UV-vis absorption spectrum of the desorbed material within 1 s of the desorption event. The CO₂ laser (Quanta-Ray EXC-1) has an $\sim 80\text{-ns}$ output spike pulse followed by an $\sim 1\text{-}\mu\text{s}$ decay pulse. The laser beam is focused by using a Ge lens (focal length $\sim 175\text{ mm}$) to an $\sim 1\text{-mm}$ spot on the Macor machinable ceramic surface on which the sample was placed, and vaporization was induced. The power density on the surface is estimated to be $\sim 10^7\text{ W/cm}^2$ in the samples studied herein, although lower power can be used for molecules with lower melting points. In each case the vaporization was performed under atmospheric pressure conditions. The position of the ceramic surface and laser beam was optimized so that as much of the desorbed plume intersected the UV-vis spectrophotometer light beam as possible. In order to concentrate the plume in the light-beam path for an extended period of time, a containment cell was placed above the ceramic desorption surface. This consists of a simple polystyrene cell with two open holes for the UV-vis

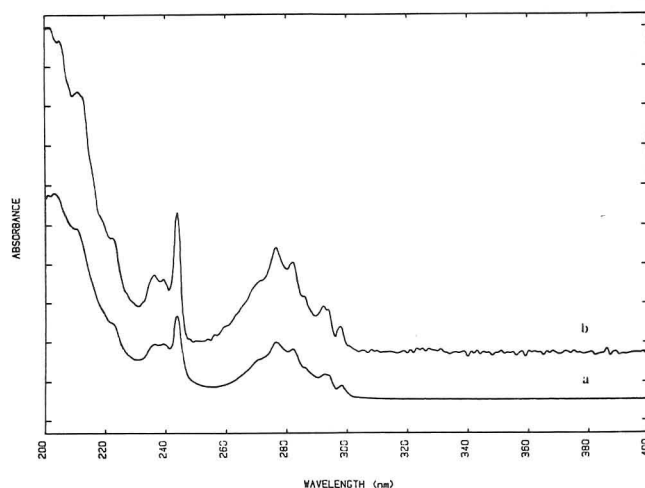


Figure 2. Comparison between the gas-phase UV spectrum of dibenzofuran obtained by (a) heating to $127\text{ }^{\circ}\text{C}$ and (b) laser-induced volatilization.

light beam to pass through and a NaCl window on top in order to allow the CO₂ laser beam to be transmitted to the ceramic surface.

This experiment is possible due to the ability of the diode array detector to acquire a complete spectrum every second. The typical sample, which generally consists of rather thick samples weighing $\sim 1\text{ mg}$, on the surface is completely desorbed within $\sim 30\text{ s}$ at the power levels used herein, although in the present configuration only a fraction of these actually traverse the beam path and contribute to the spectrum. However, spectra have been obtained with an initial sample of $<100\text{ }\mu\text{g}$. The molecules studied have absorptions in the near-UV so that the spectrophotometer was programmed to take data in the 200–400-nm region. The CO₂ laser power and pulse repetition rate ($\sim 10\text{--}100\text{ Hz}$) have been optimized in each case to produce the best spectrum. A Nd:YAG laser ($1.06\text{ }\mu\text{m}$) could also be used for laser-induced volatilization. We have found in our earlier work though (8) that the advantage of the CO₂ laser is that lower energy photons are less likely to cause subsequent multiphoton absorption/fragmentation/ionization that might interfere with the spectrum. In addition, scattered $10\text{-}\mu\text{m}$ radiation from the CO₂ laser is not detected by the diode array device and thus background noise is minimized from this source, whereas the spectrophotometer may respond to scattered near-IR or visible light from the Nd:YAG laser or its second harmonic.

RESULTS AND DISCUSSION

The purpose of this work is to provide a means of obtaining gas-phase UV-vis absorption spectra of nonvolatile molecules as a guide for investigators involved in studying the spectroscopy of these species by various laser-based techniques. The first question that must be addressed is whether the spectra obtained by laser desorption is the same as that obtained by heating the material in a gas-phase sample cell. In Figure 2a we show a spectrum of dibenzofuran obtained by heating the sample to $127\text{ }^{\circ}\text{C}$ and in Figure 2b a spectrum obtained by laser-induced volatilization at room temperature. The spectra are essentially identical, as was the case for other molecules studied whose spectra could be obtained by both methods. The reasons why they might be different could be due to excessively hot molecules present or a significant number of ions produced by the vaporization process. The desorption is performed at atmospheric pressure in air so that the large number of collisions probably relaxes any initially formed hot molecules back to thermal conditions. In addition, if ions were found in a significant quantity one would expect to observe a strong spectral peak in the green region of the spectrum since it has been shown that the ionic absorption in these aromatic species is shifted toward the visible (9). No extra bands due to ion production are observed. In previous

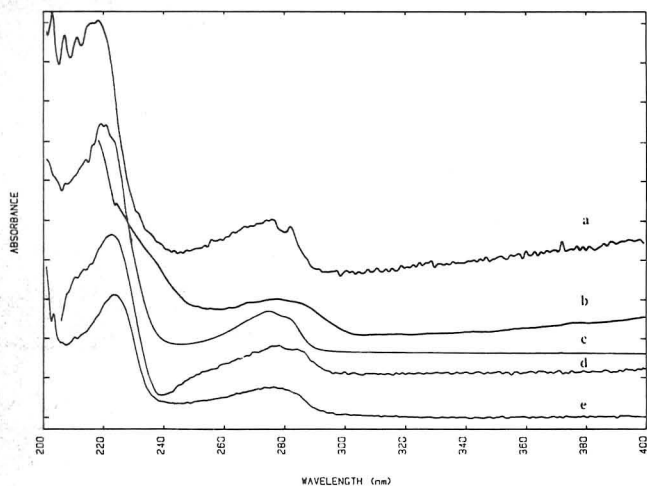


Figure 3. UV spectra of tyrosine (a) in gas-phase by laser-induced volatilization and in various solvents in the liquid phase including (b) cyclohexane, (c) water, (d) ethanol, and (e) methanol.

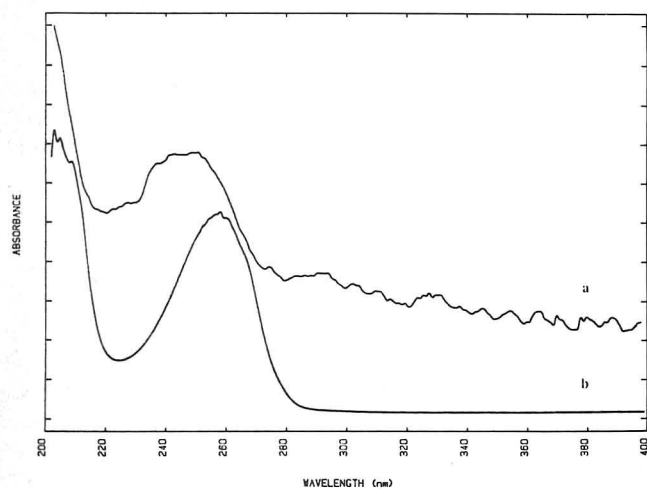


Figure 4. UV spectra of adenine in (a) gas phase obtained by laser-induced volatilization and (b) methanol solvent.

experiments under both vacuum (8) and atmospheric pressure conditions (10) almost no ion production was observed under the desorption conditions used.

The next problem examined is whether this method will produce spectra for molecules with very high melting points or that are thermally labile. One example shown in Figure 3 is tyrosine (mp $\sim 325^\circ\text{C}$ (dec)), where a gas-phase spectrum produced by laser desorption is compared to spectra obtained in various solvents. The spectra in solution are generally slightly shifted by several nanometers compared to the gas-phase spectrum. In addition, more vibrational structure can be observed in the LIVE gas-phase-produced spectrum than in the liquid phase. The shifts in solution generally appear at longer wavelengths as expected (11) in a $\pi-\pi^*$ transition. We have observed similar results for other species such as tryptophan where the liquid-phase spectra in water and methanol are shifted at least 3 and 5 nm, respectively, to longer wavelengths than the laser-induced gas-phase spectrum. In Figure 4 are shown spectra of adenine (mp $> 360^\circ\text{C}$) in the gas phase and in methanol. In this case a strong displacement of the liquid-phase spectrum to longer wavelengths is observed. In Figures 5 and 6 are demonstrated gas-phase UV-vis absorption spectra of several thermally labile compounds volatilized by laser desorption. These include Dopa, dopamine, and norepinephrine, which rapidly decompose upon heating to form a tarlike polymer. However, gas-phase spectra can be obtained by using the LIVE method, which resemble the

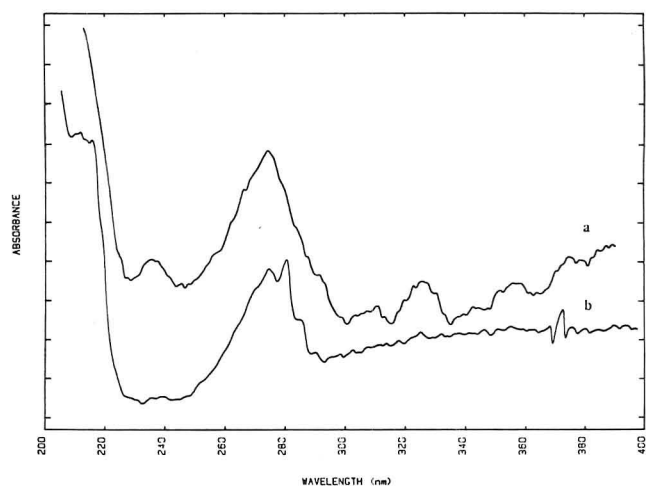


Figure 5. Gas-phase UV spectra of (a) dopamine and (b) norepinephrine obtained by LIVE technique.

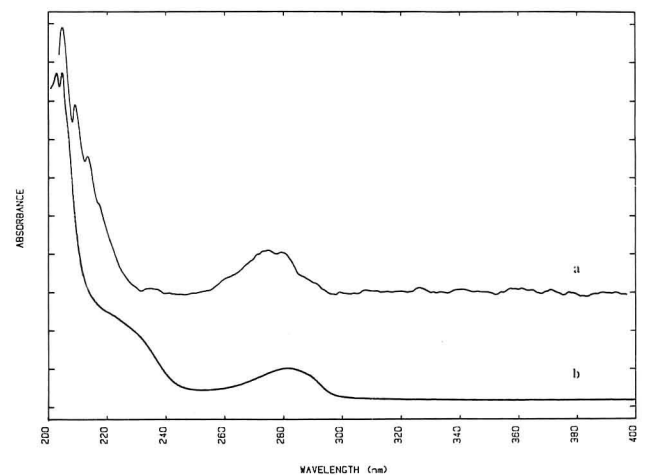


Figure 6. UV spectra of Dopa in (a) the gas phase obtained by laser-induced volatilization and (b) methanol solvent.

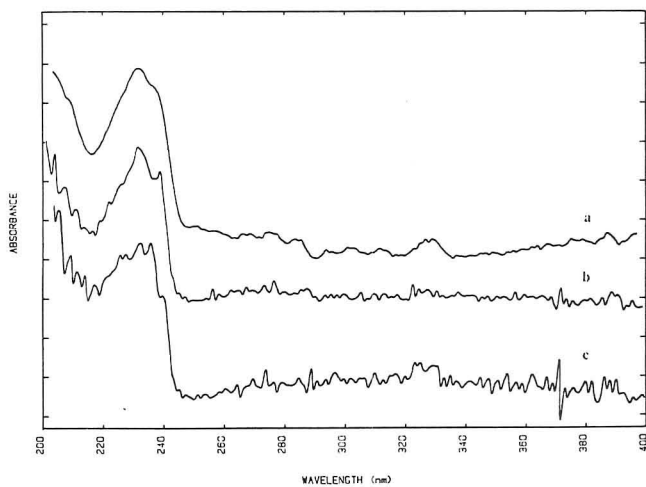


Figure 7. Gas-phase UV spectra of dipeptides obtained by LIVE technique: (a) phenylalanyltirosine, (b) phenylalanylleucine, and (c) tyrosylglycine.

spectra obtained when these molecules are dissolved in various solvents, although the liquid spectra are shifted several nanometers to longer wavelengths as demonstrated in Figure 6. It should be noted that norepinephrine was purchased in the hydrochloride form; however, previous LD experiments under vacuum (8) and at atmospheric pressure (10) show that neutral norepinephrine desorbs with the detachment of the

HCl group. This was generally found to be true of compounds prepared in the HCl form (8, 10).

One last example of the utility of the laser-induced vaporization method is shown for the case of several dipeptides. In Figure 7 are shown in the gas-phase spectra of tyrosine-glycine, phenylalanine-tyrosine, and phenylalanine-leucine performed by laser-induced vaporization. The basic tyrosine spectrum has its origin around 282 nm; however, the tyrosine aromatic ring π - π^* absorption is strongly shifted to the UV by other amino acids, which appear to act as electron-withdrawing groups in this case (12). Thus strong absorption bands are observed around 220-240 nm for these peptides, but only a very weak absorption is present at \sim 280 nm.

In conclusion, the LIVE technique can be used to obtain gas-phase UV-vis absorption of thermally labile molecules in a diode array spectrophotometer. The absorption contours are similar to those obtained in liquid solvents except they are shifted by several nanometers or in some cases 10-20 nm and the gas-phase spectra exhibit more vibrational structure. This technique is useful for obtaining spectral contours for spectroscopic purposes; however, in its present form is not useful for sensitivity or quantitation results.

Registry No. Dopa, 59-92-7; dibenzofuran, 132-64-9; L-tyrosine, 60-18-4; dopamine, 51-61-6; norepinephrine, 51-41-2; phenylalanyltirosine, 17355-18-9; adenine, 73-24-5; phenylalanylleucine, 3303-55-7; tyrosylglycine, 673-08-5.

LITERATURE CITED

- (1) Warren, J. A.; Hayes, J. M.; Small, G. J. *Anal. Chem.* **1982**, *54*, 138.
- (2) Smalley, R. E.; Wharton, L.; Levy, D. H. *Acc. Chem. Res.* **1977**, *10*, 139.
- (3) Amirav, A.; Even, U.; Jortner, J. *Anal. Chem.* **1982**, *54*, 1666.
- (4) Fukuoka, H.; Imasaka, T.; Ishibashi, N. *Anal. Chem.* **1986**, *58*, 375.
- (5) Imasaka, T.; Hirata, K.; Ishibashi, N. *Anal. Chem.* **1985**, *57*, 59.
- (6) Lubman, D. M.; Kronick, M. N. *Anal. Chem.* **1982**, *54*, 660.
- (7) Tembreull, R.; Lubman, D. M. *Anal. Chem.* **1984**, *56*, 1962.
- (8) Tembreull, R.; Lubman, D. M. *Anal. Chem.* **1986**, *58*, 1299.
- (9) Turner, D. W.; Baker, C.; Baker, A. D.; Brundle, C. R. *Molecular Photoelectron Spectroscopy*, 1st ed., Wiley-Interscience: London, 1970.
- (10) Kolaitis, L.; Lubman, D. M. *Anal. Chem.* **1986**, *58*, 2137.
- (11) Skoog, D. A. *Principles of Instrumental Analysis*, 3rd ed.; Saunders College Publishing: New York, 1984; Chapter 6 and 7.
- (12) Tembreull, R.; Sin, C. H.; Li, P.; Pang, H. M.; Lubman, D. M. *Anal. Chem.* **1985**, *57*, 1186.

RECEIVED for review March 2, 1987. Accepted July 9, 1987. We gratefully acknowledge support of this work under NSF Grant CHE-8419383. David M. Lubman is a Sloan Foundation Research Fellow.

Measurement of Vapor Deposition and Extraction Recovery of Polycyclic Aromatic Hydrocarbons Adsorbed on Particulate Solids

Robert J. Engelbach,¹ Arlene A. Garrison, E. L. Wehry,* and Gleb Mamantov*

Department of Chemistry, University of Tennessee, Knoxville, Tennessee 37996

Polycyclic aromatic hydrocarbons (PAHs), released (in the vapor phase) into the atmosphere via combustion of fossil fuels, are believed to adsorb on atmospheric particulate surfaces (1, 2). The chemical behavior of an adsorbed PAH is strongly dependent on the characteristics of the adsorbent (3-5).

Studies of chemical transformations of adsorbed PAHs usually require that the PAHs and/or their transformation products be extracted from the adsorbent and then analyzed by conventional spectrometric or chromatographic methods (3-5). Some adsorbents (especially coal ashes and other carbonaceous substrates) retain PAHs with such avidity that recoveries by conventional solvent (or even supercritical fluid) extractions are much less than 100% (6-11).

Measurement of extraction recovery is straightforward when a PAH is adsorbed onto a particular solid from a liquid solution but is less facile when the adsorbate is deposited onto the adsorbent from the vapor phase. (For example, radiotracer techniques (6) are not readily applicable with adequate safety to vapor-deposition experiments.) Herein we describe techniques for measuring the quantity of organic adsorbate vapor that deposits on a particulate solid and determining the subsequent recovery of that adsorbate by extraction. The principal component of the apparatus is a gas-chromatographic flame ionization detector (FID), used to measure the mass flow rate of PAH to which the adsorbent is exposed. Pyrene is used as an example adsorbent; the chemical reactivity of pyrene adsorbed on particulate solids has been studied extensively (3).

EXPERIMENTAL SECTION

Apparatus and Vapor-Deposition Technique. Deposition of a PAH is performed by passing a stream of PAH vapor through

a bed of adsorbent at elevated temperature. The apparatus is shown schematically in Figure 1. The PAH vapor is produced in a diffusion cell (12) placed in an oven ("oven 1") held at a temperature slightly below the melting point of the PAH. The vapor is swept from the diffusion cell by a stream of N_2 at a constant flow rate (typically 40 mL/min) and downstream pressure drop (7.3 kPa) maintained by a flow controller (Varian 57-000285-00). For pyrene, the mass flow rate of vapor emanating from the diffusion cell can be varied over the range 50-400 g/h by altering the diffusion-cell temperature over the range 383-417 K.

The PAH/ N_2 stream is then directed into a second oven ("oven 2" in Figure 1), which is maintained at a slightly higher temperature than oven 1. Oven 2 contains two valves (Valco V-4-HT), each of which can channel the PAH/ N_2 stream directly from valve inlet to outlet (dashed lines, Figure 1) or divert the vapor stream through an alternate loop (solid lines). With valve 1 in deposit mode, the PAH/ N_2 stream passes through a cell (12) containing a bed of adsorbent. With valve 1 in bypass mode, the cell is circumvented. Similarly, with valve 2 in collect mode, the vapor stream is routed to a coil of tubing immersed in a cold bath; with Valve 2 in detect mode, the vapor stream proceeds directly to an FID (Gow-Mac 12-800).

To compensate for changes in pressure drop as the route of the vapor stream is altered, pressure regulators 1 and 2 (Nupro SS-2SG) are adjusted whenever valve 1 or 2 is switched, to maintain a constant gauge pressure.

Two types of pyrene vapor deposition experiments were performed. In the first, 1-g samples of adsorbent were exposed for 1 h to a pyrene mass flow rate of 60 μ g/h (hence, the maximum quantity of pyrene that could be deposited on any adsorbent was 60 μ g). A second procedure consisted of depositing pyrene on an adsorbent until its adsorptive capacity was "saturated" (i.e., further exposure to pyrene vapor produced no detectable adsorption). These experiments are termed "60- μ g" and "capacity" depositions, respectively.

Quantification of Vapor Deposition. To determine the quantity of PAH that adsorbs on the substrate, the mass flow rate of PAH before (M_d) and after (M_e) the cell is measured.

¹Present address: National Center for Toxicological Research, Jefferson, AR 72079.

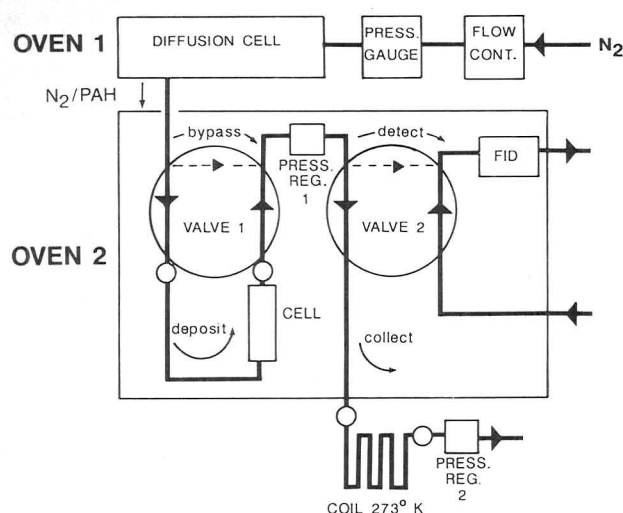


Figure 1. Apparatus for vapor deposition and quantification of polycyclic aromatic hydrocarbons on particulate solid substrates.

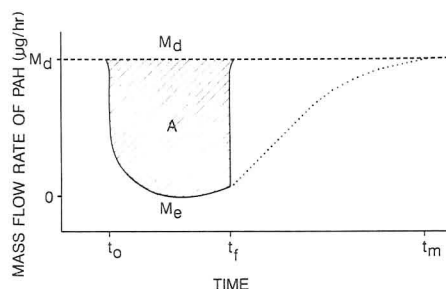


Figure 2. FID plots of mass flow rate of PAH vs. time. Rate M_d (indicated by the dashed line) is constant. Rate M_e changes with time. Area A is proportional to the total mass of PAH deposited on the substrate. The dotted line signifies a "capacity" deposition.

Integrating the difference $M_d - M_e$ over the total time of deposition yields the quantity of PAH depositing in the adsorption cell. M_d is held constant during a given experiment and is measured prior to deposition (with valve 1 in bypass and valve 2 in detect mode). M_e varies with time and is continuously monitored by the FID during adsorption of PAH on the substrate (valve 1 in deposit and valve 2 in detect mode).

The FID response is calibrated by setting valves 1 and 2 to bypass and collect, respectively, and trapping the PAH for a known period of time in a stainless steel coil immersed in ice water. The PAH so collected is dissolved in a known volume of methanol and determined by UV absorption. From the quantity of trapped PAH and the deposition time, a relationship between the mass flow rate of PAH and the FID signal is obtained.

Typical plots of M_d and M_e with time are shown in Figure 2. Deposition of PAH onto the adsorbent begins at time t_0 . If it is not desired to "saturate" the adsorbent with PAH, deposition is terminated at time t_f . The hatched area A between t_0 and t_f yields the total quantity of PAH deposited. If a capacity deposition (as defined above) is carried out, deposition is not terminated at t_f , but instead continues to t_m (defined as the time at which M_e first becomes equal to $0.99 M_d$). The dotted curve in Figure 2 represents the variation of M_e with time in a capacity deposition.

The above procedure measures the total quantity of PAH deposited in the adsorption cell. One cannot assume that the PAH deposits only on the adsorbate; some PAH may (and does) deposit on the (glass) cell walls, even if the glass is silanized. To avoid errors from this source, PAH must be deposited to full capacity on the walls of the empty cell prior to insertion of the adsorbent. When this is done, competition of the cell with the adsorbent for PAH is eliminated. However, the PAH may then desorb from the cell walls during deposition on an adsorbent, causing the measured value of M_e to be too large. To correct for this potential source of error, it is necessary to remove the adsorbent from the cell following cessation of deposition, reinsert the empty cell into

Table I. Vapor Deposition and Extraction Recovery for Pyrene on KA Coal Ash

adsorbent weight, g	deposition time, h	M_d , $\mu\text{g/h}$	C_d , $\mu\text{g/g}$	C_e , $\mu\text{g/g}$	% recovery
60- μg Depositions					
1.00	1.00	60	59	28	47
1.00	1.00	60	60	32	53
1.00	1.00	60	59	29	49
Capacity Depositions					
1.15	13.00	289	1060	875	82
1.14	13.00	341	1048	850	81
1.06	9.00	387	1082	879	81
0.56	8.00	372	1083	880	81

oven 2, and measure the total quantity of pyrene that must be passed through the empty cell for M_e to equal M_d . This quantity is then added to that determined for the adsorbent (from Figure 2) to determine the total quantity of pyrene retained by the adsorbent.

Adsorbents. The following particulate solids were used: silica gel (Brinkman); flaked graphite (Southwestern Graphite Co.); a commercially available coal fly ash (Alpha Resources; hereafter denoted AR); and fly ashes produced by combustion of Texas lignite (TX) and Kanab (KA), East Tennessee (ET), Illinois (IL), and Western Kentucky (WK) coals. The origins, compositions, and physical properties of the coal ashes are described elsewhere (3).

Solution Depositions. Adsorbent samples weighing 1.00 g were inserted into 15-mL centrifuge tubes. A solution of pyrene in CH_2Cl_2 was added to each tube; the total quantity of pyrene delivered to each tube was 60 μg . The solvent was allowed to evaporate (a process requiring several hours, during which the ash-solvent slurry was stirred at approximately 30-min intervals to promote uniformity of exposure of the ash particles to pyrene); the adsorbent was then removed from the tube. Adsorption of pyrene onto the walls of the centrifuge tube was found to be negligible under these conditions.

Extractions. Pyrene was extracted from adsorbents by conventional Soxhlet technique for 24 h with methanol as the extractant. The pyrene concentration in the extracts was determined by UV absorptiometry.

RESULTS AND DISCUSSION

The percentage recovery in extraction of adsorbed pyrene is defined as $100(C_e/C_d)$, where C_d denotes the concentration of pyrene deposited on the adsorbent and C_e is the concentration of pyrene recovered by extraction, both expressed as micrograms of pyrene per gram of adsorbent. Table I summarizes data for both 60- μg and capacity vapor depositions of pyrene on KA coal ash. These results indicate the reproducibility of deposition and recovery data attained by this method. That the extraction recovery is greater for capacity than for the 60- μg depositions is expected; coal ash is a heterogeneous adsorbent with a variety of adsorptive site energies. Thus, the enthalpy of adsorption of a PAH, averaged over all occupied adsorption "sites", increases as the concentration of adsorbed pyrene decreases (i.e., the most energetic surface sites are covered first during deposition and uncovered last by extraction) (13).

Table II compares deposition and extraction recovery data for all eight substrates subjected to 60- μg vapor depositions of pyrene vapor. Only silica and TX and KA ashes retain all (or virtually all) pyrene to which they are exposed. In addition, recoveries of the deposited pyrene vary widely, from an undetectably small recovery (IL ash) to virtually 100% recovery (silica and TX ash). The origins of these differences between adsorbents are not yet fully understood.

The extraction recovery may depend strongly on the manner in which a PAH is deposited on an adsorbent. Table III shows that extraction recoveries from some adsorbents

Table II. Vapor Deposition and Extraction Recoveries for Pyrene on Various Substrates

substrate	C_d , $\mu\text{g/g}^a$	C_e , $\mu\text{g/g}$	% recovery
silica	58	60	103
TX ash	62	64	103
AR ash	45	41	91
WK ash	31	23	74
graphite	54	28	52
KA ash	60	30	50
ET ash	53	10	19
IL ash	47	0	0

^aIn all cases, the adsorbent was exposed to 60 μg of pyrene; several adsorbents failed to retain all of the pyrene to which they were exposed.

Table III. Extraction Recoveries of Solution- and Vapor-Deposited Pyrene from Various Adsorbents

adsorbent	% recovery, vapor deposition	% recovery, soln Deposition ^a
silica	103	109
TX ash	103	93
AR ash	91	70
graphite	52	101
KA ash	50	61
ET ash	19	69
IL ash	0	88

^aSolvent: CH_2Cl_2 .

(graphite, IL, ash, and KA ash) are much lower for "vapor-deposited" than for "solution-deposited" pyrene, while the opposite is true for AR ash and silica. These results imply that the solvent used in "solution" depositions can significantly alter the affinity of an adsorbent for PAHs. Thus, it may be

inaccurate to use "solution-deposited standard" samples to infer extraction recoveries in the analysis of atmospheric particulate samples (in which the PAH deposits from the vapor phase, not from a liquid solution).

ACKNOWLEDGMENT

We gratefully acknowledge the assistance of J. S. Krueger, Zhong Jinxian, R. A. Yokley, J. W. Taylor, and J. W. Gurley.

Registry No. Pyrene, 129-00-0; graphite, 7782-42-5.

LITERATURE CITED

- (1) Schure, M. R.; Natusch, D. F. S. In *Polynuclear Aromatic Hydrocarbons: Physical and Biological Chemistry*; Cooke, M., Dennis, A. J., Fisher, G. L., Eds.; Battelle Press: Columbus, OH, 1982; p 713.
- (2) Ryan, P. A.; Cohen, Y. *Chemosphere* **1986**, *15*, 21.
- (3) Yokley, R. A.; Garrison, A. A.; Wehry, E. L.; Mamantov, G. *Environ. Sci. Technol.* **1986**, *20*, 86.
- (4) Behymer, T. D.; Hites, R. A. *Environ. Sci. Technol.* **1985**, *19*, 1004.
- (5) Dlugi, R.; Gusten, H. *Atmos. Environ.* **1981**, *17*, 165.
- (6) Griest, W. H.; Yeatts, L. B., Jr.; Caton, J. E. *Anal. Chem.* **1980**, *52*, 199.
- (7) Griest, W. H.; Caton, J. E. In *Handbook of Polycyclic Aromatic Hydrocarbons*; Bjorseth, A., Ed.; Dekker: New York, 1983; Vol. 1, p 95.
- (8) Soltys, P. A.; Mauney, T.; Natusch, D. F. S.; Schure, M. R. *Environ. Sci. Technol.* **1986**, *20*, 175.
- (9) Stenberg, U.; Alsberg, T. E. *Anal. Chem.* **1981**, *53*, 2067.
- (10) Hawthorne, S. B.; Miller, D. J. *J. Chromatogr. Sci.* **1986**, *24*, 258.
- (11) Wright, B. W.; Wright, C. W.; Gale, R. W.; Smith, R. D. *Anal. Chem.* **1987**, *59*, 38.
- (12) Miguel, A. H.; Korfmacher, W. A.; Wehry, E. L.; Mamantov, G. *Environ. Sci. Technol.* **1979**, *13*, 1229.
- (13) T. D. J. Dunstan, J. K. Sanders, R. J. Engelbach, E. L. Wehry, Mamantov, G., unpublished data, University of Tennessee, 1987.

RECEIVED for review May 14, 1987. Accepted July 7, 1987. This work was supported by the Department of Energy, Office of Health and Environmental Research, under Contract DE-AS05-81ER60006.

Vibrating Tumblers as Cleaning Devices for Mass Spectrometer Ion Source Parts

Louis R. Alexander,* Vince L. Maggio, Vaughn E. Green, James B. Gill, Elizabeth R. Barnhart, and Donald G. Patterson, Jr.

Toxicology Branch, Environmental Health Laboratory Services, Center for Environmental Health, Centers for Disease Control, Atlanta, Georgia 30333

Lance C. Nicolaysen

Chemistry Department, Emory University, Atlanta, Georgia 30322

Maintaining clean ion source parts for a high-throughput laboratory can be a major task, even for highly motivated and skilled personnel. In our laboratory, an ion source used for analyzing adipose or serum extracts usually lasts from 1 to 2 weeks before it needs to be disassembled for cleaning. A source may perform adequately for longer periods on occasion, but at any given time all mass spectrometer operators are involved at some stage in the source maintenance process.

The usual source cleaning procedures include various scrubbing techniques, sandblasting, or electrochemical baths. These procedures are rigorous and erode the source parts to some extent, especially the more fragile sliding slits and beam center plates on the Vacuum Generator (VG) Instruments.

The scrubbing action of rotary polishing tools, coupled with alumina paste, can result in surface scratches that produce a dull finish. Certain places in some of the parts, such as ion source blocks, are difficult to clean by any mechanical means.

Some of these more obstinate places can be reached by sandblasting which requires special equipment. However, one must carefully select the mesh size of the sandblasting medium. Even corn starch is too harsh for certain parts, because it can leave an etched or dull finish. In some cases, one can actually dislodge the chemical ionization restrictor from an ion source block or detach sliding slit guides from lens assemblies. The dull finish produced by sandblasting and abrasive cleaning induces rapid loss of sensitivity and expedites contamination causing degradation in source performance.

Electropolishing, the reverse of electroplating, is a nonabrasive metal cleaning technique (1). Equipment is available from Vacumetrics (Ventura, CA). It can also be assembled from items in the electrochemistry laboratory (2). Solutions for polishing various metals are easily prepared (3). During the polishing process, metal is removed from the source parts (anodic), and care must be exercised to control the amount

of metal erosion. However, erosion of the metal surfaces appears uneven and is most noticeable at the edges of the lenses and will vary with the amount of coating (contamination) present.

As an alternative method of cleaning ion sources and other mass spectrometer parts, we have developed a cleaning procedure utilizing a vibrating ammunition case tumbler (polisher), crushed corn cobs, and a metal polish. This procedure allows practically effortless cleaning and produces a mirror finish on small metal parts, of various sizes and fragility, and in many usually inaccessible spots.

EXPERIMENTAL SECTION

Apparatus. The vibrating ammunition case tumbler consists of a rubber bowl and lid attached to a motorized vibrator plate (Thumblers Tumbler, ULTRA-VIBE 18, Tru-Square Metal Products, Auburn, WA; others are also available from Buckeye Sports Supply, Canton OH, or local gun supply shops). The volume of the bowl is about 1 gallon which accommodates 5 lb of coated cleaning medium. These devices can be purchased for less than \$150. The newer vibrating tumblers are less rigorous than the conventional rotating type which reduces the probability of scratches.

Reagents and Chemicals. The cleaning medium consists of crushed corn cobs pretreated with a fine polishing (abrasive) compound. Finely crushed walnut shells are also readily available and quite acceptable. These are procurable from gun shops which handle reloading supplies for about \$2 per pound. A commonly available metal polish (Brasso, Airwick Industries, Inc., Carlstadt, NJ), was used to coat the cleaning medium. Other metal polishes, i.e. jeweler's rouge or automotive rubbing (polishing) compound, may also be used. Commercially available reagent grade organic solvents were employed for rinsing.

Procedure. The polishing medium consists of approximately 5 lb of crushed corn cobs and 4 oz of metal polish. The corn cobs can be reused many times, but the metal polish is replenished as indicated by the cleaning efficiency. Parts from one or more ion source assemblies are placed in the tumbler without any pretreatment. As a precaution, we install the shortest possible screws into all locations in ion source blocks and similar parts to prevent the polishing medium from entering the tapped screw holes. Longer screws increase the possibility of scratches on the other parts during the cleaning process.

Other small metal parts may be cleaned by using this method, namely items that can be removed from ceramics and other nonmetal parts. Adjustable source slit components, screws, and other small metal parts have been successfully cleaned.

The metal parts are usually tumbled overnight, although sometimes it takes longer to obtain the desired results. The parts are then removed from the polishing medium and excess dust is

evacuated using oil-free air. The parts are sonicated in several changes of deionized or distilled water until no trace of the polishing medium is visible. We continue sonication for three washes each in methanol, toluene, and finally acetone (total of nine washes; 10–15 min each). Other solvents may be used, provided they do not leave a residue on the metal parts. We have successfully used diethyl ether, methylene chloride, hexane, and ethanol with acceptable results. Sonication should be performed in a fume hood especially when using volatile and flammable solvents.

RESULTS AND DISCUSSION

This procedure may seem long and laborious, since it requires more than 1 day to clean and assemble an ion source. However, the actual time the operator spends cleaning the ion source parts is rarely more than 10 min. Both the abrasive method using manual and rotary polishing and the sand-blasting procedures require about an hour. Electropolishing requires somewhat less time, but it demands the operator's undivided attention due to the widely dissimilar sizes of parts. An electropolishing apparatus is also considerably more expensive, about \$500 for a basic unit compared to less than \$150 for the tumbler.

With the method described here, source parts can be tumbled while the analyst continues to run samples and rebuild the replacement source with a set of previously cleaned parts. We maintain two source assemblies and a supplementary set of source parts for each of our three high-resolution mass spectrometers. By exchanging the parts after cleaning, an analyst can reassemble an ion source in about 30 min. The total time lost due to an abrupt ion source failure is usually less than 1 h.

ACKNOWLEDGMENT

The authors thank the visiting scientists who viewed this operation in our laboratory and offered opinions on the feasibility and utility of this method.

LITERATURE CITED

- (1) Damico, J. N.; Barron, R. P. *Anal. Chem.* **1971**, *43*, 7.
- (2) Peele, G. L.; Brent, D. A. *Anal. Chem.* **1977**, *49*, 4.
- (3) Rosenbury, F. *Handbook of Electron Tube and Vacuum Techniques*; Addison-Wesley: Reading, MA, 1967; pp 18–23.

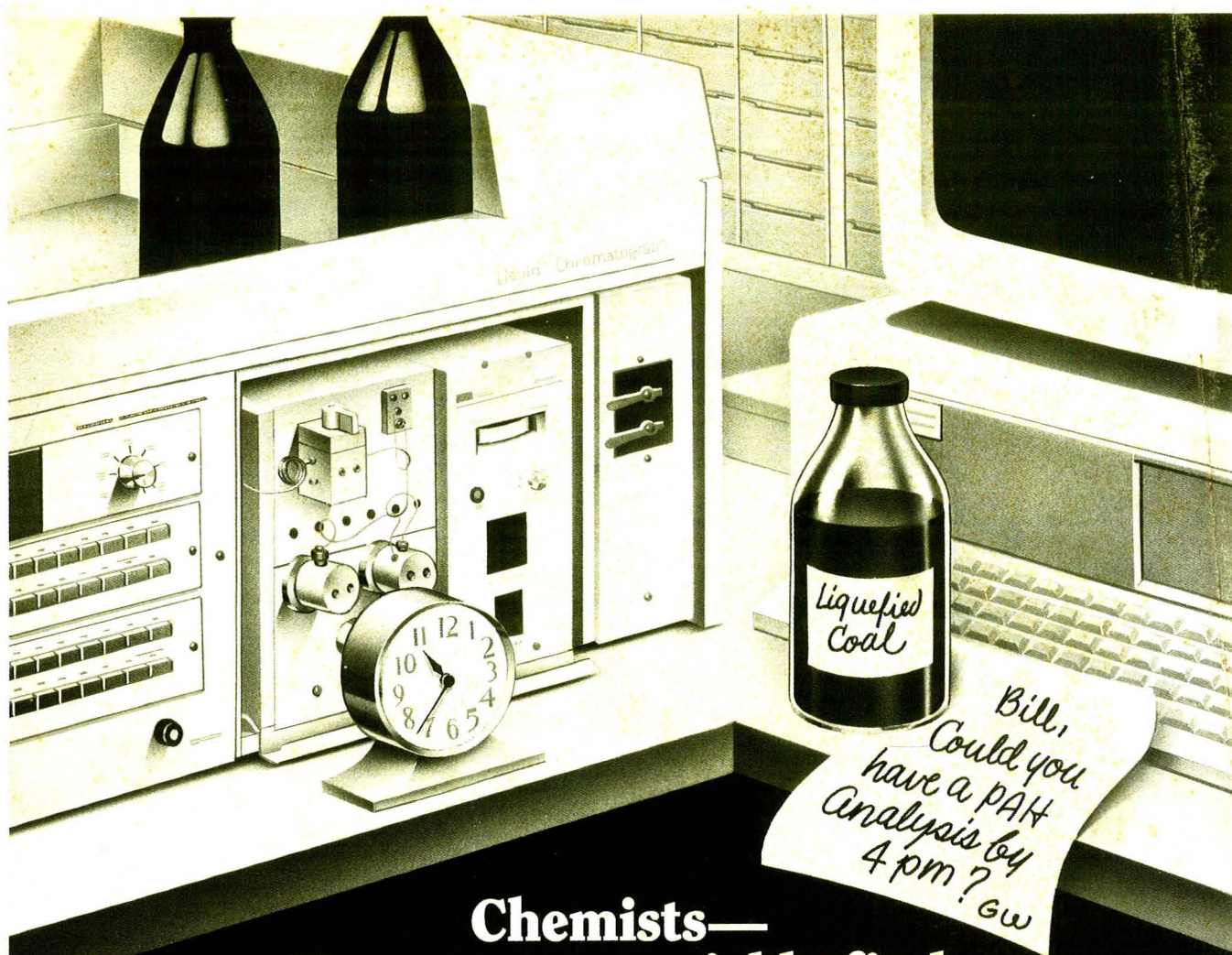
RECEIVED for review May 18, 1987. Accepted July 20, 1987. Use of tradenames is for identification only and does not constitute endorsement by the United States Public Health Service or the United States Department of Health and Human Services.

CORRECTION

Comparison of Inorganic Mobile Phase Counterions for Cationic Indirect Photometric Chromatography

Jeffrey H. Sherman and Neil D. Danielson (*Anal. Chem.* **1987**, *59*, 490–493).

On p 492, Figures 3 and 4 should be switched. The figure captions are correct.



**Chemists—
How can you quickly find
an analytical procedure
to solve this problem?**

Search CHEMICAL JOURNALS ONLINE.

CHEMICAL JOURNALS ONLINE is the new powerful information search system that permits you to quickly search over 45,000 journal articles and display:

- Experimental Procedures • Experimental Data
- Preparation Techniques • New Chemical Names • Synthesis Information
- **PLUS CROSSOVER CAPABILITIES WITH CAS ONLINE**

As part of STN, International, **CHEMICAL JOURNALS ONLINE** provides you with the unique ability to instantaneously cross over from **CAS ONLINE** to the full-text of appropriate journals.

CHEMICAL JOURNALS ONLINE is not only precise in its searching but also cost effective. In minutes you can save yourself days of tedious work.

CHEMICAL JOURNALS ONLINE contains:

- The American Chemical Society's 18 primary journals with over 45,000 articles dating back to 1982.
- A learning file for training and teaching purposes for one low connect hour charge.
- John Wiley & Son's Polymer Journals Online dating back to 1984. (Available Summer 1987)
- Other publisher's journals in the future.

To put **CHEMICAL JOURNALS ONLINE** to work for you, call an American Chemical Society sales representative today at 800-424-6747. The call is free.

Or write, Sales Office, American Chemical Society, 1155 Sixteenth Street, N.W., Washington, D.C. 20036.

CHEMICAL JOURNALS
Your Research
Is Not Complete
Until You Search
ONLINE

HP offers you more ways to do organic analysis than the EPA has methods.

And your analytical options keep growing.

For example, we've just added an infrared detector, an FPD, 601/602 water analyzer, and MS software specifically tailored to the newest EPA-reporting requirements.

These further expand what is already one of the broadest selections of analytical instruments and automation systems available for organic analysis. They reflect, too, HP's continuing commitment to provide the application solutions you need for your organic environmental analysis methods—and the EPA's.

Our support of your environmental laboratory needs includes a full range of automated systems for data analysis, management and EPA-approved reporting. Whether you need general or application specific instrumentation, GC/MS, GC/FTIR, or LC, HP has a data system to fit.

Breadth of line also means HP can give you the bonus of one-source support. You know the value of that if you've ever had to track down and coordinate multiple vendor support teams! Contrast those complexities and frustrations with the comprehensive across-the-board response that a

single phone call to HP can provide.

Plus, there's HP's time-proven quality and reliability. It's reflected in tens of thousands of HP analytical instruments that are working day-in, day-out around the world. You also see it in the 99% uptime guarantee available for our industry standard HP 5890A GC.

Quality, breadth of line and support are all a result of our "What If..." approach that sets your needs, always, as our starting point.

See for yourself.

Call the HP office listed in your telephone directory white pages and ask for an analytical products representative. Or write to Hewlett-Packard Analytical Group, 1820 Embarcadero Rd., Palo Alto, CA 94303.



 **HEWLETT
PACKARD**

AGO4701

CIRCLE 64 ON READER SERVICE CARD